Visualising the role of presynaptic calcium in hippocampal circuits using a novel, genetically encoded calcium sensor

Thesis submitted for the degree of Doctor of Philosophy

By:

Ibrahim Mahmoud Al-Osta

Department Of Neuroscience, Psychology and Behaviour

College Of Medicine, Biological Sciences and Psychology

University Of Leicester

United Kingdom

February 2018

In the name of Allah, the most gracious, the most merciful

[Have they not gone about in the land so as to make their hearts think and ears hear? The fact, however, is that it is the hearts in the breasts and not the eyes that become blind].

The Holly Quran (22:46)

Abstract

Topic: Visualising the role of presynaptic calcium in hippocampal circuits using a novel, genetically encoded calcium sensor

Author: Ibrahim Mahmoud Al-Osta

In this project we used a combination of electrophysiology and fluorescent imaging to monitor synaptic transmission and calcium signalling in synaptic terminals. The study as a whole intended to examine how presynaptic calcium contributes to normal synaptic transmission within different hippocampal neuronal pathways. To this end, we used a transgenic mouse strain known as SyG37 that stably expresses a calcium sensor, SyGCaMP2-mCherry that is expressed in subsets of CNS neurones under the control of the Thy1 promoter. Our findings indicate that this new ratiometric sensor, in the SyG37 mouse strain, provides an excellent tool for detecting neural activity in acute brain slices. First, we showed that evoked calcium transients can be detected in acute brain slices prepared from SyG37 mice where electrical activation of Schaffer collaterals or mossy fibres elicited large calcium transients in area CA1 and CA3, respectively. Using immunohistochemical techniques, SyGCaMP2-mCherry co-localised with presynaptic proteins such as Bassoon, VGLUT1 and VGAT, confirming that it is expressed presynaptically in both excitatory and inhibitory terminals. Blocking fast glutamatergic and GABA/Glycinerergic transmission reduced the size of calcium transients in CA1 and CA3 by only 25 and 20% respectively indicating that the majority of the signals originated from first order presynaptic terminals. Pharmacologically, manipulating the adenosine receptor signalling pathway showed that the actions of adenosine, via the A1 receptor subtype, were different in the CA3 region compared to those in CA1. Forskolin also caused a small, concentration dependent effect on SyGCaMP2 fluorescence in response to electrical stimulation within both CA1 and CA3 regions with pronounced effects on field potential recordings. Together, with this SyG37 strain of transgenic mouse, it is possible to detect neuronal activity with fast temporal and high spatial resolution without the need for pre-incubation with organic calcium dyes or invasive viral transduction procedures.

Acknowledgements

In the name of Allah, the most gracious, the most merciful

I would like to express my deep gratitude to my research supervisor, Professor Nicholas Hartell for his patient guidance, enthusiastic encouragement and useful critiques of this research work. His guidance helped me in all the time of research and writing of this thesis. I could not have imagined having a better advisor and mentor for my PhD study. With the greatest pleasure, I would also like to thank my co-supervisor Professor John Challiss, for his continuous support and advice. My sincere thanks also goes to my committee members Professor Ruth Luthi-Carter as well as Professor Martyn Mahaut-Smith for their brilliant and valuable contributions and feedback. In addition, I would like to thank the Libyan Ministry of Higher Education Scholarship Programme for generously supporting and funding my PhD. My grateful thanks are also extended to the past and present lab members for their friendship and their advice and assistance in keeping my progress on schedule. I would also like to acknowledge all the members of the Cell Physiology & Pharmacology and Neuroscience, Psychology and Behaviour departments.

A special thanks to my family. Words cannot express how grateful I am to my parents, brothers, sister and kids for all the sacrifices that you've made on my behalf and their continuous encouragement. To my beloved wife, I would like to express my thanks for being such good partner and always cheering me up. Your prayer for me was what sustained me thus far.

Thanks again to all who helped me.

Table of contents

List of Figures

List of Tables

List of Abbreviations

ABC	ATP-binding cassete transporter
AC	Adenylate cyclase
ACh	Acetylcholine
ACPD	1-Amino-1,3-dicarboxycyclopentane
AD	Alzheimer's Disease
ADA	Adenosine deaminase
ADP	Adenosine 5′-diphosphate
AK	Adenosine kinase
AMP	Adenosine 5′-monophosphate
AMPA	α-amino-3-hydroxyl-5-methyl-4-isoxazole propionic acid receptors
ANOVA	Analysis of variance
APP/PS1 mice	Amyloid precursor protein/presenilin 1 Mice
APV or AP5	2-amino-5-phosphono-valerate
ATP	Adenosine tri phosphate
ATP	Adenosine 5′-triphosphate
AUC	Area under the curve
AZ	Active zone
Aβ	Amyloid-beta
BAPTA	1,2-bis(o-aminophenoxy)ethane-N,N,N′,N′-tetraacetic acid
BKs	large (big)-conductance, calcium-activated potassium channels
CA1	Cornu Ammonis 1
CA2	Cornu Ammonis 2
Ca^{2+}	Calcium
CA3	Cornu Ammonis 3
CaM	calmodulin
CaMKII	Calcium/calmodulin-dependent kinase II
cAMP	Cyclic adenosine monophosphate
CMAH	Cytidine monophospho-N-acetylneuraminic acid hydroxylase
CNS	Central nervous system
cpEGFP	Circularly permuted enhanced GFP
CREB	Cyclic AMP response element-binding protein

CSF	Cerebrospinal fluid
CTx	Cortex
D	Dopamine
DAG	Diacylglyceride
DG	Dentate Gyrus
DMSO	Dimethyl sulfoxide
DNA	Deoxyribonucleic acid
DNQX	6,7-dinitroquinoxaline-2,3-dione
DPCPX	8-Cyclopentyl-1,3-dipropylxanthine
EC	Entorhinal cortex
EGTA	Ethylene glycol-bis(2-aminoethylether)-N,N,N',N'-tetraacetic acid
ELISA	Enzyme-linked immunosorbent assay
EMCCD	Electron Multiplying CCD
EN	Equilibrative nucleoside transporter
EPSPs	Excitatory postsynaptic potentials
ERK	Extracellular signal-regulated kinase
F	Fluorescence
FAD	Flavin adenine nucleotide
fEPSP	Field excitatory post synaptic potential
GABA	Gamma-Aminobutyric Acid
GDP	Guanosine diphosphate
GECI	Genetically encoded calcium indicator
GFP	green fluorescent protein
GluK R	Kainate receptors
GluRs	Glutamate receptors
GPCR	G-protein coupled receptors
GTP	Guanosine triphosphate
HCL	Hydrochloric acid
HP	Hippocampus
Hz	Hertz
IHC	Immunohistochemistry
InsP3Rs	Inositol trisphosphate receptor
IP3	Inositol trisphosphate
IPSP	Inhibitory postsynaptic potential
KCl	Potassium chloride
kDa	Dissociation constant
KO mice	knockout mice
LLP	Lateral performant pathway
LPP	lateral performant pathway
LTD	Long term depression
LTP	Long term potentiation
MAGUK	Membrane-associated guanylate kinase
MAPK	Mitogen-activated protein kinase
MCPG	α-Methyl-4-carboxyphenylglycine
MF	Mossy Fibers

MF-LTP	Mossy Fibre-Long term potentiation
Mg^{2+}	Magnesium
mGluRs	Metabotropic glutamate receptors
MPP	Medial perforant pathway
ms	Millisecond
Munc	Mammalian uncoordinated
n	Number of release sites at the terminal
N1	First negative component of the fEPSP
N2	Second negative component of the fEPSP
nAChRs	Neuronal nicotinic acetylcholine receptors
NADH	Nicotinamide adenine dinucleotide
NADPH	Nicotinamide adenine dinucleotide phosphate
NaOH	Sodium hydroxide
NBQX	2,3-dihydroxy-6-nitro-7-sulfamoyl-benzo[f]quinoxaline-2,3-dione
NMDA	N-methyl-D-Aspartate
NSF	N-ethylmaleimide-sensitive factor
p	Probability
PCR	Polymerase chain reaction
PDEI	Phosphodiesterase inhibitor
PKA	Protein kinase A
PKC	Protein kinase C
PLC	Phospholipase C
PP	Perforant path
PP-1	Protein phosphatases-1
PPD	Paired-pulse depression
PPF	Paired-pulse facilitation
PSD	Postsynaptic density
PSD95	Postsynaptic density protein-95
PTP	Post-tetanic potentiation
q	Quantal
R^2	The square of the sample correlation coefficient
GEP	GDP/GTP exchange protein
Rab	Ras-related protein
RIM	Regulating synaptic membrane exocytosis protein
RNA	Ribonucleic acid
ROIs	Regions of interests
RRP	Readily releasable pool
RSET factor	Repressor element-1 silencing transcription factor
RyRs	Ryanodine receptor
SAH	S-adenosyl-L-homocysteine
SC	Schaffer collateral
SC-CA1 pathway	Schaffer-collateral-CA1 pathway
SEM	Standard error of means
Ser	Serine

SKs	Small-conductance calcium-activated potassium channels
SL	*Stratum lucidum*
SNAP-25	Synaptosomal-associated protein 25
SNAREs	Soluble N-ethylmaleimide- sensitive factor attachment protein receptors
SNR ratio	Signal to noise ratio
STD	Short term depression
STP	Short term plasticity
Syp1	Synaptophysin 1
Syb2	Synaptobrevin 2
TA pathway	Temporoammonic pathway
TAE	Tris base, acetic acid and EDTA
TARPs	Transmembrane AMPAR regulatory proteins
Thy-1 promoter	Thymus cell antigen 1
t-SNAREs	Target membrane SNARES
V	Voltage
VAMP2	Vesicle-associated membrane protein 2
VDCCs	Voltage-dependent calcium channels
VGCCs	Voltage-gated calcium channels
v-SNARE	Vesicular SNARE
WT mice	Wild Type mice

Chapter 1-General Introduction

1.1 The importance of hippocampal function in memory

Memories are believed to be formed deep within the brain. Many structures are involved in the complex process of encoding memories, however, how each structure contributes to this process is not fully known. One brain structure known to be involved in forming, sorting, and storing memories is the hippocampus. The hippocampus is a major component of our brains. Mammals have two hippocampi; each side of the brain has one hippocampus (O'Keefe and Dostrovsky, 1971, Eichenbaum, 1999, Bird and Burgess, 2008). In 1957, Scoville and Milner discovered that bilateral lesions to the human hippocampus led to a severe impairment of a type of memory that is required for everyday activities called episodic memory (Scoville and Milner, 1957). In the early 1970's "place cells" were discovered leading to the idea that the hippocampus was involved in acquiring and maintaining a spatial representation of the external world (O'Keefe and Dostrovsky, 1971). Rats that had undergone selective lesions of the hippocampus following targeted injections of the excitotoxic neurotoxin ibotenic acid were unable to carry out tasks that required the utilization of contextual and spatial information (Jarrard, 1993). The discovery of hippocampal long-term potentiation (LTP) provided a possible synaptic mechanism for memory storage (Bliss and Lomo, 1973). In the CA1 region, LTP was shown to be dependent upon NMDA receptors (Collingridge *et al.*, 1983). Local application of a selective N-methyl-D-aspartate receptor (NMDA-R) antagonist influenced both the acquisition of spatial forms of memory and hippocampal LTP (Morris *et al.*, 1986). Induction of other forms of synaptic plasticity elsewhere in the brain may be mediated by NMDARs but not all forms of LTP require the activation of NMDARs (for review see; Volianskis *et al.*, 2015). Although the role of the CA1 region of the hippocampus in spatial memory acquisition is well reported, other areas of the hippocampus, and of course other brain regions, contribute to memory acquisition and storage. Procedural memory, for example, appears to be largely unaffected by hippocampal damage, indicating that other brain regions are responsible for its acquisition and storage (Diana *et al.*, 2007). Rolls (1996)

suggested that the CA3 region is important for both episodic and spatial memories with the neocortex being necessary for later retrieval.

Memory impairments that accompany aging and conditions such as Alzheimer's disease also highlight the crucial role of the hippocampus in memory formation. Cognitive function in normal ageing is associated with memory impairments that are linked with specific alterations in prefrontal and hippocampal synapses (Morrison and Baxter, 2012). Examples of these alterations include a reduction in synaptophysin immunoreactivity (synaptophysin is a presynaptic protein that participate in synaptic transmission) in the CA3 *lacunosum-moleculare* layer of rats with spatial-learning impairment (Smith *et al.*, 2000), a decrease in postsynaptic density size of CA1 perforated synapses in spatial learning-impaired aged rats (Nicholson *et al.*, 2004), a reduction in hippocampal NMDA and AMPA receptors (Shi *et al.*, 2007), an alteration in the densities of glutamate receptors in intact complexes of axospinous synapses of the hippocampus (Morrison and Baxter, 2012). However, there is no clear evidence on neuronal loss of the prefrontal and hippocampal synapses in the normal aging process (Rapp and Gallagher, 1996). Calcium influx through L-type calcium channels in aged hippocampal neurones is also increased, leading to prolonged hyperpolarization due to activation of calcium-sensitive potassium channels (Foster, 2007). Manipulation of dopamine levels is also directly related to ageing and cognition, where, blocking of dopamine (D1) receptors in young adults leads to a reduction in activation of frontal and parietal regions during a task of high-load working memory to levels similar to those seen in older adults (Fischer *et al.*, 2010, Grady, 2012). In Alzheimer's disease, the histological findings and the patterns of cell death suggests that the entorhinal cortex is significantly affected by the disease. The CA1 region and the subiculum are both heavily affected (De Leon *et al.*, 1997, Rusinek *et al.*, 2003) whereas the CA3 region and the dentate gyrus are relatively preserved (Small *et al.*, 2011).

Brickman *et al.* (2014) reported that the dentate gyrus (DG) may be a possible hippocampal region associated with age-related decline in memory. They found that the episodic memory decline in healthy older adults associated with the dentate gyrus (DG) can be improved using a high cocoa flavanol-containing diet.

However, this diet is not effective in Alzheimer-related memory decline, since, in Alzheimer's disease, the neurones and memory circuits are already damaged (Busche and Konnerth, 2016). The hippocampus is a structure that is highly susceptible to damage and injury as a result of conditions such as medial temporal lobe epilepsy, ischemia, encephalitis and neurodegenerative conditions including, Alzheimer's disease (Chetelat and Baron, 2003). Therefore, its susceptibility to disease and its links to both LTP and memory make it a widely used model for disease and conditions that affect different types of short and long-term memory. Together with the fact that the hippocampus has a simple laminar structure, the hippocampus can be considered as a favourable model system suitable for studying memory, neuronal plasticity and the effects of ageing and degenerative conditions that affect memory formation.

1.2 Introduction to hippocampal anatomy and connectivity

The hippocampus is a popular brain structure used to study brain physiology because of its well-defined neuronal structure and importance for learning and memory. Figure 1.1 illustrates the main hippocampal regions which are the dentate gyrus (DG), the hippocampus proper (CA3, CA2 and CA1) and the subicular complex (presubiculum and parasubiculum) (for review see; Cappaert *et al.*, 2015). The traditional trisynaptic circuit (EC-DG-CA3-CA1-EC) starts from axons that project from layer II of the entorhinal cortex (EC). These axons are received by neurones within the dentate gyrus and CA3 via the perforant pathway, which can be sub-divided into medial and lateral perforant pathways. The perforant path (PP) innervates the dentate gyrus as well as CA1 pyramidal neurones. The axons of granule cells within the dentate gyrus form mossy fibres, which supply both CA3 pyramidal cells as well as interneurons. CA3 is connected to CA1 neurones (the main output of the hippocampus) via the Schaffer-collateral-commissural pathway. This pathway is so called because the CA1 pyramidal neurones receive Schaffer collaterals (SC) from the ipsilateral hippocampus as well as associational commissural (AC) fibres from CA3 neurones which are located in the contralateral hemisphere (Ramón y Cajal, 1972, Rolls, 1996, Deng *et al.*, 2010). Figure 1.1 shows the schematic diagram of the basic anatomy and neural circuitry of the rat hippocampus.

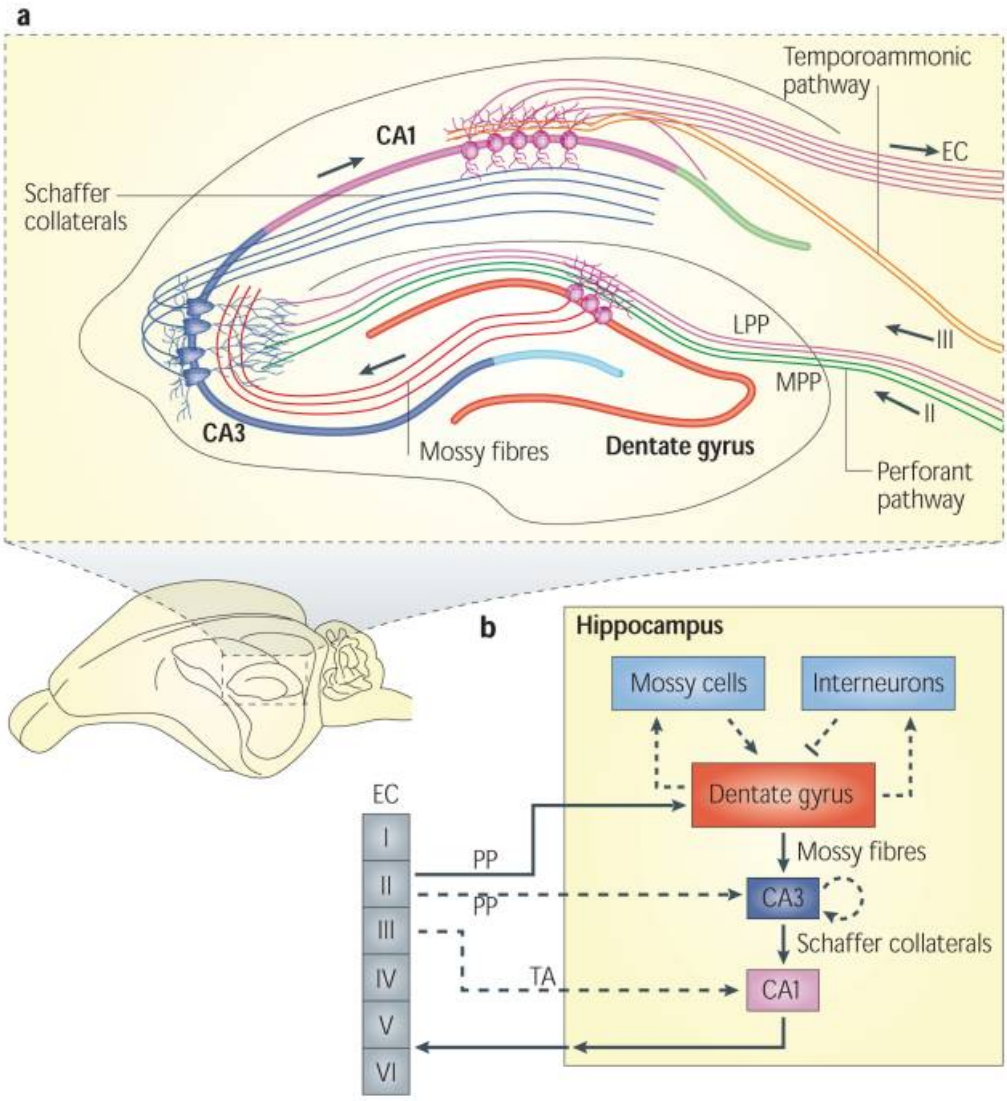

Figure 1.1. A schematic diagram of the basic anatomy and neural circuitry of the rat hippocampus.

A. The hippocampal formation. **B.** Basic hippocampal neural circuitry. The traditional trisynaptic circuit (EC-DG-CA3-CA1-EC) starts from axons that project from layer II of the entorhinal cortex (EC). These axons are received by neurones within the dentate gyrus and CA3 via the perforant pathway, which can be sub-divided into medial and lateral perforant pathways. The perforant path (PP) innervates the dentate gyrus as well as CA1 pyramidal neurones. The axons of granule cells within the dentate gyrus form mossy fibres supply both CA3 pyramidal cells as well as interneurons. CA3 is connected to CA1 neurones (the main output of the hippocampus) via the Schaffer-collateral-commissural pathway. CA1 receives direct input from EC layer III neurons through the TA pathway. Abbreviations: CA-Cornu Ammonis, EC-entorhinal cortex, PP-

performant path, TA-temporoammonic pathway, LPP-lateral performant pathway and MPP- medial perforant pathway. Adapted from Deng *et al*. (2010)

There is a direct connection between CA1 pyramidal neurones and layer III of the entorhinal cortex via the temporoammonic pathway (TA-CA1 pathway). The entorhinal cortex deep-layer neurones receive back-projections from CA1 pyramidal neurones via subicular complex neurones which are considered as the last stage in the pathway. All these pathways are glutamatergic but there are also inhibitory GABA-ergic neurones intrinsic to the hippocampus that mediate feedback as well as feed-forward inhibition. The mossy fibres in the hilus receive projections from dentate granule cells and these dentate granule cells receive inhibitory and excitatory projections from the mossy cells (Rolls, 1996, Squire *et al.*, 2004).

Computational theories have suggested different functions in memory between the CA1 and CA3 hippocampal subfields. Rolls (1987) described a theory of the hippocampus where he suggested that the CA3 neurones operated as an auto-association memory to store object and place memories (episodic memories). Behaviourally, it has been shown that the CA3 supports learning of arbitrary associations where space is a component, such as in spatial rapid one-trial learning, pattern completion, spatial short-term memory, and spatial sequence learning by associations formed between successive items. The granule cells in dentate gyrus support spatial pattern separation during learning (encoding) (the ability to differentiate one memory from other stored memories is called pattern separation (Moser *et al.*, 2008), so, for each memory to be stored in the CA3 cells, the mossy fibre pathway could act to set up different representations. He also suggested that the CA1 cells operate as a re-coder for the information recalled from the CA3 cells to a partial memory cue, and sets up associatively learned back-projections to the neocortex to allow information's subsequent retrieval from the neocortex, and confirms the CA1 findings on consolidation. Therefore, the input from the entorhinal cortex to the DG via the perforant pathway is implicated in learning, the CA3 is implicated in retrieval from CA3, and the CA1 is implicated in retrieval after longer time intervals and in the temporal sequence memory for objects (Rolls, 1987). This theory was further developed to explain the clearer role of each hippocampal region in memory (for review see:

Kesner and Rolls, 2015). Lee *et al.* (2004) provided data in support of that the CA3 plays a crucial role in the rapid formation of representations of new spatiotemporal sequences (as is necessary for episodic memory), whereas CA1 plasticity may be more important in comparing present experienced sequence information with stored sequences in the CA3 network, so it is proposed to play a role in matching the CA3 output with afferent input from the entorhinal cortex. Morphologically, in addition to the differences in the size of pyramidal cells in CA3 and CA1, there is a clear difference in connectivity. The CA3 pyramidal cells receive a mossy fibre input from DG while CA1 pyramidal cells do not. In the CA3 field, but not in CA2 and CA1, there is a narrow acellular zone, called the *stratum lucidum*, which is located just above the pyramidal cell layer; this layer is occupied by the mossy fibre axons (for review see: Cappaert *et al*., 2015). The CA1 area has another property distinct from the CA3 area where there is a pathway referred to as the temporoammonic (TA) or perforant path (pp) that directly connects layer III of the entorhinal cortical (EC) neurones to neurones of the CA1 region (pp-CA1) (Witter *et al.*, 1988). The other cortical input to the hippocampus originates from layer II of the EC and innervates the CA1 region via the DG and CA3. These two separate projections to the CA1 area are thought to play different roles. The Schaffer collateral-CA1 pathway is thought to transfer pre-processed information arising from the CA3 region, and the pp-CA1 synapses are thought to transfer unedited information directly to the CA1 area. The unedited information transferred via the pp-CA1 pathway might serve as a reference copy for newly stored information in the CA1 area, or support mismatch and/or error detection (Lisman and Otmakhova, 2001, Izumi and Zorumski, 2008, Aksoy-Aksel and Manahan-Vaughan, 2015). Understanding how information flows within and between these brain circuits is one of the many unsolved mysteries of neuroscience. Communication between individual cells is primarily chemical in nature within these precise neural circuits. The fundamental step in this process is neurotransmitter release via exocytosis of neurotransmitter-filled synaptic vesicles. In the following paragraph, the presynaptic release site architecture, where these vesicles present, will be covered, in brief.

1.3 The presynaptic release site architecture.

Neurotransmitter release is mediated by a calcium-dependent synaptic vesicular release process. This process involves vesicle docking, priming, fusion, endocytosis, and recycling (Li and Chin, 2003). In brief, at the presynaptic nerve terminal, synaptic vesicles filled with neurotransmitter are docked at an active zone. The maturation process of docked vesicles is called priming. When Ca^{2+} influx follows an action potential, these primed vesicles rapidly fuse with the presynaptic membrane to release their contents through the process of exocytosis. The membranes of the synaptic vesicle and their constituent vesicular proteins are recycled locally for future exocytosis through the process of endocytosis (Klenchin and Martin, 2000). The presynaptic molecular machinery of vesicle exocytosis involves proteins which play a crucial role in guiding vesicles to the active zone, retaining vesicles in place and sensing the Ca^{2+} influx as the trigger for exocytosis (figure.1.2). The entire story of the role of these identified proteins is still a major ongoing topic in neuroscience research (Li and Chin, 2003, Sudhof, 2013).

The protein families which are involved in the fusion molecular machinery include: ATPase N-ethylmaleimide-sensitive factor (NSF), soluble N-ethylmaleimide- sensitive factor attachment protein receptors (SNAREs), Rab GTPases, Munc18/Sec1, and the protein components of the exocytosis complex such as complexin, RIM, Munc 13 and synaptotagmin (Li and Chin, 2003). The SNARE family are small proteins with molecular masses of 10-35 kDa (Burri and Lithgow, 2004, Jahn, 2004). This protein family plays a role in the mechanisms of vesicle membrane fusion which include VAMP2/synaptobrevin, which is a vesicular SNARE (v-SNARE) and syntaxin 1 and SNAP-25 which are target membrane SNARES (t-SNAREs). The initial complex of a tetrahelical core of SNAREs is formed from domains of synaptobrevin, syntaxin-1 and SNAP-25. This complex is formed between the presynaptic membrane and the vesicle. Synaptobrevin and syntaxin allow presynaptic and vesicle membranes to be recognized to each other (Sudhof, 1995, Sutton *et al.*, 1998, Martens and McMahon, 2008, Sudhof and Rizo, 2011).

Synaptotagmins-1 and 2 are vesicle proteins that have Ca^{2+} binding sites. They are thought to work as Ca^{2+} sensors that can start the process of exocytosis upon Ca^{2+} influx; there is no formation of a fusion pore without Ca^{2+} influx. In the absence of calcium, the 5 calcium binding sites on the C2A and C2B calcium binding domains of synaptotagmin are unbound and vesicle fusion is inhibited. Synaptotagmin does not seem to be directly involved in the vesicle fusion process; it is does, however, pull the presynaptic membrane and vesicle together to position them in close proximity to ease pore formation. SNARE gene disruption in mice leads to failure in neurotransmitter release which further explains the crucial role of SNARE proteins in synaptic vesicle exocytosis which is stimulated by Ca^{2+} influx (Washbourne *et al.*, 2002, Kennedy and Ehlers, 2011). Interestingly, however, whilst fast, synchronous release is prevented, spontaneous and asynchronous release were enhanced suggesting that at least one other protein exists within the presynaptic terminal that acts as a calcium sensor (Kennedy and Ehlers, 2011). Recently, neuronal polarity and axon differentiation were found to be regulated by Synaptotagmin 1 in cultured hippocampal neurones (Inoue *et al.*, 2015).

Rab3a is a member of a G protein family that consists of Rab3A, -3B, -3C, and -3D. Rab3a has the ability to bind GTP and is activated by GDP/GTP exchange protein (Rab3 GEP). Rab3a is thought to be involved in the docking process by guiding vesicles to active zones (Tanaka *et al.*, 2001). The Munc18-1, Sec/Munc (SM) protein family member, which seems to be important for membrane trafficking pathways and the binding of munc 18-1 to syntaxin through its N-terminal Habc domain, is important for neurotransmitter release. Munc 18 interacts with munc 13 to alter the conformational state of syntaxin allowing priming to take place (Verhage *et al.*, 2000, Weimer and Richmond, 2005, Hu *et al.*, 2011).

Complexin (synaphin) is a cytoplasmic neuronal protein that has the ability to bind to the complex of SNARE proteins with high affinity and there is competition between complexins and synaptotagmins to bind to the SNARE protein complex. In the presence of Ca^{2+} synaptotagmin replaces complexin allowing the SNARE protein complex to bind to vesicle and presynaptic membrane to facilitate pore

formation. When there is no Ca^{2+} influx, complexin acts as neurotransmitter release inhibitor by clamping the SNARE protein complex and inhibiting vesicle fusion (Sudhof, 1995, Brose, 2008, Giraudo *et al.*, 2009, Kennedy and Ehlers, 2011).

Synaptophysin (major synaptic vesicle protein p38; 38kDa) is a four transmembrane domains vesicular protein present in virtually all brain and spinal cord neurones (Wiedenmann and Franke, 1985, Südhof *et al.*, 1987, Calhoun *et al.*, 1996). This protein has unknown function; however, previous molecular studies have shown that synaptophysin plays a crucial role in synaptic functions including exocytosis, synapse formation and endocytosis of synaptic vesicles (Thomas *et al.*, 1988, Eshkind and Leube, 1995, Spiwoks-Becker *et al.*, 2001, Tarsa and Goda, 2002). Surprisingly, in synaptophysin (Evans and Cousin, 2005), this is might be the reason for choosing to use it to create our sensor. The lack of an obvious phenotype was attributed to abundant expression of synaptophysin isoforms such as synaptogyrin or synaptoporin. Consistent with this, mice lacking both synaptogyrin and synaptoporin showed exacerbation in synaptic depression and delay in the replenishment of releasable synaptic vesicle pools (Janz *et al.*, 1999, Kwon and Chapman, 2011). In disease, research has shown that synaptophysin elimination in mice creates behavioral changes such as impaired object novelty recognition, increased exploratory behavior and reduced spatial learning (McMahon *et al.*, 1996, Schmitt *et al.*, 2009). Most recently, Adams *et al.* (2017) found that synaptophysin is a target of β-Amyloid that regulates synaptic plasticity and seizure susceptibility in an Alzheimer's model, where they found a subtle yet critical role for synaptophysin in the synaptic vesicle cycle and the Alzheimer's disease etiology. Many mechanisms of how synaptophysin works have been proposed, for example, Rehm *et al*. (1986) suggested that there is a direct interaction between synaptophysin and the dynamin (a GTPase responsible for endocytosis in the eukaryotic cell) where dynamin only associates with synaptophysin in vivo after synaptobrevin enters the SNARE complex, suggesting that synaptophysin plays a role in synaptic vesicle recycling by recruiting dynamin to the vesicle membrane. Gordon *et al.* (2011) found that synaptophysin is specifically required for sybII-pHluorin (Synaptobrevin 2- pHluorin) retrieval, while its absence slowed the retrieval of

other synaptic vesicle protein cargo. Thus synaptophysin is specifically required for synaptobrevin 2 retrieval during synaptic vesicle endocytosis. Recently, Rajappa *et al.* (2016), identified the key mechanisms mediating release site clearance for preventing cis-SNARE complex formation at the active zone. This could happen by self-assembly of exocytosed synaptobrevin 2 and Synaptophysin 1 by homo- and hetero-oligomerization into clusters (figure 1.2). They also found that loss of synaptophysin II induced frequency-dependent STD confirming the importance of synaptophysin in the release site clearance process during synaptic vesicle recycling.

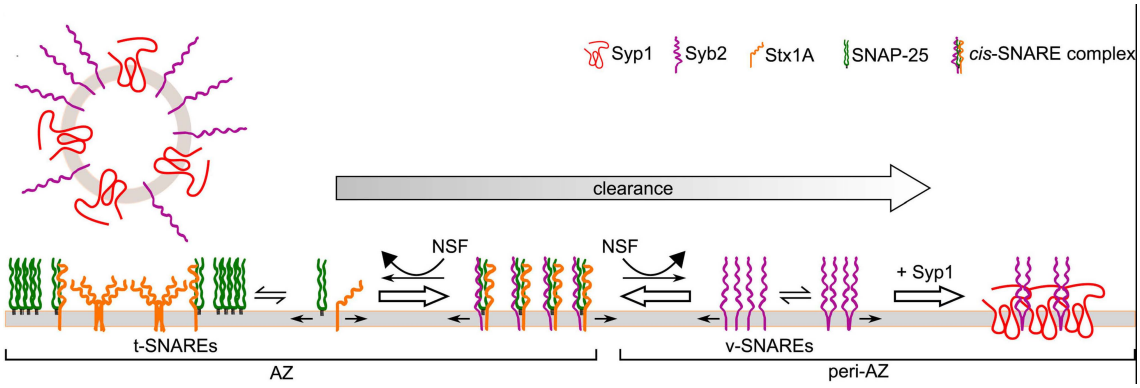

Figure 1.2. A schematic diagram of the proposed role of Synaptophysin 1 in release site clearance process.

For release site clearance, Syb2 is pushed away by NSF, which disassembles cis-SNARE complexes, and pulled by Syp1, which clusters Syb2 dimers outside of the active zone (AZ). Loss of either one leads to accumulation of cis-SNARE complexes at sites of SV fusion, thereby perturbing its function, which results in short term depression. Syb2-Syp1 clusters in the peri-AZ and t-SNARE clusters form stable domains in the active zone, thereby maintaining its integrity, whereas all other components diffuse freely. Abbreviations: Syp1- Synaptophysin 1, Syb2- synaptobrevin 2, Stx1A- Syntaxin 1A, NSF- ATPase N-ethylmaleimide-sensitive factor, SNARE-Soluble N-ethylmaleimide- sensitive factor attachment protein receptors. Adapted from Rajappa *et al.* (2016).

At the molecular level, there are many studies that have dealt with the function and the structure of presynaptic proteins. However, as yet, our understanding of the exocytosis process remains somewhat incomplete. Figure 1.3 summarizes the mechanism of synaptic exocytosis and its conserved protein components and the synaptic vesicle exocytosis at the molecular level.

A

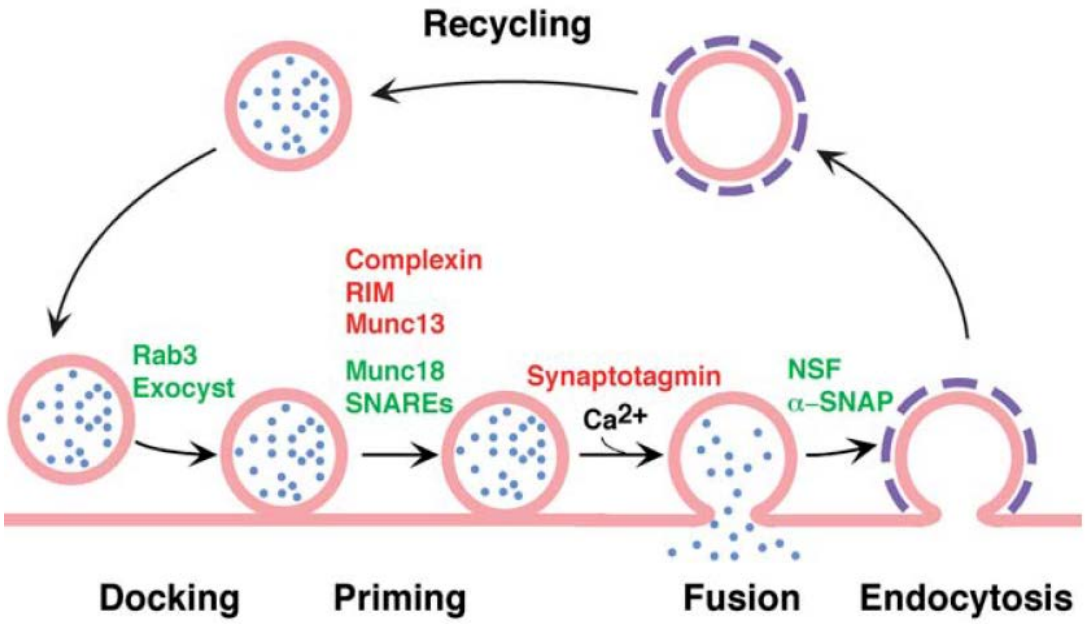

B

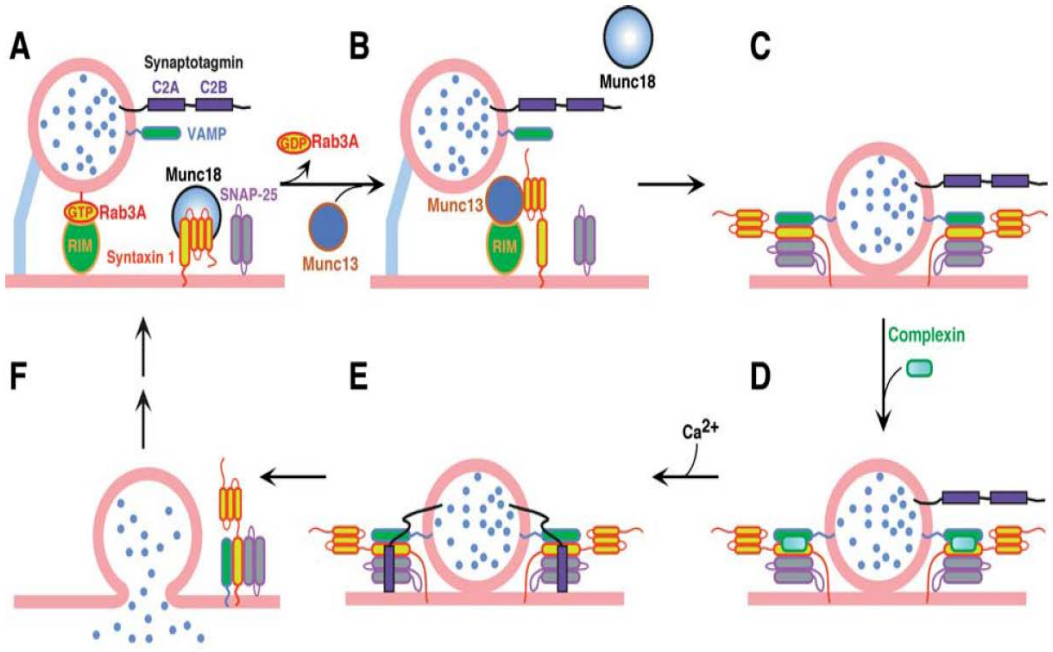

Figure 1.3. A. The mechanism of synaptic exocytosis and its conserved protein components.

Synaptic vesicle exocytosis unique components are written in red whereas fusion machinery protein components are shown in green. **B. Synaptic vesicle exocytosis at the molecular level:** (A) Docking of a synaptic vesicle to the active zone. In this stage, there is an interaction between the closed form of syntaxin 1 and Munc18. Bassoon, piccolo and the interaction between GTP bound Rab3A and RIM proteins are thought to be involved in this process. (B)

Hydrolysis of GTP to GDP leads to dissociation of Rab3A from the Rab3A-RIM complex. Binding of RIM with Munc13 leads to activation of Munc13 to displace Munc18 from its site on syntaxin 1. This process leads to the conversion of syntaxin 1 from closed state to opened state. (C) The opened state of syntaxin 1 permit to syntaxin 1 to be reunited with SNAP-25 and VAMP2 as a trans-SNARE complex, which bring the plasma membrane and synaptic vesicle in close proximity. (D) When there is no Ca2+ influx, Complexin acts as neurotransmitter release inhibitor by clamping the SNARE protein complex and inhibiting vesicle fusion. (E) In the presence of Ca2+, the synaptotagmin replaces complexin, and therefore, the SNARE protein complex then can bind vesicle and presynaptic membranes to put them in close proximity to facilitate pore formation. (F) Dissociation of cis-SNARE complex by NSF/a-SNAP will make the SNARE proteins ready to be involved in a new exocytosis cycle. Adapted from Li and Chin (2003).

Many other proteins located at the presynaptic terminals. In this study, some of antibodies against them will be used in immunohistochemistry experiments. For example, bassoon is a presynaptic protein involved in the organisation of the neurotransmitter release site, and is specifically localised at the active zone. In cultured hippocampal neurones, bassoon was found to co-localise with glutamate receptor-1 (GLUR1) and GABAA receptors and, therefore, is considered to be a component of the active zone of both excitatory glutamatergic and inhibitory GABAergic synapses (Richter *et al.*, 1999). The vesicular glutamate transporter 1 (vGLUT1), and the related vGLUT-2 are both highly important transporters for the uptake and storage of glutamate, and thus comprises the sole determinant for a glutamatergic phenotype. The vesicular glutamate transporter mediates glutamate uptake into the synaptic vesicles of excitatory neurones (Bellocchio *et al.*, 2000, Ziegler *et al.*, 2002). In the CNS, their expressions seem to be largely complementary. Together, they are currently considered as the best markers for glutamatergic nerve terminals and glutamatergic synapses. VGLUT1 is preferentially expressed in the neocortex and hippocampus, while vGLUT2 mainly occurs in the thalamus (Herzog *et al.*, 2006). The vesicular GABA transporter (VGAT) is responsible for the uptake and storage of gamma-aminobutyric acid (GABA) and glycine by synaptic vesicles in the central nervous system (McIntire *et al.*, 1997, Chaudhry *et al.*, 1998b).

Therefore, VGAT is currently considered as a good marker for GABAregic inhibitory nerve terminals.

Postsynaptic density (PSD) is a postsynaptic marker, however, it can be used in IHC experiments, where the absence of co-localisation with this protein can be used to confirm a presynaptic locus of any target protein. PSD95 is the most abundant scaffolding protein, almost exclusively located in the postsynaptic density (PSDs) of neurones. PSD95, which is a member of the membrane-associated guanylate kinase (MAGUK) family, interacts with the cytoplasmic tail of NMDA receptor subunits and potassium channel clusters to regulate synaptic plasticity associated with NMDA receptor signalling (Hunt *et al.*, 1996, Garner *et al.*, 2000, Kim and Sheng, 2004, Chen *et al.*, 2011).

1.4 Regulation of neurotransmitter release by synaptic receptors

There are many receptors (metabotropic and ionotropic families), which are involved in neurotransmitter release modulation. Ionotropic receptors affect release mainly by changing the membrane potential; in contrast, most metabotropic receptors are coupled to G proteins and modulate release by an interaction between calcium channels and G protein βγ-subunits (Frerking and Wondolowski, 2008). The possible mechanisms for modulation include Ca^{2+} channel inhibition, vesicle release complex regulation or by activation of presynaptic ion channels. Sometimes, all of these mechanisms are recruited simultaneously (Miller, 1998). Therefore, presynaptic receptors represent a wide class of molecules that can influence synaptic transmission with a high degree of synapse-specificity (Wang, 2008). Thanawala and Regehr (2013) suggested that neuromodulators that regulate presynaptic voltage-gated calcium channels (VGCCs) regulate both the probability of vesicular exocytosis (p) and the effective size of the readily releasable pool (RRP). Therefore, neurotransmitter release and synaptic strength are profoundly dependant on presynaptic calcium channels. In the following section, a number of receptors that have been reported to play a role in neurotransmitter release modulation will be discussed briefly.

1.4.1 Glutamate Receptors

Glutamate receptors play a role in modulating pre- and post-synaptic neuronal Ca^{2+} influx and postsynaptic activity. Because of the importance of these receptors, both pre and postsynaptic glutamate receptors will be discussed briefly. Glutamate receptors can be classified into: G-protein-coupled (GPCR; metabotropic) and ionotropic (ligand-gated ion channels) receptors. GPCRs initiate a series of intracellular signalling events within postsynaptic neurones upon activation whereas ionotropic receptors gate ion channels leading to conductance changes such that the postsynaptic neuronal polarization state will be altered. Metabotropic glutamate receptors (mGluRs) are a group of GPCRs that act via second messenger pathways. These receptors can be subdivided into Group I mGlu receptors (mGlu1 and mGlu5), group II (mGlu2 and mGlu3) and group III receptors (mGlu4, mGlu6, mGlu7 and mGlu8). These receptors can indirectly modulate postsynaptic ion channels (Bortolotto *et al.*, 1999, El Moustaine *et al.*, 2012). Group I mGlu receptors influence calcium signalling through phospholipase C (PLC), whereas group II and group III receptors have inhibitory effects on adenylyl cyclase. In the hippocampus, group I mGluRs are mainly postsynaptic, whereas group II (mGluR2) and most of group III mGluRs are mainly localized to presynaptic neurones. Moreover, mGluR2, mGluR7a, and mGluR7b were identified in mossy fibre terminals, whereas Schaffer collateral terminals were labelled only for mGluR7a (Shigemoto *et al.*, 1997, Hinoi *et al.*, 2001).

Ionotropic glutamate receptors (GluRs) are subdivided into three main types: N-methyl-D-aspartic acid (NMDA), α-amino-3-hydroxy-5-methyl-4-isoxazolepropionic acid (AMPA), and kainate receptors. Glutamate has a high affinity to all of them (Palmada and Centelles, 1998, Erreger *et al.*, 2004, Meyerson *et al.*, 2014). In the CNS, fast excitatory synaptic transmission is mediated in large part by AMPA receptors. AMPA receptors conduct sodium and potassium ions, however, depending on the composition of their subunits, they can be permeable to Ca^{2+} as well (Gouaux, 2004). NMDA receptors are non-selective ion channels; NMDA receptors have the ability to conduct Na^{+}, K^{+} and Ca^{2+} only when the Mg^{2+} block within the channel is removed when the cell is sufficiently depolarized. The ligand gating in NMDA receptors requires co-

activation by two ligands: glutamate and either D-serine or glycine. These receptors have a large capacity to increase Ca^{2+} concentration within the postsynaptic neuron, which then works as a second messenger in more downstream signalling pathways and processes. These properties of NMDA receptors are widely thought to be the basis of information storage at synapses (Purves, 2008). The NMDA receptor antagonist AP5 (2-amino-5-phosphono-valerate) can be used to differentiate between AMPA/kainate and NMDA responses. The EPSPs produced by AMPA/kainate receptors are faster and short-lasting than the those produced by NMDA receptors (Purves, 2008).

Kainate receptors are permeable to sodium and potassium ions but they have a low permeability for calcium (Ferrer-Montiel and Montal, 1996, Sun *et al.*, 2009). Kainate receptors are located both at presynaptic and postsynaptic terminals and can be either metabotropic or ionotropic. Presynaptic metabotropic kainate receptors are responsible for suppression of release probability during postnatal development (Lauri *et al.*, 2006). Interestingly, kainate receptors are only expressed presynaptically at CA3 cell terminals. These receptors are involved in release probability modulation (Jane *et al.*, 2009, Riebe, 2010). Kainate receptors act as modulators of synaptic transmission. They have pre- and postsynaptic effects and their function is not fully understood. The kainate receptor agonist, kainic acid, can induce seizures through GluK2 subunit activation; therefore, it is a favorable target for the development of new antiepileptic therapeutics (Contractor *et al.*, 2011, Fritsch *et al.*, 2014).

General mechanisms of action of the above glutamate receptors can be summarized as follows: presynaptic metabotropic glutamate receptors generally depress neurotransmitter release by activating $K+$ conductance, inhibiting Ca^{2+} channels, modulating the levels of cyclic AMP or by modulating the exocytotic machinery. They can also increase neurotransmitter release by activating calcium-induced calcium release. Whereas, presynaptic ionotropic glutamate receptors often facilitate neurotransmitter release and have short-lived effects. They achieve this through mechanisms that involve the direct modulation of calcium channels, the depolarization of the nerve terminal, the induction of calcium-induced calcium release from internal stores, the direct influx of

calcium through the receptor channel, or the synthesis of nitric oxide (for review see: Engelman and MacDermott, 2004, Pinheiro and Mulle, 2008). There is a big difference between the actions of ionotropic and GPCRs receptors on presynaptic terminals; for example, ionotropic receptors activate within a few milliseconds whereas, GPCRs might act in the order of seconds or minutes. These differences in activation can lead to different temporal regulation of neurotransmitter release (Kidd et al., 2002). Ionotropic and GPCRs receptors can also differ in their desensitization characteristics. Ionotropic receptors desensitize over widely variable time courses, whereas, GPCRs desensitize within seconds of agonist activation (Luttrell and Lefkowitz, 2002). In addition, ionotropic and GPCRs receptors that respond to the same agonist can have markedly different affinities (Siegel, 2005).

1.4.2 Voltage gated calcium channels

Voltage-gated calcium channels (VGCCs), also called voltage-dependent calcium channels (VDCC) are a group of ion channels that are highly sensitive to changes in membrane potential. They contribute to many physiological functions in excitable cells including transmission at the neuromuscular junction, synaptic transmission and hormonal secretion to name but a few. According to their voltage dependence, single-conductance kinetics and their pharmacological sensitivity, VGCCs can be classified into L (Cav1.1, Cav1.2, Cav1.3 and Cav1.4), N ($Ca_v2.2$), P/Q ($Ca_v2.1$), R ($Ca_v2.1$) and T-types ($Ca_v3.1$, $Ca_v3.2$, and $Ca_v3.3$) (Reuter, 1996, Voglis and Tavernarakis, 2006). L-type ion channels are activated by high-voltage threshold. They are involved in a form of NMDAR-independent LTP that occurs within the mossy fibre pathway (Kapur *et al.*, 1998). Administration of an antagonist to L-type calcium channels (nimodipine) inhibits this NMDA-independent LTP and leads to loss of memory in animals receiving chronic administration of nimodipine (Veng *et al.*, 2003). L-type VGCC current is highly increased in the hippocampal CA1 neurones of aged rats. Moreover, L-type VGCC are also highly expressed in aged and Alzheimer's patients suggesting that these channels might be involved in both learning and memory processes as well as in pathological and physiological neurological conditions where plasticity and memory are affected (Thibault and Landfield, 1996, Voglis and Tavernarakis, 2006). T-type calcium channels are activated at a low-voltage threshold and this property enables them to contribute to bursting activity in various brain regions. P-, Q- and R-type of VGCCs are also involved in the neurotransmitter release process and as such contribute to various forms of synaptic plasticity. LTP induction at the hippocampal mossy fibres pathway requires a presynaptic calcium rise but its expression is independent of postsynaptic calcium currents. R-type calcium channels are not involved in fast neurotransmitter release in general, but they are involved in synaptic LTP, most notably within the mossy fibre pathway (Dietrich *et al.*, 2003).

1.4.3 Adenosine receptors

Adenosine is a purine nucleoside widely found in nature that plays an important role in biological processes such as in energy transfer (ATP and ADP), signal transduction (cAMP) and as a neuromodulator believed to play a role in suppressing arousal and promoting sleep (Buckingham, 1987, Huston *et al.*, 1996, Belardinelli and Pelleg, 2012). In the CNS, adenosine modulates synaptic responses via A_1 and A_{2A} receptors, which mainly localize at excitatory glutamate synapses (Rebola *et al.*, 2003a, Rebola *et al.*, 2003b, Rebola *et al.*, 2005). A_1 receptors are the most abundant G protein-coupled receptors in the brain that suppress synaptic transmission and therefore, control basal network activities (Dunwiddie and Masino, 2001), whereas A_{2A} receptors play essential roles in some forms of synaptic plasticity (Rebola *et al.*, 2008). A_{2B} and A_3 receptors are located mainly peripherally and are involved in processes such as immune responses and inflammation (For review see, Sheth *et al.*, 2014). Adenylate cyclase is the primary second messenger target of all adenosine receptor subtypes. Adenylate cyclase is either activated or inhibited depending on the stimulated receptor type. A_1 and A_3 receptors are coupled to G_i and their activation results in a decrease of cAMP levels, a decrease of transient Ca^{2+} conductance and an increase of K^+ conductance. Whereas adenosine A_{2A} and A_{2B} receptor subtypes increase cAMP levels as they are coupled to the G_s subunit (Sperlágh and Sylvester Vizi, 2011, Sheth *et al*., 2014). In the hippocampus, adenosine mediates its inhibitory effect on synaptic transmission via A_1 receptors (Bruns *et al.*, 1987b). Adenosine acts presynaptically (via A1 receptors) to decrease the release of neurotransmitters such as glutamate (Dunwiddie, 1985) and postsynaptically via an increase in a potassium conductance's (Gerber *et al.*, 1989, Thompson *et al.*, 1992). Gundlfinger *et al*., (2007), using imaging and electrophysiological techniques, demonstrated that adenosine has a direct inhibitory effect on presynaptic calcium channels to modulate transmission at the hippocampal mossy fibre synapse (Gundlfinger *et al.*, 2007). Many studies have suggested that extracellular adenosine can be elevated via several pathways, including exocytosis (Klyuch *et al.*, 2012), transport (Lovatt *et al.*, 2012) and enzymatic breakdown of extracellular nucleotides (Mi and Jackson, 1998). Endogenous adenosine is released

metabolically from active brain cells by adenosine triphosphate (ATP) degradation such that it is then generated extracellularly (Kase *et al.*, 1999). By means of bidirectional nucleoside transporters, normally, intra and extracellular adenosine concentrations are kept in equilibrium (Deckert *et al.*, 1988). The concentration gradient between the cytosol and the extracellular space is the determinant of the direction of adenosine transport. Several enzymes can regulate the intracellular level of adenosine, for example, phosphorylation of intracellular adenosine by adenosine kinase keeps the intracellular concentration low. Released adenine nucleotide in the extracellular space is rapidly hydrolysed by ecto-nucleotidases to form adenosine. That is why the basal extracellular levels of adenine nucleotides are low. Ecto-5'-nucleotidase is a nucleotide catabolizing enzyme which is abundant in the central nervous system (Richardson *et al.*, 1987, Zimmermann *et al.*, 1993, Pak and Yetkin, 2014). The imbalance in adenosine concentrations is an indicator of many health problems where adenosine levels are drastically elevated during metabolic stress, seizures (During and Spencer, 1992), epilepsy (Gouder *et al.*, 2003, Boison, 2012) and hypoxia or ischemia (Winn *et al.*, 1981) with the consequence of profound inhibition of synaptic transmission and neuronal excitability (Pak and Yetkin, 2014). Figure 1.4 summarizes the adenosine cycle between cytosolic and extracellular compartments.

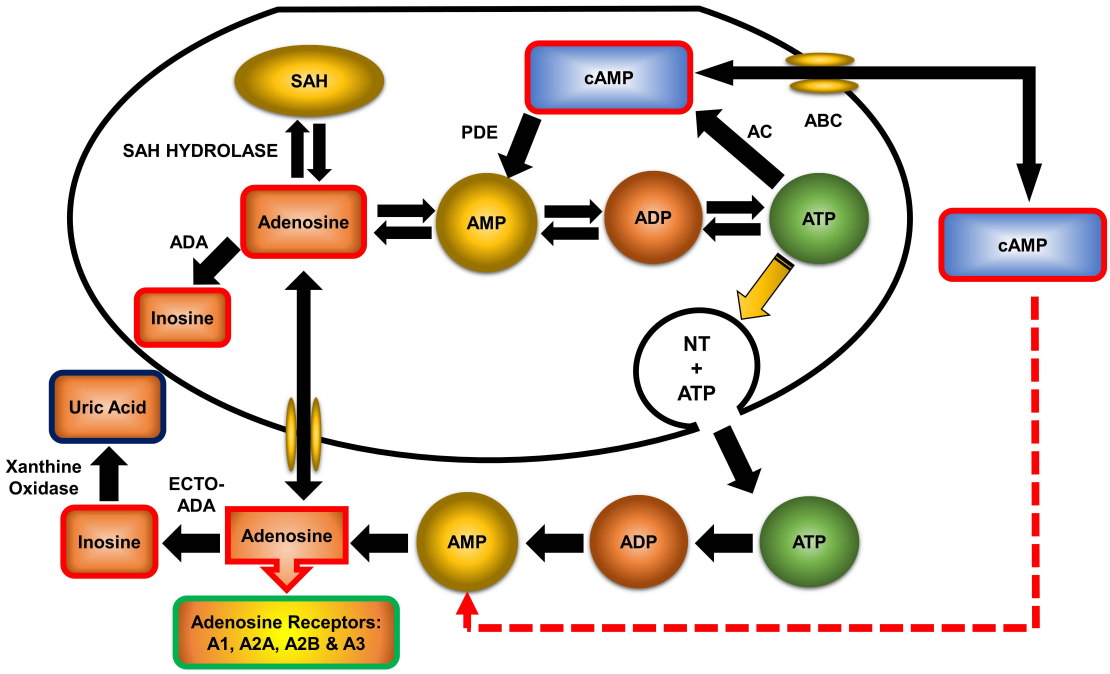

Figure 1.4. Schematic diagram of adenosine metabolism.

Extracellular adenosine concentrations can be increased via intracellular sources (synthesis from intracellular dephosphorylation of ATP, ADP or AMP by 5'-nucleotidases and hydrolysis of SAH), transport of extracellular cAMP followed by its hydrolysis, or rapid hydrolysis of released nucleotides by ecto-nucleotidases. The balance between intra- and extracellular concentrations of adenosine is obtained by bidirectional transport through equilibrative nucleoside transporter (ENT). Once in the extracellular space, adenosine can act via two high affinity receptors (the A1 and A2A receptors) and two low-affinity receptors (A2B and A3 receptors). Adenosine metabolisation to inosine occurs intra- and extracellularly through local adenosine deaminase activity. Intracellularly adenosine can also be metabolized through AK-mediated phosphorylation to AMP. Abbreviations: ABC: ATP-binding cassette transporter; AC: adenylate cyclase; ADA: adenosine deaminase; ADP: adenosine 5′-diphosphate; AK: adenosine kinase; AMP: adenosine 5′-monophosphate; ATP: adenosine 5′-triphosphate; cAMP: cyclic AMP; PDE: phosphodiesterase; SAH: S-adenosyl-L-homocysteine. Sourced from Marro *et al.* (1997), Park and Gupta (2013), Rombo *et al.* (2016).

1.4.4 Potassium channels

Potassium channels are a group of potassium conducting ion channels that can be classified as voltage-gated (K_V), inwardly rectifying, tandem pore domain and those which are modulated by intracellular calcium called calcium-activated potassium channels (K_{Ca}). There are three types of calcium activated potassium channels: small-conductance calcium-activated potassium channels (SKs = $K_{Ca}2.1$, $K_{Ca}2.2$ and $K_{Ca}2.3$), large (big)-conductance, calcium-activated potassium channels (BKs = $K_{Ca}1.1$) and intermediate conductance channels (IK = $K_{Ca}3.1$) that seem to be the least studied of all of the channels (Wei *et al.*, 2005, Alexander *et al.*, 2015). In CA1 hippocampal neurones, (SKs) are localized at presynaptic terminals and in their activated state they have the ability to modulate postsynaptic potentials by increasing potassium efflux and, therefore, hyperpolarizing the membrane after an action potential (Faber *et al.*, 2005). Hippocampal LTP can be enhanced by blocking SKs while it is diminished by SK over expression (Hammond *et al.*, 2006). BKs, on the other hand are generally located in both post- and presynaptic compartments of hippocampal pyramidal neurons (Sailer *et al.*, 2006). They are involved in neuronal excitability and the contractility of smooth muscle. BKs are dual regulated through intracellular Ca^{2+} and membrane voltage. BKs have a negative-feedback effect on membrane depolarization through membrane hyperpolarization by their modulation by calcium influx (Furukawa *et al.*, 2008, Yuan *et al.*, 2010).

1.4.5 GABA Receptors

GABA also has a substantial impact on neurotransmitter release. It is a common inhibitory neurotransmitter in the adult mammalian brain. There are three types of GABA receptors; $GABA_A$ and $GABA_C$ receptors are inotropic, whereas $GABA_B$ receptors are metabotropic. GABA receptors play an inhibitory role on postsynaptic cells, either by increasing chloride ion conductance (ionotropic GABA receptors) or by blocking Ca^{2+} channels or by activation of K+ channels ($GABA_B$) which leads to hyperpolarization (Purves, 2008). There is a specific $GABA_A$ receptor subtype (containing α5-subunit) which is highly expressed in hippocampal CA1-CA3 regions. Mice lacking the GABA-$_{A\alpha\text{-}5}$ subunit showed a

decrease in inhibitory currents of postsynaptic neurones and increase in the capacity of spatial learning. These findings suggest a role for $GABA_A$ receptors in hippocampal synaptic plasticity (Collinson *et al.*, 2002). Furthermore, activation of postsynaptic $GABA_B$ receptors results in second messenger modulation through inhibition of adenylyl cyclase activity. Mutation of S783 in $GABA_B$ receptors led to deficits in memory consolidation and long-term spatial memory and so enhancing of $GABA_B$ receptor signalling could be a good target for enhancement of memory (Terunuma *et al.*, 2014).

1.5 Ca^{2+} and its role in synaptic transmission.

The complex networks of neurones and glial cells in our brains are connected via around one hundred trillion synapses (Squire, 2013). The major excitatory neurotransmitter at these synapses is glutamic acid, which is released from presynaptic terminals to exert its effects on postsynaptic cells to influence neuronal function and synaptic plasticity (McEntee and Crook, 1993, Meldrum, 2000, Kennedy and Ehlers, 2011). Neurotransmitter release is mediated by a calcium-dependent synaptic vesicular release process. As mentioned above, this process involves vesicle docking, priming, fusion, endocytosis, and recycling. At rest, neurotransmitters are stored in presynaptic vesicles. A few of these vesicles are concentrated at the "active zone" (a zone in a presynaptic terminal where a neurotransmitter is released). Most presynaptic vesicles are held in a protein matrix near the active zone that includes actin and synapsin-I (Kennedy and Ehlers, 2011). When there is enough neuronal excitation, an action potential will be generated along neuronal axons and the depolarisation of the presynaptic terminal will trigger calcium entry into the presynaptic terminal. Calcium influx is a crucial step in the exocytotic process. The increase in calcium ion concentration primarily arises from Ca^{2+} influx via voltage-gated Ca^{2+} channels (Zucker and Regehr, 2002). Ca^{2+} influx may then trigger further Ca^{2+} release from intracellular stores including the mitochondria and the endoplasmic reticulum and for these ryanodine receptors (RyRs) or inositol trisphosphate receptor (InsP3Rs) play an important role. Whereas rapid and substantial increases in presynaptic calcium trigger transmitter release, smaller changes in the residual calcium concentration within the terminal have a major role in modulating transmitter release. Residual

presynaptic calcium is well known to modulate forms of short-term transmitter release including paired-pulse facilitation at many different synapses within the central nervous system (see Zucker and Regehr, 2002 for a review on presynaptic plasticity).

In the central nervous system, there are three known modes of neurotransmitter release; synchronous release, asynchronous release, and evoked release. If the presynaptic bouton is invaded by an action potential, transmitter release will occur synchronously within several milliseconds or occur asynchronously and lasts for tens of milliseconds to tens of seconds. Spontaneous release occurs in the absence of presynaptic depolarization (Kaeser and Regehr, 2014). Synchronous release is well defined and involves a synaptic vesicle's readily releasable pool, voltage-gated Ca^{2+} channels, a fast Ca^{2+} triggering mechanism and a tight coupling between the primed vesicle, the Ca^{2+} sensor, and the Ca^{2+} channel. The major Ca^{2+} sensors for synchronous release are synaptotagmins 1, 2, and 9, but Ca^{2+} sensors for asynchronous release have not been completely identified (Kaeser and Regehr, 2014). All of these three modes of transmitter release appear to involve the canonical SNARE proteins synaptobrevin 2/VAMP2, syntaxin-1 and SNAP-25. Further multiple alternative molecular mechanisms may be involved in asynchronous and spontaneous release. Synchronous, asynchronous release and a significant portion of spontaneous release depend on Ca^{2+} (Chung and Raingo, 2013, Kaeser and Regehr, 2014).

Under resting conditions, Ca^{2+} sparks, a tonic levels of Ca^{2+} in the presynaptic pulsatile or milieu release of Ca^{2+} from internal stores, can potently regulate neurotransmitter release (Llano et al., 2000). Even in the absence of presynaptic action potentials, nerve terminals manifest brief bursts of high fusion activity, clearly deviating from the low frequency, random nature of spontaneous release (Abenavoli et al., 2002). The fluctuations in intracellular Ca^{2+} typically trigger these presynaptic bursts (Glitsch, 2008), although some studies suggest that resting neurotransmitter release also strictly relies on intracellular Ca^{2+} without these large Ca^{2+} fluctuations (Xu et al., 2009). In contrast to the steep Ca^{2+} dependence of evoked transmission, spontaneous neurotransmitter release displays close to linear Ca^{2+} dependence. This suggests that at low

Ca^{2+} concentrations, Ca^{2+} signalling may selectively impact spontaneous release but not evoked release (Ramirez and Kavalali, 2011).

It is worth mentioning that the transmitter release could also occur through a Ca^{2+}-independent, carrier mediated process. The best example of this type is the case for synaptic transmission between photoreceptors and second order neurons of the vertebrate retina. The proposed mechanism for this type of transmitter release is that by lowering extracellular Ca^{2+}, Ca^{2+} influx through voltage-activated Ca^{2+} channels can be promoted via a modification of surface potential of plasma membranes (Piccolino *et al.*, 1999). In general, calcium is involved in the conversion of the action potential (electrical signal) into neurotransmitter release (chemical signal) and so calcium can be considered as a controller of electrochemical transduction. Factors that affect both peak and residual presynaptic calcium concentration within the terminal have a huge potential to influence synaptic signalling and plasticity.

1.6 Ca^{2+} and its role in neurodegenerative diseases

Cytosolic calcium levels are major sources of influence for synaptic activity. Calcium levels can be modulated through extracellular calcium influx via VGCCs or calcium permeable ionotropic receptors such as the NMDAR. Calcium can also come from intracellular sources including mitochondria or the endoplasmic reticulum and for this RyRs or InsP3Rs play an important role. De-regulation or failure of calcium homeostasis is central to the calcium hypothesis of ageing as well as in neurodegenerative diseases such as Alzheimer's disease. Factors that affect calcium homeostasis, including changes in the expression levels of calcium binding proteins, alteration of mitochondrial function and NMDAR or AMPAR activities are all disrupted in the neurodegenerative conditions. In AD, α-Synuclein and Aβ-peptides as building blocks for senile plaques, can form channels which can be permeable to calcium ions at the plasma membrane (Marambaud *et al.*, 2009).

In AD, the activities of glutamate receptor agonists are increased and there is evidence of reduced protein levels of NMDAR subunits NR1, NR2A and NR2B. NMDAR subunit phosphorylation is also reduced in AD. Therefore, these abnormalities may be involved in cognitive impairments (Sze *et al.*, 2001, Mota

et al., 2014). It also has been observed that calcium is overloaded in dendritic spines in neurones adjacent to amyloid plaques (Kuchibhotla *et al.*, 2008). Moreover, the frequency of spontaneous calcium transients is increased in neurones adjacent to amyloid plaques as well (Busche *et al.*, 2008). Properly controlled Ca^{2+} flux through the plasma membrane is crucial for the normal function of neurones. Hence drugs that influence Ca^{2+} regulation represent a potentially viable treatment neurodegenerative disease. For example, nimodipine (L-type Ca^{2+} channel blocker), memantine (NMDA open channel blocker) both showed significant beneficial effects in AD patients (Mattson, 2007). The majority of published studies about the calcium effect on aging have primarily focused on post-synaptic processes since measuring presynaptic calcium is extremely difficult. A better understanding of early presynaptic compensatory mechanisms could be a crucial step in the discovery of novel AD therapies of aimed to improve cognitive function before starting of neuronal loss.

1.7 Calcium measurement during synaptic signalling

Calcium ions play a crucial rule in a large number of different physiological processes and over the past few decades various methods have been devised for calcium detection. Electrophysiological methods and bioluminescent probes are two examples of older methods employed for calcium ion detection. Today, the most widely used calcium detection methods are based on fluorescent bioproteins. In the following sections, there will be a brief introduction to non-optical and optical techniques used for neuronal calcium detection.

1.7.1 Electrophysiology as a non-optical technique for monitoring Ca^{2+} in synaptic signalling.

Electrophysiological techniques are non-optical methods that have been used to assess calcium signalling in neurones. Intracellular calcium changes can be estimated by recording the current changes through the plasma membrane that are generated by calcium-dependent ion channels and transporters. Associated conductance changes are considered to be very sensitive indicators of local calcium flux however the correlation between these calcium currents and signals from fluorescent calcium indicators are often very poor (Takahashi *et al.*, 1999,

Bennett and Guthrie, 2003). For example, calcium current activation is generally transient, reaching a peak while there is a continued increase in fluorescent signal from optical calcium sensors (Takahashi *et al*., 1999). Calculation of the intracellular ion concentration using this method is still impossible because this depends highly on the effects of intracellular buffering. Moreover, it is necessary to collect information from more than one cell, therefore, researchers have developed an automated patch clamp methods for that reason (Benitah *et al.*, 2002). Patch clamping up to 16 cells simultaneously on a planar array to record ion channel function has been developed as well (Bennett and Guthrie, 2003). Calcium-selective electrodes represent another non-optical technique that can be used to measure calcium ion concentrations potentiometrically. This method is used to calibrate calcium solutions and can be used to calibrate fluorescent indicators signals *in vivo*. However, there is a large gap between the response time to changes in free calcium of these electrodes (0.5-1s) and the response time to changes in free calcium of a fluorescent indicator (ms scale) (Gründig and Krabisch, 1989, Ammann, 2013). However, electrophysiology can be used as an experimental tool to determine the locus of action of experimentally tested drugs, where, paired-pulse ratio can be used as indicator of presynaptic changes.

1.7.1.1 Paired-pulse ratio as an indicator of presynaptic changes.

Synaptic transmission efficiency is not a fixed parameter but it can be regulated positively and negatively according to ongoing presynaptic activity (Regehr, 2012). The paired-pulse ratio (i.e. the ratio of the amplitude of the first response to the second; PPR) can be used as an experimental tool to determine the locus of action of externally applied drug or an intrinsic neuromodulator. If the drug was interacting at the presynaptic site and changing the way the presynaptic neuron acts when it receives an action potential, then there will be a change in the way the presynaptic terminal responds to a paired pulse stimulus and therefore, there will be a change in PPR accordingly. This change in PPR after a drug treatment, indicates that the drug may be acting at the presynaptic terminal. Paired-pulse facilitation, as an example of STP, is due to calcium accumulation in the presynaptic terminals. If there is some residual calcium from the first pulse at the

time of the second pulse, this will lead to greater peak calcium concentration that can cause more vesicles to be released at the time of the second pulse than by a single pulse (Zucker, 1987, Tank *et al.*, 1995, Regehr, 2012). It should be noted that the residual calcium concentration is several orders of magnitude smaller than that required to trigger release which indicates that proteins involved in release modulation are likely to be different from those responsible for triggering release. Paired pulse depression (PPD) is also due to the presynaptic mechanism where changes in the quantum content affect this phenomenon (Jensen *et al.*, 1999), This is consistent with the residual calcium hypothesis (Zucker, 1987) where Debanne *et al*., (1996) concluded that PPD results from a decrease in quantal content, perhaps due to that readily releasable vesicles undergo short-term depletion (Debanne *et al.*, 1996). On the other hand changes in the post-synaptic neuronal membrane potential (size of the quantum) do not affect PPR (Wilcox and Dichter, 1994, Ivanova *et al.*, 2002). While these electrophysiological methods are advancing in terms of their ability to measure calcium ion concentration, the fluorescent bioproteins and fluorescent probes are still more widely used.

1.7.2 Monitoring Ca^{2+} in synaptic signalling using Optical techniques.

Optical techniques for measuring calcium use calcium indicators that have the ability to change their fluorescence properties when they bind to Ca^{2+} ions. There are two main classes of calcium indicators: chemical (organic dye) indicators and genetically encoded calcium indicators (GECIs) (Stosiek *et al.*, 2003). In addition to these two methods, autofluorescence imaging can also be used to detect changes in calcium-dependent processes.

1.7.2.1 Synthetic fluorescent calcium indicators

Electrophysiological methods are associated with various difficulties outlined above and so the more widely used technology used to detect cytosolic Ca^{2+} levels utilizes chemical indicators whose fluorescent response changes in the presence of calcium ions (Tsien *et al.*, 1982). These dyes have the ability to

chelate Ca^{2+} and upon chelation, they change their fluorescent properties in a way that is directly proportional to the free [Ca^{2+}] in the sample. These chemical indicators are a group of dyes based on the structures of well-known calcium chelators such as EGTA or BAPTA which bind and chelate calcium ions with high selectivity. The cell permeable forms of these dyes are the acetoxymethyl ester forms that have the ability to perfuse into the cell freely after a long incubation period. Once the dyes enter inside the cell, these acetoxymethyl esters turn into the de-esterified form which are less permeable and are therefore maintained inside the cells for the duration of the experiment (Gee *et al.*, 2000). These indicators include indo-1, Calcium Green-1, fura-2, fluo-3 and fluo-4, etc. See table 1.1 for high affinity calcium indicators. Recently, Tada et al., (2014), demonstrated a new BAPTA-based fluorescent calcium indicator, Cal-520. This dye yields calcium transients with large amplitudes and high SNR in different neural subsets, which are reliably, sufficient to detect single APs in the intact brain (Tada *et al.*, 2014). In this study we used fluo-4 AM as a control for our genetically encoded sensor. Fluo-4 has Ca^{2+} affinity at K_D~345 nM, and its absorption maximum is shifted ~12 nm compared to fluo-3, making it more suitable for 488 excitation using an argon laser. Fluo-4 has many advantages such as, it is brighter at a lower dye concentration, less phototoxic, has very low background absorbance and it requires shorter incubation times (Gee et al., 2000, Paredes *et al.*, 2008).

Table 1.1. High affinity calcium indicators.

Adapted from Paredes *et al*. (2008).

Indicator	K_d for Ca^{2+}(nM)	Excitation (nm), emission (nm)	Notes	Reference
Calcium Green-1	190	490 ex, 531 em	Single wavelength	[39,40]
Fluo-3	325	506 ex, 526 em	Single wavelength	[41,42]
Fluo-4	345	494 ex, 516 em	Single wavelength	[43–45]
Fura-2	145	363/335 ex, 512 em	Dual excitation/single emission	[39,46,47]
Indo-1	230	488 ex, 405/485 em	Single excitation/dual emission	[47]
Oregon Green 488 Bapta-1	170	488 ex, 520 em	Single long wavelength	[48]
Fura-4F	0.77	336/366 ex, 511 em	Ratiometric excitation/single emission	[49]
Fura-5F	0.4	336/363 ex, 512 em	Ratiometric excitation/single emission	[50]
Calcium Crimson	185	590 ex, 615 em	Single long wavelength	[39]
X-Rhod-1	0.7	580 ex,602 em	Single excitation/emission	[51,52]

According to Paredes *et al* (2008), and others, a major disadvantage of chemical calcium indicators is that the cellular localization of Ca^{2+} indicators cannot be easily controlled or specifically targeted to a particular organelle. In addition, chemical indicators tend to compartmentalize and are eventually extruded from the cell during long experiments. Moreover, at times of compartmentalization into cellular organelles, they are rendered inaccessible in the cytoplasm (Del Nido *et al.*, 1998, Gee et al., 2000, Paredes et al., 2008, Russell, 2011). Therefore, it was necessary to create advanced technology that can precisely and accurately detect small changes in [Ca^{2+}] *in situ*. The most recent advances in calcium detection technology are photoproteins that can generate signals in the presence of Ca^{2+}.

1.7.2.2 Autofluorescence

Intrinsic signals can also be used to measure calcium indirectly as an index of neuronal activity. There are autofluorescent molecules, such as flavoproteins, within excitable tissue that have the ability to change their fluorescence

properties when they bind to Ca^{2+} ions (Fein and Tsacopoulos, 1988). Neuronal excitation does not produce clear optical signals by itself. However, activity-dependent aerobic energy metabolism facilitation has fast dynamics (Fein and Tsacopoulos, 1988, Vanzetta and Grinvald, 1999) and produces changes in intrinsic, optical signals. It is known that endogenous fluorescence changes are due to intracellular energy metabolism because endogenous substances that have fluorescence such as NADH and flavoproteins are involved in oxygen metabolism. For example, high levels of flavin adenine nucleotide (FAD) in the brain cause a green fluorescence emission with a peak at approximately 520 nm in the presence of blue light (Kunz and Gellerich, 1993, Frostig, 2009). Enhancement of the metabolism of mitochondrial energy converts the reduced form to the oxidized form of flavoproteins and this is associated with an increase in green fluorescence (Chance *et al.*, 1979). The increase in green fluorescence of intrinsic proteins can be used to monitor neural activity, since the relationship between aerobic energy metabolism and neural activity is correlated with changes in intracellular calcium, which plays a crucial role in neural functions described previously, including synaptic transmission and the induction of neural plasticity (Frostig, 2009). Kwan *et al.* (2009) suggested that there are distinct intrinsic emissions obtained from tissues of AD transgenic models. It is possible that these endogenous intrinsic emission signals could help to contrast and distinguish between normal and neurodegenerative tissues. Therefore, intrinsic signals may provide useful and important information about the onset and progression of disease mechanisms.

1.7.2.3 The fluorescent proteins

The other optical technique that is now widely used for measuring calcium uses genetically encoded calcium indicators (GECIs). Since the discovery of the green fluorescent protein (GFP), there has been a widespread use of it in cell biological research (Tsien, 1998). GFP traditionally refers to the protein (26.9 kDa) first isolated from the jellyfish *Aequorea victoria*. This protein produces green fluorescence when exposed to light in the blue-ultraviolet range (Prendergast and Mann, 1978, Tsien, 1998). Fluorescent protein-based Ca^{2+} indicators are Ca^{2+}-sensitive fluorescent or luminescent proteins that can

be expressed in specific subsets of target cells in the tissue, by the use of specific promoters (Miyawaki *et al.*, 1997, Hasan *et al.*, 2004, Heim, 2005). Using molecular biology and transgenic techniques, these proteins were then, non-invasively, genetically targeted and expressed in specific cells and cellular compartments. These fluorescent proteins were then mutated to produce a widely differing spectral emission properties (Heim *et al.*, 1994, Tian and Looger, 2008, Tian *et al.*, 2012). Fluorescent protein chimeric constructs and Ca^{2+}-binding proteins such as calmodulin and troponin-C were engineered yielding cell targetable Ca^{2+} indicators. Some of these new generation fluorescent protein Ca^{2+} indicators were designed with two different GFP mutants; e.g. cyan fluorescent protein (CFP) and yellow fluorescent protein (YFP) based on changes in Fluorescence Resonance Energy Transfer (FRET) efficiency upon Ca^{2+} binding (For review see: Russell, 2011). Since GFP was discovered, at least 17 different forms of fluorescent protein based calcium sensor have been developed, ranging from the Cameleons (Miyawaki et al., 1997), Camgaroo, Pericams (Baird *et al.*, 1999), and the GCaMP family (Nakai *et al.*, 2001, Dana *et al.*, 2014).

1.7.2.3.1 Thy1 as a neuron specific expression promoter.

There are many promoters can be used to target expression specifically to neurones, one of them is Thy1 promoter. The antigen Thy-1, also called CD90 (Cluster of Differentiation 90), was the first T cell marker to be discovered, by Reif and Allen in 1964 (Reif and Allen, 1964). Due to its prior identification in thymocytes, it is named Thy-1; THYmocyte differentiation antigen 1 (Ades *et al.*, 1980). In mice, there are two alleles: Thy1.1 and Thy1.2. The only difference between them is that the amino acid at position 108 in Thy-1.1 is an arginine, whereas in Thy-1.2 promoter is glutamine. Thy 1.2 is expressed by most mice strains (Ades et al., 1980), predominantly in neurons (Kemshead *et al.*, 1982), where, ELISA reports have shown that the highest concentrations of Thy1 protein in the striatum and hippocampus. The mouse thy1 promoter "Neuron specific" has been used to drive neuronal forced expression of proteins e.g. in transgenic animal models of Alzheimer's disease, mutated Amyloid precursor protein (APP) was preferentially directed to the neuronal cells (Moechars *et al.*, 1999). As the

Thy-1 gene expression has been extensively characterized in transgenic mice (Gordon *et al.*, 1987) and the expression of heterologous genes in the CNS have been driven by Thy-1 gene (Aigner *et al.*, 1995, Campsall *et al.*, 2002). Therefore, in this study, The Thy-1.2 expression cassette was used to drive strong constitutive expression of SyGCaMP2-mCherry sensor, specifically in the neurons of the SyG transgenic mice.

1.7.2.3.2 GCaMP family sensors

The genetically encoded calcium indicator (GCaMP) is the first variant of a protein family that was initially developed by Junichi Nakai (Nakai *et al.,* 2001) and based on a fusion of GFP, calmodulin (CaM), and M13 (a domain of myosin light chain kinase). Upon calcium binding, conformational changes through this complex interaction induce a subsequent structural shift in the fluorophore of an attached FP leading to an increase in fluorescence (Nakai *et al.,* 2001). In the absence of calcium, due to chromophore protonation by water, these fluorescent proteins will be in a reduced fluorescent state. Binding of Ca^{2+} to the calmodulin results in solvent pathway removal and therefore, rapid chromophore de-protonation, and bright fluorescence (Wang *et al.*, 2008, Akerboom *et al.*, 2009). The GCaMP family of calcium indicators have, through several rounds of genetic engineering, become particularly popular (see figure 1.5). One of the first useful variants was GCaMP2 which was engineered from its predecessor to be stable at mammalian body temperatures (Tallini *et al.*, 2006). It is created by subsequent mutation of GCaMP1.6 at A206K and the plasmid leader sequence RSET was added to the N-terminal segment of the M13 peptide (Tallini *et al.,* 2006). GCaMP2 was later targeted to specific sub-cellular compartments to detect even small Ca^{2+} signals in specific cellular compartments such as vesicular membrane proteins - synaptophysin; SyGCaMP2 (Dreosti *et al.*, 2009a) and isoforms of adenylate cyclase; GCaMP2-AC8 (Willoughby *et al.*, 2010). Tethering GCaMP2 to synaptic vesicles by fusion to 4 transmembrane domain vesicular protein synaptophysin, led to the development of SyGCaMP2 that has two advantages over existing cytoplasmic GECIs in detecting the electrical activity of neurones: the presynaptic location which is very close to the location of voltage gated Ca^{2+} channels and the linear response to change in intracellular

calcium concentration over a wide range of spike frequencies. This linearity arises because SyGCaMP2 detects the brief calcium transient passing through the presynaptic compartment rather than changes in bulk calcium concentration (Dreosti et al., 2009a). Moreover, SyGCaMP2 provides a good SNR and it has the ability to even detect a single action potential, which its parent (GCaMP2) cannot (Dreosti et al., 2009a).

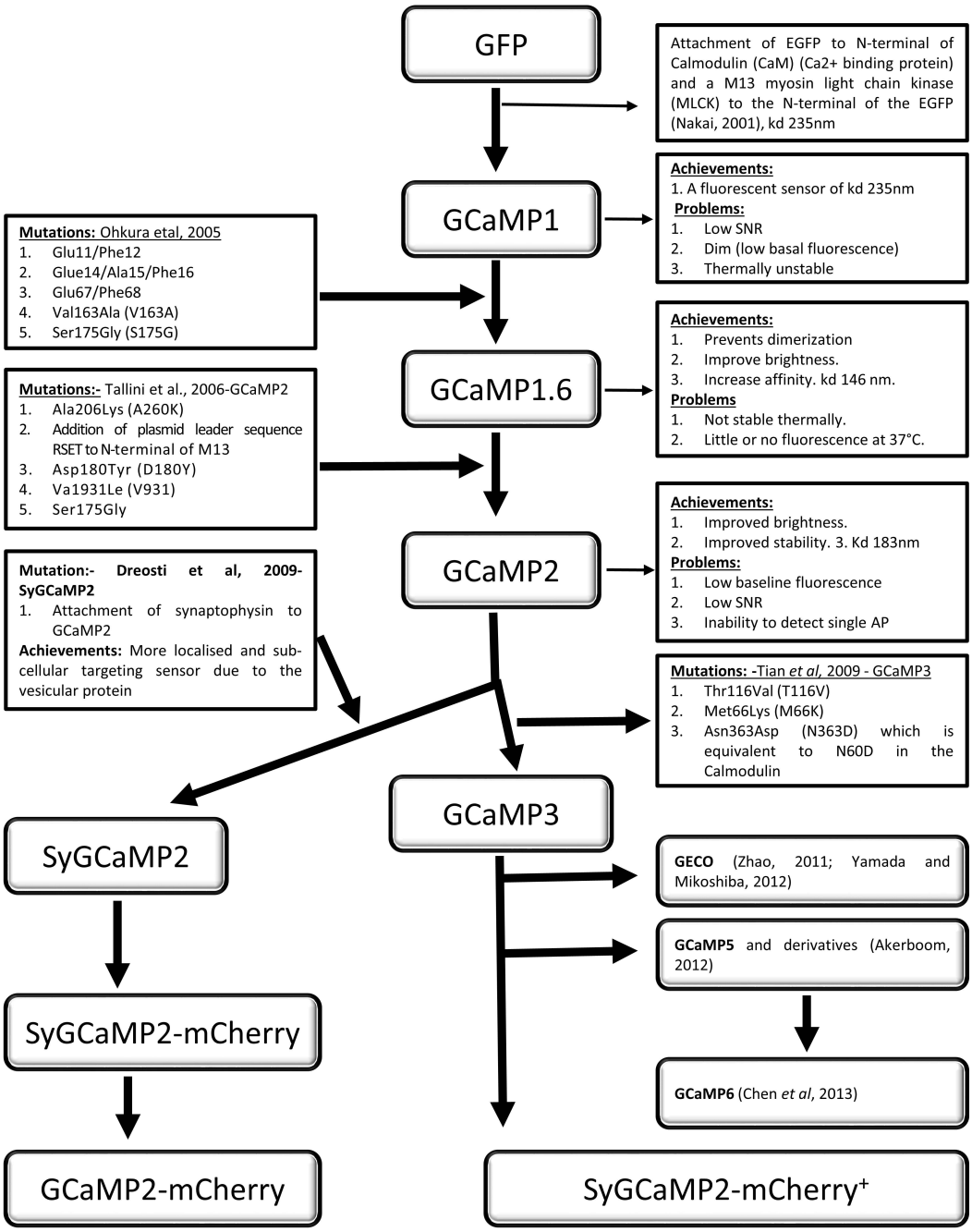

Figure 1.5. Schematic diagram of the development of the GCaMP family fluorescent protein calcium sensors.

Adapted from Okorocha (2016).

1.7.2.3.3 SyGCaMP2-mCherry as a new fluorescent protein calcium sensor

Ratiometric imaging offers the opportunity to measure the absolute concentration of intracellular ions reliably in the face of numerous confounding factors including differences in cell diameter and optical properties of the imaging setup (Thestrup *et al.*, 2014, Cho *et al.*, 2017). Over the last few years, Professor Hartell's lab has developed a series of fluorescent protein-based sensors that are designed to allow the direct, real-time visualisation and quantification of presynaptic calcium signalling, transmitter release and vesicle reuptake. In this study we used a strain of transgenic mice called SyG37. These mice express a sensor called SyGCaMP2-mCherry under control of a Thy1-2 promotor. SyGCaMP2 is a fusion of GCaMP2 to the vesicular protein synaptophysin (Dreosti *et al.*, 2009b). This calcium sensor is located on the intracellularly facing terminus of synaptophysin. SyGCaMP2 was modified by attaching the red fluorescent protein mCherry and the Thy1-2 promotor used to target expression to neurones (figure 1.6). The addition of mCherry served two purposes. The first was to facilitate the identification of presynaptic terminals because GCaMP2 on its own displays very weak fluorescence at low calcium concentrations (Dreosti et al., 2009a). The second was to allow a ratiometric calibration of the sensor such that the calcium dependent change in GCaMP2 can be expressed as a proportion of the amount of sensor expressed. This can be estimated from the fluorescence level of mCherry using the fluorescent intensity ratio (F.I.R) equation as the following:

$$F.I.R = \frac{F(SyGCaMP2) - F(Background\ SyGCaMP2)}{F(mCherry) - F(Background\ mCherry)}$$

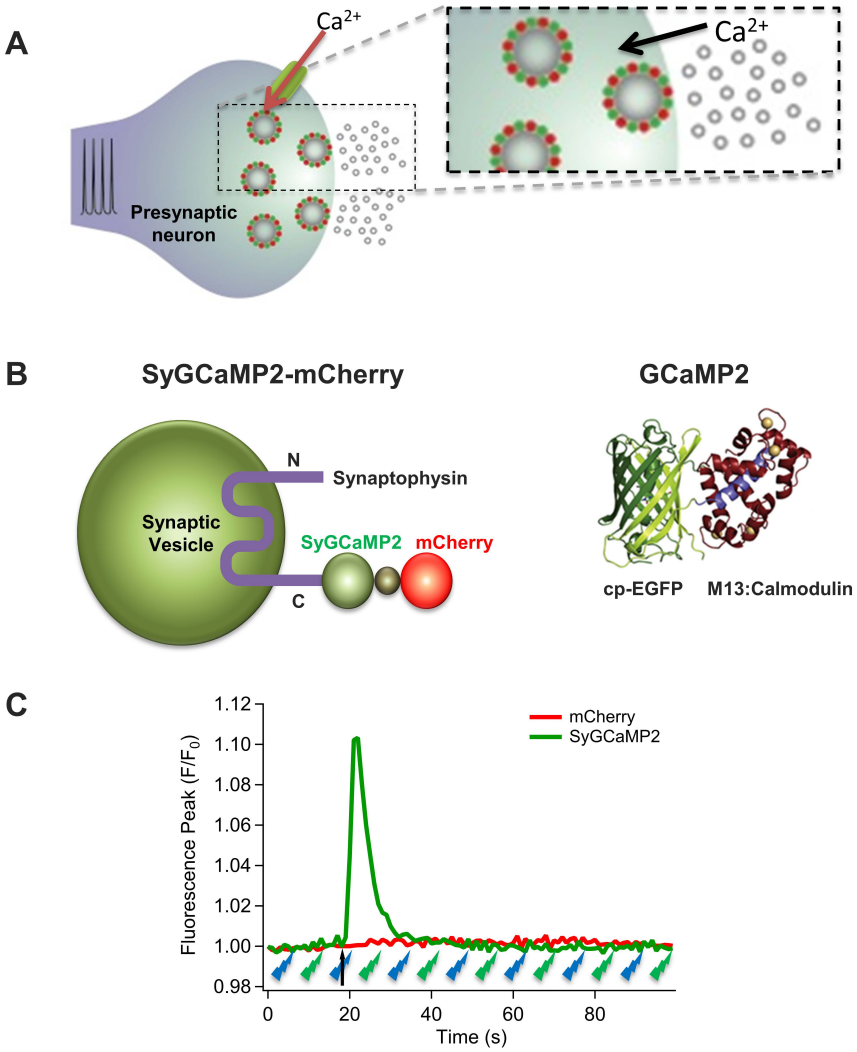

Figure 1.6. Schematic diagram of the SyGCaMP2-mCherry sensor.

A. shows the presynaptic location of the sensor. B. left panel shows the schematic diagram of the SyGCaMP2-mCherry sensor components; the synaptic vesicle, vesicular transmembrane protein, synaptophysin, the GCaMP2 and mCherry. Right panel shows the crystal structure of GCaMP2 where the cpEGFP on the left and the Calmodulin + M13 molecules on the right. C. Shows the mean responses to 20 AP, 20 Hz at 20 V collected from 9 ROIs placed within the *stratum radiatum* of the CA1 hippocampal region were plotted against time. A monochromator (Till Photonics, Germany) was synchronised with image capture such that it alternated rapidly between 470 ± 10 nm and 560 ± 10 nm excitation wavelengths to record an interleaved image stack of emitted fluorescence measured at wavelengths of 520 ± 20 nm and 620 ± 25 nm as “green” and “red” images, respectively; for this, a dual band emission filter (Chroma Technology) was used. Right panel in B is a*dapted from* (Wang *et al.,* 2008).

Optical techniques for measuring calcium have numerous advantages over electrophysiological recordings. First, there is minimal tissue damage because there is no physical contact of the tissue with an electrode. Second, confocal and two-photon laser scanning microscopy can be used to explore fine neuronal structures deep in living tissue. Third, multiple active sites in neurones can be monitored at the same time (Siegel and Lohmann, 2013). Moreover, In electrophysiological recordings, differentiation between pre- and postsynaptic responses requires an application of further statistical analysis that require more time and effort (Sims and Hartell, 2005). Despite certain limitations of GECIs, such as reduced dynamic range and limited range of affinities, they have certain distinct advantages as their ability to be targeted to particular sub-cellular compartments by fusing the sensor to a protein of interest.

1.8 Aims and Objectives

The over-arching aim of developing the transgenic strains of mice described in this thesis was to examine how presynaptic calcium contributes to normal synaptic transmission in different circuits within the hippocampus. It was therefore necessary to first confirm that the expression of SyGCaMP2-mCherry was indeed presynaptic as we had predicted. Immunohistochemical (IHC) methods were also used to examine the tissue distribution of antigens of interest. Therefore, we performed double labelling for mCherry in combination with a variety of synapse-specific markers to establish first whether the sensor was expressed selectively in presynaptic terminals – as predicted – and, second, which type of synapse the SyGCaMP2-mCherry was expressed in. This study also required an evaluation of the suitability of the mouse model for measuring presynaptic calcium activity. Therefore, we decided to use a range of different methods of measuring neuronal activity and presynaptic calcium signalling for comparison. This included the SyGCaMP2-mCherry sensor (within our SyG37 mouse model), the organic calcium indicator fluo-4, in combination with electrophysiological recordings and pharmacological manipulation. Therefore, the first aim was to examine the effects of pharmacological manipulations that are known to affect synaptic transmission through presynaptic effects and to establish whether these manipulations led to an associated change in SyGCaMP2 fluorescence. We chose to examine the effects of the receptor blockers AP5, DNQX and picrotoxin that were used to block NMDA, AMPA and GABA receptors, respectively. The purpose of blocking these receptors was to distinguish between calcium signals originating from the first synaptic terminals in the pathway, namely the SCs pathway in the CA1 region of the hippocampus and mossy fibre terminals in recordings made from the CA3 region. This was necessary because although SyGCaMP2-mCherry is expressed selectively in presynaptic terminals, we are unable to distinguish between the sources of calcium signals in polysynaptic pathways which contain presynaptic terminals but in cells that are postsynaptic to the first synaptic relay.

Having established what proportion of the total signal originated from the first set of synaptic terminals, we then examined the effects of adenosine, an agonist at adenosine receptors, as this has been shown to reduce synaptic transmission at

both CA1 and CA3 synapses through presynaptic processes (Wu and Saggau, 1994). Next, we examined the effects of the adenosine receptor subtype 1 antagonist DCPCX in the presence of adenosine in both the presence and absence of the postsynaptic blockers (picrotoxin, AP5 and DNQX). Having characterised how these pharmacological manipulations altered SyGCaMP2 fluorescence in response to activity at CA1 and CA3 hippocampal regions, we next examined what mechanisms are responsible for shaping calcium signals. Therefore, the second aim was to examine whether forskolin, a promotor of adenylyl cyclase activity combined with rolipram, a type IV phosphodiesterase inhibitor (Otmakhov *et al.*, 2004) altered presynaptic calcium within the hippocampus. Forskolin has been shown to induce potentiation within the hippocampus at both CA1 and CA3 although in very different ways. Forskolin is known to enhance spontaneous transmitter release in many brain regions as well as facilitating potentiation within the CA1 region and we wished to find out first whether forskolin induced changes in synaptic strength within CA1 and second, whether these were associated with changes in presynaptic calcium signalling. Shaw and Hartell (unpublished results) have previously found that forskolin enhances baseline calcium levels within presynaptic terminals in hippocampal cultures.

Chapter 2: Materials and methods

2.1 Experimental animals used in this study

Wild type mice (C57 Blk6) and two transgenic mouse lines (SyG14 and SyG37) were used in this study. SyG37 strain of these transgenic mice expresses a sensor called SyGCaMP2-mCherry under control of a Thy1-2 promotor. SyGCaMP2 (a gift from Lagnado) is a fusion of GCaMP2 to the vesicular protein synaptophysin (Dreosti et al., 2009b). This calcium sensor is located on the intracellularly facing terminus of synaptophysin. SyGCaMP2 was modified by attaching the red fluorescent protein, mCherry. The Thy1.2 promoter was used to target expression of this sensor specifically to neurones. SyGCaMP2-mCherry sensor was made, by Dr Mariusz Mucha as described below. Using the site directed mutagenesis with primers F5'CAAATGATGACAGCGAAGGCAGCGGCCGCGACTCTAG and R5'CTAGAGTCGCGGCCGCTGCCTTCGCTGTCATCATTTG, the STOP codon (TAA) located at the 3' end of the SyGCaMP2 coding sequence was substituted with alanine coding GCA. To clone 0.7kb mCherry, coding sequence and primers; F5'GCGGCCGCTATGGTGAGCAAGGGCGAGGA, R5'GCGGCCGCTTACTTGTACAGCTCGTCCATGC was used at the NotI restriction site located directly downstream of the mutated STOP codon. Single nucleotide (T) was inserted between the NotI site and the START codon at the 5' end of the forward primer, to avoid a "frame-shift" of the mCherry coding sequence caused due to cloning into the NotI site (for more details see; Okorocha, 2016). The integrity and orientation of these clones were verified by restriction analysis and DNA sequencing, and the SyG mice were then bred in the animal house of the University of Leicester. See appendix 1, for SyGCaMP2-mCherry cloning vehicle.

2.2 Genotyping using polymerase chain reaction (PCR)

Ear snips from the SyG14 and SyG37 mouse colonies were collected as necessary and the genotypes of samples verified by PCR. Genomic DNA extraction involved incubating ear snips in 70 µl 0.05 M NaOH and then heating with a heating block to 95°C for 20 minutes followed by subsequent neutralisation

with 7 µl of 1 M Tris-HCL at pH 7.5. Extracted DNA was then analysed by PCR using 2x ReddyMix (ThermoFisher Scientific; USA) and the following primers: SyGCaMP2 forward primer (5'-CGACAACCACTACCTGAGCA) and SyGCaMP2 reverse primer (5'GAACTTCAGGGTCAGCTTGC). The Cmah (cytidine monophospo-N-acetyl-neurmanic acid hydroxylase) forward primer (5'CAGCTTGCTTATCACGTGTG) and Cmah reverse primer (5'TGGTGCTCACGTCTAACTTC) were used as controls to ensure that DNA had been recovered from the samples. PCR tubes were placed in the PCR machine (Techne-TC.512; Bibby Scientific, UK) that was set to a SyGCaMP2 protocol, which consisted of 5 minutes at 94°C to heat and activate the polymerase followed by 30 seconds (denature DNA) on 35 cycles of 94°C, 30 seconds (anneal primers to DNA) at 60°C, 30 seconds (elongation) at 72°C and, finally, one round of 5 minutes (final elongation) at 72°C. PCR products were stained by SYBR® safe DNA gel stain (Invitrogen; U.K.) and separated by 3% agarose gel electrophoresis and then visualised under a blue light source.

2.3 mCherry detection using western blotting

Wild type, SyG14 and SyG37 mice (3–8 weeks old) were used for these experiments. All experiments were conducted according to the Scientific Procedures Act, 1986. Animals were placed in a small box and provided with 100% oxygen and anesthetised with isoflurane until they were no longer breathing. Once this was verified, they were quickly decapitated; the brains were immediately removed and tissue samples were homogenised in lysis buffer (10% Triton X-100, 5 M NaCl, 0.1% SDS, 1 M tris, 0.5%, phosphatase inhibitor cocktail-3 (Sigma-Aldrich; U.K) and cOmplete™ Roche protease inhibitors, pH 8 (Roche Diagnostics; Switzerland). Samples were mixed with equal volumes of 2x standard loading buffer (50% glycerol, 10% SDS, 1% bromophenol blue and 5% 2-mercaptoethanol) and denatured at 100°C for 5 min. 35 µl of sample protein per lane were separated by sodium dodecyl sulphate-polyacrylamide gel electrophoresis (SDS-PAGE; 12% gel, 180 V for 90 min) and then transferred (15-30 V overnight at room temperature) onto an Immobilon-P PVDF transfer membrane. A three-colour protein ladder (10 µl per lane; Prism Ultra Protein Ladder - 10-180 kDa) was used adjacent to the sample lanes to check protein

transfer onto the PVDF membrane, and later to determine the molecular weights of detected bands. Membranes were blocked for 30 minutes at room temperature using 5% dry skimmed milk in PBS-T with 0.1% Tween-20 (PBS-T; pH 7.6). Membranes were then incubated for 1 hour at room temperature with primary antibody diluted in PBS-T containing 5% dry skimmed milk. The primary antibodies used were goat anti-mCherry (AB0040-200; 1:2,000; Sicgen, Portugal) and guinea pig anti-vGlut-1 (135 304; 1:5000; Synaptic Systems, Germany). After 1 hour, membranes were washed 3x for 10 min in PBS-T and incubated with horse radish peroxidase-coupled secondary antibodies; donkey anti-goat (sc-2020; 1:5000; Santa Cruz Biotechnology, U.S.A.) and rabbit anti-guinea pig (61-4620; 1:4000; ThermoFisher Scientific, U.S.A.) in PBS-Tween with 5% dry skimmed milk for 1 hour at room temperature, followed by washing 3 x for 10 min. The visualisation was performed by Western Blotting Luminol Reagent detection and detected with Amersham hyperfilms and hyper-processor (GE Healthcare Ltd, U.K). The X-ray film images were scanned, saved in PDF format and then FIJI software (ImageJ-1.49O, National Institute of Health, USA) was used to measure the relative signal intensities of the bands on the Western blots.

2.4 SyGCaMP2-mCherry expression in SyG37 mouse's brain slice.

For SyGCaMP2-mCherry expression analysis, SyG37 and WT adult mice (3–8 weeks old) were deeply anesthetised with isoflurane as previously described. The brains were immediately removed and 400 µm-thick coronal slices were prepared on a Microslicer™ DTK-1000 (Dosaka-EM; Japan) and stored in artificial cerebrospinal fluid gassed with 95% oxygen:5% carbon dioxide and stored at room temperature for at least 1 hour to recover from the cutting process. The aCSF composition was, in mM: 120 NaCl; 2.7 KCl; 2.5 $CaCl_2.2H_2O$; 25 $NaHCO_3$; 1.2 NaH_2PO_4; 1.2 $MgSO_4$.7H2O and 11 D-glucose. A slice was then transferred to a recording chamber perfused with carbogenated aCSF containing a saturated solution of calcium (5 mM) at a rate of > 1 ml/min at room temperature. Once imaging was started the perfusion was stopped to prevent the slice from moving. These slices were then imaged using a custom epifluorescent

microscope built around a Scientifica Slicescope with Nikon FNI epifluorescence attachment and equipped with an optiMOS Scientific CMOS Camera (QImaging; Surrey, Canada) and controlled by Igor Pro software. A CoolED pE-4000 (CoolLED Ltd; U.K.), a universal illumination system for fluorescence microscopy, was used to control individual wavelengths. The excitation wavelengths were 470 ± 10 nm and 550 ± 10 nm to record images of emitted fluorescence measured at wavelengths of 520 ± 20 nm and 620 ± 25 nm as green and red images respectively; for this, the single band filter sets ET-EGFP (FITC/Cy2) and ET-mCherry, Texas Red® (Chroma Technology; U.S.A.) were used. To identify the different regions of the brain in the slice, a Nikon Plan (4X/0.20 NA) water immersion lens was used and images collected for the whole brain slice. To allow the software to recognise images during tiling and stitching, the individual images were taken in a systematic manner to form a panoramic image, with evenly spaced overlaps between each image. The panoramic images were then analysed using FIJI (ImageJ-1.49O) software. The same brightness adjustments were performed using the adjust brightness/contrast, unsharp mask features and the illumination profile of the individual images was flattened to allow direct comparison between SyG37 and WT mice (Ferreira and Rasband, 2012, Bankhead, 2014).

2.5 Immunohistochemistry

For immunohistochemistry experiments, mice were deeply anesthetised with intraperitoneal sodium pentobarbital and transcardially perfused with normal saline containing protease inhibitors, followed by 4% paraformaldehyde in phosphate buffer. After perfusion, the brains were removed and post-fixed overnight at 4^{O}C and then rinsed three times in tris-HCl and incubated for 12h in 20% sucrose in tris-HCl of pH 7.2. The brains were removed and cut into two hemispheres. Each hemisphere was embedded in Surgipath FSC 22 clear freezing medium (Leica Biosystems; UK) in the desired orientation and fast frozen in liquid nitrogen. Transverse hippocampal slices of 10-20 µm thickness were obtained from SyG37 and wild-type mice using a Bright cryostat-OTF-5040 (Bright Instruments, UK). For autofluorescence quenching, slices were incubated in 0.1 M glycine in PBS for 1 hour and washed with 0.1 M NH_4Cl in PBS for one

minute. Slices were then incubated for 1 hour at room temperature in TBS with 0.1% Triton X-100 (TBS-T) and 10% normal goat serum (NGS) or donkey serum. Slices were then incubated in primary antibodies in tris-buffered saline with Triton X-100 (TBS-T) and 10% NGS overnight at 4^{o}C. Slices were rinsed in TBS, incubated with secondary antibodies, then rinsed in TBS and mounted on super-frost glass slides (VWR International, U.K.). Sections in which primary antibodies were omitted were considered as controls. The primary antibodies used were anti-vGLUT1 guinea pig polyclonal (135 304; 1:1000; Synaptic Systems, Germany), anti-mCherry goat polyclonal (AB0040-200; 1:1000; Sicgen, Portugal), anti-bassoon rabbit polyclonal (141002; 1:1000; Synaptic Systems, Germany), anti-PSD95 rabbit polyclonal (ab18258; 1:1000; Abcam, U.K.), and anti-vGAT mouse monoclonal (131011BT; 1:1000; Synaptic Systems, Germany). The secondary antibodies used were goat anti-guinea pig Alexa Fluor 488 (1235789; 1:2000; Life Technologies, USA), donkey anti-goat Alexa Fluor-594 (1180089; 1:2000; Life Technologies, USA), donkey anti-rabbit Alexa Fluor-488 (1387792; 1:2000; Thermo Fisher Scientific, USA), and goat anti-mouse Alexa Fluor-546 (1787787; 1:2000; Thermo Fisher Scientific, USA). The sections were examined with a Zeiss LSM 7 MP multiphoton microscope (Carl Zeiss Microscopy GmbH, Jena, Germany) equipped with green and red fluorescence filter sets, magnified with a (x20, 0.8 NA) water immersion lens using ZEN 2009 software. Series of images from hippocampal slices were taken in the axial plane (*z*-stacks) at a pixel resolution of 1024x1024 and a stack of at least five images was ultimately created. For Hoechst stain experiments, the slices were imaged using a custom-built epifluorescent microscope equipped with an optiMOS Scientific CMOS Camera (QImaging; Canada) and controlled using Igor Pro software. A Nikon Intenslight C-HGFI (Nikon Limited, U.K), was used as a light source. The excitation wavelengths were 470 ± 10 nm and 550 ± 10 nm to record images of emitted fluorescence measured at wavelengths of 520 ± 20 nm and 620 ± 25 nm as green and red images, respectively; for this, the single band filter sets ET-EGFP (FITC/Cy2) and ET-mCherry, Texas Red® (Chroma Technology; U.S.A.) were used. To image the whole hippocampus and to identify the different regions of the hippocampus in the slice, a Nikon Plan Apo (x4/0.2 NA) and a Nikon NIR Apo (x60/1.0 NA) lens were used. Sets of images collected by both

microscopes were then processed using FIJI. Brightness adjustments were performed using the adjust brightness/contrast and unsharp mask subtraction features and for protein co-localisation, dual-stained images were co-localised using the colour merge channels feature (MBF-ImageJ/plugins; written by Tony Collins) in the FIJI software (ImageJ-1.49O) (Collins, 2007, Brettle and Carmichael, 2011, Dunn *et al.*, 2011).

2.6 Slice preparation and maintenance for imaging and electrophysiology experiments.

Mice were anesthetised with isoflurane according to the Schedule 1 protocol described above. The brains of mice (3–8 weeks old) were immediately removed so that 400 µm thick transverse slices could be prepared and stored in artificial cerebrospinal fluid bubbled with carbogen prior to use. A slice was then transferred to a recording chamber and perfused with carbogenated aCSF at a rate of > 1 ml/min at room temperature (25-28 C^{o} , as the laser is worming up the chamber). For fluo-4 calcium indicator experiments, a small amount of fluo-4 AM was dissolved in DMSO and 20% Pluronic F-127 to yield a dye concentration of 5 mM, after which a borosilicate glass patch pipette was filled with 0.5 µl dye solution and 4.5 µl aCSF. Under visual control, when the pipette reached the desired depth, the dye was applied to the *stratum radiatum* of area CA1 using gentle positive pressure. Following dye loading, the pipette was removed and the slice left for an hour to ensure complete de-esterification of the dye (Eichhoff *et al.*, 2010) and to obtain a stable maximal fluorescence level in stained cells (Stosiek *et al*., 2003). Fluorescence was then imaged from the *stratum radiatum* of the CA1 area, approximately 500 µm from the injection site (for more details see; Wu and Saggau, 1994).

2.7 Imaging data acquisition and analysis

Because of the diversity and complexity of this step, we have divided this paragraph into two sections; data acquisition and data analysis.

2.7.1 Imaging data acquisition.

An Olympus BX50WI upright microscope equipped with a QuantEM EMCCD camera (Photometrics, USA) was used in experiments to visualise signals from brain slices (see figure 2.1). To identify the different regions of the hippocampus in the slice, an Olympus (LUMPlanFI x20/0.5 NA) water immersion lens was used. Slices were placed under the microscope and held in place using a harp which consisted of a flattened silver ring with thin nylon strands glued to one side. Slices were stimulated using a glass capillary electrode with a carefully broken tip to increase the resistance to around 2–3 MΩ when filled with aCSF. The electrode was connected to an isolated stimulator (Digitimer, UK) which was used to control the stimulus pulse width and stimulus intensity. A micromanipulator was used to place the stimulating electrode in between the CA3 and CA1 areas to stimulate SCs fibres. A recording electrode (2-3 MΩ), also filled with aCSF but not broken, was placed in the *stratum radiatum* of the CA1 region. Fluorescence recordings and electrophysiological field potential recordings were taken from the same field of view. In MF-CA3 pathway experiments, stimulating electrodes were placed in the *stratum granulosum* of the dentate *gyrus* and the recording electrode was placed in the *stratum lucidum* of CA3. A monochromator (Till Photonics, Germany) was synchronised with image capture such that it alternated rapidly between 470 ± 10 nm and 560 ± 10 nm excitation wavelengths to record an interleaved image stack of emitted fluorescence measured at wavelengths of 520 ± 20 nm and 620 ± 25 nm as “green” and “red” images, respectively; for this, a dual band emission filter (Chroma Technology) was used. For transgenic mice experiments, the imaging protocol was as follows: image pixel binning was x2, digital gain was 400 and the exposure time was 80 ms. The protocol used for these experiments was to stimulate synaptic pathways with 10/20 stimuli at a rate of 20 Hz and at 20 V. For Fluo-4 experiments, only a 470 ± 10 nm wavelength was used as this is a single wavelength calcium indicator. Therefore, the imaging protocol was as follows: image pixel binning was x4,

digital gain was 400 and the exposure time was 30 ms. Recordings were taken at 5 minute intervals and stable baseline recordings for 15-20 min were obtained before applying drugs. During this time, at least three image stacks were collected. Images were saved on a computer at a 256×256 pixel density as TIFF format files for analysis. In CA1 region experiments, a NMDA-dependant long-term potentiation could arise as a result of this type of repeated stimulation, so the selective NMDA receptor antagonist DL-AP5 (Collingridge et al., 1983) was added to the aCSF in all experiments to prevent this phenomenon.

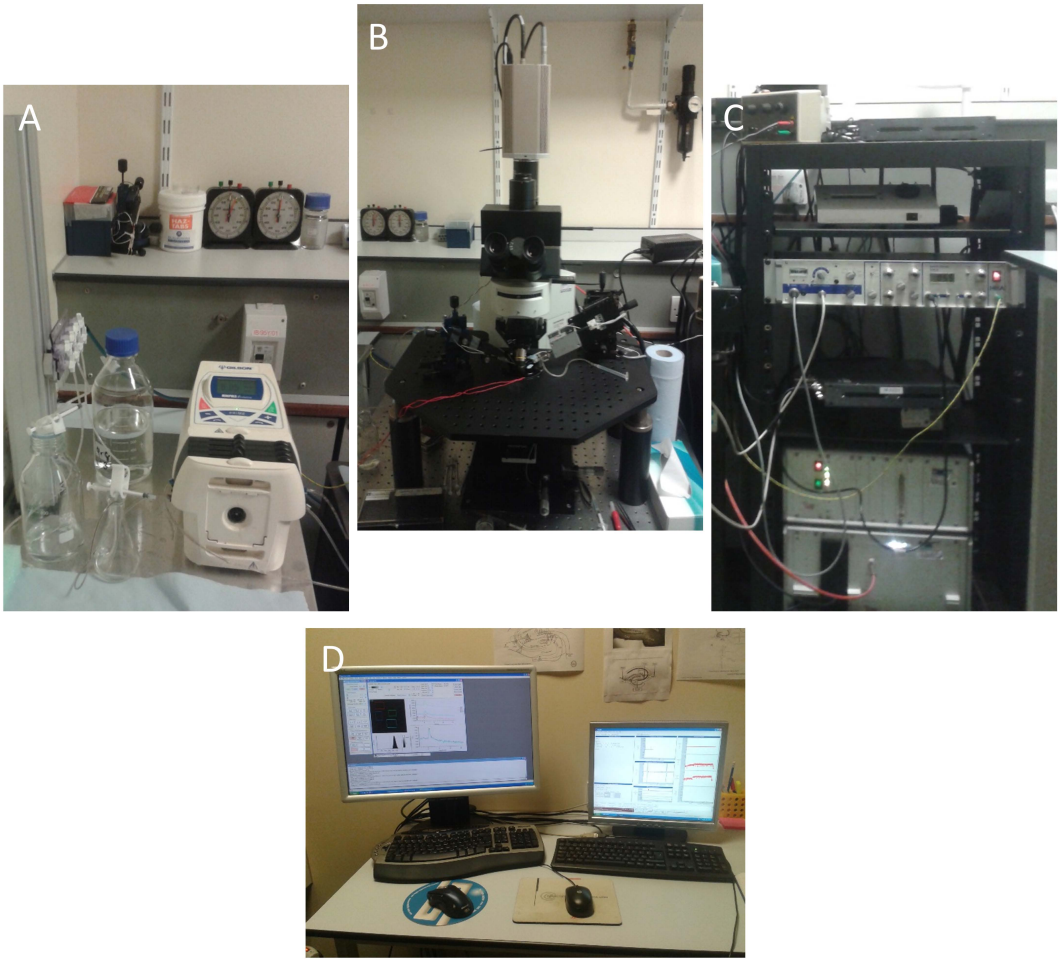

Figure 2.1. An Olympus upright fluorescent imaging microscope equipped with a QuantEM EMCCD camera and connected to an electrophysiology system.

Figures show the whole recording system, including: A. A peristaltic perfusion pump and carbogen gas line; B. stimulating and recording electrodes, micromanipulator, perfusion chamber, QuantEM EMCCD camera; C. the stimulator, the light source Polychrome II (Photonics), the data acquisition-

NIDAQ-board break out box (CA-1000) (National Instruments), electrophysiology system; patch clamp amplifier (HEKA; Germany) connected to imaging system; and D. two PCs for monitoring and controlling imaging and electrophysiology experiments.

2.7.2 Imaging data analysis.

Igor Pro software and Microsoft Excel were used to analyse imaging experiment data. The first step in the data analysis was splitting the interleaved image stacks into two separate stacks; one for GCaMP2 and the other for mCherry. Because it was difficult to accurately assess background fluorescence for ratiometric imaging, only the GCaMP2 images were analysed and used in this study (see chapter 6). Regions of interest (ROI) were selected according to the various strata within the hippocampus, and the absolute fluorescence was obtained for each image in the stack using batch analysis routines written in Igor Pro. A bleach compensation routine was applied with a double-exponential function to help compensate for the bleaching that occurred during data acquisition. After bleach compensation, and to allow clearer visualisation of fluorescence responses, the mean value of fluorescence prior to stimulation (F_0) and the fluorescence at any given time (F) were calculated. The peak (F/F_0) fluorescence was measured and a value of 1 subtracted to give the change in fluorescence from baseline. Any subsequent change in absolute fluorescence could be expressed as a proportion of (F/F_0) plotted against relative time. To compare the responses over time, data from up to nine separate ROIs were averaged and plotted against time, and the peak amplitudes of the responses, the initial slope, the area under the curve and the decay time constant, tau (τ), of the peak F/F_0 response was obtained and compared in order to observe any changes in the basic kinetics of calcium signalling. Data were normalised by taking percentages of means of peak amplitudes so that changes in relative fluorescence could be detected across these experiments. In some cases, three different image sets were extracted from different collection periods. As an example; baseline, drug and wash out were plotted using the Igor software to provide a visual indication of any drug effects. A similar methodology was used for all experiments, and the example

illustrated in figures 2.2 and 2.3 demonstrates how the imaging data were recorded and analysed.

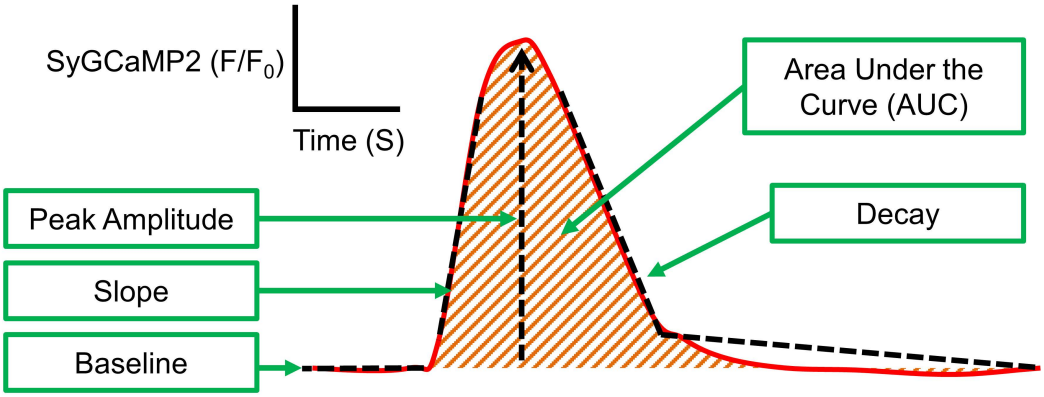

Figure 2.2. Schematic diagram of the SyGCaMP2 fluorescence trace.
Figure shows a schematic diagram of the responses to electrical stimulation collected from ROI placed within a target place within the collected image and then plotted against time. The excitation wavelength was 470 ± 10 nm to record an emitted SyGCaMP2 fluorescence measured at 520 ± 20 nm as “green”. Using Igor pro software, the peak amplitude, the initial slope, AUC and the decay of the SyGCaMP2 fluorescence can be extracted from these curves.

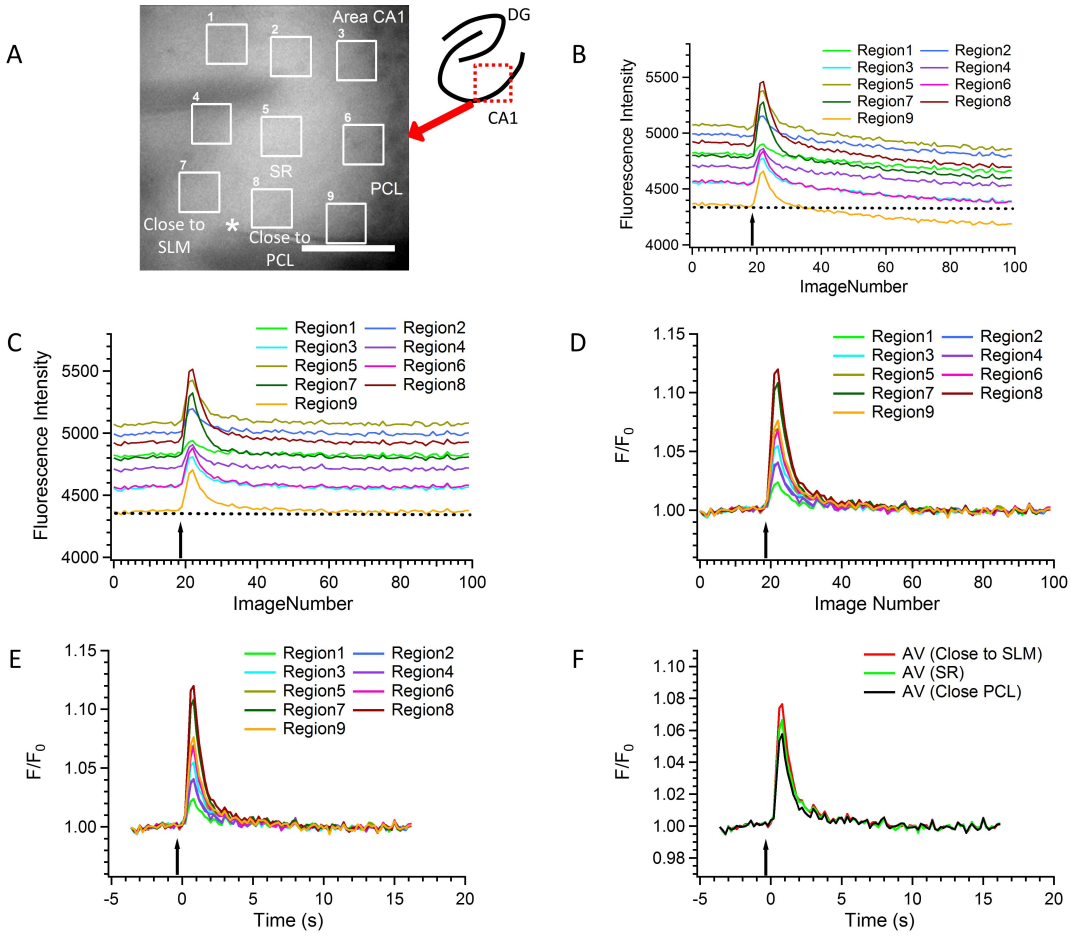

Figure 2.3. Imaging data analysis steps using Igor Pro software.

As an example, only SyGCaMP2 images were analysed in here. A shows the positions of nine regions of interest (ROIs) positioned within the CA1 hippocampal area, which were later arranged into three groups and averaged. ROIs 1, 4 and 7 were grouped in the *SR-close to stratum lacunosum moleculare,* whilst ROIs 2, 5 and 8 were grouped in the *stratum radiatum* and ROIs 3, 6 and 9 in the *SR*-close to the pyramidal cell layer. The small diagram in black is for the whole hippocampus with red squared area for CA1 region. The small diagram is for the hippocampus and the red boxed area is CA1 area. B and C show raw data and the subsequent effect of application of bleach compensation. D and E show the absolute fluorescence measurements from each ROI and the data expressed as F/F_0 over image number and time, respectively. Figure F shows the averaged data of three ROIs for the SR-*close to stratum lacunosum moleculare* (Av close to SLM), *stratum radiatum* (Av SR) and SR-close to pyramidal cell layer (Av close to PCL). The asterisk in A indicates the top of the stimulating electrode. Arrows indicate the beginning of the period of electrical stimulation (stimulus intensity

was 20 V, stimulus number = 20 stimuli at a fixed frequency (20 Hz). SR: *stratum radiatum*; PCL: *pyramidal cell layer.* The scale bar in A is 100 µm

2.7.3 Imaging of individual synaptic boutons within the CA1 region and puncta analysis (Puncta experiments).

Transverse slices (400 µm thick) obtained from SyG37 transgenic mice were also used in this set of experiments. As before, slices were transferred to a recording chamber perfused with carbogenated aCSF at a rate of > 1 ml/min at room temperature. Slices were then stimulated using a glass capillary electrode with a carefully broken tip. A micromanipulator was used to place the stimulating electrode between the CA3 and CA1 area to stimulate SCs fibres. The CA1 area was examined with a Zeiss LSM 7 MP multiphoton microscope equipped with a (x20, 1 NA) water immersion lens (Zeiss; U.K) and coupled to a Mai-Tai HP-Sapphire-pulsed laser (Spectra-Physics, USA). Images were acquired using Zen 2009 software (Zeiss) at intervals of 110 ms, under the control of an Arduino Uno programmed using a sequencer program running under Igor pro software. The intention was to record only GCaMP2 fluorescence. The following imaging protocol was as follows: the laser was tuned to 920 nm and set to 22% power, the pixel resolution was 512 x 64, and the zoom was at 3. A band emission filter 500-550 nm was used (Chroma Technology, USA). The protocol used for these experiments was to stimulate the synaptic pathway with 20 stimuli at a rate of 20 Hz at 50 V with a pulse width of 200 µs. Recordings were taken at 5 minute intervals and stable baseline recordings for 15-20 min were obtained before applying drugs. During this time, at least three images were collected and saved on the computer.

Single bouton responses were analysed using Igor Pro. Averages of images taken before stimulation were used to create F/F_0 images using averages of images taken during stimulation at the maximum intensity tested of 40V. This revealed the position of boutons that responded at this maximum intensity. These locations were then used to define 3x3 pixel ROIs that just circumscribed these single, responding boutons. These ROIs were used to measure responses at the other intensities tested along with a separate group of neighbouring ROIs that were used to measure the background fluorescence. As a control, we drew a

number of regions of interest around regions of identical size where there was no response. The absolute fluorescence was obtained by subtracting the average fluorescence from the control ROIs from each puncta's fluorescence (figure 2.4).

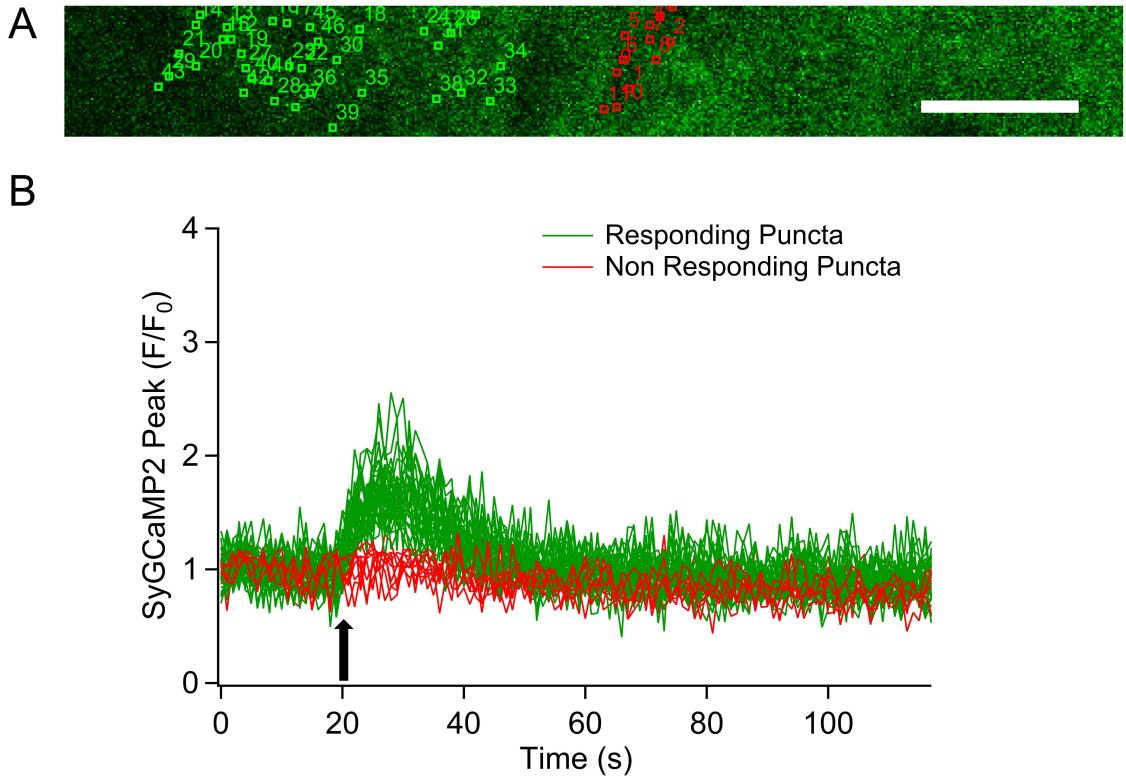

Figure 2.4. Puncta analysis steps using Igor Pro software.

A. shows a GCaMP2 image of area CA1 responding to bursts of 20 stimuli delivered at 20 Hz at an intensity of 50 V with individual puncta identified with green regions of interest centred on puncta that were responsive to stimulation and non-responsive regions of interest shown in red. B. shows traces of control red puncta and selected green puncta. Black arrows indicates the beginning of the stimulation period. The scale bar in A is 10 µm.

2.8 Electrophysiological recordings

Evoked synaptic field potentials (fEPSPs) were recorded using a patch clamp amplifier (HEKA, Germany) linked to an analogue-to-digital converter (National Instruments, U.K.) and custom-programmed acquisition software (WinLTP version-2.01, U.K.). This software was used to trigger imaging experiments that were controlled using a separate computer running custom procedures written by Prof. Nick Hartell in Igor Pro (v6.34A; Wavemetrics, USA). Synaptic fEPSP

were filtered at 3 kHz, digitized at 20 kHz and stored on a PC. To compare between electrophysiology and imaging experiments, the tip of the recording electrode was placed in the centre of the imaging field. While the electrical stimulation was delivered, the image stack was recorded. This was repeated at 5-minute intervals over the course of the experiment. Drugs were applied only after recording a stable baseline for about 15-20 min.

Electrophysiological data were analysed using WinLTP (Anderson and Collingridge, 2007). The initial slopes and amplitudes of N2 component of fEPSPs (and N1 components in puncta experiments) were measured (see figure 2.5) for the entire duration of the experiments and normalised to a 15 min baseline and expressed as the mean ± SEM. Between periods where imaging data were being collected (i.e., 10/20 pulses delivered at 20 Hz and 20 V stimulus intensity), pairs of stimuli separated by 50 ms were applied every 10 seconds and the electrophysiogical signals recorded. This was to evaluate the ongoing synaptic strength of the synaptic pathways. The ratio of the amplitude or slope of the second pulse to the first is called the paired-pulse ratio, and changes in this ratio can be used to reveal a synaptic change with a presynaptic origin (Xu-Friedman and Regehr, 2004, Regehr, 2012, Yang and Calakos, 2013). The magnitudes of any drug effects were calculated by comparing the average size of the fEPSCs in control, drug and wash-out periods.

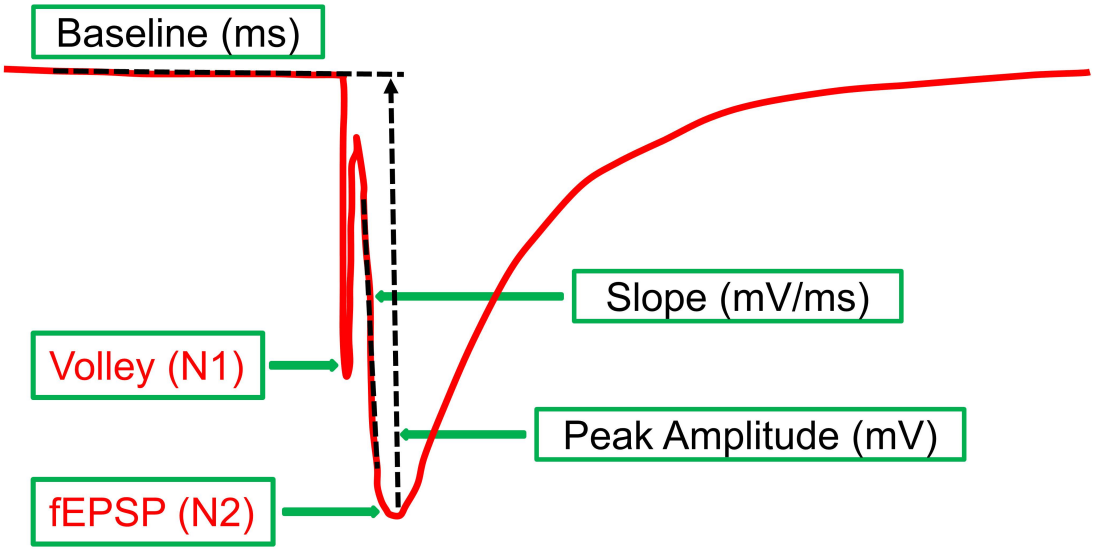

Figure 2.5. Schematic diagram of a field potential recording.

Figure shows a schematic diagram of a typical fEPSP recording. The first, smaller deflection is the fibre volley (N1) which corresponds to the action potentials evoked by the stimulation. The action potentials will subsequently promote release of transmitter in the presynaptic terminals, leading to the second larger deflection (N2) which is the postsynaptic potential. A custom-programmed acquisition software (WinLTP version-2.01, U.K.) was used to measure the peak amplitude and the initial slope of both N1 and N2 components.

2.9 Reagents

The following reagents were purchased from Sigma-Aldrich (Gillingham, U.K.): NaCl, $CaCl_2.2H_2O$, KOH, tris acetate-EDTA buffer, glycerol, agarose, phosphatase inhibitor cocktail-3, DNQX, picrotoxin, 2-mercaptoethanol, SDS, dry skimmed milk, donkey serum, DMSO, Dulbecco's phosphate-buffered saline, paraformaldehyde, pluronic® F-127, Tween-20 and Triton-X 100. Reagents obtained from R&D Systems (Minneapolis, U.S.A) were DMSO, DL-AP5, forskolin, rolipram, adenosine, DCG-IV and DPCPX. Reagents obtained from VWR International (Lutterworth, U.K.) were NaH_2PO_4, $NaHCO_3$ and $MgSO_4.7H_2O$. Fluo-4-acetoxymethyl ester (fluo-4-AM), sucrose, D-glucose, normal goat serum, tris-base and KCl were obtained from Fisher Scientific (Loughborough, U.K.). Polyvinylidene fluoride (PVDF) transfer membrane was purchased from Millipore, Ltd. (Watford, U.K.). ReddyMix PCR master mix was obtained from ThermoFisher Scientific (New Jersey, U.S.A.). COmplete™, Mini

Protease Inhibitor Cocktail was obtained from Roche Diagnostics (Basel, Switzerland). Acrylamide/bis-acrylamide stock solution (30%, w:v) was supplied by National Diagnostics, Ltd. (Hessle, U.K.). Luminol Reagent detection was obtained from Santa Cruz (California, U.S.A.). Pentobarbitone sodium 20% w/v solution was obtained from Animalcare, Ltd. (York, U.K.). PKI (14-22) amide (myristoylated) was obtained from Enzo Life Sciences (Exeter, U.K.). Prism ultra-protein ladder was obtained from Abcam (Cambridge, U.K.). Isoflorane (IsoFlo®) was obtained from Abbott Laboratories (Chicago, U.S.A.). Bromophenol Blue was obtained from Amersham Biosciences (GE Healthcare, Ltd., Chalfont, U.K.). Cmah R, Cmah F, SyGCaMP2 R, SyGCaMP2 F and SYBR® safe DNA gel stain were obtained from Invitrogen (Paisley, U.K.).

2.10 Statistics

Excel, Igor and GraphPad Prism 7 (GraphPad, USA) software were used to carry out basic statistical analyses. Data in each experiment were normalised to baseline, then pooled together and expressed as mean ± SEM. Unless stated otherwise, the time points used in the statistical tests are as the following: adenosine and forskolin experiments, -5, 25, 55, 75 minutes; synaptic blocking experiments, -5, 15, 30, 45, 70 minutes. Statistical significance was tested using unpaired t test, Mann-Whitney U-test, one-way ANOVA, followed by Dunnett's test, Kruskal-Wallis with Dunn's test post hoc correction or two-way ANOVA, followed by Sidak’s post hoc test; p values of 0.05 were considered significant and are indicated with asterisks with *, ** or *** according to the level of significance. For co-localisation analysis, a Pearson correlation coefficient was calculated for the co-variation of fluorescence from pairs of antibodies along lines drawn through immunohistochemically stained sections.

CHAPTER 3- CHARACTERISATION OF THE EXPRESSION OF SYGCAMP2-mCHERRY IN SYG TRANSGENIC MOUSE LINES.

3.1 Introduction

In the first part of this study, we characterised and evaluated the suitability of two different strains of transgenic mouse. We began by exploring and identifying the individual genotype of animals in our mouse colonies using the polymerase chain reaction (PCR) technique. Having established that the DNA for the SyGCaMP2-mCherry construct was present using PCR, it was then important to confirm that the SyGCaMP2-mCherry sensor was properly created and expressed. For this, we first used Western blot analysis to confirm the presence of mCherry. Having established that SyG37 mice contain the genetic code for mCherry and expressed a protein that was recognised by an antibody to mCherry, we then examined the fluorescence expression levels for mCherry and SyGCaMP2 in acute coronal slices from the SyG37 mouse line. We then attempted to confirm that the expression of SyGCaMP2-mCherry was indeed presynaptic, as predicted. For this, we undertook a series of immunohistochemical (IHC) studies to determine, in more detail, the cellular and subcellular expression patterns of the SyGCaMP2-mCherry sensor using an antibody raised against mCherry. We performed double labelling for mCherry in combination with a variety of synapse-specific markers to establish first whether the sensor was expressed selectively in presynaptic terminals – as predicted – and, second, which type of synapse the SyGCaMP2-mCherry was expressed in.

3.2 Results

3.2.1 Gene Amplification by PCR

Identification of an individual genotype for animals is important for proper maintenance of transgenic mouse lines and in reducing the number of animals that need to be used during research. Monitoring the transgenic status of the mice can be achieved using the PCR technique by analysing small amounts of DNA extracted from tissues obtained from ear snip or tail biopsies of young

rodents. DNA doubling occurs in every PCR cycle, leading to an exponential amplification of the target gene and, therefore, genotype is judged by the differential bands produced with flanking primers, which are designed to distinguish between wild-type (-WT) and transgenic (+TG) alleles by amplicon length (Mullis *et al.*, 1987, Bartlett and Stirling, 2003). An example of the genotype check is shown in figure 3.1, where the genotyping of two mouse lines, SyG14 and SyG37 is determined by the differential bands on a gel. In this case, primers were designed so that each mouse can be represented by two potential bands; the first band represents the control DNA (Cmah), while the second band represents the DNA for the SyG mouse construct. Samples with two bright bands (red coloured, +/+) indicate a positively genotyped mouse, whereas samples with only one bright band with the second band missing (black coloured, +/-) indicate a negatively genotyped mouse. The first two bands in each gel represent a control positive mouse that was already tested in a previous genotyping experiment.

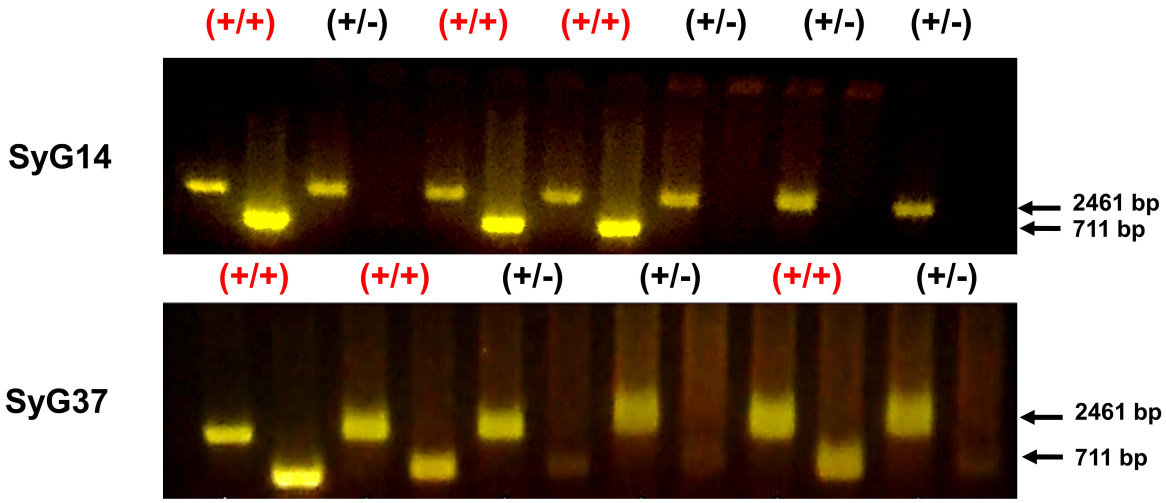

Figure 3.1. Typical examples of PCR genotyping for detection of a transgene from mouse ear snips from both SyG14 and SyG37 colonies.
Each mouse is represented by two lanes; the first lane is the control DNA while the second lane is the DNA for the SyG mouse construct under test. Samples with two bright lanes (red coloured, +/+) indicate a positively genotyped mouse, whereas a sample with one bright lane and a missing second lane (black coloured, +/-) indicate a negatively genotyped mouse (WT).

3.2.2 Western Blotting

PCR can be used to detect whether a target gene is present within a tissue sample but it does not reveal whether the gene of interest has been successfully expressed as a protein. The Western blot (protein immunoblot) is an antibody-based analytical technique widely used in molecular biology to detect specific proteins in samples of tissue homogenate or extract. Gel electrophoresis is first used to separate proteins according to their molecular weight and then they are transferred to a membrane where they are stained with antibodies specific to the target protein (Towbin *et al.*, 1979). As mentioned previously, our sensor, SyGCaMP2, was modified by attaching the red fluorescent protein mCherry to make the SyGCaMP2-mCherry sensor. Therefore, we decided to test for mCherry expression levels in three different mouse lines: WT (as a control), and SyG14 and SyG37 mice. The vesicular Glutamate transporter 1 (VGlut1), which is widely expressed within the CNS (Ni *et al.*, 1995, Kaneko *et al.*, 2002), was used as a positive control. vGLUT1, was expressed as a protein with a size of 60 kDa in each of the three different mouse lines (figure 3.2A). Only the SyG37 mice displayed a band with a size of 27 kDa. This band, representing mCherry, was completely absent in SyG14 animals. For better data visualisation, mCherry expression levels were normalised to vGLUT1 expression levels and plotted in figure 3.2. These experiments clearly confirm that the SyG14 mouse model is either entirely lacking in or, at best, contains undetectable levels of the SyGCaMP2-mCherry sensor.

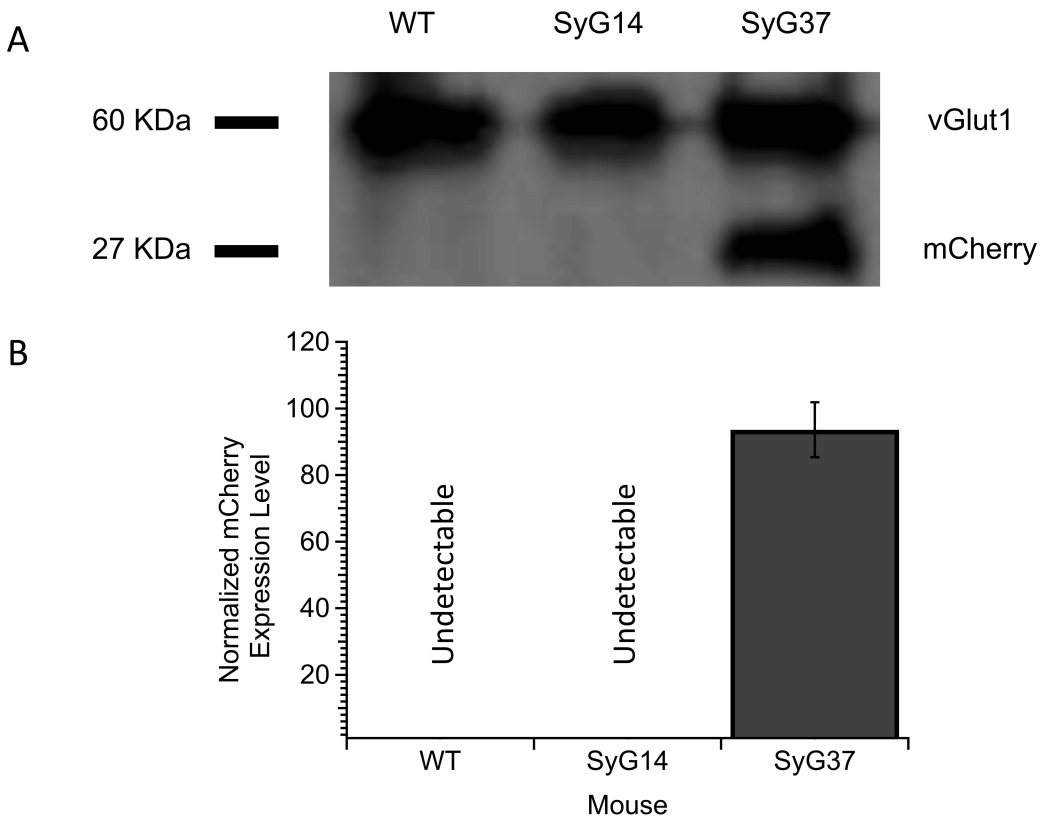

Figure 3.2. Assessment of SyG14 and SyG37 mice by Western blot analysis of mCherry protein expression.

A. A band with a molecular weight of 27kDA that reacted to the mCherry antibody was detected in SyG37 but not in SyG14 or WT mice. VGlut1 (60 kDa), used as a positive control was expressed in all three groups. B. The bar chart showing mCherry protein expression levels normalised to VGlut1 levels in WT, SyG14 and SyG37 mouse lines; n = 3.

3.2.3 SyGCaMP2-mCherry expression in SyG37 mouse's brain.

Having established that SyG37 and SyG14 mice contain the genetic code for mCherry but that only SyG37 mice expressed a protein that was recognised by an antibody to mChery, we then examined the fluorescence expression levels for mCherry and SyGCaMP2 in acute coronal slices from the SyG37 mouse line. The SyG14 mouse line was not tested here as we have shown and we will show later that fluorescence levels for mCherry and SyGCaMP2 in SyG14 mice are indistinguishable from age matched WT animals indicating that neither fluorescent protein appears to be expressed. Brains from young, SyG37 and WT mice were cut into 400 µm-thick slices which were perfused with aCSF containing

a saturating concentration of calcium (5 mM) to maintain maximal fluorescence levels of GCaMP2 during image acquisition. The excitation wavelengths were 470 ± 10 nm and 550 ± 10 nm to record images of the emitted fluorescence measured at wavelengths of 520 ± 20 nm and 620 ± 25 nm as green (SyGCaMP2) and red (mCherry) images, respectively. Figure 3.3-B shows fluorescence expression patterns in coronal sections of the brains from a young, SyG37 positive animal. The yellowish colour in the merged images of the SyG37 mouse indicates that GCaMP2 (green) and mCherry (red) are both generally expressed in same places (co-localised). Ratio images from SyG37 show GCaMP2: mCherry fluorescence ratio which might give an idea of calcium levels. A WT mouse of the same age was used as a control. Images were collected using identical light intensities, camera exposure settings and illustrated using identical brightness and contrast settings. Under these conditions, the fluorescence levels were clearly very much lower in the WT mouse (figure 3.3A). Figure 3.4 shows that mCherry expression was present throughout the brain of SyG37 positive mice. Within the hippocampus, mCherry and SyGCaMP2 expression was particularly evident in the DG, CA3, CA1 and subiculum. mCherry expression was also present shown in the layers of the cortex, amygdala and in thalamic nuclei.

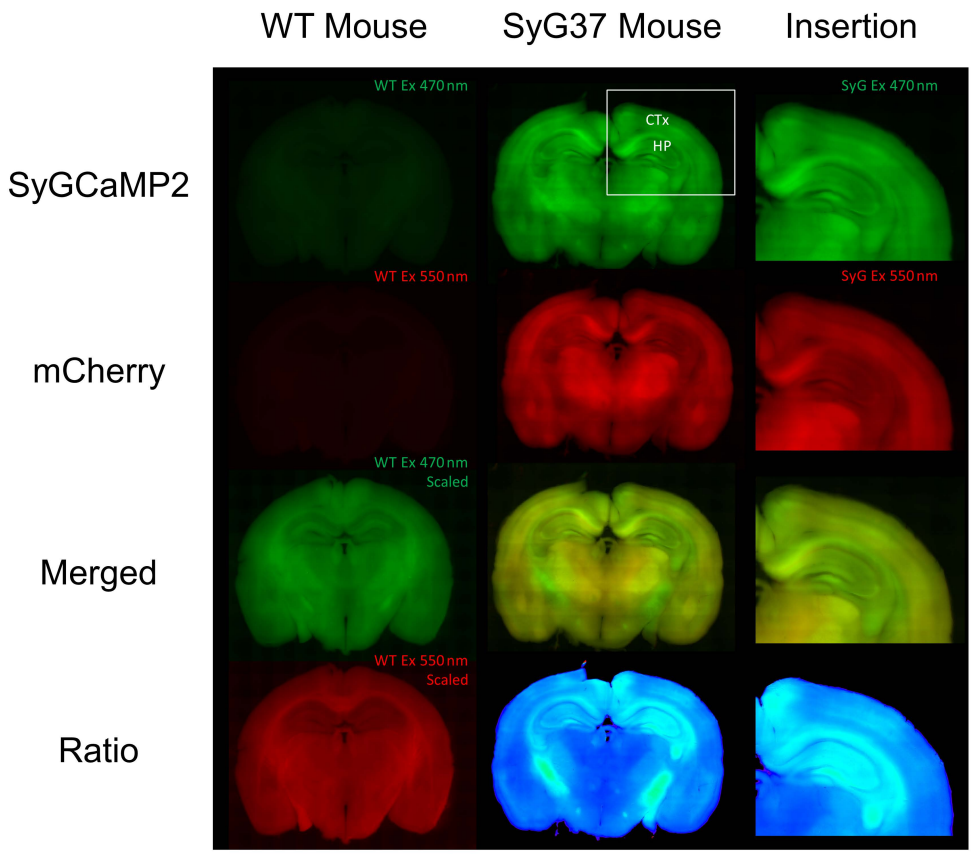

Figure 3.3. Fluorescence images of acute coronal brain slices from a SyG37 positive mouse showing the expression patterns of the SyGCaMP2-mCherry sensor in direct comparison with a WT mouse.

Left panel shows coronal images of the whole brain of the WT mouse (control). Images were constructed from arrays of sub-images that were flattened to adjust for uneven illumination and stitched together. Middle panel shows similar image of the whole brain taken from a SyG37 mouse, illustrating the widespread distribution of both GCaMP2 (green) and mCherry (red). Right panel shows the magnified view (white box) in the middle panel. Merged images show an overlay of GCaMP2 and mCherry fluorescence. Ratio images show GCaMP2: mCherry fluorescence ratio which might give an idea of calcium levels. Merged and ratio images from WT mouse shows images where the brightness was increased (scaled) as it is difficult to make any observations when the brightness of all the images were the same. Excitation was at 470 nm, 550 nm and emission was at 525 ± 50 nm and 620 ± 60 nm for GCaMP2 and mCherry, respectively. CTx, Cortex and HP, Hippocampus. The mouse brain was cut at about 2.15 mm posterior to bregma.

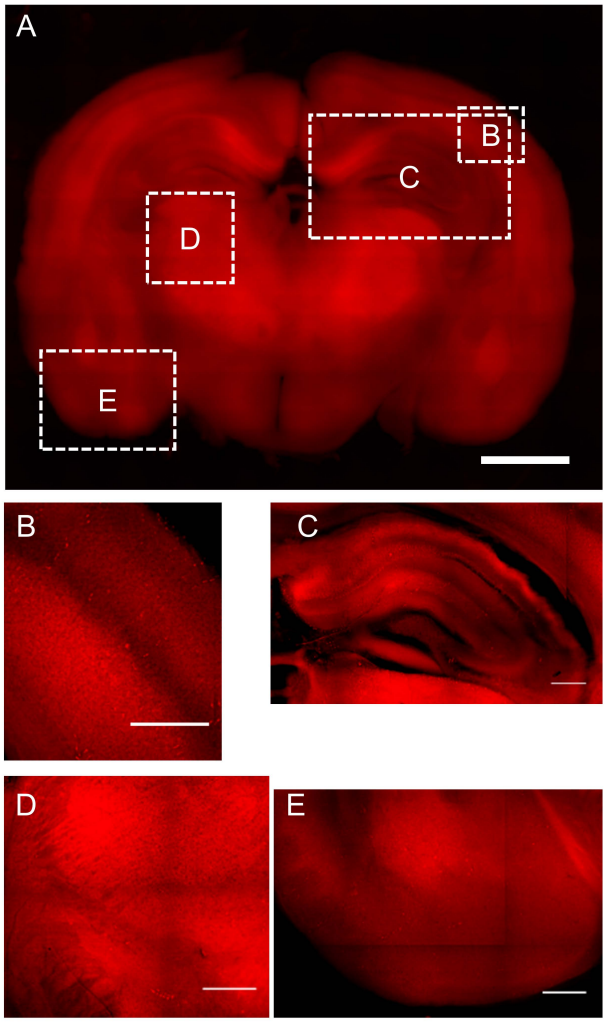

Figure 3.4. Fluorescence images of acute coronal brain slices of a SyG37 mouse showing the expression patterns of mCherry in different brain regions.

Panel A shows a stitched image of the same coronal slice from a SyG37 mouse shown in figure 3.3 indicating widespread distribution of mCherry. B, C, D and E are expanded views from panel A illustrating the expression patterns in the cerebral cortex, hippocampal regions (dentate gyrus, CA3, CA1, subiculum), thalamus and amygdala, respectively. The scale bars represents 1 mm in A and 300 µm in B-E.

3.2.4 Immunohistochemistry

We next undertook a series of immunohistochemical (IHC) studies to determine, in more detail, the cellular and subcellular expression patterns of the SyGCaMP2-mCherry sensor using an antibody raised against mCherry. This technique was first described in the mid-1930s, and the first study of such was published in the mid-1940s (de Matos *et al.*, 2010). We performed double labelling for mCherry in combination with a variety of synapse-specific markers to establish first whether the sensor was expressed selectively in presynaptic terminals – as predicted – and, second, which type of synapse the SyGCaMP2-mCherry was expressed in. In order to generate reproducible and reliable immunohistochemical data, an antibody test matrix was undertaken in order to establish the optimal conditions for fixation, as well as the optimal dilutions for each primary and associated secondary antibody. The following sections describe in detail the immunohistochemical data that were collected to determine the SyGCaMP2-mCherry localisation; for this, antibodies against specific proteins were applied to sections of WT and SyG37 mouse hippocampus. It is worth mentioning that the following IHC experiments have repeated several times with different fixatives and different buffer saline (phosphate and tris-base buffer saline) and then the results were imaged using both microscopes (one and multi-photon microscope), just to confirm IHC data.

3.2.4.1 Validation of antibody expression in hippocampal slices.

All the secondary antibodies used in this study were commercially available and had previously been assessed for use in immunohistochemical studies but we needed to determine the staining specificity of the primary antibodies. Transverse brain slices from the SyG37 mice (for anti-mCherry experiments) and from WT mice (for the other primary antibodies) were incubated with primary antibodies. The primary and secondary antibodies used in this project were as in table 3.1. Sections in which the primary antibodies were omitted were considered as controls. The reason for using antibodies against mCherry was to increase the

fluorescence intensity during labelling as fluorescent proteins tend to lose some of their fluorescence following fixation.

Table 3.1. The primary and secondary antibodies used in this project.
Single and multi-photon excitation and emission wavelengths. Cited from Franke *et al.* (2014)

Primary antibodies	Marker of	Secondary antibodies	Single Photon Ex (nm)	Multi Photon Ex (nm)	Em (nm)
Goat Anti-mCherry	SyGCaMP2-mCherry sensor marker	Donkey anti-goat Alexa Fluor-594	590	780	618
Rabbit Anti-Bassoon	Presynaptic marker	Donkey anti-rabbit Alexa Fluor-488	495	720	519
Rabbit Anti-PSD95	Postsynaptic marker	Donkey anti-rabbit Alexa Fluor-488	495	720	519
Guinea pig Anti-vGlut1	Excitatory neuronal marker	Goat anti-guinea pig Alexa Fluor 488	495	720	519
Mouse Anti-vGAT	Inhibitory neuronal marker	Goat anti-mouse Alexa Fluor-488	495	720	519

The results of these experiments are shown in figure 3.5. mCherry was expressed in all hippocampal regions of SyG37 mice and showed a strong punctate distribution. At high magnification, labelling for mCherry was not observed in cell bodies but showed a clear punctate expression that was particularly pronounced around the dark areas within the pyramidal cell layer of area CA1, which presumably represent unstained cell bodies (figure 3.5; first row). Bassoon staining was also widespread throughout the hippocampus. Higher magnification images also showed a punctate staining similar to that of mCherry (figure 3.5; second row). PSD95 staining showed a similar pattern of staining to that of Bassoon and mCherry at low magnification. At high magnification, labelling for PSD95 was subtly different and although punctate, and largely absent from cell bodies, there was evidence of some staining in dendrites, consistent with a post-synaptic expression (figure 3.5; third row). VGLUT1 staining was also punctuate (figure 3.5, fourth row) and clearly evident around the dark areas that presumably represent cell bodies in area CA1. The fifth row of figure 3.5 shows an example of VGAT staining which was again punctuate and outside cell bodies. For the control slides shown in column D, only

the secondary antibodies were added. In the absence of the primary antibodies, only low levels of non-specific staining were present as shown by ensuring that the fluorescence acquisition and image presentation conditions were identical. In the case of mCherry staining, the background fluorescence was slightly more obvious but it is important to remember that mCherry is fluoresce and this remained even after fixation. These experiments provide confirmation of the specificity of the antibodies used.

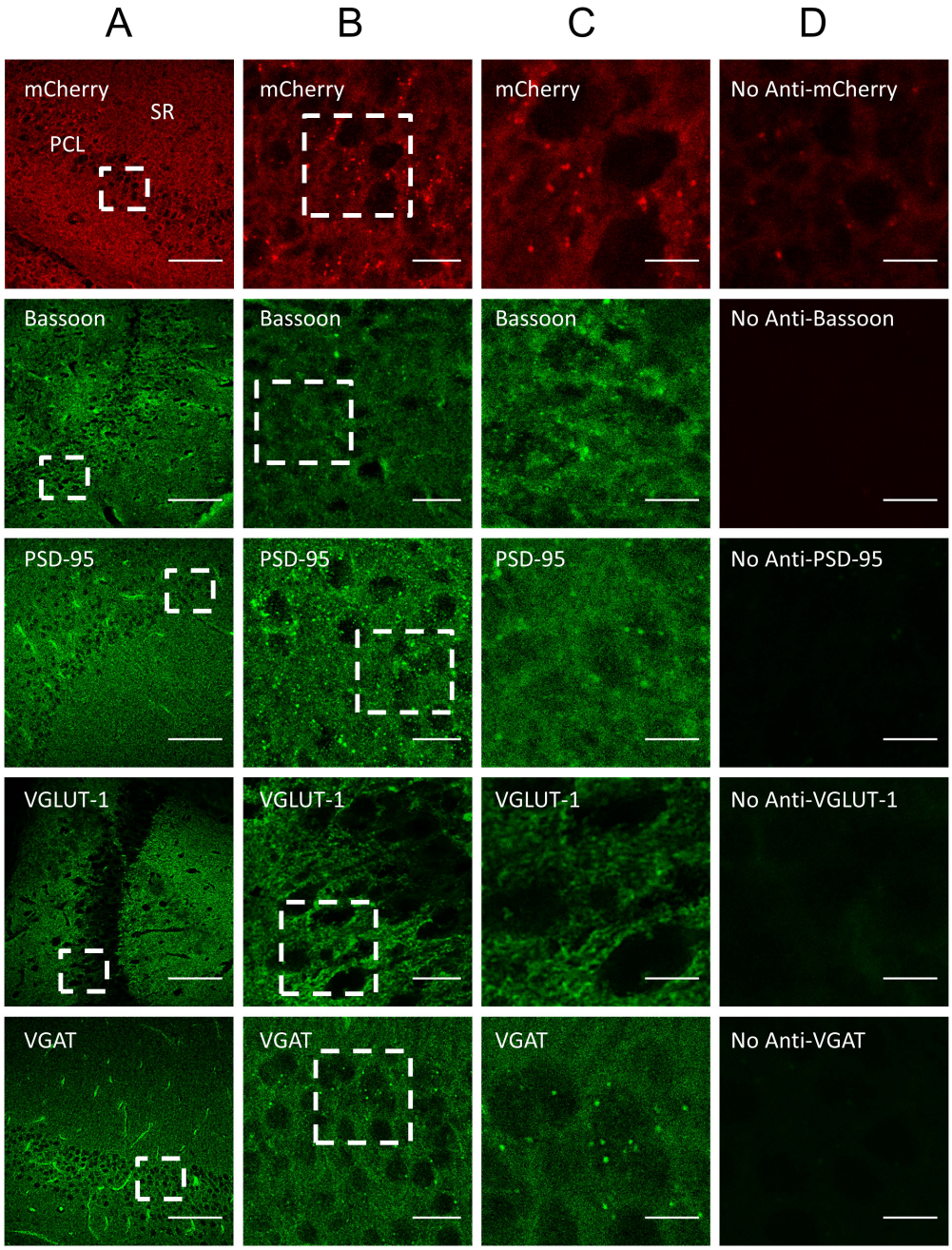

Figure 3.5. Fluorescent labelling of hippocampal area CA1 using 5 different primary antibodies against; mCherry, bassoon, PSD95, vGLUT1 and vGAT.

Panels A, B and C show the expression patterns of the primary antibodies used against different synaptic proteins; mCherry, bassoon, PSD95, vGLUT1 and vGAT at different magnification levels. Inset in B shows the magnified image of the boxed area in A, whereas, inset in C shows the magnified image of the boxed area in B. Panel D shows a control slice stained with secondary antibodies only. PCL, *pyramidal cell layer*; SR, *stratum radiatum*. The scale bars in panels A, B, C and D are 100 µm, 30 µm, 10 µm and 10 µm, respectively.

3.2.4.2 Dual staining of anti-mCherry and a nuclear stain, Hoechst-33342, in hippocampal slices of SYG37 mouse.

If SyGCaMP2-mCherry is expressed presynaptically, we would not expect it to be expressed in the cell bodies as suggested from the results shown in figure 3.5. This was further confirmed by co-staining mCherry with the nuclear stain Hoechst 33342 (Latt and Stetten, 1976). Immunostaining showed that there was no mCherry labelling in wild-type mouse hippocampal slices. However, cell nuclei in all layers of the hippocampus could be detected (figure 3.6-A). mCherry immunostaining revealed expression in SyG37-positive mouse hippocampal slices (figure 3.6-B) and images taken at higher magnification showed that labelling for mCherry was never observed in cell bodies. There was a clear evidence of punctate expression around the Hoechst-stained areas within the pyramidal cell layer (figure 3.6-C).

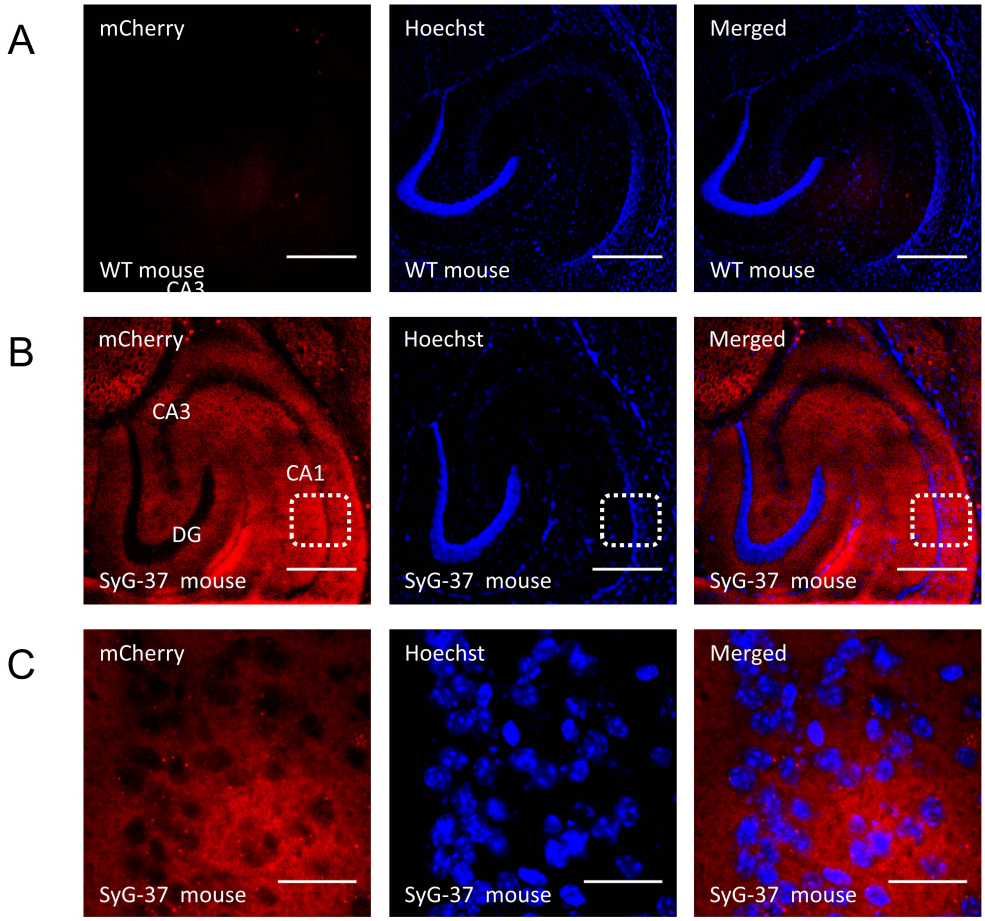

Figure 3.6. Comparison of Hoechst 33342 staining and mCherry immunohistochemistry in SyG37 and WT mouse hippocampal slices.

Panel A shows labelling for anti-mCherry in WT mouse hippocampal slices with an overlay of Hoechst 33342 staining (blue). Panel B shows labelling of anti-mCherry in a SyG37 mouse. Panel C shows a higher magnification image of the region highlighted in panel B. Images were collected with a custom-made epifluorescent microscope equipped with 4X and 60X objectives (Nikon) and a set of suitable filters. The scale bars for panels A and B were 1 mm, and for C was 10 µm.

Figure 3.7 compares mCherry expression in SyG37 mice in different regions of the hippocampus at different magnifications. Expression was punctate in all regions of the hippocampus including CA1, CA3, DG and subiculum. mCherry was not present in cell bodies but puncta were present around the cell bodies. From these data, we conclude that mCherry is not present in cell bodies and is at least consistent with a presynaptic expression. However, further evidence is required before we can conclude that the sensor is expressed presynaptically.

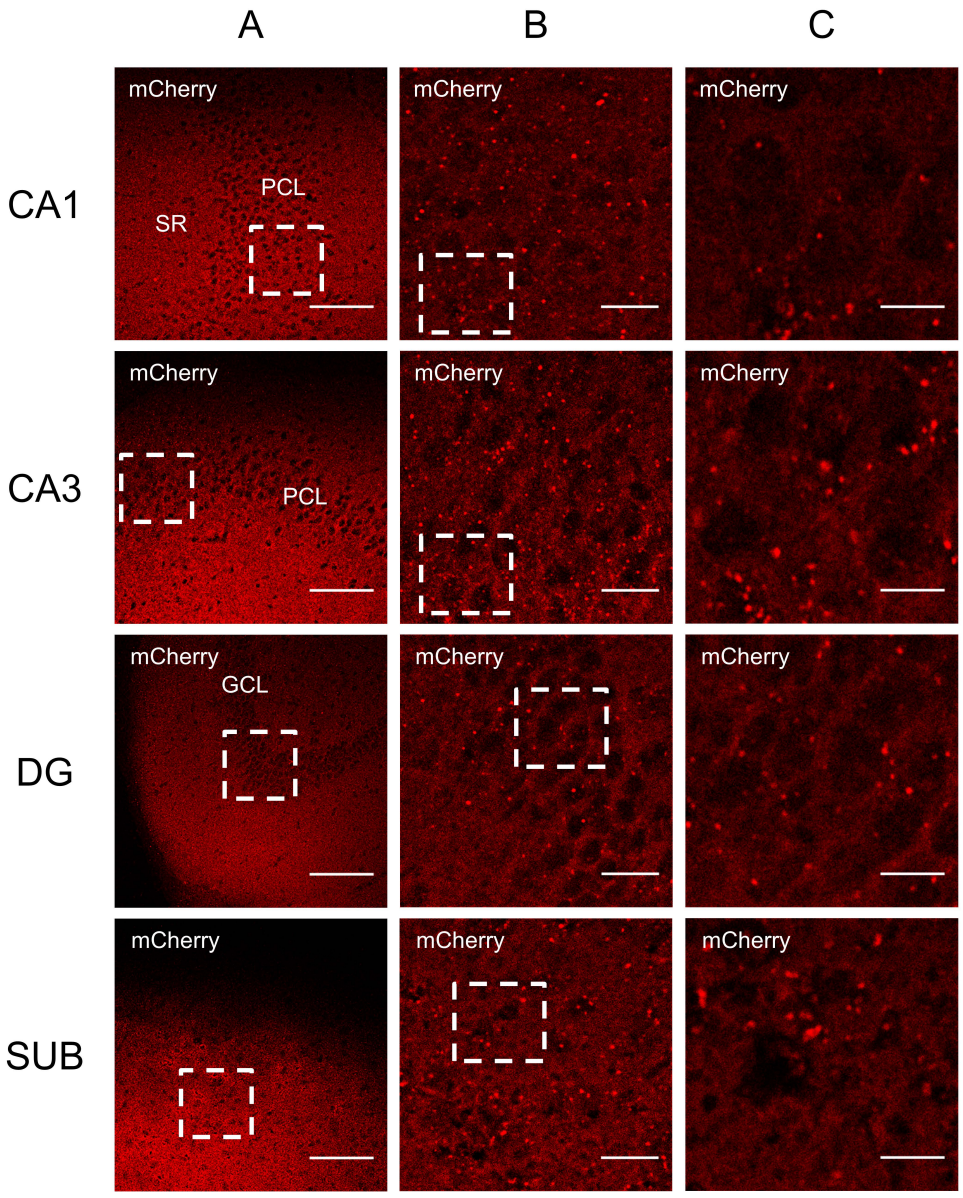

Figure 3.7. mCherry localisation within different hippocampal regions of a SyG37 mouse.

Panels A, B and C show mCherry is expression in hippocampal regions CA1, CA3, DG and subiculum, at different magnifications. Inset in B shows the

magnified image of the boxed area in A, whereas, inset in C shows the magnified image of the boxed area in B. The scale bars for panels A, B, and C represent 100 µm, 30 µm and 10 µm, respectively.

3.2.4.3 Dual staining of anti-mCherry and anti-bassoon in hippocampal slices from SyG37 mice.

To better verify that SyGCaMP2-mCherry was expressed in presynaptic boutons, a series of double labelling experiments were undertaken combining labelling for anti-mCherry with anti-bassoon. In cultured hippocampal neurones, bassoon was found to co-localise with glutamate receptor-1 (GLUR1) and $GABA_A$ receptors and, therefore, is considered to be a component of the active zone of both excitatory glutamatergic and inhibitory GABAergic synapses (Richter et al., 1999). Figure 3.8 shows that their relative distributions were similar and that there was a clear co-localisation of mCherry and bassoon labelling in the *stratum radiatum* of CA1 hippocampal area. A correlation of green and red fluorescence along line profiles drawn through puncta showed a very high correlation between mCherry and Bassoon (figure 3.8-D). This suggests that mCherry, and by inference the SyGCaMP2-mCherry sensor, was expressed in presynaptic terminals. It should be noted that bassoon was distributed more widely than mCherry, suggesting that mCherry was not expressed in all presynaptic terminals.

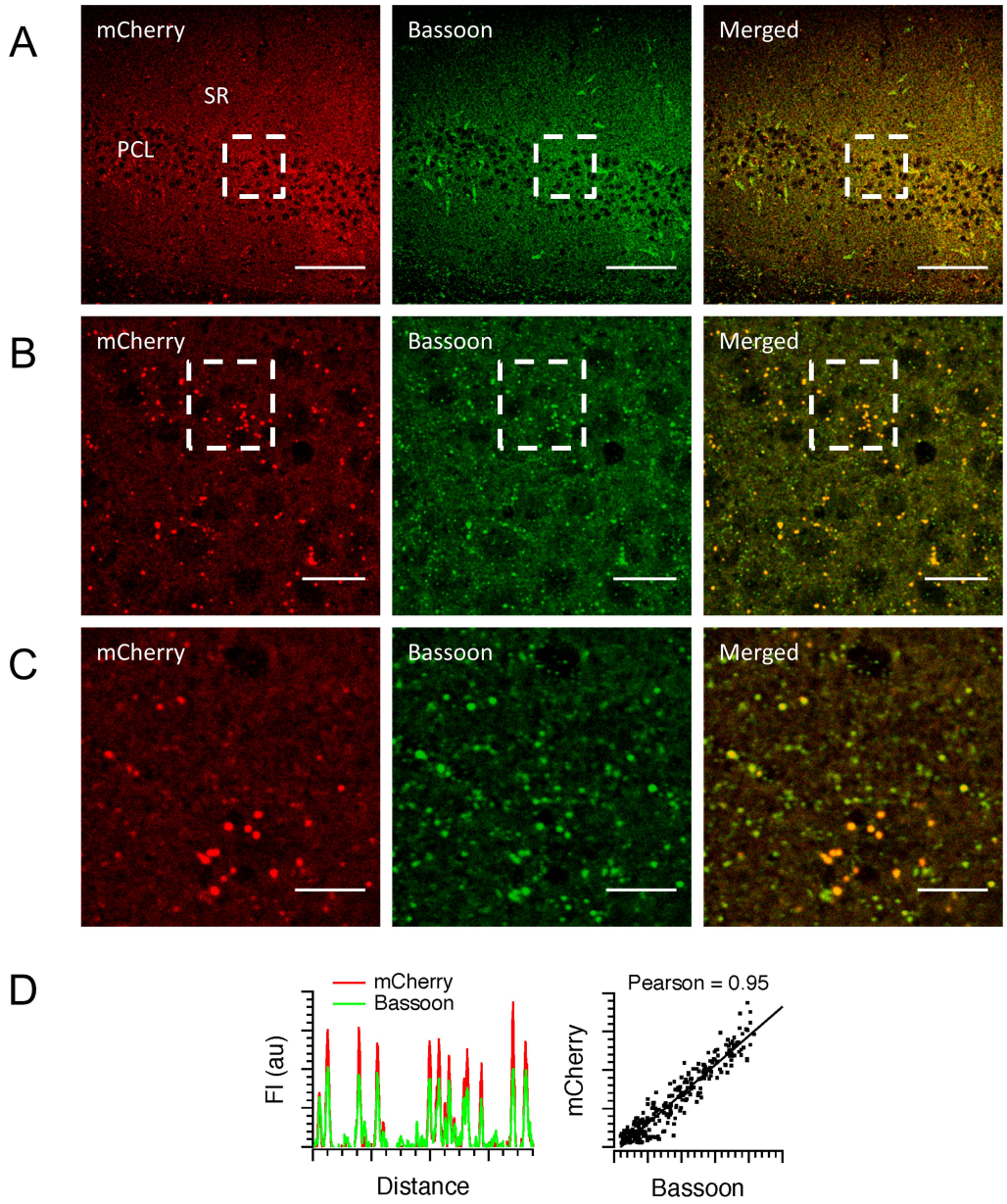

Figure 3.8. Co-localization of mCherry and bassoon in hippocampal area CA1 of a SyG37 mouse.

Panels A, B and C show different magnifications of double staining (anti-mCherry and anti-bassoon) of horizontal sections from hippocampal area CA1 of a SyG37 mouse. Inset in B shows the magnified image of the boxed area in A, whereas, inset in C shows the magnified image of the boxed area in B. The overlay shows that mCherry is co-localised with bassoon in many but not all puncta. D illustrates fluorescence values extracted from lines drawn through punctate regions of the magnified images in B. To the right are graphs showing the relationship between bassoon and mCherry along with the Pearson correlation. The scale bars for panels A, B, and C represent 100 µm, 30 µm and 10 µm, respectively. Abbreviations: SR- *stratum radiatum*, PCL-pyramidal cell layer.

3.2.4.4 Dual staining of anti-mCherry and anti-PSD95 in hippocampal slices of SyG37 mice.

Postsynaptic density protein 95 (PSD95) is the most abundant scaffolding protein almost exclusively located in the postsynaptic density (PSDs) of neurones (Hunt et al., 1996, Garner et al., 2000, Kim and Sheng, 2004, Chen et al., 2011). We next co-stained hippocampal slices from SyG37 positive mice for mCherry and a specific antibody against PSD95 (figure. 3.9). PSD95 expression was also punctate, however, unlike bassoon which co-localised very clearly with mCherry, PSD95 expression was much less obviously co-localised. The higher magnification images shown in figure 3.9 demonstrate that PSD95 did not co-localisation with mCherry in the *stratum radiatum* of area CA1. A correlation of green and red fluorescence along line profiles drawn through puncta showed a very little overlap between mCherry and PSD95. This is Likely due to the low signal-to-noise ratio in the magnified images and the strong background, the synaptic staining could not be very clearly detected. Generally, these results further confirming a presynaptic localisation of the SyGCaM2-mCherry sensor to hippocampal synapses formed by SCs to CA1 pyramidal cells (figure. 3.9).

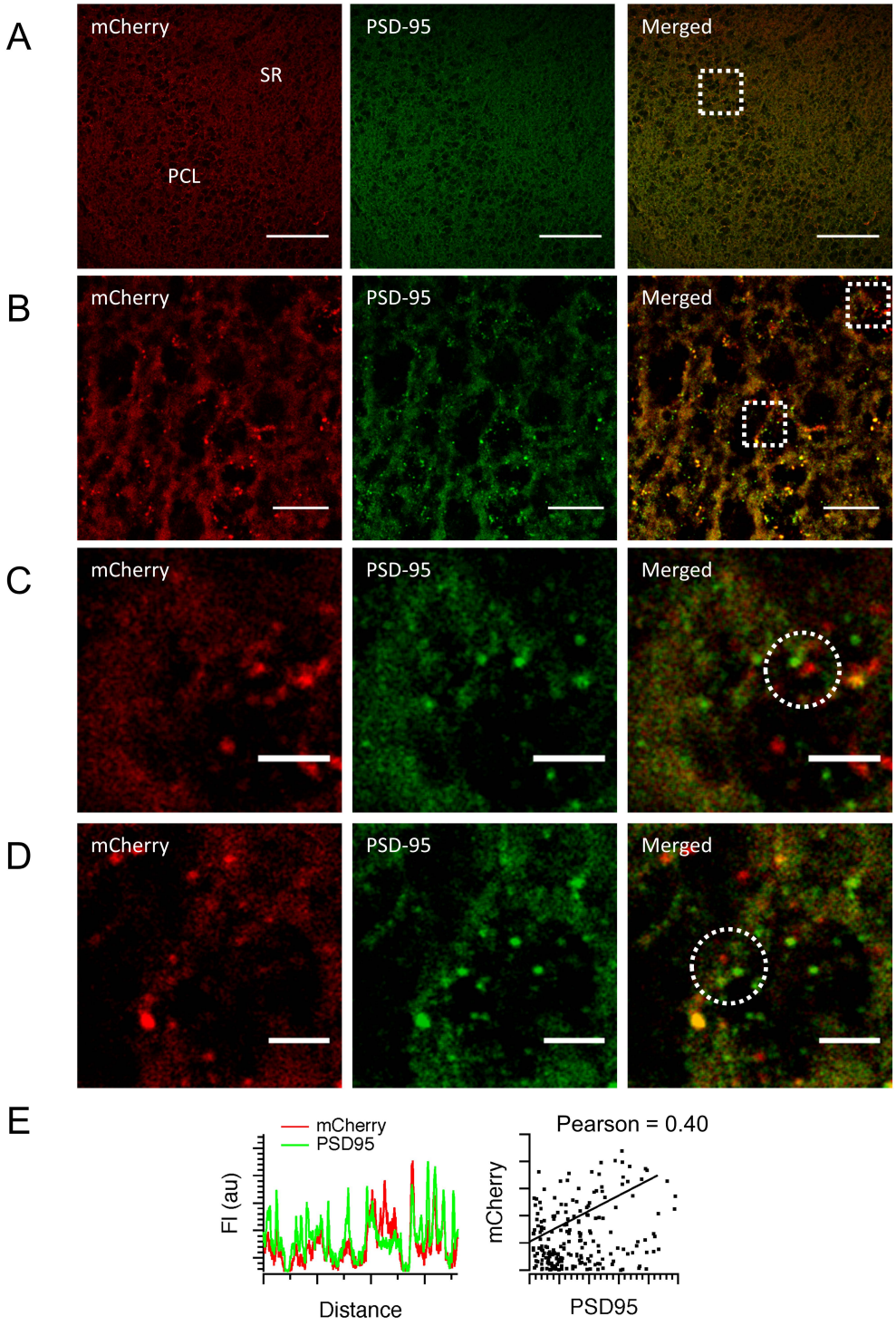

Figure 3.9. Dual staining of mCherry and PSD95 in hippocampal area CA1 of a SyG37 mouse.

Panel A shows double staining of anti-mCherry and anti-PSD95 of horizontal sections from hippocampal area CA1 of a SyG37 mouse. Panels B and C show selected portions of panel A magnified to show the punctate nature of staining. The overlay (right panel) shows an absence of co-localisation between the

mCherry and Anti-PSD95 labelled sides. E, illustrates fluorescence values extracted from lines drawn through punctate regions of the magnified images in B. To the right are graphs showing the relationship between PSD95 and mCherry along with the Pearson correlation. The scale bars for panel A is 100 µm, B is 30 µm and 5 µm for C and D panels.

3.2.4.5 Dual staining of anti-mCherry and anti-vGLUT1 in hippocampal slices of SyG37 mice.

The vesicular glutamate transporter 1 (vGLUT1) mediates glutamate uptake into the synaptic vesicles of excitatory neurones (Bellocchio et al., 2000, Ziegler et al., 2002). In the CNS, vGLUT1 and vGLUT2 are, together, currently considered the best markers for glutamatergic nerve terminals and glutamatergic synapses (Herzog et al., 2006). Therefore, a series of combined labelling experiments for mCherry with vesicular vGLUT1 were performed to identify whether our sensor is expressed in excitatory neurones. Figure 3.10 showed possible co-localisation of SyGCaMP2-mCherry with vGLUT1 in the hippocampal slices, demonstrating that mCherry was present in glutamatergic excitatory presynaptic terminals. Moreover, mCherry was not expressed in all anti-vGLUT1 stained terminals, indicating that mCherry might be expressed in a different neuronal subset of excitatory neurones or inhibitory neurones.

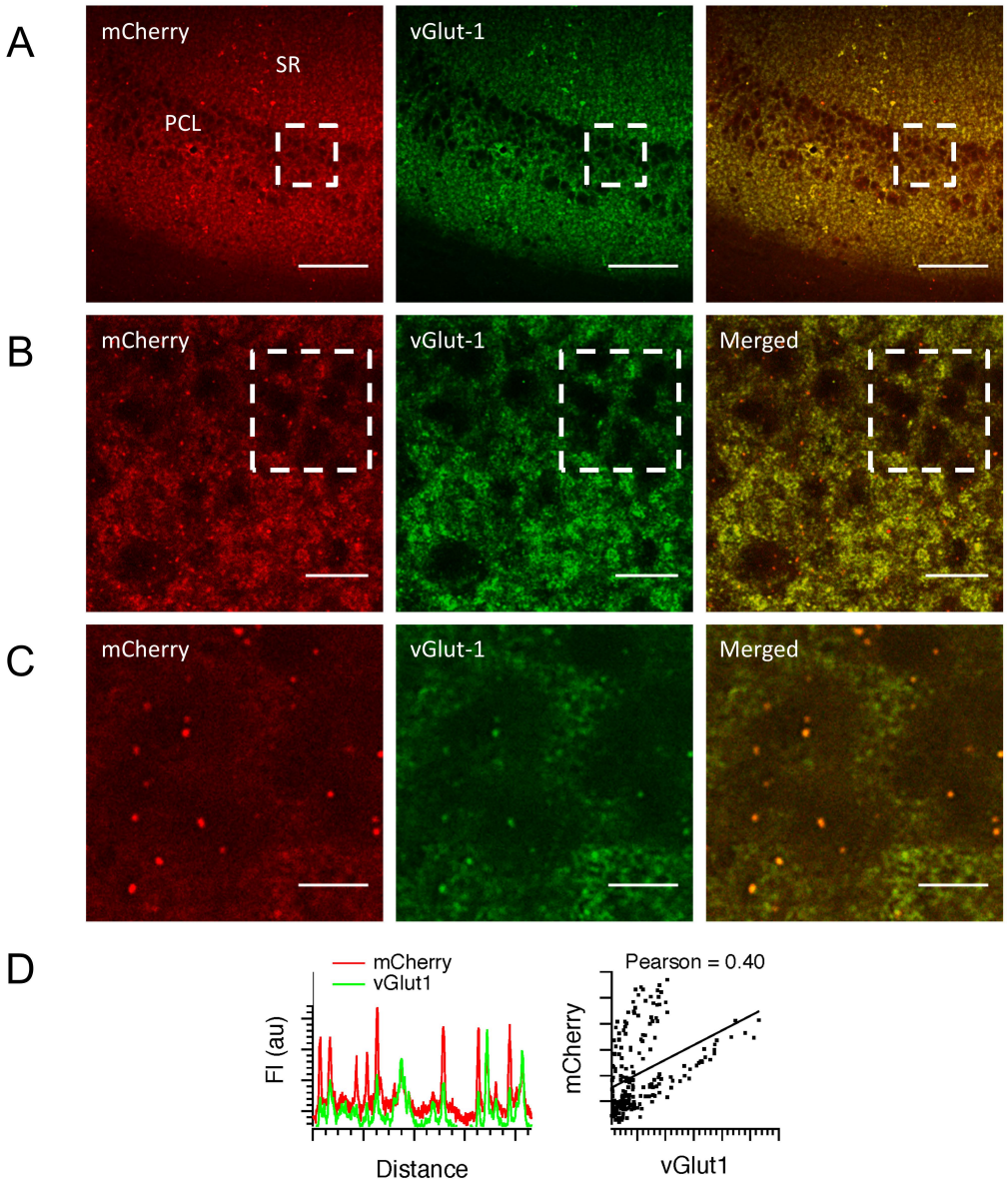

Figure 3.10. Co-localisation of mCherry and vGLUT1 in hippocampal area CA1 of a SyG37 mouse.

Panels A, B and C show different magnifications of double-stained (anti-mCherry and anti-vGLUT1) horizontal sections taken from the hippocampal area CA1 of a SyG37 mouse. The overlay (right panel) shows co-localisation between mCherry and anti-vGLUT1-labelled terminals. D illustrates fluorescence values extracted from lines drawn through punctate regions of the magnified images in B. To the right are graphs showing the relationship between vGLUT1 and mCherry along with the Pearson correlation. The scale bars for panels A, B, and C represent 100 µm, 30 µm and 10 µm, respectively.

3.2.4.6 Dual staining of anti-mCherry and anti-vGAT in hippocampal slices of SyG37 mice.

We next examined whether SyGCaMP2-mCherry was expressed in inhibitory neurones of presynaptic terminals by double staining with mCherry and vGAT. The vesicular GABA transporter (vGAT) is responsible for the uptake and storage of gamma-aminobutyric acid (GABA) and glycine by synaptic vesicles in the central nervous system and can be used as a marker for inhibitory nerve terminals (McIntire et al., 1997, Chaudhry et al., 1998b). Figure 3.11 showed possible co-localisation of mCherry and vGAT labelling in area CA1 of the hippocampal area, demonstrating that mCherry is present in GABA/glycine-inhibitory presynaptic terminals as well.

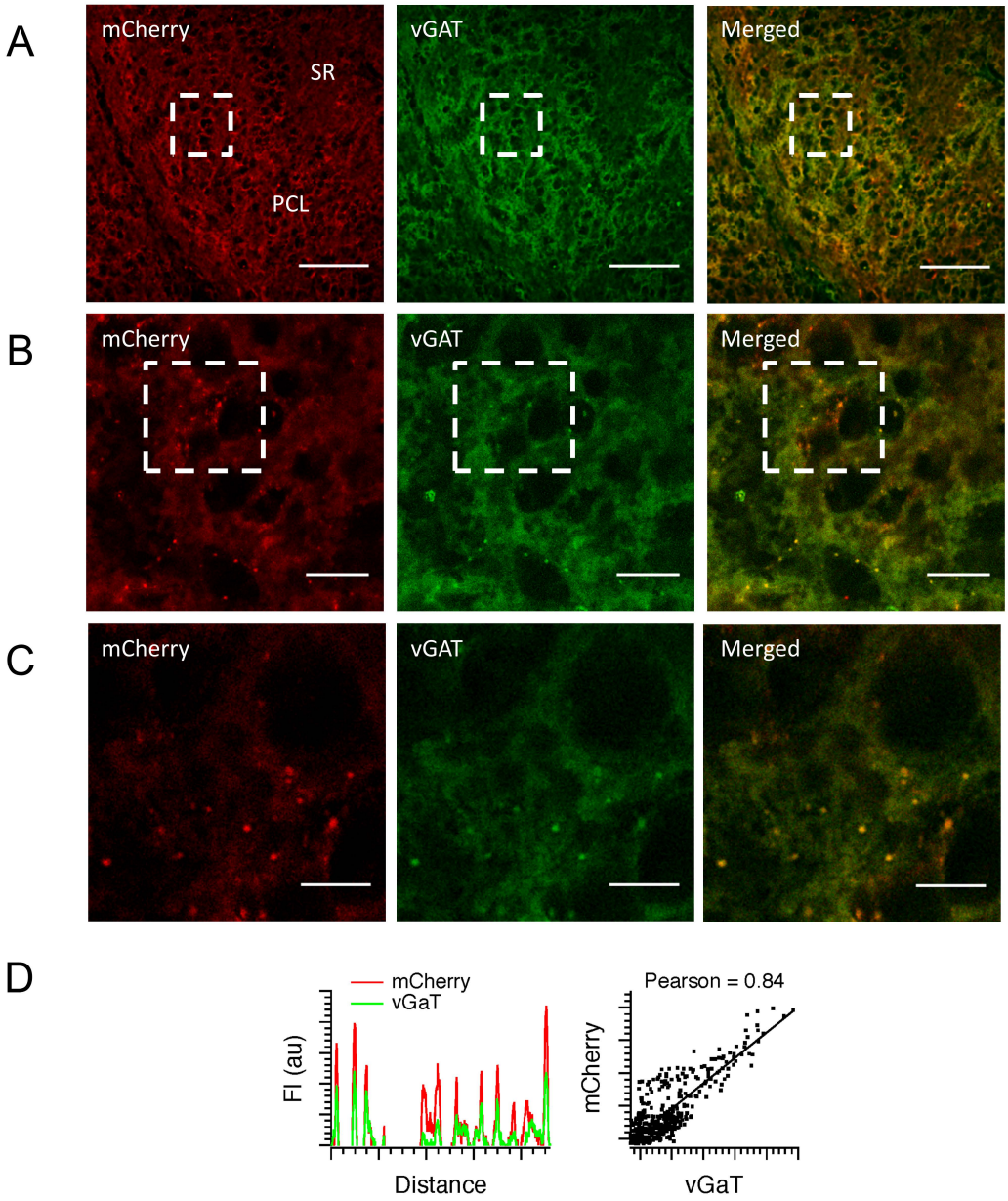

Figure 3.11. Co-localisation of mCherry and vGAT in the hippocampal CA1 area of a SyG37 mouse.

Panels A, B and C show different magnifications of double-stained (anti-mCherry and anti-vGAT-1) horizontal sections taken from the CA1 hippocampal area of a SyG37 mouse. At higher magnification, within the pyramidal cell layer, co-labelling for anti-mCherry and anti-vGAT showed a clear punctate expression around cell bodies and the merged image exhibited possible co-localisation. D illustrates fluorescence values extracted from lines drawn through punctate regions of the magnified images in B. To the right are graphs showing the relationship between vGAT and mCherry along with the Pearson correlation. The

scale bars for panels A, B, and C represent 100 µm, 30 µm and 10 µm, respectively.

3.3 Discussion

3.3.1 mCherry was expressed in the SyG37, but not in SyG14, mouse line.

SyG-mice were screened for SyGCaMP2 gene sequences by PCR of genomic DNA obtained from ear snip lysates according to the methods described above. The PCR technique allowed us to determine the genotype of two mouse lines: SyG14 and SyG37 where both lines were positive (figure 3.1). Using the WB technique, we found that only the SyG37 mouse line displayed a band at the protein size expected for mCherry; 27 kDa (figure 3.2). But work performed by another member of the lab (Dr Roisin Thomas) showed that the SyG37 mouse line displayed a band at the protein size expected for the whole sensor (between 100 and 110 kDa). This might be because of the too harsh conditions during the Western blot experiment that made the mCherry protein became separated from the entire sensor. Nevertheless, the mCherry band was completely absent in SyG14 animals, despite the fact that both mouse lines were healthy with no apparent behavioural abnormality and were born at the expected Mendelian rate in terms of PCR product. These results clearly confirm that the SyG14 mouse model was lacking in, or had undetectable levels of the SyGCaMP2-mCherry sensor. These results are consistent with our imaging data collected from area CA1 of SyG14 and SyG37 mice (see Chapter 4), where SyG14 mice responded in a similar manner to WT mice in terms of their fluorescence signals. The question arises as to why the PCR technique was able to determine the genotype of two mice lines, but the Western blot technique failed to detect mCherry protein expression and, therefore, the SyGCaMP2-mCherry sensor in the SyG14 mouse line. Modulation or failure of gene expression at any of many different stages is possible from DNA-RNA transcription to post-translational modification of a protein. Final gene product stability is also crucial to gene expression levels, where a low expression level could be due to an unstable product. In the case of the SyG14 mouse line, there are many possibilities as to why mCherry remained undetected, including, but not limited to, possible errors in RNA splicing (Berget, 1995, Scotti and Swanson, 2016), failure of the mCherry protein to fold into the intended well-defined three-dimensional structure which usually produces

inactive proteins (Selkoe, 2003) or post-formation protein degradation (Peters *et al.*, 1994, Lodish, 2004).

Low gene expression levels in the world of genetically modified animals seems to be common. Caroni, 1997, who generated a Thy-1 promoter, noted that expression patterns differ considerably among transgenic lines due to the strong genetic context sensitivity of the expression construct. Accordingly, he found that about a fifth of the transgenic lines only displayed a quite generalised expression in neurones (Caroni, 1997). In agreement with Caroni (1997), Chen *et al*. (2012), and others, found that all founder lines that have been generated under Thy1-control differed in levels and patterns of expression. The Thy1-driven transgene is often stochastically and differentially expressed in subsets of neurones in different transgenic lines due to the strong transgenic position effect of the variegation bulb (Feng *et al.*, 2000, Heim, 2005, Young *et al.*, 2008, Chen *et al.*, 2012, Dana et al., 2014). Chen et al. (2012) then decided to focus only on the two mouse lines that have the highest levels of transgene expression, the Thy1-GCaMP2.2c line and the Thy1-GCaMP3 line. Although, in the central nervous system, the transgene expression in these two lines was widespread, there were some notable differences between the two lines. For example, high expression in the olfactory bulb was observed in Thy1-GCaMP3 mice, but not Thy1-GCaMP2.2c mice.

The reasons for these differences in transgene expression and this loss of function are unknown, though there are many possibilities that might explain them. One theory supposes that the use of the combination of calmodulin-M13 as a calcium-binding domain could be responsible for the modification or inactivation of probes encountered in certain expression systems (Heim, 2005). Imaging data from experiments in Drosophila flies, however, did not confirm this hypothesis (Reiff *et al.*, 2005). Hasan *et al*. (2004) attribute this problem to genetic factors such as gene silencing (Redberry, 2006), which is the ability of a cell to prevent the expression of a certain gene, or the formation of protein precipitates in inclusion bodies (Hasan et al., 2004), since this problem is most likely due to intrinsic protein properties as the targeting tag proteins used originate from non-mammalian species (Gradinaru *et al.*, 2010, Madisen *et al.*, 2015).

For more explanation, when genes are knocked out, they are completely removed from the genome of the organism and, thus, have no expression. In contrast, when genes are silenced, which is considered a gene knockdown mechanism, their expression is reduced by at least 70% but is not completely eliminated (Hood, 2004, Mocellin and Provenzano, 2004, Deng *et al.*, 2014). From the above, one could support the idea of the gene-silencing theory because the integrity and the orientation of the clones of SyG14 had already been verified by restriction analysis and DNA sequencing (Muscha and Hartell-unpublished observations). Therefore, one could argue that the SyG14 mouse line has expressed a SyGCaMP2-mCherry gene that can be detected by PCR; however, this expressed gene could not be translated to the target protein, and the Western blot subsequently failed to detect it. Many studies support this postulation, mentioning that there is a lack of any strict correlation between gene expression and protein levels (Guo *et al.*, 2008, Gingold and Pilpel, 2011, Payne, 2015). It is worth mentioning that the SyG14 mouse definitely used to work. Looking at older data, the responses to stimulation were large and possibly larger than those with SyG37. Therefore we think that we lost the sensor expression when the mice were moved to the new animal unit because we bred from a restricted line and at that time, there must have been a mutation in the DNA, since the DNA is still there but expression is lost. This is most likely caused by a mutation which prevented the DNA being transcribed or prevented protein folding/expression so badly that the antibody to mCherry failed to recognise the protein. Therefore transgene expression in mice is unpredictable and always needs to be examined and confirmed experimentally.

3.3.2 Expression patterns and expression levels of SyGCaMP2-mCherry in SyG37 mouse brain.

Since Western blot experiments failed to detect mCherry protein expression in the SyG14 mouse line, this mouse line was excluded from anatomical and immunohistochemical experiments (figure 3.2). Initially, the fluorescence expression patterns of SyGCaMP2 and mCherry in the SyG37 mouse line were explored (figure 3.3). Live coronal slices of SyG37 and WT mice where perfused with aCSF containing a saturating concentration of calcium to ensure that

GCaMP brightness would be maximal, and subsequently examined using standard single photon epifluorescence. The SyG37 mouse model showed a typical Thy1.2-promotor transgene expression distribution where the expression was observed in cortex and hippocampal areas. Cortical layers 4/5 showed strong fluorescence, as did the hippocampal regions DG, CA3, CA1 and subiculum. While, the highest expression was typically seen in the thalamus, expression can be also seen in the hypothalamus (figure 3.4). The yellowish colour in the merged images of SyG37 mice reveal the pattern of expression in both GCaMP2 (green) and mCherry (red) was very similar, demonstrating that GCaMP2 and mCherry are linked and essentially expressed in the same places; co-localised (figure 3.3). Care was taken to flatten the illumination pattern across each of the images that comprised the final stitched montages but the slices moved slightly during image acquisition and so there are some differences in fluorescence that were caused by images moving. What is very clear, however, is that the fluorescence levels were very much lower in WT mice, indicating that SyGCaMP2-mCherry expression is strongly expressed in SyG37 mice (figure 3.3-left panel).

3.3.3 Immunohistochemical characterisation of SyGCaMP2-mCherry sensor in the SyG37 mouse model.

Further morphological characterisation was performed using immunohistochemical methods to confirm whether the sensor was expressed in presynaptic terminals as predicted and, if so, whether it had any preferential expression in excitatory or inhibitory synapses.

3.3.3.1 Antibody validation

All the antibodies used in this study are commercially available and have previously been assessed in both Western blot and immunohistochemistry experiments. With Western blot, they showed bands at the anticipated molecular weights, with no sign of non-specific binding or cross-reactivity being observed (See the following references in the same order for anti-VGAT, anti-PSD95, anti-mCherry, anti-vGLUT1 and anti-Bassoon: Chakrabarti *et al.*, 2007, Guo *et al.*,

2009, Falkner *et al.*, 2016, Chen *et al.*, 2017, Thakar *et al.*, 2017). In this project, we validated two of these primary antibodies ourselves, vGLUT1 and mCherry, using Western blots (figure 3.2). All the antibodies used in this study showed a reasonable degree of specificity in immunohistochemistry experiments at least in as much as we observed little if any non-specific binding of the secondary antibodies (figure 3.5). We were not in a position to verify selectivity using knockout mice except for mCherry for which WT mice can be considered an equivalent of a KO for SyG37 mice (figure 3.6). Some background fluorescence was apparent in all of the experiments, even in the absence of a primary antibody, although this was relatively small (figure 3.5). Brightness levels were carefully matched so that it is possible to compare non-specific background from fluorescence arising from primary antibody binding. In the case of mCherry, images from control slides without primary antibody were still quite bright suggesting that either the antibody was not very selective or that a significant amount of mCherry fluorescence was still present even after fixation (figure 3.5). The greatest challenge we faced in the immunohistochemistry experiments was the expression of autofluorescence in our slides, which makes IHC experiments very difficult as they had to be repeated many times using different protocols. The most common sources of autofluorescence are NADPH and flavins in biological structures such as mitochondria and lysosomes; moreover, collagen and elastin can also contribute to autofluorescence in the extracellular matrix; therefore, autofluorescence interferes with the detection of specific fluorescent signals, as the emission wavelength of the autofluorescent substance can be visible from 425 to 700 nm (Georgakoudi *et al.*, 2002, Zipfel *et al.*, 2003, Monici, 2005, Menter, 2006, Yang and Honaramooz, 2012). Autofluorescence can also be induced by the fixation step, particularly when we use aldehydes as a fixative because they react with amines to generate fluorescent products (Brock *et al.*, 1998, Chen and Barkley, 1998). Therefore, using quenching agents such as glycine and ammonium chloride might be helpful in the reduction of the strong autofluorescence background. With these caveats in mind, these data show that all the primary antibodies used in this study were specific and thus suitable for the investigation of the localisation of the SyGCaMP2-mCherry sensor in brain slices by immunostaining.

3.3.3.2 SyGCaMP2-mCherry is expressed in SyG37 mouse hippocampal slices but not in WT mouse slices.

The expression patterns of SyGCaMP2-mCherry were examined in SyG37 and WT mice, the latter as a control, using immunohistochemical approaches with an antibody raised against mCherry. In order to confirm that the SyGCaMP2-mCherry sensor was expressed presynaptically, we first confirmed that it was not expressed in the cell bodies by co-staining of mCherry with the nuclear stain Hoechst 33342 (Latt and Stetten, 1976); the reason for choosing the Hoechst 33342 dye in particular is that it shows a considerable Stokes shift between the excitation and emission spectra (Excitation at 350 nm and emission at 461 nm) that makes it useful in multi-staining experiments (Haugland *et al.*, 2005). Immunostaining also showed that there was no labelling for mCherry in wild-type mouse hippocampal slices (figure 3.6-A). In contrast, immunostaining showed mCherry expression in SyG37 mouse hippocampal slices with a clear punctate expression around but never inside the Hoechst-stained areas (figure 3.6-B & C). mCherry was shown to be expressed throughout the hippocampus of SyG37 mice with a strong punctate expression, suggesting a presynaptic distribution. Puncta were clearly observed in CA1, CA3, DG and subiculum (figure 3.7), indicating that they can be used to investigate all of the pathways within the hippocampus that make up the trisynaptic pathway from the entorhinal cortex to the subiculum. Labelling for mCherry showed a clear expression around cell bodies within the pyramidal cell layer. The location around cell bodies might suggest expression in the inhibitory terminals that tend to form in such regions (Megías *et al.*, 2001, Spruston, 2008).

3.3.3.3 SyGCaMP2-mCherry co-localises with the presynaptic, excitatory and inhibitory marker proteins, in the CA1 hippocampal area of SyG37 mice.

Having characterised mCherry's localisation and expression in the SyG37 mouse hippocampus, a series of double-labelling experiments were performed with mCherry and specific synaptic markers (Bassoon, VGluT1 and vGAT). Bassoon is a presynaptic protein involved in the organisation of the neurotransmitter release site, and is specifically localised at the active zone. In cultured hippocampal neurones, bassoon was found to co-localise with glutamate receptor-1 (GLUR1) and GABA (A) receptors and, therefore, is considered to be a component of the active zone of both excitatory glutamatergic and inhibitory GABAergic synapses (Richter et al., 1999). The vesicular glutamate transporter 1 (vGLUT1), and the related vGLUT-2 are both highly important transporters for the uptake and storage of glutamate, and thus comprises the sole determinant for a glutamatergic phenotype. The vesicular glutamate transporter mediates glutamate uptake into the synaptic vesicles of excitatory neurones (Bellocchio et al., 2000, Ziegler et al., 2002). In the CNS, their expressions seem to be largely complementary. Together, they are currently considered as the best markers for glutamatergic nerve terminals and glutamatergic synapses. VGLUT1 is preferentially expressed in the neocortex and hippocampus, while vGLUT2 mainly occurs in the thalamus (Herzog et al., 2006). The vesicular GABA transporter (VGAT) is responsible for the uptake and storage of gamma-aminobutyric acid (GABA) and glycine by synaptic vesicles in the central nervous system (McIntire et al., 1997, Chaudhry et al., 1998b). As illustrated in figures 3.8, 3.10 and 3.11, the merged images show an extensive co-localisation of mCherry and bassoon, vGLUT-1 and vGAT labelling in the hippocampal slices, respectively, directly demonstrating that mCherry was present in presynaptic terminals in both, excitatory and inhibitory terminals. However, bassoon labelling was distributed more broadly than mCherry labelling, suggesting that mCherry was strictly confined to the active zone but was not expressed in all presynaptic terminals. It is worthwhile noting that Zander *et al.* (2010) found that immunogold double-labelling revealed coexistence of vGLUT1, vGLUT2, and VGAT in mossy

fibre terminals of the hippocampal CA3 area which might explain the co-localisation of our sensor with both vGLUT1 and VGAT presynaptic proteins.

3.3.3.4 SyGCaMP2-mCherry does not co-localise with the postsynaptic marker protein, PSD95, in the hippocampal CA1 area of SyG37 mice.

We also examined mCherry and postsynaptic density protein (PSD95) co-localisation to confirm that our sensor was expressed presynaptically in excitatory synapses, but not postsynaptically. PSD95 is the most abundant scaffolding protein, almost exclusively located in the postsynaptic density (PSDs) of neurones. PSD95, which is a member of the membrane-associated guanylate kinase (MAGUK) family, interacts with the cytoplasmic tail of NMDA receptor subunits and potassium channel clusters to regulate synaptic plasticity associated with NMDA receptor signalling (Hunt et al., 1996, Garner et al., 2000, Kim and Sheng, 2004, Chen et al., 2011). Our results show the absence of co-localisation between mCherry and anti-PSD95 labelled spins in the hippocampal slices, where PSD95 labelling is particularly dense in dendrites of pyramidal neurones in the *stratum radiatum* of area CA1 (figure 3.9). These data confirm our findings that mCherry is not localised in the dendrites of the pyramidal cells of area CA1, and indicate its presynaptic location.

3.4 Conclusion

The results presented in this chapter have provided a description of the expression and localisation of the SyGCaMP2-mCherry sensor in the SyG37 mouse hippocampus. WB data showed that the SyG14 mouse model seemed to either be completely lacking in, or have otherwise undetectable levels of the SyGCaMP2-mCherry sensor. Therefore, it was excluded from expression and immunohistochemistry experiments. By examining the subcellular co-localisation with several pre- and post-synaptic markers, we have shown that there is very strong evidence that SyGCaMP2-mCherry expression within the hippocampus is presynaptic and likely to be present in both inhibitory and excitatory terminals. This validation allows us to thoroughly investigate hippocampal physiology in the next chapters.

CHAPTER 4: A Comparative evaluation of organic dyes and intrinsic fluorescence with the SyGCaMP2-mCherry sensor expressed in the SC-CA1 pathway of the SyG37 transgenic mouse model.

4.1 Introduction

In this study, we have used SyG37 mice to examine how presynaptic calcium contributes to normal synaptic transmission in the SC-CA1 pathway within the CA1 region of the hippocampus and how presynaptic calcium homeostasis is altered during synaptic plasticity. For this, we set our sensor a real challenge, the nature of which required an evaluation of the suitability of the SyG37 mouse model for measuring presynaptic activity in both short- and long-term synaptic plasticity. In the first part of this chapter, we performed a basic characterisation of the SC-CA1 pathway in SyG37 mice to varying stimulus intensity, number and frequency. In the second part, we examined the effects of pharmacological manipulations that are known to affect synaptic transmission through presynaptic effects, and attempted to establish whether these manipulations led to an associated change in SyGCaMP2 fluorescence. We first chose to examine the effects of adenosine, an agonist at adenosine receptors, as this has been shown to reduce synaptic transmission at CA1 synapses through presynaptic processes (Wu and Saggau, 1994). Next, we examined the effects of the adenosine receptor subtype 1 antagonist DCPCX in both the absence and presence of adenosine. All adenosine receptor modulation experiments were repeated after blocking synaptic transmission with AP5, NBQX and picrotoxin which inhibit NMDA, AMPA and $GABA_A$/Glycine receptors, respectively. The reason for blocking synaptic transmission was to isolate responses of SCs terminals from those from secondary/tertiary neurones that were activated through synaptic or polysynaptic transmission. We reasoned then that this would reveal the presynaptic effect on calcium of each of the drug manipulations used. After that, we used multiphoton microscopy to examine the calcium transients measured at individual presynaptic boutons in the CA1 area using the SyGCaMP2 sensor. The third part of this chapter was aimed at examining whether manipulation of the cAMP-PKA signalling cascade affected presynaptic calcium. Forskolin, a

promotor of adenylyl cyclase activity, combined with rolipram, a type IV phosphodiesterase inhibitor, are known to enhance spontaneous transmitter release in many brain regions, including the calyx of Held (Kaneko and Takahashi, 2004), parallel to Purkinje cell synapses in the cerebellar cortex, mossy fibre synapses in the CA3 region of the hippocampus as well as facilitating postsynaptic potentiation within the CA1 region (Lu and Gean, 1999, Otmakhov et al., 2004). Therefore, we wished to first examine whether forskolin induced changes in synaptic transmission within the CA1 area, and second whether these were associated with changes in presynaptic calcium signalling. For this, a combination of imaging (SYG37, SyG14 mice and Fluo-4 calcium indicators) and field potential recordings were carried out in the hippocampal CA1 area using electrical and pharmacological stimulation. Imaging data were used to assess the basic kinetics of calcium signalling by measuring the peak response, the initial slope, the area under the curve and the decay constant, tau. Therefore, we had the opportunity to localize SyGCaMP2-mCherry sensor and to simultaneously explore the synaptic transmission, modulation within the SC-CA1 pathway. Moreover, we examined the relationship between presynaptic calcium levels and postsynaptic potentials during normal synaptic transmission, paired-pulse facilitation (PPF), and chemically induced long-term plasticity in CA3-CA1 synapses of the hippocampus.

4.2 RESULTS

4.2.1 Electrode positions for SC-CA1 pathway activation and recording.

Figure 4.1-A shows a schematic drawing of the hippocampus with its different regions, DG, CA3, CA1 and subiculum, and its different microcircuits that connect the entorhinal cortex to the subiculum, forming what is often referred to as the trisynaptic pathway. Image 4.1-B was obtained using a x20 objective on an upright microscope and shows the CA1 region where recordings were made. This light transmission image shows the different layers in area CA1; *st. oriens*, *st. pyramidale*, *st. radiatum* and *st. lacunosum moleculare*. It also shows the positions of the stimulating and recording electrodes. A micromanipulator was used to place the stimulating electrode between the CA3 and CA1 areas to stimulate the SCs fibres. A recording electrode was placed in the *stratum radiatum* of the CA1 region. To compare between electrophysiology and imaging experiments, fluorescence and field potential recordings were taken from the same field of view, and an example trace of a fEPSP is shown in figure 4.1-C. In CA1 area experiments, an NMDA-dependent long-term potentiation could arise as a result of repeated stimulation and so the selective NMDA receptor antagonist DL-AP5 was added to the aCSF in all experiments to prevent this phenomenon (Collingridge et al., 1983).

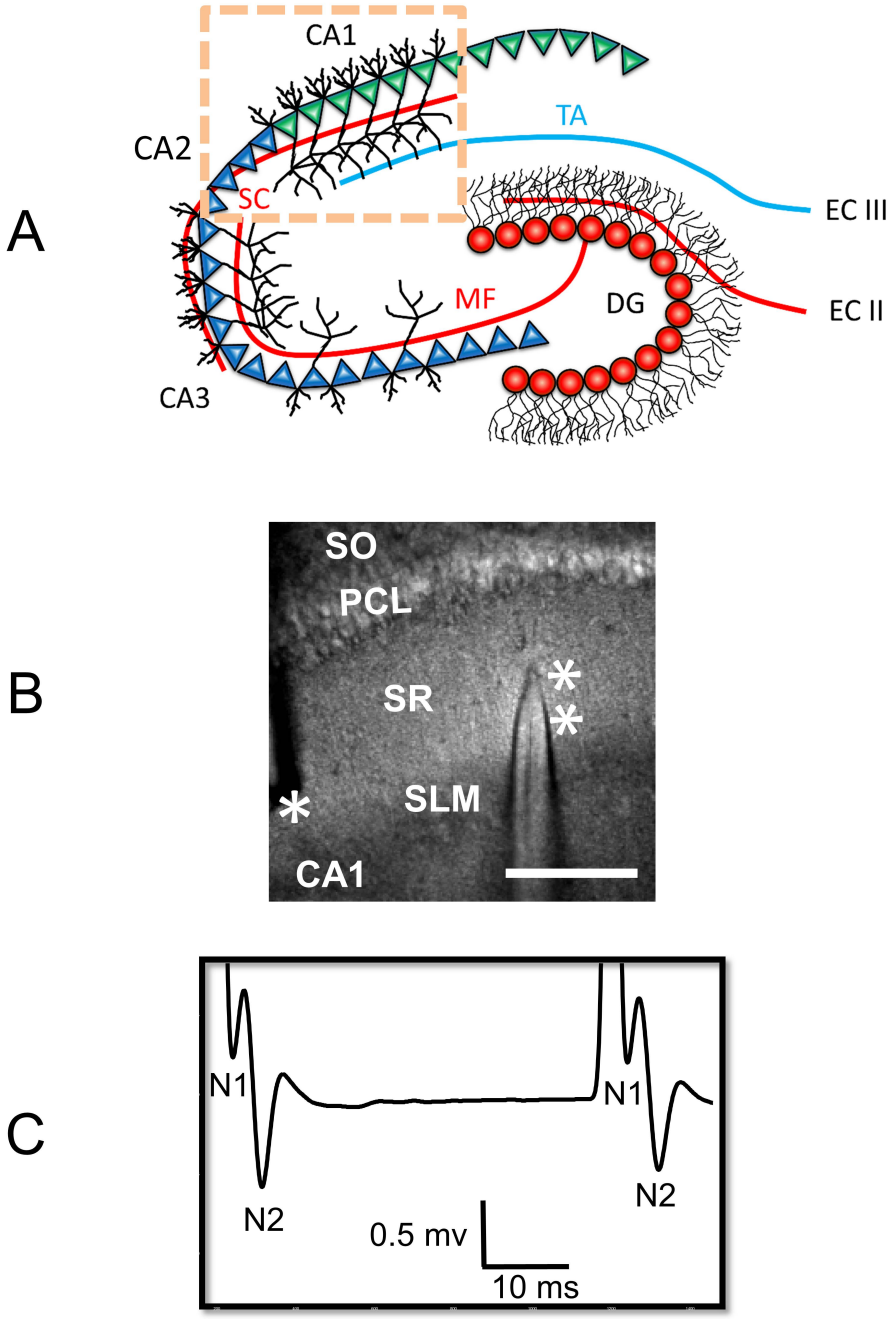

Figure 4.1. Schematic drawing of a transverse section of the mouse hippocampus and a transmission image of the CA1 area of a hippocampal slice showing electrode positions and a sample fEPSP trace recorded from the same area.

A. shows a schematic diagram of a transverse section of the mouse hippocampus. B. shows the light transmission image of a transverse section of SyG37 mouse CA1 region of the hippocampus illustrating stimulating and recording electrode positions indicating the different layers and regions of the

hippocampal CA1 area which contains the following layers: SO = *stratum oriens*, PCL = *pyramidal cell layers*, SR = *stratum radiatum* and SLM= *stratum lacunosum moleculare*, the EC = *entorhinal cortex*. The single asterisk indicates the stimulating electrode position and the double asterisks indicate the recording electrode position. C. shows the N1 and N2 components of the field recordings in the *stratum radiatum* of the hippocampal CA1 area as a result of the SCs activation. The scale bar in B is 50 µm.

4.2.2 Electrical activation studies of the SC-CA1 pathway of SyG37 mouse model expressing SyGCaMP2-mCherry sensor.

Little work has been done on presynaptic calcium monitoring or measurement to date because it is difficult to target calcium sensors to presynaptic terminals because of their size. In this study, we aimed to use the SyGCaMP2-mCherry sensor to characterise the properties of presynaptic calcium signalling upon activation of the SC-CA1 pathway. In this part of this chapter, we define the optimal stimulus intensity, number and frequency that would evoke consistent and physiologically relevant responses. To achieve this, each variable was independently altered and the effects on responses recorded.

4.2.2.1 The effects of altering the stimulus intensity on the SC-CA1 pathway of the SyG37 mouse model.

We first established the stimulus strengths required to reliably activate the SC/CA1 pathway for optical and electrophysiological responses during SC-CA1 pathway activation. For this, the stimulus intensity was increased gradually from 0 to 70 V using a fixed stimulus number (20 stimuli) at a fixed frequency (20 Hz). Figure 4.2, obtained from the CA1 hippocampal area of a slice taken from a SyG37 mouse, provides an example of the effects of increasing stimulus intensity on SyGCaMP2 fluorescence after SC/CA1 activation. As mentioned previously, the first step in the data analysis was splitting the interleaved image stacks into two separate image stacks; one for SyGCaMP2 and the other for mCherry; however, only the SyGCaMP2 images were analysed in this particular study. As an exception, in the following example, we analysed mCherry images as well, to

show that mCherry fluorescence is not sensitive to presynaptic calcium changes (figure 4.2-A). SyGCaMP2 was, on the other hand, very sensitive to any changes in presynaptic calcium, as can be seen from the larger changes in fluorescence intensity indicated by brighter colours recorded at 70 V, as shown in figure 4.2-B.

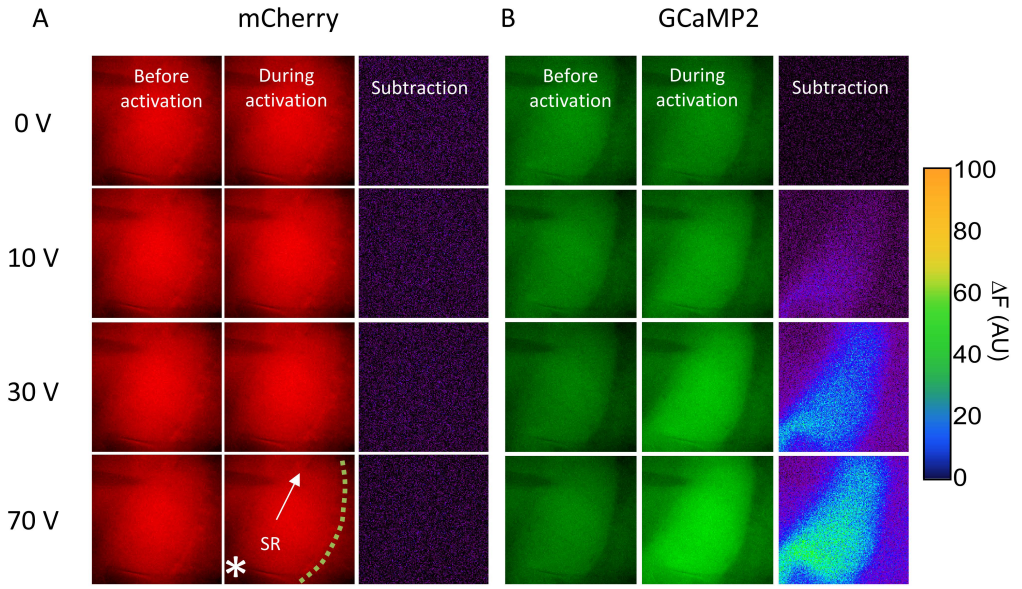

Figure 4.2. Visualization of the effect of increasing stimulus intensity on both SyGCaMP2 and mCherry fluorescence after SC/CA1 activation in the hippocampal CA1 region of a SyG37 mouse.

Images of mCherry and SyGCaMP2 fluorescence were collected before and during SC/AC stimulation at different stimulus intensities (20 stimuli at 20 Hz). A. shows the averages of three consecutive mCherry images taken immediately before stimulation (left panel). These were subtracted from the peak responses taken during (middle panel) electrical stimulation to create a subtraction image right hand panel. B. SyGCaMP2 images were collected and illustrated in the same way. A warm/cold look up-table (right panel) was used to illustrate the difference in the size of the responses in both. Larger changes in fluorescence, and assumed calcium concentration are indicated by brighter colours in the SyGCaMP2 images. The asterisk indicates the stimulating electrode position and the border between the pyramidal cell layer (to the right) and *stratum radiatum* (to the left) is shown as a dotted line. The white arrow in A shows the schaffer collateral pathway direction.

By analysing images of SyGCaMP2 using Igor Pro software, we were able to quantify these effects and assess the basic kinetics of fluorescence changes by measuring the peak response, the time taken to reach the peak, the slope, the area under the curve and the decay constant (tau) of fluorescence values from regions of interest, converted in F/F_0 (figure 4.3). Data where normalized to 20 V as this stimulus strength was much less than the maximum but gave consistent and robust responses in the more linear part of the intensity-response curve. Therefore, this normalization of data might help us to hold a direct comparison between different hippocampal areas, later. Altering the stimulus intensity increased the peak amplitude of the fluorescence response in a roughly linear manner up to about 20 V after which responses in the *stratum radiatum* tended towards a plateau eliciting a near maximal response at 70 V which was approximately 165% of the response measured at 20V. It is unlikely that responses would reach a complete maximum because increasing intensities will simply recruit more and more fibres, further from the stimulus electrode (figure 4.3-B). The initial slopes of the rising phase of the SyGCaMP2 fluorescence responses to stimulation were also measured. The effects of increasing stimulus intensity were similar to those of the peak responses (~170% of the response at 20V); this measure has the advantage of being less susceptible to either saturation of the sensor or the synapse during prolonged or high-frequency stimulation (figure 4.3-C). At these intensities, frequencies and stimulus numbers, the similarity between peak and slope responses suggests that little or no saturation of either kind occurred. The area under the curve (AUC) was also measured. Again these were very similar to those of the peak responses as shown in figure 4.3-D. The decay time constant was also measured by measuring the time to recover to 63% of the peak where there no effect of increasing stimulus intensity on the 63% decay time of SyGCaMP2 fluorescence was observed, as shown in figure 4.3-E.

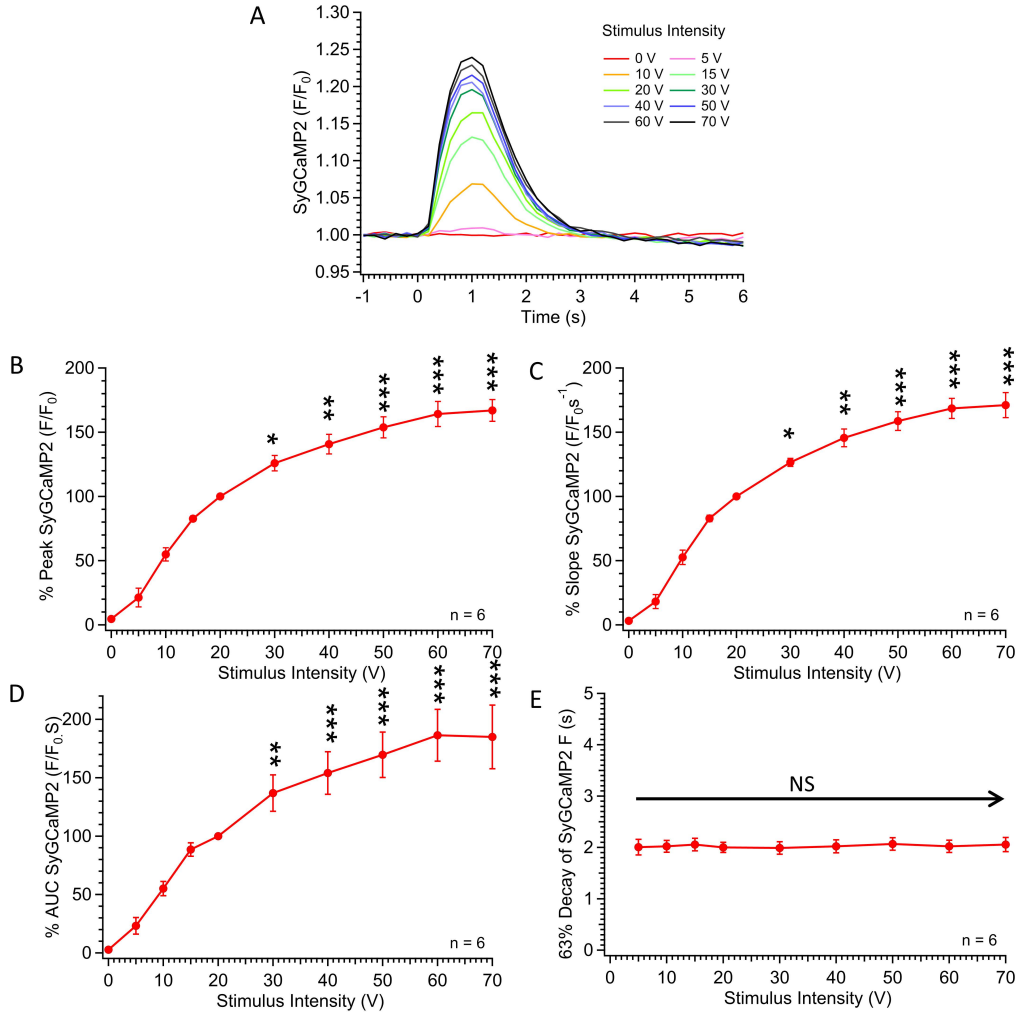

Figure 4.3. The effect of increasing stimulus intensity on SyGCaMP2 fluorescence in the hippocampal CA1 region after SC/CA1 activation.

A. shows the mean responses to different stimulus intensities from ROIs placed within the *stratum radiatum* of the CA1 hippocampal region plotted against time. Panels B to E illustrate the effects of increasing stimulus intensity on peak (B), slope (C), AUC (D) and 63% decay time (E). Values in B-D are normalized to the response at 20 V. The means and standard errors from 6 separate experiments are shown. The statistical test were performed between 0V and other stimulus intensities. (B), 30V, P=0.0120; 40V, P=0.0120; 50V, P=0.0120; 60V, P=0.0120; 70V, P=0.0120; (C), 30V, P=0.0211; 40V, P=0.0014; 50V, P=0.0001; 60V, P=<0.0001; 70V, P=<0.0001; (D), 30V, P=0.0052; 40V, P=0.0009; 50V, P=0.0002; 60V, P=<0.0001; 70V, P=<0.0001; Kruskal-Wallis test followed by Dunn's multiple comparisons test; (E), no significant difference, Ordinary one-way ANOVA followed by Dunnett's multiple comparisons test.

Field potential recordings produced results that were entirely consistent with the imaging results. The N2 component of the field potential curve was also increased by increasing the stimulus intensity. A stimulus intensity of 20 V produced a distinct and characteristic field potential response which increased with intensity and did not show signs of saturation even at 70V. The paired-pulse ratio was also affected, but non-significantly, by changing the stimulus intensity, especially at 60 V as shown in figure 4.4. It is worth mentioning that whenever the stimulus intensity was increased, the SEM increased as well, showing high variation between individual slice mean responses; it should be noted that this was not the case for the imaging data where individual responses were remarkably consistent leading to relatively small SEM values even at higher stimulus intensities. The N1 component of the field potential curve will be presented with different set of data later to show the effect of increasing the stimulus intensity on the presynaptic fibre volley as well. Both imaging and electrophysiology results show that the supra-threshold is not clear as there was no saturation, as can be seen in figures 4.3 and 4.4. On the other hand, the impact of increasing stimulus intensity on SyGCaMP2 fluorescence is much lower than its impact on the N2 component of the fEPSP; this may reflect the non-linear relationship between presynaptic calcium and transmitter release such that a small increase in presynaptic calcium can lead to a large increase in synaptic transmission. For example, when the peak amplitude of SyGCaMP2 (F/F_0) at 70 V was 165% of the response at 20 V, the peak amplitude of field potential was 250% at the same voltage with a ratio of ~ 3:5.

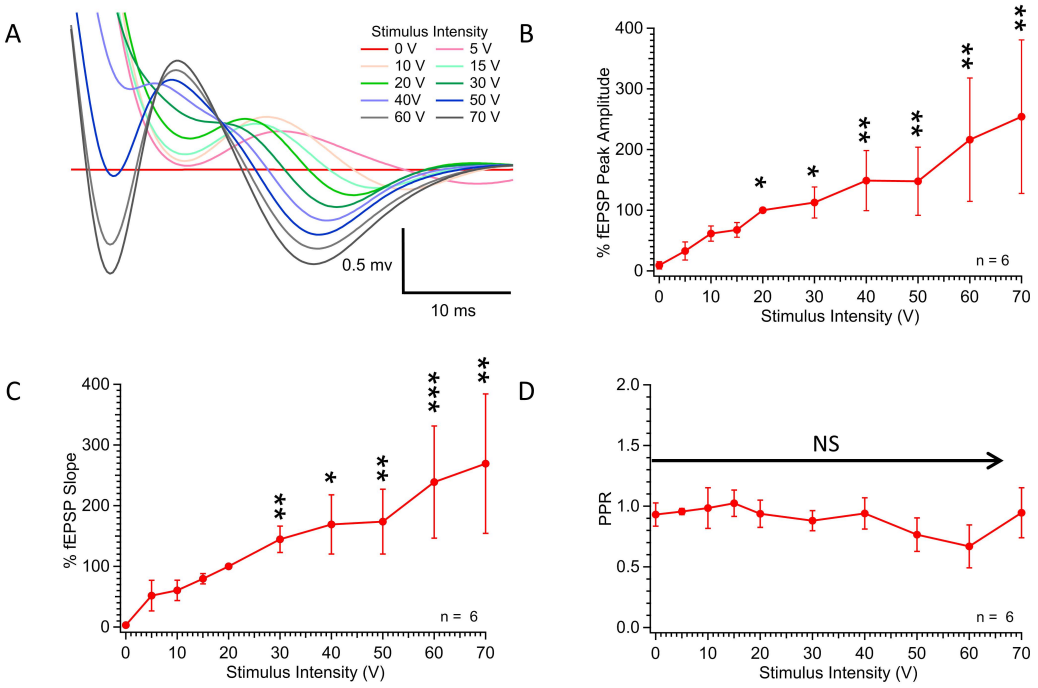

Figure 4.4. The effect of increasing stimulus intensity on fEPSP in the hippocampal CA1 region after SC/CA1 activation. A. shows the field potential curve illustrating the action of increasing stimulus intensity on SC/CA1 activation, where the trace depicts the average of six sweeps. B., C. and D. show the change in peak amplitude, slope and PPR of field excitatory postsynaptic potentials (fEPSPs) during increasing stimulus intensity, respectively. The values shown in B and C are normalized to response at 20 V. The means and standard errors from 6 separate experiments are shown. The statistical test were performed between 0V and other stimulus intensities. (B), 20V, P=0.0101; 30V, P=0.0261; 40V, P=0.0035; 50V, P=0.0095; 60V, P=0.0120; 70V, P=0.0120; (C), 30V, P=0.0067; 40V, P=0.0127; 50V, P=0.0020; 60V, P=0.0009; 70V, P=0.0014, Kruskal-Wallis test followed by Dunn's multiple comparisons test; (D), no significant difference was observed, Ordinary one-way ANOVA followed by Dunnett's multiple comparisons test.

Next, we examined the correlation between peak SyGCaMP2 fluorescence and the corresponding field excitatory postsynaptic potential whilst changing the stimulus intensity in the SC-CA1 pathway. Figure 4.5 indicates the peak amplitude of the N2 component of the field EPSP is approximately proportional to SyGCaMP2 fluorescence, which represents the change in presynaptic Ca^{2+}.

The relationship between the amplitude of the SyGCaMP2 fluorescence and the amplitude of the corresponding field EPSP was approximately linear, where a direct correlation between peak amplitude and the SyGCaMP2 fluorescence peak was observed, and had an R^2 values of 0.86 (figure 4.5-A). The linearity of the correlation appears to reduce over the final two stimulus intensities, i.e., at 60 V and 70V, showing the possibility of the sensor saturation at those stimulus intensities. In figure 4.5-B, we excluded those final two stimulus intensities to see an improved correlation with R^2 values of 0.96.

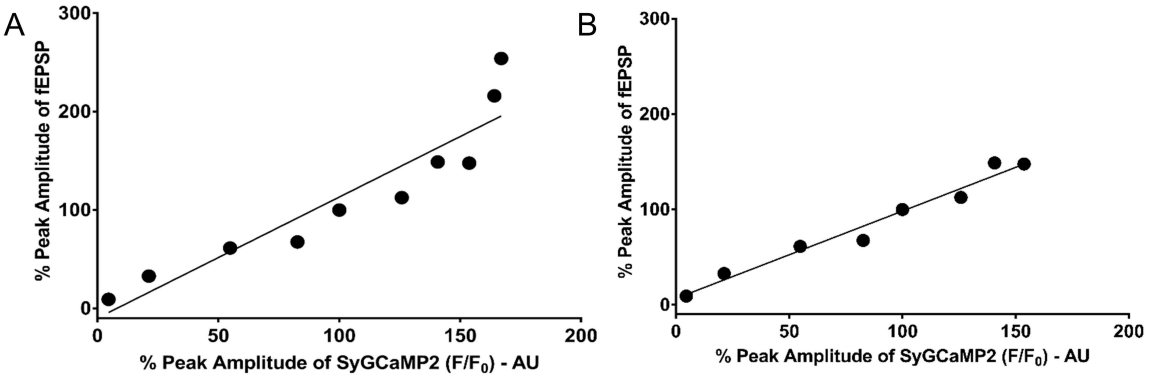

Figure 4.5. The relationship between SyGCaMP2 fluorescence and the corresponding fEPSP at different stimulus intensities.

A shows a scatter plot of the relationship between the peak amplitudes of SyGCaMP2 fluorescence (presynaptic Ca^{2+}) and the peak amplitudes of fEPSP. A linear regression line was fitted (r = 0.96) using the equation Y = 1.231*X - 9.841. B shows the same scatter plot in A, but without final two stimulus intensities (r = 0.98; Y = 0.9164*X + 6.703). Each group of data in this figure was collected from six experiments; data were recorded during the sequential application of 0, 5, 10, 15, 20, 30, 40, 50, 60 and 70 V.

4.2.2.2 The effects of altering the stimulus frequency on the SC-CA1 pathway of the SyG37 mouse model.

The second step in our electrical activation studies was aimed at first testing the effects of changing stimulus frequency on SyGCaMP2 fluorescence and its corresponding fEPSP, and second to determine the optimal stimulus frequency for use in our experiments. For the latter, we have tested different frequencies at a fixed stimulus intensity of 20 V and using a fixed stimulus number of 20. The

same parameters as described in the previous section were analysed. Imaging data showed that the peak amplitude and the initial slopes of the rising phase of SyGCaMP2 fluorescence responses increased in a roughly linear manner up to ~ 10 Hz in the *stratum radiatum* and then reached a plateau at around 50 Hz. There was a decline in the peak SyGCaMP2 fluorescence at 100 Hz as shown in figure 4.6-A, B and C. The decay time was also measured by measuring the time to recover to 63% of the peak value, where an inverse relationship between the increase in stimulus frequency and the 63% decay time of SyGCaMP2 fluorescence was observed (figure 4.6D).

In this example of the field potential recordings, only the last pulse in the train of the field potential was measured. The peak amplitude and the slope of the N2 component were non-significantly increased, by increasing the stimulus frequency with the 15-20 Hz required to elicit a suitable response in the stratum radiatum and 100 Hz eliciting a maximal response, as shown in figure 4.6-E, F and G. This is unlike what happened with the SyGCaMP2 fluorescence, which decreased slightly at 100 Hz. Moreover, the effect at lower frequencies is more pronounced for SyGCaMP2 fluorescence than on field potential recordings.

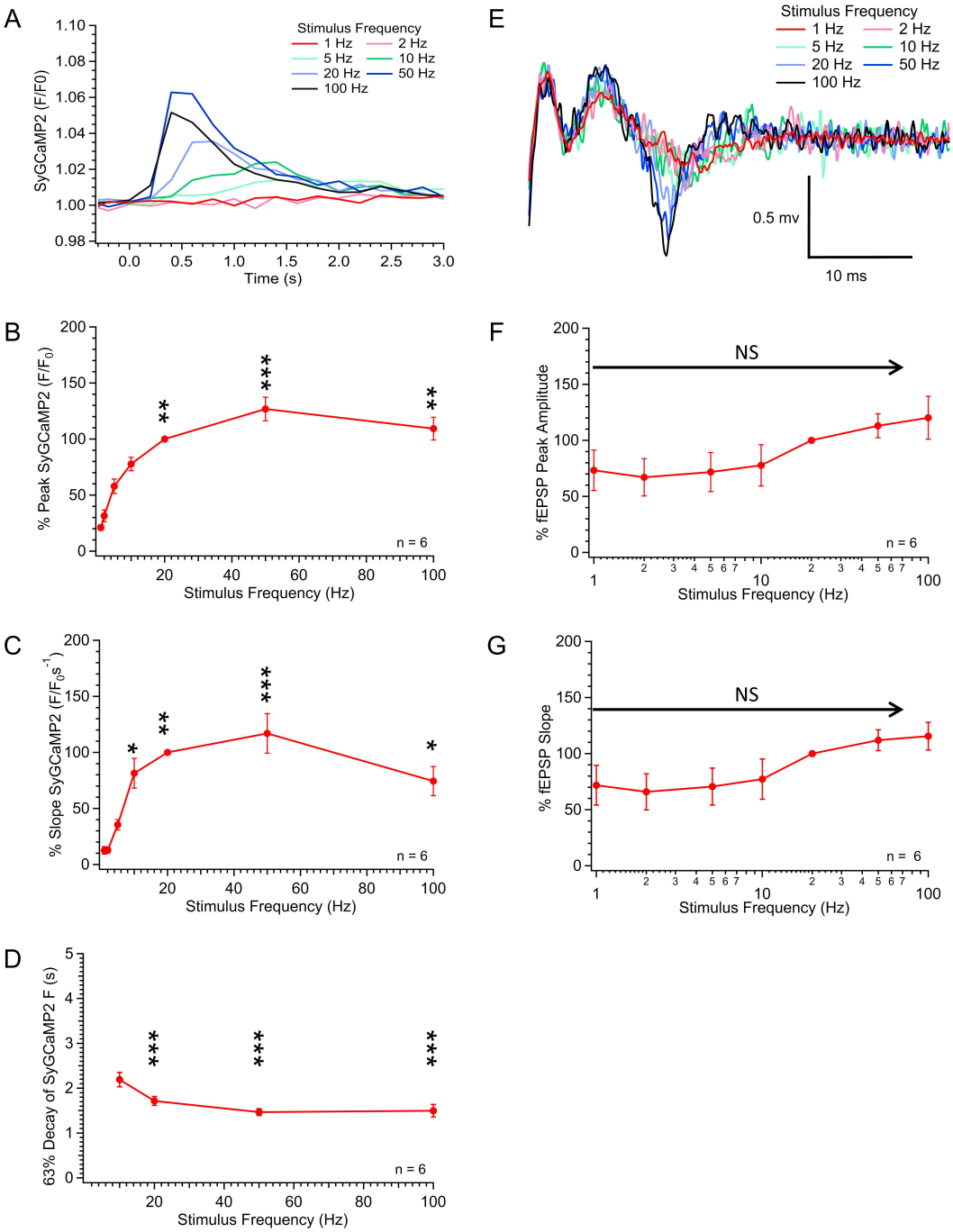

Figure 4.6. The effect of increasing stimulus frequency on both SyGCaMP2 fluorescence and its corresponding fEPSP in the hippocampal CA1 region in response to SC activation.

A. shows the mean responses to 20 stimuli delivered at 20 V over a range of different stimulus frequencies from ROIs placed within the *stratum radiatum* of the CA1 hippocampal region plotted against time. B. to D. illustrate the effects of increasing stimulus frequency on Peak (B), slope (C), and 63% decay time (D)

over time for SyGCaMP2 fluorescence, respectively. E. shows field recordings of the last one sweep in the train illustrating the action of increasing stimulus frequency on SC/CA1 activation. F & G show the change in peak amplitude and slope of field excitatory postsynaptic potentials (fEPSPs) whilst increasing stimulus frequency (logarithmic scale). The values shown in B, C, F and G are normalized to the response at 20 Hz. The means and standard errors from 6 separate experiments are shown. The statistical test were performed between 1Hz and other stimulus frequency. (B), 20Hz, P=0.0029; 50 Hz, P=<0.0001; 100 Hz, P=0.0011; (C), 10 Hz, P=0.0376; 20 Hz, P=0.0029; 50 Hz, P=0.0002; 100 Hz, P=0.0261; Kruskal-Wallis test followed by Dunn's multiple comparisons test; (D), F=27.5; 10 Hz, P=0.0001; 20 Hz, P=0.0001; 50 Hz, P=0.0001; 100 Hz, P=0.0001; Ordinary one-way ANOVA followed by Dunnett's multiple comparisons test. Electrophysiology data showed no significant difference, Kruskal-Wallis test followed by Dunn's multiple comparisons test.

4.2.2.3 The effects of altering the stimulus number on the SC-CA1 pathway of the SyG37 mouse model.

The third step in our study on the characterisation of responses to electrical stimulation was to test the effects of changing the stimulus number on SyGCaMP2 fluorescence and its corresponding fEPSP. For this, we tested different numbers of stimuli delivered at 20 Hz and 20 V. Both the peak amplitude and the initial slopes of the rising phase of the SyGCaMP2 fluorescence responses increased with increasing stimulus number (figure 4.7-A, B and C). Increasing the stimulus number from 1-15 AP increased the peak SyGCaMP2 fluorescence in a roughly linear manner. Further increases in stimulus number were not linear and reached a plateau at around 30 stimuli. Although the peak response only declined slightly with 100 stimuli, the shape of the response clearly altered. The initial slope of the response remained linear up to 20 stimuli. The time taken to recover from 63% of the peak was also measured and there was a positive relationship between the increase in stimulus number and the 63% decay time constant of SyGCaMP2 fluorescence. These results are confirmed by the AUC results, which show the same trend as the 63% decay time (figure 4.7-D and E).

Field potential recordings were not exactly consistent with imaging data. The peak amplitude and the slope of the N2 component of field potential increased with increasing stimulus intensity. The peak response reached near maximum after 30 stimuli, followed by a small decline at 100 stimuli (figure 4.7-F and H). It is worth mentioning that the slope of fEPSP shows a clear deeper decline at later stimulus number in each series. In general, as for the stimulus frequency results, the effect at lower stimulus numbers is more pronounced on SyGCaMP2 fluorescence than on field potential recordings. The SyGCaMP2-mCherry sensor shows a high sensitivity even to as few as a single stimulus.

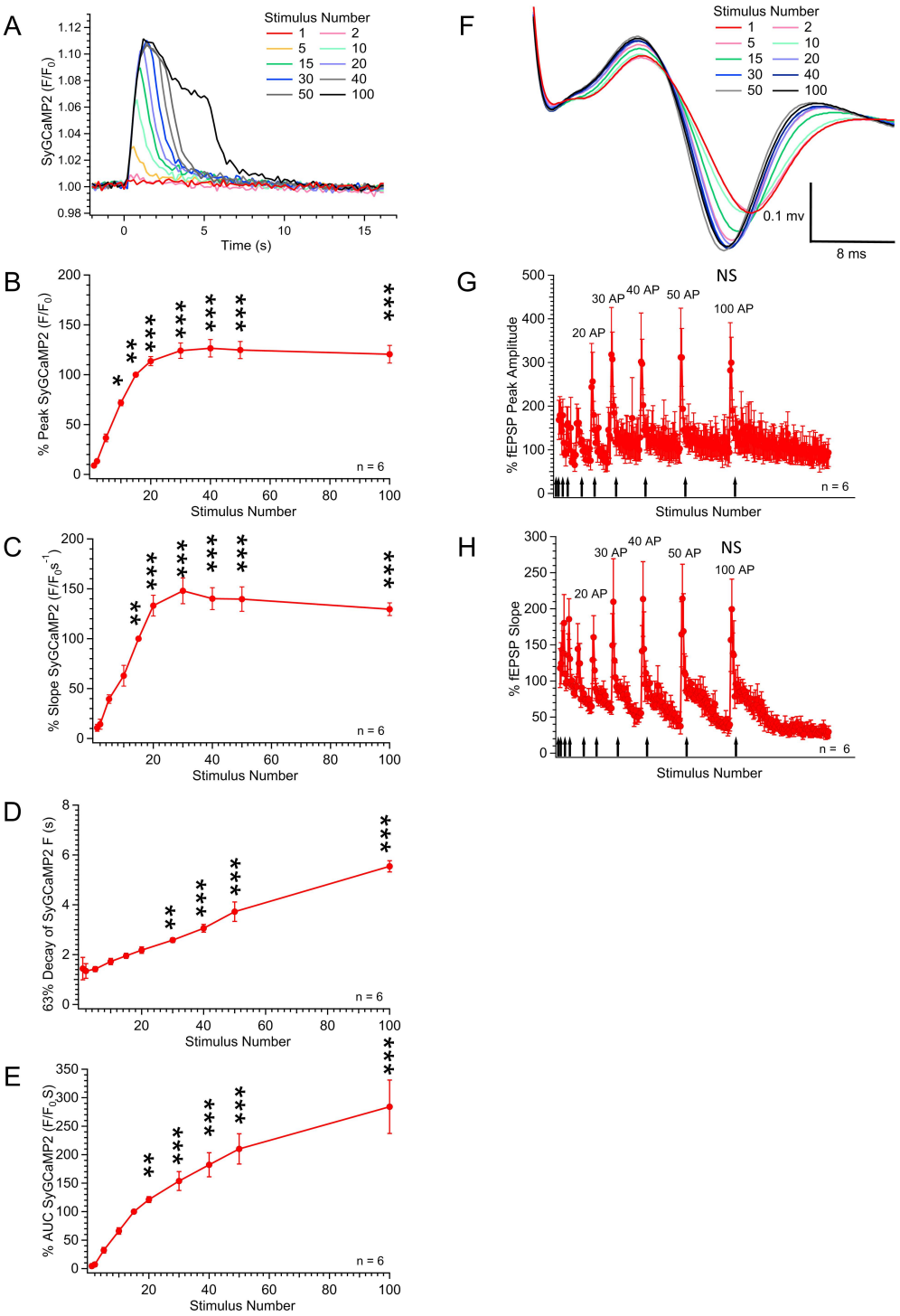

Figure 4.7. The effect of increasing stimulus number on both SyGCaMP2 fluorescence and its corresponding fEPSP in the hippocampal CA1 region in response to SC activation.

A. shows the mean responses to different numbers of stimuli from ROIs placed within the *stratum radiatum* of the CA1 hippocampal region plotted against time. B. to E. illustrate the effects of increasing stimulus number on Peak (B), slope (C), 63% decay time (D) and AUC (E) over time on SyGCaMP2 fluorescence,

respectively. F. shows field potential recordings illustrating the action of increasing stimulus number on SC activation. G to H show the change in the peak amplitude and slope of field excitatory postsynaptic potentials (fEPSPs) with increasing stimulus number, respectively. The values shown are mean values ± SEM; values are normalized to response at 20 stimuli except for D and I which are represented as relative absolute values. The statistical test were performed between 1AP and other stimulus numbers. (B), 15AP, P=0.0380; 20AP, P=0.0026; 30AP, P=0.0003; 40AP, P=0.0002; 50AP, P=0.0004; 100AP, P=0.0003; (C), 15AP, P=0.002; 20AP, P=0.0005; 30AP, P=0.0002; 40AP, P=0.0003; 50AP, P=0.0004; 100AP, P=0.0003; (E), 20AP, P=0.0041; 30AP, P=0.0009; 40AP, P=0.0001; 50AP, P=<0.0001; 100AP, P=<0.0001; Kruskal-Wallis test followed by Dunn's multiple comparisons test; (D), F=36.1; 30AP, P=0.0016; 40AP, P=0.0001; 50AP, P=<0.0001; 100AP, P=<0.0001, Ordinary one-way ANOVA followed by Dunnett's multiple comparisons test. Electrophysiology data showed no significant difference, Kruskal-Wallis test followed by Dunn's multiple comparisons test.

The above results indicated that stimulus strength of 20 Volts, at 20Hz and 10/20 stimulus number, is sufficient to produce a reliable response within the appropriate range of these stimulation parameters.

4.2.3 A comparative evaluation of the SyGCaMP2-mCherry sensor in a SyG37 transgenic mouse model showing the relative mono- and poly-synaptic contributions of presynaptic SyGCaMP2 fluorescence within the CA1 microcircuit.

To characterise the usefulness of the SyG37 mouse model for measuring presynaptic calcium, we investigated the effects of various pharmacological manipulations on SC activation in the CA1 area via four different methods. These were imaging of the SyGCaMP2-mCherry sensor (in the SyG37 mouse model), imaging of intrinsic fluorescence (in the SyG14 mouse model), imaging the fluo-4 organic calcium indicator loaded into presynaptic terminals, and electrophysiology. Even though it became apparent that the SyG14 mouse model stopped expressing a functional sensor, we used this model as a control for the SyG37 mouse and used it to examine intrinsic fluorescence. With each of these 4 models, we examined the effects of pharmacological manipulations that are known to affect synaptic transmission through presynaptic effects to establish whether these manipulations led to a corresponding change in SyGCaMP2 fluorescence.

4.2.3.1 Effect of adenosine receptor modulation on the CA1 area of a SyG37 mouse.

Adenosine has been shown to reduce synaptic transmission at CA1 synapses through presynaptic processes (Wu and Saggau, 1994), therefore, we first chose to use the SyG37 mouse model to examine the effects of adenosine on fluorescence responses to electrical stimulation. Next, we examined the effects of the removal of endogenous adenosine “tone” by inactivating A1 receptor activity using DPCPX as a specific competitive antagonist. In later experiments, synaptic transmission was blocked to investigate the relative contributions of direct and poly-synaptically activated terminals on SyGCaMP2 fluorescence within the CA1 microcircuit. A similar methodology was used for all experiments whereby bursts of 20 stimuli were delivered at 20 Hz at an intensity of 20 V to elicit field potential and SyGCaMP2 recordings as described already.

4.2.3.1.1 Effect of 50 µM Adenosine on SC activation in the CA1 area of a SyG37 mouse.

In the first series of these experiments we wanted to test whether adenosine, which is known to produce a presynaptic inhibition of synaptic transmission within the CA1 region of the hippocampus, reduced SyGCaMP2 fluorescence. After obtaining a stable baseline of synaptic responses, 50 µM adenosine was bath applied for 30 minutes and then washed out for at least 20 minutes. Data were analysed and pooled and the adenosine-mediated effects expressed as a percentage of the baseline peak responses. Pairs of field potentials, activated at intervals of 50 ms, were collected every 10 s to provide a further assessment of the source of changes in synaptic activity by changes in the paired pulse ratio (figure 4.8-B). Figure 4.8-A illustrates the spatial changes that accompanied electrical stimulation and the effects of adenosine. The SyGCaMP2 response was highly sensitive to adenosine addition as its fluorescence decreased dramatically in the presence of adenosine as indicated by the cooler colours during stimulation. Adenosine produced a pronounced effect on both optically recorded fluorescence (SyG37 mouse, ~50%; SyG14 mouse, ~35%; and Fluo4, ~35% reduction) and concurrently recorded field potentials (~60% reduction), reaching a minimum within 10 minutes of application (figure 4.9-A-D). Both the fluorescence and the N2 component of the field potential were significantly reduced compared to baseline responses. Both the fluorescence and the fEPSP peak amplitude recovered and even exceeded baseline levels during the wash-off period except for the Fluo-4 experiments, which remained at approximately the same level as during drug application. It is worth mentioning that responses from fluo-4 calcium dye and SyG37 experiments were bigger and faster than those from SyG14 animals as shown in the insertions in figure 5.9.A-C. This issue will be discussed later (see subsection 4.2.3.3 in this chapter). If adenosine-induced depression involves presynaptic mechanisms, then it might be associated with a change in the paired-pulse ratio (PPR) because manipulations that change transmitter release usually change the magnitude of PPR (Manabe *et al.*, 1993, Schulz *et al.*, 1994) Therefore, we compared the PPR before and after the treatment with adenosine. Synaptic responses to a pair of stimuli were recorded with an ISI of 50 ms, and the PPR was expressed as the ratio of the

second response to the first. Figure 4.9-E shows that application of adenosine increased the magnitude of the PPR from about 0.7 to 2.0, which is consistent with a presynaptic action of adenosine. By chance and interestingly, in a small number of experiments in which transverse slices were cut to separate the lower part of the slice that contained the thalamus, hypothalamus, amygdala, leaving just the hippocampus, we found that there was no any change in PPR when we applied adenosine (data not shown).

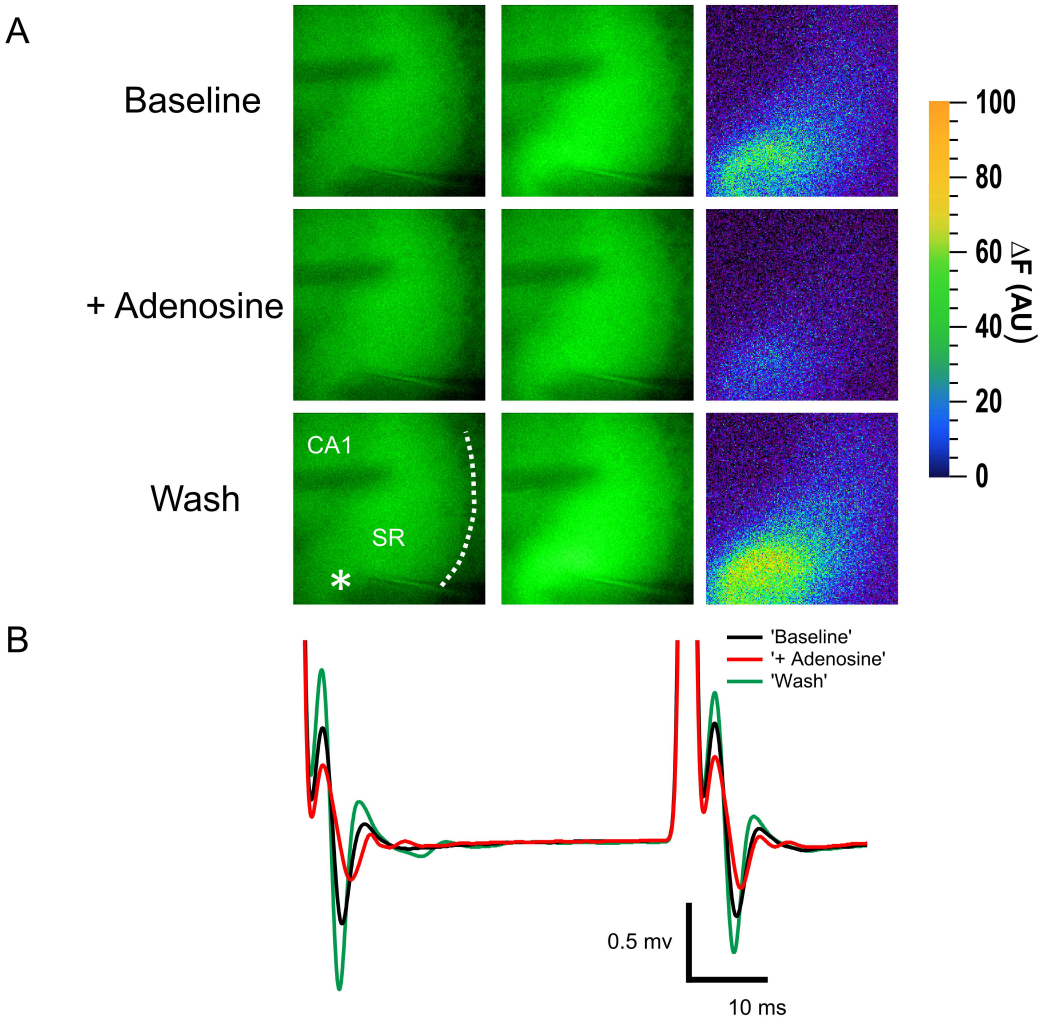

Figure 4.8. Visualization of the effect of 50 µM adenosine on SyGCaMP2 fluorescence after SC/CA1 activation with its corresponding field potential recordings in the hippocampal CA1 region of a SyG37 mouse.

Images of SyGCaMP2 fluorescence were collected before, during, and after adding 50 µM adenosine. A. shows the averages of three SyGCaMP2 images taken immediately before stimulation (left panel), the peak responses taken

during electrical stimulation (middle panel) and the difference (right panel). A warm/cold look-up table (right panel) was used to illustrate the difference in the size of the responses in both. Larger changes in calcium concentration are indicated by brighter colours in the SyGCaMP2 Images. The asterisk indicates the stimulating electrode position, and the border between the pyramidal cell layer (lower right corner) and *stratum radiatum* are shown as a dotted line. B. shows the representative traces of field potentials collected before, during, and after wash-out of adenosine.

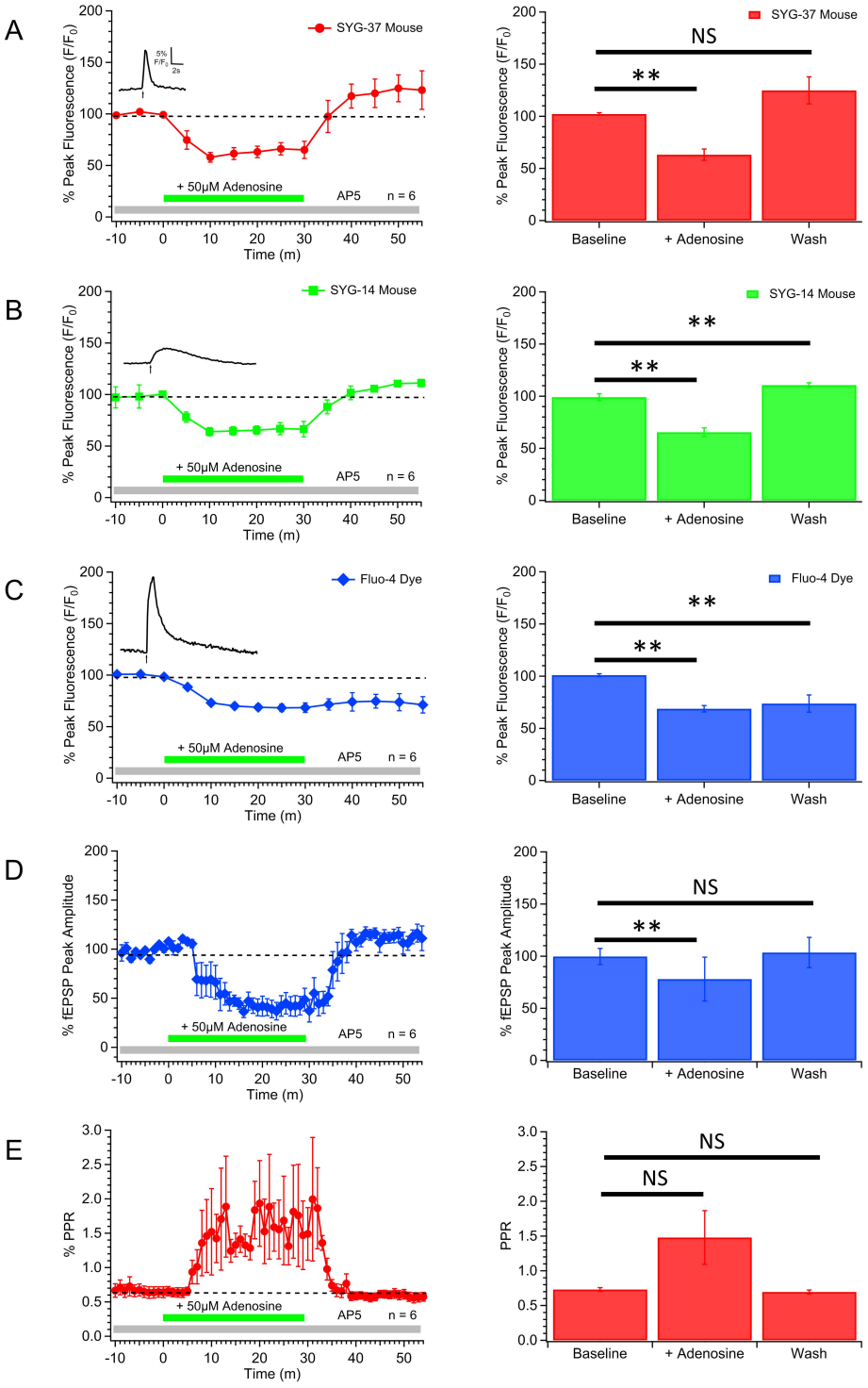

Figure 4.9. Effect of 50 µM adenosine on SC activation in the CA1 area of the hippocampus.

Figures A, B and C. show the pooled analysis of the effects of adenosine on CA1 responses to stimulation, using images from the SyGCaMP2-mCherry sensor of SyG37 mice, the intrinsic fluorescence of SyG14 mice and fluo-4 calcium dye, respectively. These data are represented as a percentage of the mean peak

response before drug application, plotted against time, along with the standard error of the mean (n = 6). Insertions in A, B and C show responses (F/F_0) of fluorescence collected during the baseline period (-5 minutes) from SyG37, fluo-4 calcium dye and SyG14 mice experiments, respectively. The black arrow shows the point where the stimulation (20 V, 20 AP at 20 Hz) was delivered. Figures D. and E. show the change in peak amplitude and the PPR of the field potential before, during, and after addition of adenosine. The statistical test were performed between baseline and the other periods. The degree of the statistical significance was presented on the histograms (right panel). Statistics: (A), adenosine, U= 0, P=0.0022; (B), adenosine, U= 0, P=0.0022; wash, U= 0, P=0.0022 (C), adenosine, U= 0, P=0.0022; wash, U= 1, P=0.0043; (D), adenosine, U= 0, P=0.0022; Mann Whitney test; (E), no significant difference was observed; Ordinary one-way ANOVA followed by Dunnett's multiple comparisons test.

4.2.3.1.2 Effect of the 250 nM A1-adenosine receptor antagonist DPCPX on SC activation in the CA1 area of a SyG37 mouse.

Next, we wanted to test the effects of DPCPX, an A1-adenosine receptor antagonist, which is known to antagonise the inhibitory effect of adenosine on synaptic transmission within the CA1 region of the hippocampus (Martinson *et al.*, 1987, Schubert, 1988, Alzheimer *et al.*, 1989, Pak *et al.*, 1994, Vollert *et al.*, 2013). After obtaining a stable baseline for synaptic responses and in the continued presence of 50 µM AP5, 250 nM DPCPX was applied for 30 minutes and then washed out for 25 minutes. In fluo-4 and SyG14 mouse experiments, there was no significant difference between the control and drug application periods, whilst in SyG37 mouse experiments, there was a significant increase in responses between the control and drug application periods, as shown in figure 4.10-A., B. and C. It is worth mentioning that, in SyG14 mouse experiments, there was no significant difference between the control and drug application periods even at higher concentrations of DPCPX (data not shown). In field potential recordings, the N2 component of the field potential was clearly changed after DPCPX application. The reason that the Mann-Whitney test was unable to detect any significant difference in this set of experiments, might be, due to the large

dispersion of sample means around the population mean. The paired pulse ratio changed as well, giving another indicator as to the locus of the action of adenosine (figure 4.10-D. and E.). In both SyG37 and electrophysiological experiments, there were increases in fluorescence, and the fEPSP did not recover during the wash-out period, as shown in figure 4.10-A. and D.

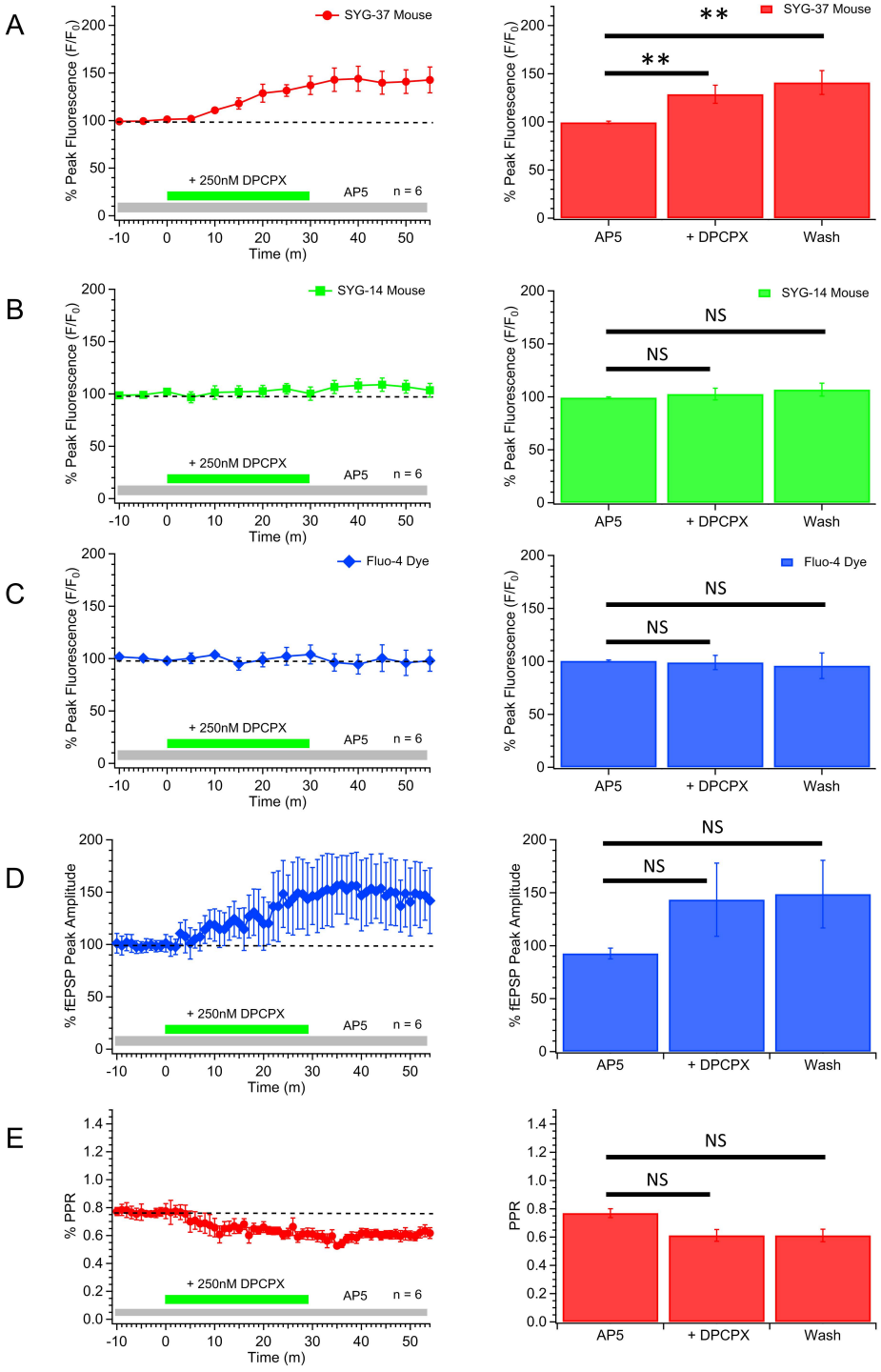

Figure 4.10. Effect of 250 nM DPCPX on SC activation in the CA1 area of the hippocampus.

Panels A., B. and C. show the pooled analysis of the effect of DPCPX on the CA1 area, using imaging from the SyGCaMP2-mCherry sensor, intrinsic fluorescence of SyG14 mice and fluo-4 dye, respectively. These data are represented as a percentage of the averaged peak amplitude plotted against time, along with the standard error of the mean (*n* = 6). Panels D. and E. show the changes in peak

amplitudes of the fEPSPs and PPR after adding DPCPX, respectively. The statistical test were performed between the baseline and the other periods. The degree of the statistical significance was presented on the histograms (right panel). Statistics: (A), DPCPX, U= 0, P=0.0022; wash, U= 0, P=0.0022. In B, C and D, no significant difference was observed; Mann Whitney test; (E), no significant difference; Ordinary one-way ANOVA followed by Dunnett's multiple comparisons test.

4.2.3.1.3 Effect of 50 µM Adenosine in the presence of 250 nM DPCPX on SC activation in the CA1 area of a SyG37 mouse.

We next tested whether pre-incubation with 250 nM DPCPX, an A_1-adenosine receptor antagonist, prevented the adenosine-mediated reduction in fluorescence and field potential recordings within the CA1 region of the hippocampus. After obtaining a stable baseline for the synaptic responses in the presence of 50 µM AP5 and DPCPX, 50 µM adenosine was applied for 30 minutes and then washed out for 20 minutes. In SyG37 mice, SyG14 experiments and field potential recordings, there was no significant difference between the baseline responses and those recorded in the presence of adenosine. In experiments using fluo-4 calcium dye, the peak amplitude of F/F_0 gradually declined over time and there was no significant difference between the baseline and adenosine application periods. Both the fluorescence and the fEPSP peak amplitude remained at approximately the same level as during the baseline period except for the SyG14 and Fluo-4 experiments, which significantly declined during the wash-off period, as shown in figure 4.11-A., B., D. and E. This decline in fluo-4 fluorescence was most likely due to a gradual reduction in the amount of this dye in the tissues over time due to the organic sensor redistributing within the tissue.

In summary, DPCPX on its own increased both SyGCaMP2 fluorescence and the fEPSP suggesting a causal relationship. Moreover, the inhibitory effects of adenosine were blocked by DPCPX indicating that they were mediated by the A1 receptor subtype.

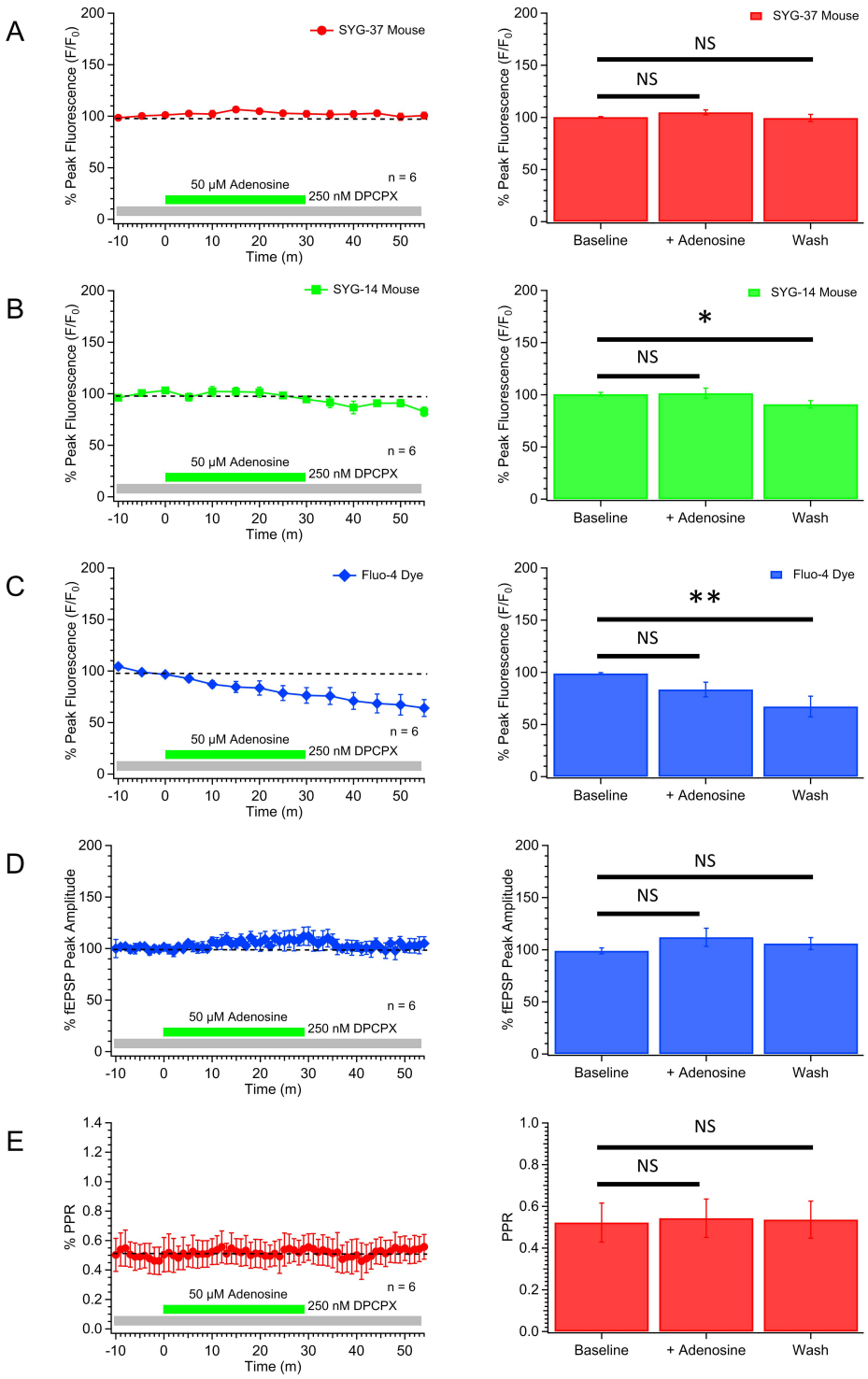

Figure 4.11. The effect of 50 µM adenosine in the presence of 250 nM DPCPX on SC activation in the CA1 region of the hippocampus.

Panels A., B. and C. show the pooled analysis of the effect of adenosine on the CA1 area in the presence of DPCPX, using imaging of the SyGCaMP2-mCherry sensor, imaging of SyG14 autofluorescence and fluo-4 dye, respectively. These data are represented as a percentage of the averaged peak amplitude plotted

against time, along with the standard error of the mean (*n* = 6). Panels D. and E. show the change in peak amplitude and the PPR of the field excitatory postsynaptic potentials (fEPSPs) after adding adenosine in the presence of DPCPX and AP5, respectively. The asterisks show the level of significance. The statistical test were performed between baseline and the other periods. The degree of the statistical significance was presented on the histograms (right panel). Statistics: (A), no significant difference; (B), wash, U= 4, P=0.0260; (C), wash, U= 0, P=0.002; (D), no significant difference was observed; Mann Whitney test; (E), no significant difference was observed; Ordinary one-way ANOVA followed by Dunnett's multiple comparisons test.

4.2.3.2 The effect of adenosine receptor modulation in the presence of inhibitors of excitatory and inhibitory synaptic transmission.

The main classes of excitatory and inhibitory receptor in the hippocampus are glutamatergic and GABA/Glycinergic receptors. Once we had established that application of adenosine reduced SyGCaMP2 fluorescence we next attempted to establish whether the effects that we observed were mediated primarily at SC terminals or whether there were contributions from presynaptic terminals that were postsynaptic to the SC terminals. We therefore chose to examine the sequential effects of picrotoxin, AP5 and DNQX, which could be used to block the $GABA_A$/Glycine, NMDA and AMPA receptors, respectively. We then examined the effects of adenosine alone and in the presence of the A_1 receptor blocker DPCPX, having blocked the major excitatory and inhibitory synaptic pathways formed by the SC terminals.

4.2.3.2.1 Effect of block synaptic transmission inhibition on SC activation in the CA1 area.

Each slice was stimulated as described previously in a drug-free standard extracellular solution before washing on cumulatively 10 μM picrotoxin (PTX), then after 15 minutes 50 μM AP5, and then 10 μM DNQX after a further 15 minutes. All these drugs were then washed off using the drug-free standard extracellular solution. 10 μM PTX produced a small but not statistically significant enhancement of responses compared to the baseline in the SyG14 mouse

experimental group but no effects were seen in the SyG37 or fluo-4 groups. Application of AP5 in the continued presence of PTX caused a reduction in the optically measured responses in all experimental groups; however, this effect was only significant in the SyG37 and fluo-4 groups. Application of DNQX led to a further reduction in the amplitudes of the responses in all groups. Figure 4.12-A., B. and C. illustrate the effects of the three cumulative drug applications on the optically recorded responses for the SyGCaMP2, SyG14 intrinsic fluorescence and fluo-4 calcium dye experimental groups, respectively. Concurrent field potential recordings were also taken. The N2 component of the field potential, which represents the postsynaptic component of the responses, was reduced slightly upon adding AP5 but was reduced significantly when AMPA receptors were blocked with DNQX. The paired-pulse ratio changed as well, as shown in figure 4.12-D. and E. Whilst this might normally be considered to represent a presynaptic effect, this is probably more artefactual as DNQX reduced fEPSP amplitudes to nearly zero making measurement of the PPR noisy. Responses recovered fully after 30 minutes of washout in the SyG37 and SyG14 experimental groups, and partially recovered in terms of fEPSP recordings. As was the case in other experiments, fluo-4 responses showed a gradual decrease in peak amplitude over time, suggesting gradual loss of sensor.

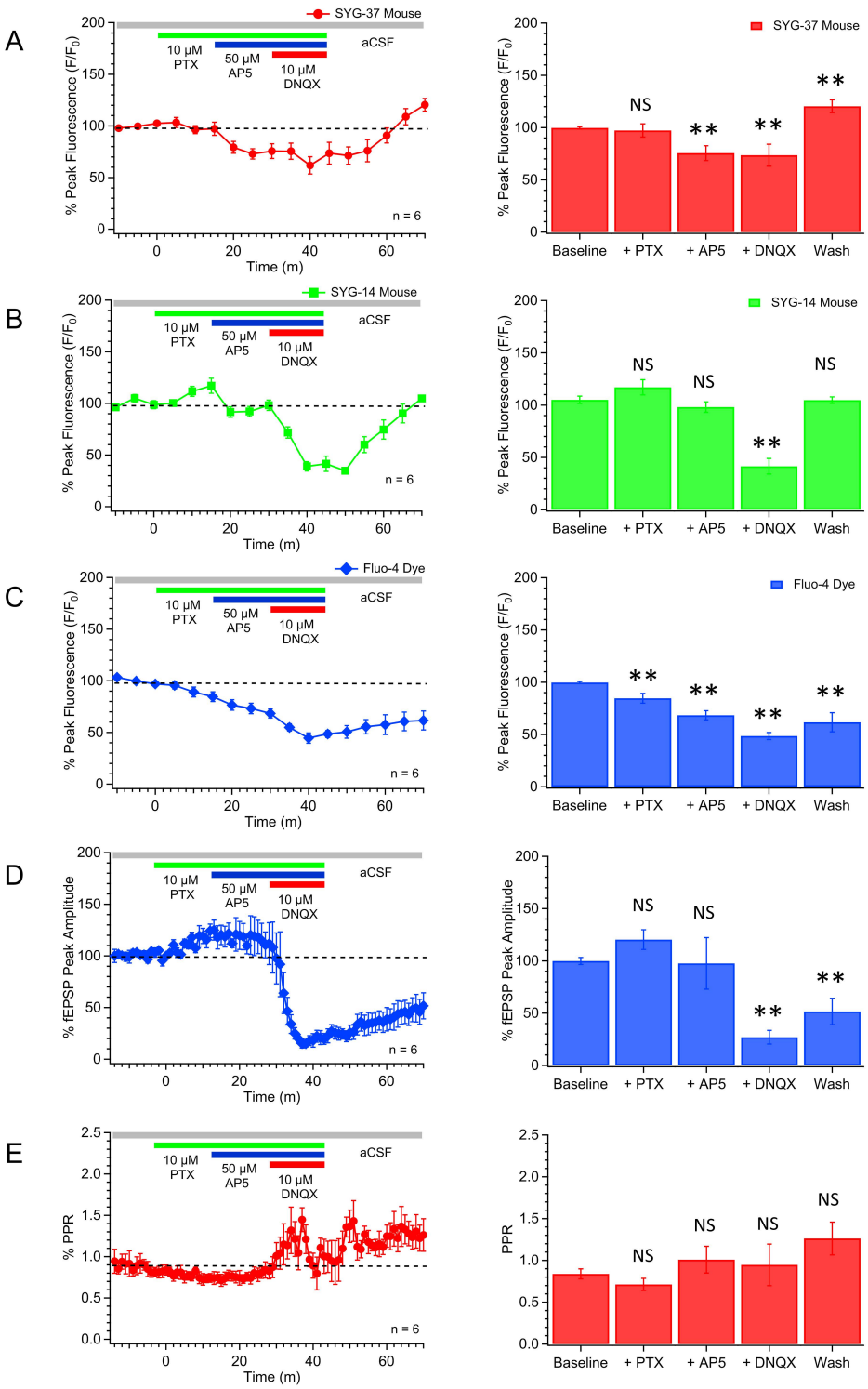

Figure 4.12. Effects of cumulative blockade of GABA/Glycine, NMDA and AMPA receptors on optically and electrophysiologically recorded responses to SC activation in the CA1 area of the hippocampus.

Panels A., B. and C. show the pooled analysis of the effect of cumulative applications of 10 µM PTX, 50 µM AP5 and 10 µM DNQX on optically recorded responses in the CA1 region for the SyGCaMP2-mCherry, SyG14 mouse intrinsic

fluorescence and fluo-4 experimental groups, respectively. These data are represented as a percentage of average peak amplitudes plotted against time, along with the standard error of the mean. Panels D. and E. show the change in peak amplitude and the PPR of the field excitatory postsynaptic potentials (fEPSPs) after adding each of the postsynaptic blockers. The statistical test were performed between baseline and the other periods. The degree of the statistical significance was presented on the histograms (right panel). Statistics: (A), AP5, U= 0, P=0.0022; DNQX, U= 1, P=0.0043; wash, U= 0, P=0.0022; (B), DNQX, U= 0, P=0.0022; (C), PTX, U= 0, P=0.0022; AP5, U= 0, P=0.0022; DNQX, U= 0, P=0.0022; wash, U= 0, P=0.0022; (D), DNQX, U= 0, P=0.0022; wash, U= 0, P=0.0022; Mann Whitney test; (E), no significant difference; Ordinary one-way ANOVA followed by Dunnett's multiple comparisons test.

4.2.3.2.2 The effects of 50 µM adenosine, 250 nM DPCPX, and then both 50 µM adenosine and 250 nM DPCPX, on SC activation in the CA1 area in the presence of postsynaptic blockers.

The effects of adenosine and DPCPX were next examined in the presence of a postsynaptic receptor blockade to establish the proportion to which their overall effects on the SC-CA1 synaptic pathway were mediated on SC synaptic terminals and, therefore, to estimate the relative contribution of poly-synaptic circuits of SyGCaMP2 fluorescence responses to SC/AC stimulation. As before, in the presence of PTX, AP5 and DPCPX, applications of adenosine produced the same pattern of results as the experiments without postsynaptic blockers in each of the three different imaging methods used; adenosine reversibly reduced the size of SyGCaMP2 responses, as shown in figure 4.13-A. Applications of DPCPX had no effect in either the SyG14 or fluo-4 groups, but an increase in responses was observed in the SyG37 group, as seen in figure 4.13-B. The inhibitory actions of adenosine observed in the SyG37 model experiments were blocked in the presence of DPCPX even when $GABA_A$/Glycine and ionotropic glutamate receptors are blocked, indicating the presynaptic locus of the SyGCaMP2-mCherry sensor (4.13-C). Insertions in figure 4.13-D show that the autofluorescence response in SyG14 mice was almost completely lost in the

presence of PTX, AP5 and DNQX which suggests it is almost exclusively postsynaptic in origin.

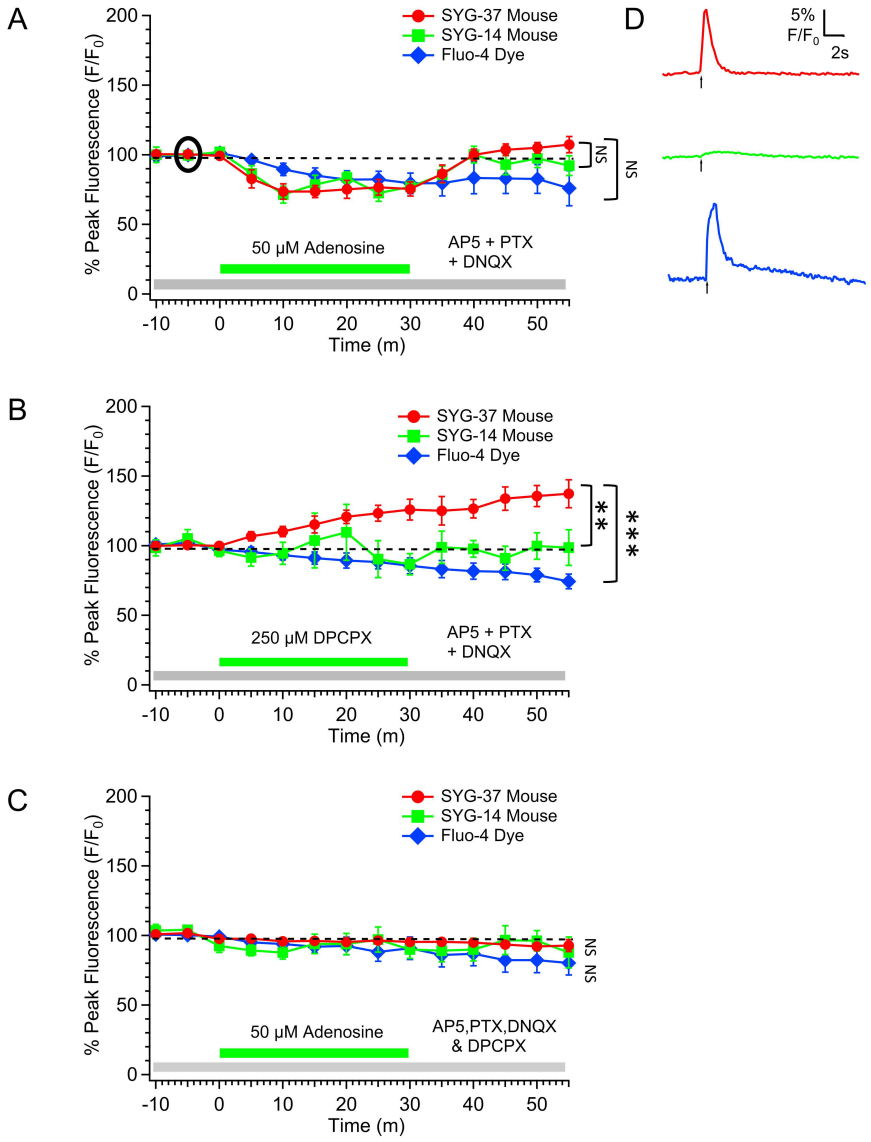

Figure 4.13. The effects of 50 µM adenosine, 250 nM DPCPX, and then both 50 µM adenosine and 250 nM DPCPX, on optically recorded responses to SC activation in the CA1 area of the hippocampus in the presence of postsynaptic blockers.

A., B. and C. show the pooled data of the three different optically recorded responses for the effect of adenosine, DPCPX, and then both adenosine and DPCPX, on CA1 area responses in the presence of 10 µM PTX, AP5 and DNQX, respectively. Insertions in D show responses (F/F_0) of fluorescence collected during the baseline period (-5 minutes, black circle) from SyG37 (red), SyG14 mice (green) and fluo-4 calcium dye (blue) experiments, respectively. The black arrow shows the point where the stimulation (20 V, 20 AP at 20 Hz) is begun.

Data are shown as the mean peak optical responses and standard errors. The numbers of experiments in each group was six. The statistical test were performed between SyG37 and the other two optic methods. Statistics: In (A), there is no significant difference; (B) SyG37 Vs SyG14, P=0.0045; SyG37 Vs Fluo-4, P=<0.0001; (C), there is no significant difference; Two-way ANOVA followed by Sidak's multiple comparisons test.

4.2.3.3 Comparison of the effects of adenosine receptor modulation on CA1 responses with and without blocking synaptic transmission.

The effects of adenosine and DPCPX in the presence of AP5 only and in the presence of AP5, 10 µM PTX and DNQX in the extracellular solution were collated and compared in figure 4.14 for each of the three experimental models examined. Each column of data represents one of the three experimental models. With the exception of the SyG14 mouse model group in adenosine experiments, addition of PTX, AP5 and DNQX did not lead to a clear reduction in the size of responses prior to application of adenosine, or DPCPX, or both. In SyG14 mouse model experiments, the fluorescence was significantly reduced in both, during adenosine addition and the wash-off period as compared to the baseline responses. The results shown in figure 4.14 indicate that neither SyG14 measurements nor fluo-4 measurements were sufficiently sensitive to detect the effects of DPCPX in the presence or absence of postsynaptic blockers. Responses recorded in SyG37 positive mice were, however, still present in the presence of postsynaptic blockers, which is consistent with the expression of the SyGCaMP2-mCherry sensor in SC/AC terminals.

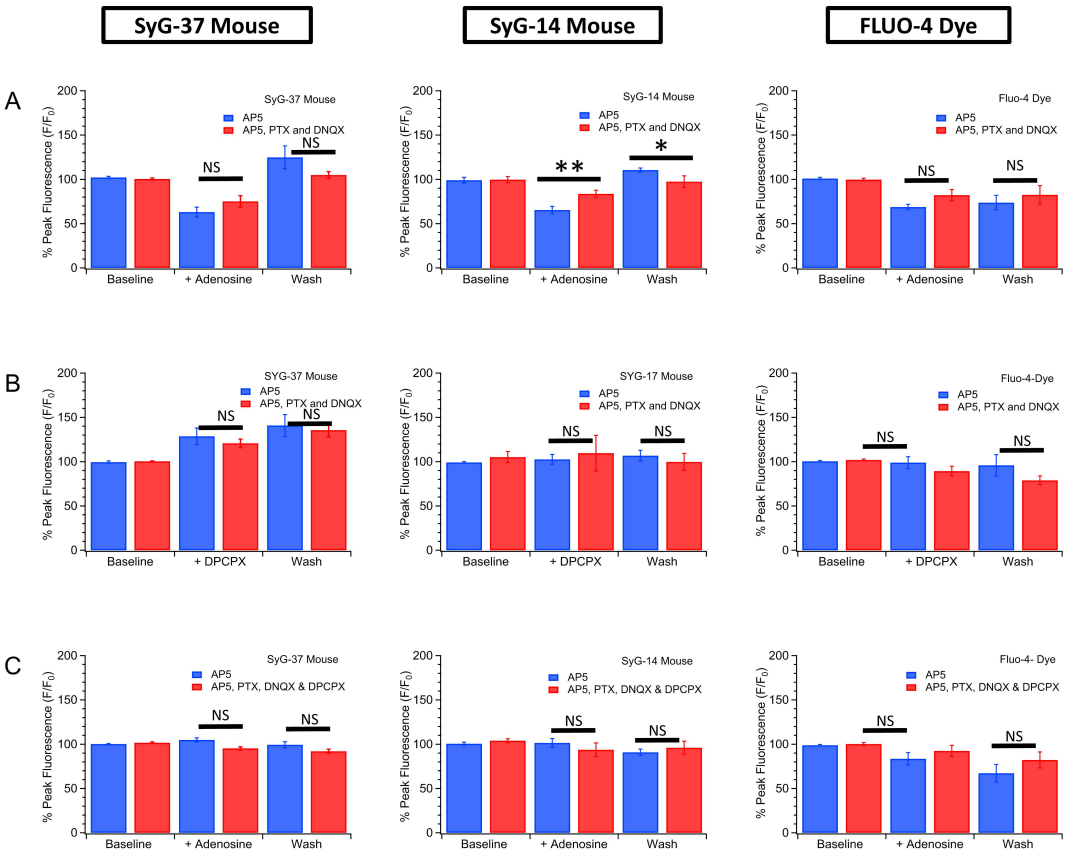

Figure 4.14. Comparison between the effects of 50 µM adenosine, 250 nM DPCPX, and both 50 µM adenosine and 250 nM DPCPX, on three different optically recorded responses to SC activation in the CA1 area of the hippocampus in the presence and absence of postsynaptic blockers.

Panels A., B. and C. show the pooled analysis of the effects of adenosine, DPCPX and the effects of adding adenosine and DPCPX together on CA1 responses to SC stimulation. The left, middle and right panels represent three different experimental groups: SyG37, SyG14 intrinsic fluorescence and fluo-4 calcium dye, respectively. The means and standard errors from 6 separate experiments are shown. Statistics: The statistical test were performed between Just AP5 and PTX, AP5, DNQX experiments. Statistics: In (A-SyG14), adenosine, P=0.0071; wash, P=0.035; Two-way ANOVA followed by Sidak's multiple comparisons test.

Although the cumulative addition of AP5, PTX and DNQX reduced the amplitudes of responses to SC/AC stimulation in all models, we noticed that the baseline peak amplitude of responses in the SyG37 mouse were actually larger in slices that had been pre-incubated in AP5, PTX and DNQX. Figure 4.15 provides

examples of responses collected using the fluo-4 calcium dye, SyG37, SyG14 and WT mouse experiments in the presence of AP5 alone and then overlain with examples from different slices in which AP5, PTX and DNQX had been included in the extracellular solution for at least 30 minutes. For each method, the mean absolute responses from nine ROIs were placed within the *stratum radiatum* of the CA1 hippocampal region and plotted against time. Responses from fluo-4 calcium dye and SyG37 experiments were faster than those from SyG14 or WT animals. With the exception of the SyG37 group, pre-incubation of slices with PTX, AP5 and DNQX for at least 30 minutes led to a clear reduction in the size of baseline responses compared to non-incubated slices. In the SyG37 group, the baseline fluorescence levels, interestingly, increased as a result of pre-incubation by about 26.9% compared to slices that had not been pre-incubated. In the absence of these blockers, the responses represent a mixture of signals originating from the SC/AC terminals and those from presynaptic terminals from cells that are postsynaptic to SC/AC terminals. It is possible, therefore, that prior stimulation in the absence of blockers had in some way influenced the size of the response that was not apparent when the blockers were present from the outset. The autofluorescence response in SyG14 and WT mice was almost completely lost in the presence of PTX, AP5 and DNQX which suggests it is almost exclusively postsynaptic in origin. The fluo-4 signal was reduced by less than 40%. Whilst this method of fluo-4 loading is reported to preferentially load presynaptic terminals, these data suggest that the signal we recorded is only partially presynaptic in origin (figure 4.15-A., B., C., D. and E.). These results are consistent with our earlier observations that SyGCaMP2-mCherry is selectively expressed in presynaptic terminals within the hippocampus and indicate that a significant component of the response to SC/AC stimulation is from the SC/AC terminals themselves. Therefore, the SyG37 gives the most “pure” indication of presynaptic effects, then it is capable of detecting an acute effect of blockers that occurs in the absence of stimulation. Our results also indicate that fluo-4 also targets presynaptic sites but not exclusively as a significant proportion of the total signal is of postsynaptic origin. The source of fluorescence collected from SyG14 and WT mouse experiments seemed to be originating from the postsynaptic

region and so these intrinsic fluorescence models are not useful for measuring presynaptic calcium signals.

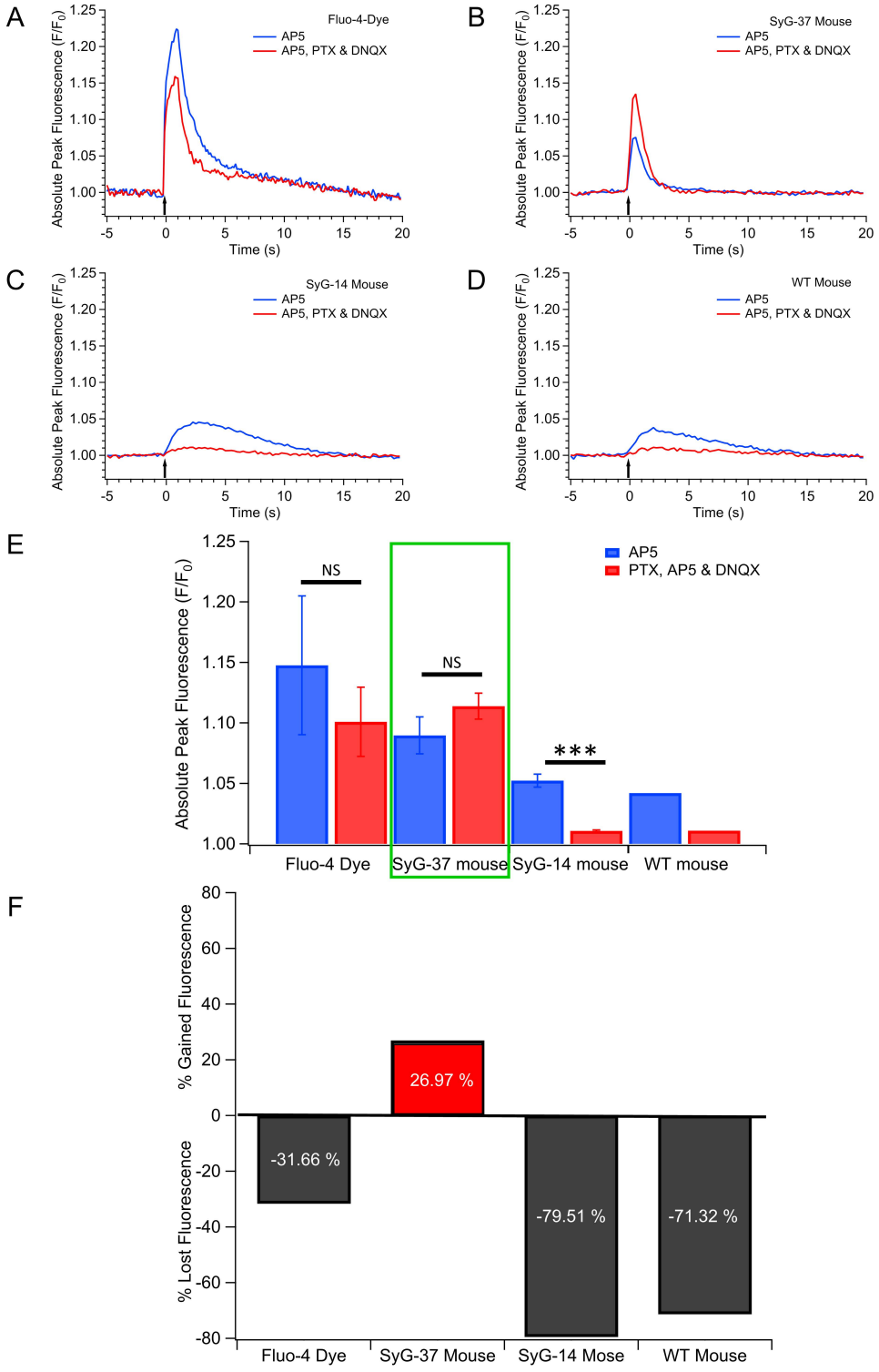

Figure 4.15. The effects of pre-incubation of postsynaptic blockers on the responses of different optical recording methods to SC/AC pathway stimulation.

A., B., C. and D. show responses (F/F_0) of fluorescence collected during the baseline period (-5 minutes) from fluo-4 calcium dye, SyG37, SyG14 and WT mice experiments, respectively, where these traces were collected during stimulation of the SC/AC from experiments in the presence of AP5 alone (blue) and then overlain with examples from different slices in which AP5, PTX and DNQX had been included (red) in the extracellular solution for at least 30 minutes. The black arrow shows the point where the stimulation (20 V, 20 AP at 20 Hz) was delivered. E. shows the pooled data of absolute fluorescence collected during stimulation of the SC/AC before and after application of 10 µM PTX, 50 µM AP5 and 10 µM DNQX. The number of experiments in E. was six, except for WT experiments where there was only one experiment. The statistical test were performed between Just AP5 and PTX, AP5, DNQX experiments at baseline level. Statistics: In (E-SyG14), t(10) = 7.6, P=<0.0001; unpaired t test. The bar chart, F., shows the percentage of lost or gained fluorescence in each optical recording method after synaptic transmission blockade. The percentage of lost or gained fluorescence for each experimental group was calculated by subtracting the absolute fluorescence collected from AP5 only experiments from the absolute fluorescence collected from PTX, AP5 and DNQX experiments, from which the percentages were then calculated.

4.2.4 Calcium transients measured at individual presynaptic boutons in the CA1 area using the SyGCaMP2 sensor.

It is not clear from our previous studies whether the changes in SyGCaMP2 fluorescence observed were due to a change in the number of contributing puncta or a whether each puncta experienced a larger or smaller peak response. Therefore, we used multiphoton microscopy to identify individual presynaptic boutons and examined the effects of stimulus intensity and adenosine on fluorescence responses in CA1. A presynaptic fibre volley, which was collected during our previous experiments, was used as a further indicator of presynaptic activity. The fibre volley is a brief, negative, extracellularly recorded wave caused by activation of presynaptic fibres when action potentials in a population of axons are evoked by extracellular stimulation. The fibre volley amplitude is proportional to the number of active presynaptic fibres, which in turn fire and activate their postsynaptic partners (Henze *et al.*, 2000a, Meeks and Mennerick, 2004).

4.2.4.1 The effect of altering the stimulus intensity on both individual presynaptic boutons and the presynaptic fibre volley during SC-CA1 pathway activation of the SyG37 mouse model.

To find the impact of altering stimulus intensity on both individual presynaptic boutons and the presynaptic fibre volley, stimulus intensity was increased gradually from 0 to 70 V using a fixed stimulus number (20 AP) at a fixed frequency (20 Hz). Image 4.16-A obtained from the CA1 hippocampal area of SyG37 mice provided an example of the effects of increasing stimulus intensity on SyGCaMP2 fluorescence after SC/CA1 activation. To test the effects of increasing stimulus intensity on individual presynaptic boutons, the amplitudes from the same ROIs placed directly over identified puncta were compared at different stimulus intensities. Figure 4-16-B clearly demonstrates that increasing the stimulus intensity caused relatively little effect on the peak amplitude of responses from single puncta obtained at 10 and 60 V although the numbers of boutons that responded at each intensity were very different. The right hand panel of figure 4-16-C shows that when only responding puncta were included in the analysis, there was no difference between the amplitudes of responses at each of the intensities tested greater than zero volts. On the other hand, full frame fluorescence responses (left-hand panel), showed a gradual increase with stimulus intensity. When the AUC of responses for each case was plotted against intensity (figure 4-16-D), there was a clear linear relationship between the full frame response. In contrast, with responding puncta, once the threshold for responses of single puncta was reached, the peak response did not change significantly with intensity. These results indicate that as stimulus intensity increases, there is a gradual recruitment of puncta. The increase in SyGCaMP2 fluorescence caused by increasing stimulus intensity was therefore due to an increase in the number of contributing terminals as opposed to an increase in the amount of calcium influx per terminal. Fibre volley recordings were consistent with imaging results where the N1 component of the field potential curve was also significantly increased by increasing the stimulus intensity with 70 V eliciting a maximal response with no saturation (figure 4-16-E. and F.).

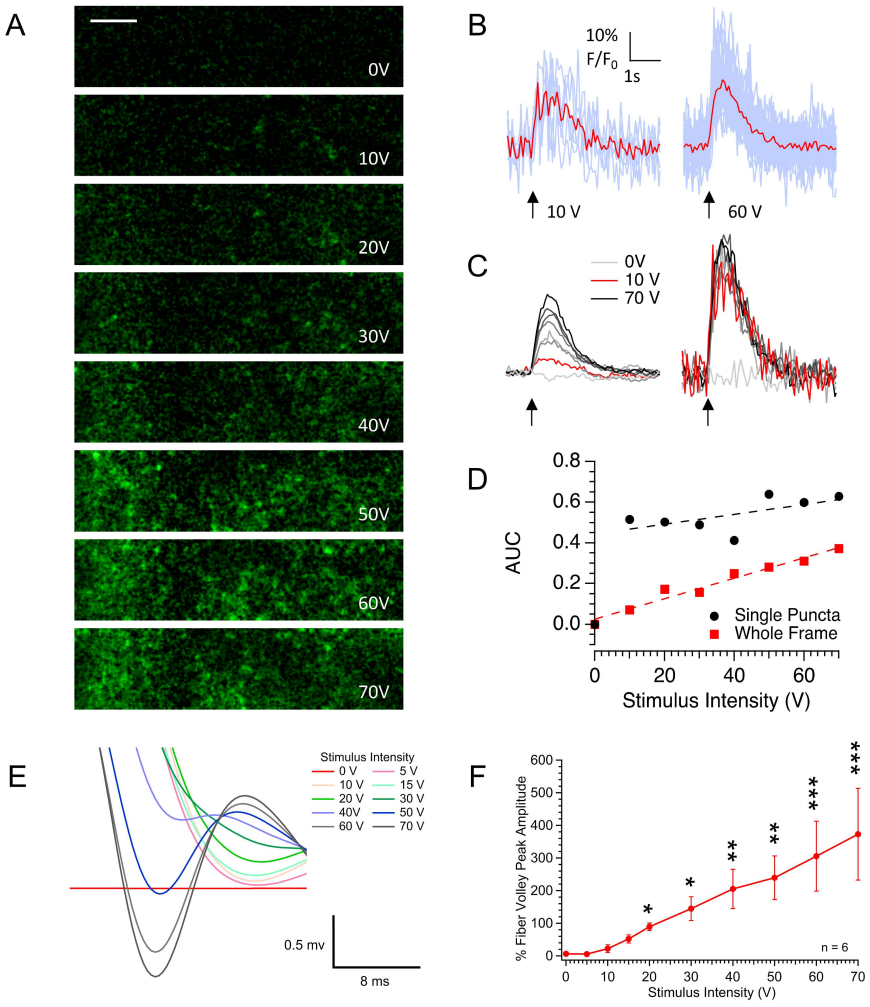

Figure 4.16. The effect of altering the stimulus intensity on both individual presynaptic boutons and the presynaptic fibre volley after SC/CA1 activation in the hippocampal CA1 region of a SyG37 mouse.

A. shows the average of three SyGCaMP2 images taken immediately before stimulation were subtracted from the peak responses taken during electrical stimulation at different stimulus intensities. B. shows responses obtained at 10 and 60 V. C. shows responses from single puncta (right) and full frame fluorescence response (left) obtained at different stimulus intensities. D. shows the AUC of SyGCaMP2 fluorescence obtained from single puncta (black) and full frame fluorescence response (red) plotted against the stimulus intensity. E. and F. show the change in the N1 component of the field potential curve at different stimulus intensities and the fibre volley peak amplitude plotted against stimulus intensity, respectively (Mean ± SEM; *n* = 6). The statistical test in F was performed between 0V and other stimulus intensities. 20V, P=0.0161; 30V, P=0.0108; 40V, P=0.0030; 50V, P=0.0013; 60V, P=0.0008; 70V, P=0.0002;

Kruskal-Wallis test followed by Dunn's multiple comparisons test. The scale bar in A is 10µ.

4.2.4.2 The effect of 50 µM adenosine on both individual presynaptic boutons and the presynaptic fibre volley during the SC-CA1 pathway activation of the SyG37 mouse model.

We have so far shown, in experiments carried out using an epifluorescence microscope and camera, that adenosine causes a reversible reduction in SyGCaMP2 fluorescence and associated reduction in synaptic transmission at the SC-CA1 synapse. We next carried out experiments using a multiphoton microscope to examine whether the reduction in SyGCaMP2 fluorescence was due to a reduction in the number of contributing boutons, a reduction in fluorescence per bouton or a combination of the two. These results were compared with the effects of adenosine on the presynaptic fibre volley, N1. Image 4.17-A obtained from the CA1 hippocampal area of SyG37 mice provided an example of the effects of 50 µM adenosine on SyGCaMP2 fluorescence after SC/CA1 activation. The SyGCaMP2 fluorescence slope obtained from the full frame fluorescence response were compared before, during, and after washout of adenosine as shown in figure 4.17-B. Traces from either the full frame fluorescence response (figure 4.17.C) or single puncta were shown in figures 4.17.D and E. These figures clearly demonstrate that 50 µM adenosine caused a decrease in the amplitude of the slope of responses from individual puncta. It is reasonable to suggest, therefore, that the decrease in fluorescence caused by adenosine is due a reduction in the amount of calcium influx per terminal. It is worth noting that the SyGCaMP2 fluorescence amplitude collected from a single punctum (as an exemplary sample) was decreased after adenosine addition with different recovery levels at wash-out (figure 4.17-D and E); therefore, there was a difference between SyGCaMP2 fluorescence collected from single punctum and the full frame fluorescence response during the wash-out period, where the SyGCaMP2 fluorescence recovered at full frame fluorescence response but not in the case of the single punctum that represented in figure 4-17-D. Fibre volley recordings were also analyzed. Interestingly, the N1 component of the field

potential curve was significantly increased after adding adenosine. This suggests that there is a significant change in the number of afferents activated by stimulation of the SCs (figure 4-17-E. and F.). Generally, there was a small effect on responses from single boutons. This might be due to the presence of fewer boutons and a small reduction in calcium influx. Of course, an AP might still occur and adenosine seems to suggest that more fibers are recruited but this recruitment does not appear to result in calcium influx.

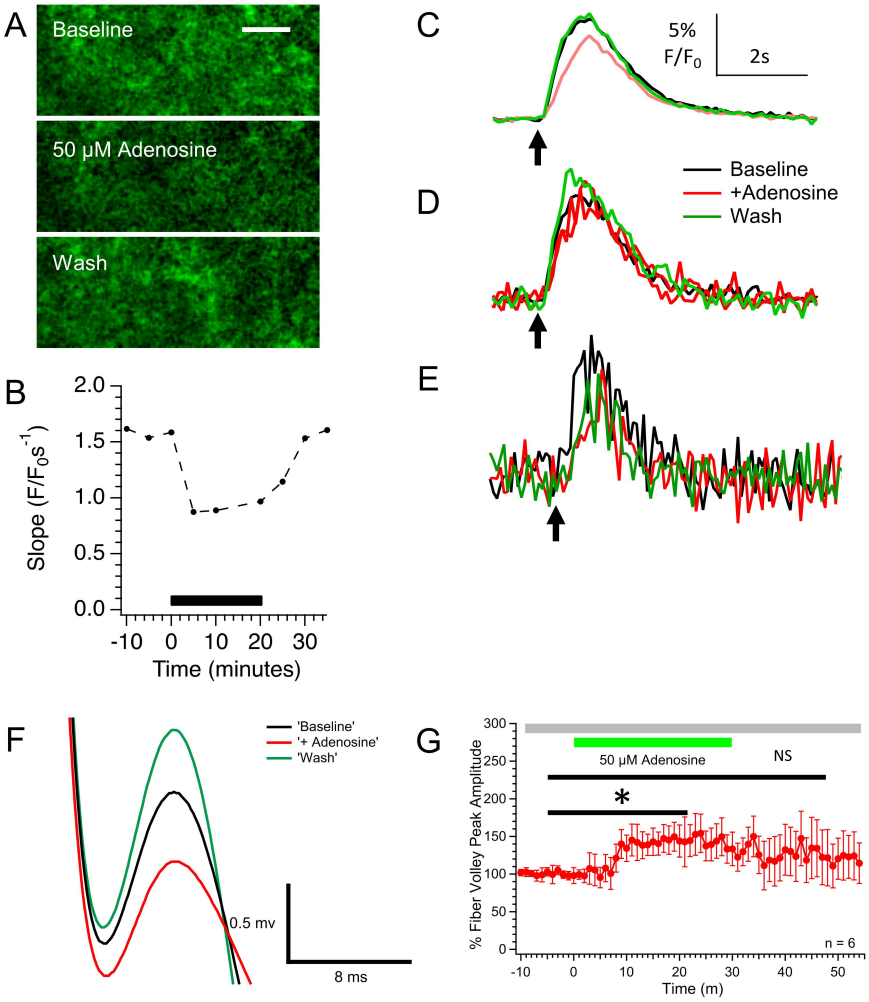

Figure 4.17. The effect of 50 µM adenosine on both individual presynaptic boutons and the presynaptic fibre volley during SC/CA1 activation in the hippocampal CA1 region of a SyG37 mouse.

Pseudo-coloured images of SyGCaMP2 fluorescence were collected before and during SC/AC stimulation at 50 V, 20 AP using 20 Hz (black arrow). A. shows the average of three SyGCaMP2 images taken immediately before stimulation when subtracted from the peak responses taken during stimulation during the baseline

and adenosine addition periods. B. shows the full frame fluorescence response change before, during, and after adenosine addition. Traces obtained from either the full frame fluorescence response (C) or from single puncta (D and E) are shown as well. F. shows the N1 component of the field potential curve where the upper traces show the averages of six sweeps each of an exemplary experiment for the baseline (black line), adenosine (red line) and for wash-out (green line). F. shows the fibre volley peak amplitude plotted against time (Mean ± SEM; *n* = 6). The statistical test were performed between baseline and the other periods. Statistics: Adenosine, U= 5, P=0.0411; Mann Whitney test. The scale bar in A is 10µ.

4.2.5 The role of the cAMP-PKA signalling cascade in SC/AC-CA1 pathway activity and the contribution of presynaptic calcium?

Long-term potentiation at the hippocampal SC/AC synapse onto CA1 pyramidal cells (Bliss and Collingridge, 1993) is perhaps the most commonly studied form of long-lasting synaptic plasticity. Long-lasting changes in synaptic efficacy can be induced either chemically, by pharmacologically stimulating the respective intracellular transduction pathways (Breakwell *et al.*, 1996, Lu *et al.*, 1999, Otmakhov et al., 2004) or synaptically using one of many different stimulus paradigms. Brief bursts of high frequency synaptic stimulation to SC/AC pathways leads to activation of AMPA and *N*-methyl-D-aspartate (NMDA) receptors which lead to large increases in intracellular Ca^{2+} and eventually LTP by activating a variety of protein kinases (Bliss and Collingridge, 1993). The cAMP-PKA signalling pathway is involved in both the pre- and post-synaptic modulation of synaptic transmission at hippocampal CA1 excitatory synapses (Bourtchouladze *et al.*, 1998, Bach *et al.*, 1999, Sharifzadeh *et al.*, 2005, Abel and Nguyen, 2008, Rutten *et al.*, 2009, Bollen *et al.*, 2014, Cavalier *et al.*, 2015). For example, forskolin mediates synaptic transmission potentiation via postsynaptic mechanisms (Sokolova *et al.*, 2006), that involves NMDARs (Otmakhov *et al.*, 2004). Many studies have shown a presynaptic effect of forskolin. For example, in the CA1 area of rat hippocampal slices, cAMP activation enhances evoked and spontaneous release of neurotransmitter in SC/AC terminals. This resulted in a significant increase in mEPSC frequency

(Chavez-Noriega and Stevens, 1994, Carroll *et al.*, 1998). Using our SyG37 mouse model, we aimed to examine whether modulation of the cAMP-PKA signalling cascade had an effect on SyGCaMP2 responses to SC/CA1 activation. Since we routinely applied AP5 in our CA1 experiments, we presume that we blocked NMDA-dependent postsynaptic effects of cAMP. We used forskolin, an adenylyl cyclase activator, and rolipram, a PDE4 inhibitor, to modulate the activity of the cAMP-PKA signalling cascade and examined signalling cross talk with the adenosine pathway using optical and extracellular recording techniques.

4.2.5.1 The effects of activation of the cAMP/PKA signalling cascade on SyG37 and fEPS responses in the CA1 area of the hippocampus.

The effects of forskolin/rolipram on the SyGCaMP2-mCherry sensor were investigated using imaging and electrophysiological experiments. In these two series of experiments we tested the effects of two different concentrations of forskolin (25 and 50 µM), each in the presence of 10 nM rolipram, on SyGCaMP2 fluorescence. After obtaining a stable baseline of evoked synaptic responses, either 25 or 50 µM forskolin and 10 nM rolipram were applied via a bath for 30 minutes and then washed out for about 20 minutes. Both concentrations of forskolin reduced SyGCaMP2 fluorescence responses to stimulation in a dose-dependent manner. 50 µM forskolin had a stronger and more significant inhibitory effect than 25 µM forskolin on the initial slope of SyGCaMP2 fluorescence. This effect was clearer from measurements of the slope than the peak amplitude of SyGCaMP2 fluorescence as shown in figure 4.18- A. and B. Responses recovered partially after applications of 25 µM forskolin but not with 50 µM. There was a significant difference between the slope of SyGCaMP2 fluorescence for the recovery period at each of these doses of forskolin. In contrast, electrophysiological recordings showed no clear effect of forskolin/rolipram on the peak amplitude of the N2 component of fEPSP (figure 4.18-C) or small non-significant effect on the slope (figure 4.18 D). The paired-pulse ratio was slightly, but not significantly, changed with either concentration of forskolin.

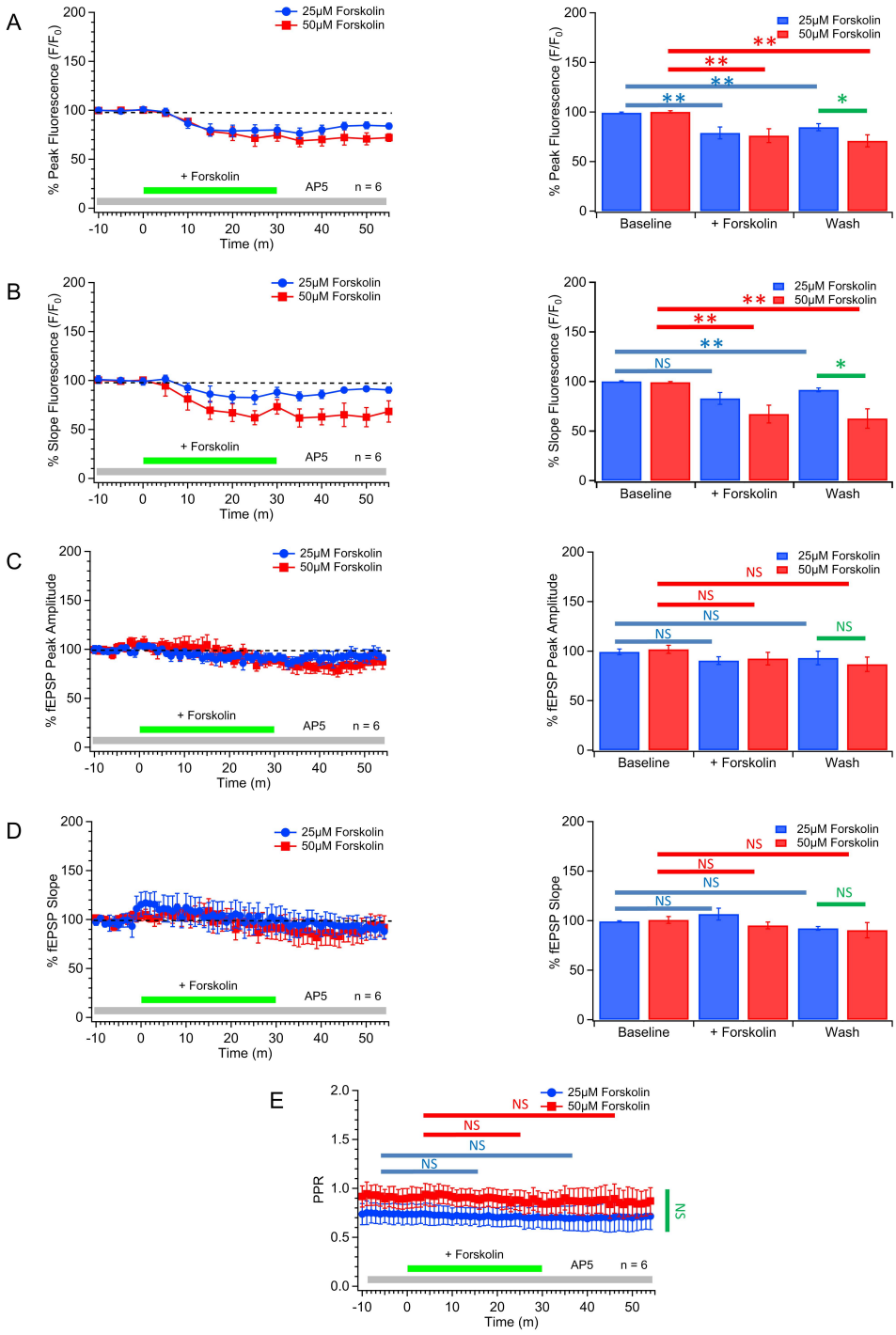

Figure 4.18. The effects of 25 and 50 μM forskolin in the presence of rolipram on SC/AC activation of the CA1 area of a SyG37 mouse.

Panels A. and B. show the effect of both 25 and 50 μM forskolin in the presence of rolipram on the peak amplitude and the slope of SyGCaMP2 fluorescence plotted against time, respectively. Panels C. and D. show the effect of forskolin/rolipram on the peak amplitude and the slope of fEPSP plotted against

time, respectively. Panel E. shows the effect of both 25 and 50 μM forskolin on PPR plotted against time. Data are represented as a percentage of averaged means (*n* = 6) of both SyGCaMP2 fluorescence and fEPSP change in the *stratum radiatum* during the control period, 30 minutes after forskolin/rolipram addition and then after a 25 minute wash out period. The statistical tests were performed between baseline and the other periods and between the effects of the two doses of forskolin. The degree of the statistical significance was presented on the histograms (right panel). Statistics: (A-blue), 25 μM forskolin, U= 0, P=0.0022; wash, U= 0, P=0.0022; (A-red), 50 μM forskolin, U= 1, P=0.0043; wash, U= 0, P=0.0022; Mann Whitney test. (A-green); wash, P=0.0394; two-way ANOVA followed by Sidak's multiple comparisons test. (B-blue), wash, U= 1, P=0.0043; (B-red), 50 μM forskolin, U= 0, P=0.0022; wash, U= 0, P=0.0022; Mann Whitney test. (B- green), wash, P=0.0216; two-way ANOVA followed by Sidak's multiple comparisons test. In E, Unpaired t test was performed between baseline and the other periods and the two-way ANOVA followed by Sidak's multiple comparisons test was used to compare between the two doses of forskolin.

4.2.5.2 Effects of forskolin and rolipram in the presence of DPCPX on SC/AC responses in the CA1 region of SyG37 mice.

We did not expect to see an inhibitory effect of forskolin/rolipram on SyG37 responses. Lu and Gean (1999) reported that forskolin-induced long-term potentiation is masked by adenosine accumulation in area CA1 of the rat hippocampus (Lu and Gean, 1999). We therefore examined whether inhibition of adenosine A_1 receptors influenced the effects of forskolin/rolipram using the lower concentration of 25 μM forskolin. Slices were pre-treated with DPCPX, a selective A_1 adenosine receptor antagonist (Bruns *et al.*, 1987a, Lohse *et al.*, 1987b). Under these conditions, 25 μM forskolin and 10 nM rolipram produced a small but non-significant increase in both the peak amplitude and the slope of SyGCaMP2 fluorescence responses, as shown in figure 4.19 A. and B. The slope of the N2 component of the field potential was also increased but non-significantly (figure 4.19-D.). The paired-pulse ratio also changed, indicating possible presynaptic action of forskolin/rolipram in the presence of DPCPX (figure 4.17-E). Inhibition of adenosine A_1 receptors by DPCPX therefore unmasked forskolin-

induced potentiation of SyGCaMP2 responses. Qualitatively similar effects were observed on the field potential recordings but the effects were not significant.

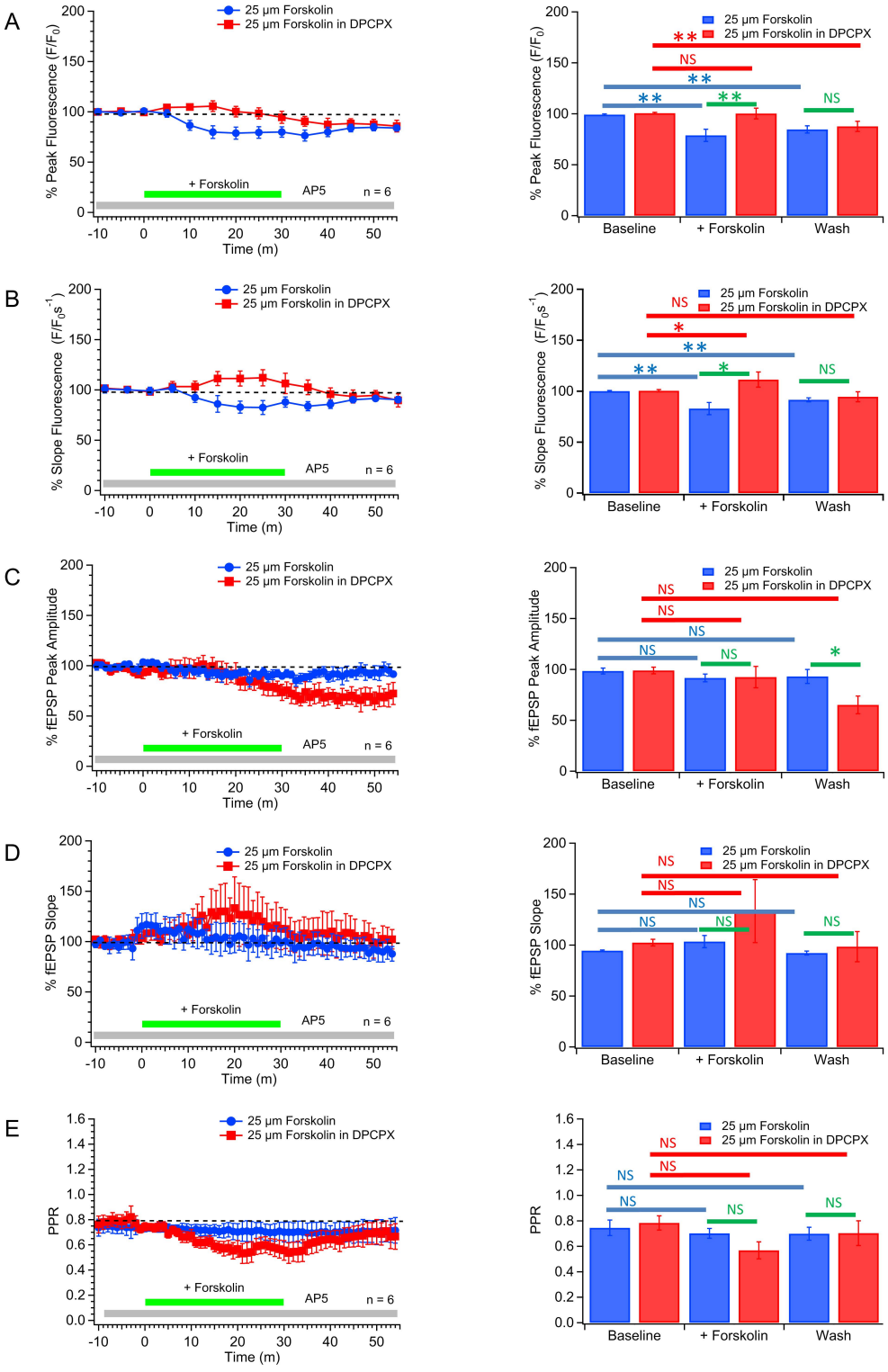

Figure 4.19. Comparison between the effect of 25 µM forskolin and rolipram in the presence and absence of DPCPX on optical and

electrophysiological responses to SC/AX activation in the CA1 area of SyG37 mice.

Panels A. and B. show the effect of 25 μM forskolin in the absence and presence of DPCPX on the peak amplitude and the slope of SyGCaMP2 fluorescence plotted against time, respectively. Panels C. and D. show the effect of 25 μM forskolin in the absence and presence of DPCPX on the peak amplitude and the slope of fEPSP plotted against time, respectively. Panel E. shows the effect of 25 μM forskolin on PPR plotted against time. The above data is represented as a percentage of averaged means (*n* = 6) of both SyGCaMP2 fluorescence and fEPSP change in the *stratum radiatum* at 15 minute control, 30 minute forskolin/rolipram addition and 25 minute washing-out periods. The statistical tests were performed between baseline and the other periods and between the two sets of experiments. The degree of the statistical significance was presented on the histograms (right panel). (A-blue), drug addition, U= 0, P=0.0022; wash, U= 0, P=0.0022; (A-red), wash, U= 0, P=0.0022; Mann Whitney test. (A-green), drug addition, P=0.0067; two-way ANOVA followed by Sidak's multiple comparisons test. (B- blue), wash, U= 1, P=0.0043; (B-red) - drug addition, U= 0, P=0.0022; wash, U= 0, P=0.0022; Mann Whitney test. (B-green); drug addition, P=0.0159; two-way ANOVA followed by Sidak's multiple comparisons test. (C-green); wash, P=0.0272; two-way ANOVA followed by Sidak's multiple comparisons test. In E, Unpaired t test was performed between baseline and the other periods and the two-way ANOVA followed by Sidak's multiple comparisons test, was used to compare between the two doses of forskolin.

4.2.5.3 Effect of forskolin and rolipram on SC/AC activation in the CA1 area in the presence of both DPCPX and PKA inhibitors.

Simultaneous application of forskolin/rolipram and DPCPX induced a potentiation of SyGCaMP2 responses. To confirm that this was mediated by protein kinase A, the experiments were repeated in the presence of the PKA inhibitor PKI (14-22) amide. Slices were incubated with aCSF containing 50 μM D-AP5, 250 nM DPCPX and 100 μM PKI (14-22) amide from the outset. After obtaining stable baselines 25 μM forskolin and 10 nM rolipram were applied for 30 minutes and then washed out for a further 20 minutes. 25 μM forskolin and 10 nM rolipram produced a significant reduction of the slope of SyGCaMP2 fluorescence which

did not recover to the baseline levels upon washout (figure 4.20-B). The slope of the N2 component of the field potential was also significantly reduced and this also did not recover to the baseline levels as shown in figure 4.20-D. The paired-pulse ratio reduced slightly in the presence of DPCPX and PKI but not significantly (figure 4.18-E). A two-way ANOVA test detected a significant difference between the two groups (with and without PKI); in terms of SyGCaMP2 fluorescence. None of the electrophysiological parameters demonstrated any significant changes between two groups as the SEM were very large, as shown in figure 4.20-D. and E.

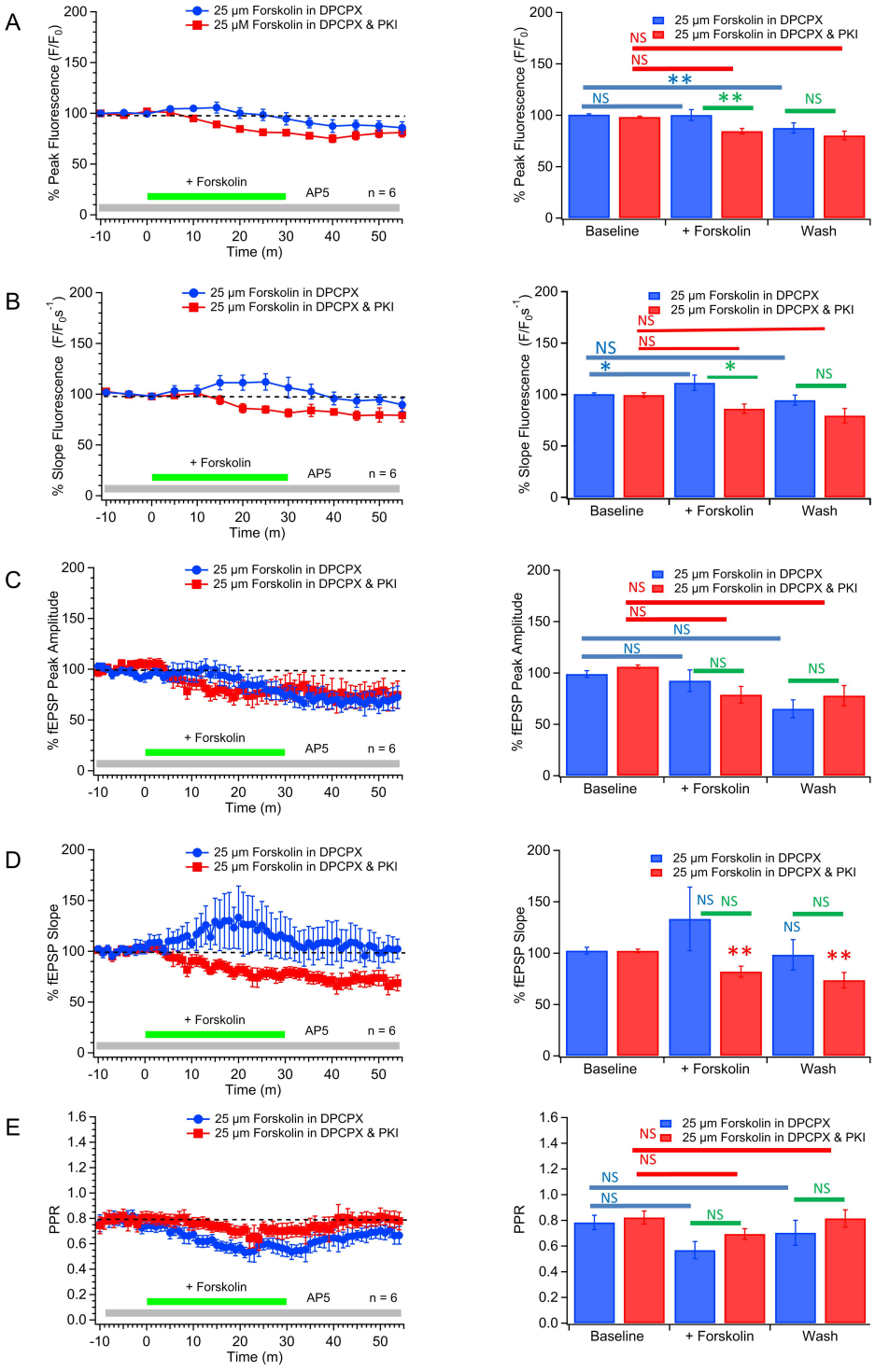

Figure 4.20. Comparison between the effect of 25 µM forskolin and 10 nm rolipram in the presence of DPCPX in the presence and absence of protein kinase inhibitor (PKI) on SC/AC activation in the CA1 area of a SyG37 mouse.

Panels A. and B. show the effect of 25 µM forskolin/10 nm rolipram in the presence of DPCPX in the absence and presence of the PKI inhibitor (14-22)

amide on the peak amplitude and the slope of SyGCaMP2 fluorescence plotted against time, respectively. Panels C. and D. show the effect of 25 μM forskolin and DPCPX in the absence and presence of PKI on the peak amplitude and the slope of fEPSP plotted against time, respectively. Panel E. shows the effect of 25 μM forskolin and DPCPX in the absence and presence of PKI on PPR plotted against time. Data are represented as a percentage of averaged means (n = 6) of both SyGCaMP2 fluorescence and fEPSP change in the *stratum radiatum* during 15 minute control, 30 minute forskolin/rolipram addition and after a 25 minute wash out period. The statistical tests were performed between baseline and the other periods and between the two sets of experiments. The degree of the statistical significance was presented on the histograms (right panel). Statistics: (A- blue), wash, U= 0, P=0.0022; Mann Whitney test. (A- green), drug addition, P=0.0075; two-way ANOVA followed by Sidak's multiple comparisons test. (B- blue), drug addition, U= 5, P=0.0043. (B-green); drug addition, P=0.0488; two-way ANOVA followed by Sidak's multiple comparisons test. (D-green); Drug addition, P=0.0087; wash, P=0.0021; Mann Whitney test. In E, Unpaired t test was performed between baseline and the other periods and the two-way ANOVA followed by Sidak's multiple comparisons test, to compare between the two doses of forskolin.

4.3 Discussion

In this chapter we evaluated the sensitivity of a new, ratiometric fluorescent calcium indicator, SyGCaMP2-mCherry by characterising its responses to activation of SC-CA1 pathway. In the CA1 region there is general agreement that LTP is dependent upon NMDA-receptors (Collingridge et al., 1983). Little is known about the exact role of presynaptic calcium signalling in the CA1 region. However, several studies have reported concomitant changes in presynaptic vesicle recycling associated with long-term potentiation in area CA1 (Stanton *et al.*, 2006). A combination of imaging and field potential recordings was carried out in the hippocampal CA1 area using electrical stimulation and pharmacological manipulation to confirm whether the SyGCaMP2-mCherry sensor was capable of reporting presynaptic changes in calcium signalling.

4.3.1 Electrical activation studies of the SC-CA1 pathway reveals the sensitivity of the SyGCaMP2-mCherry sensor.

The effects of altering the stimulus intensity in the SC-CA1 pathway of SyG37 mice revealed that responses increased in a roughly linear manner, particularly at lower intensities, indicating a gradual recruitment fibres (figure 4-4). SyGCaMP2 fluorescence, as an indicator of a presynaptic calcium, showed a direct correlation with the postsynaptic potentials except at the two highest stimulus intensities examined, 60 and 70 V (figure 4-5). This loss of linearity might be due to the sensor saturation because fEPSP responses continued to increase. The single bouton experiments showed that raising stimulus intensity recruits more fibres/boutons rather than leading to substantial increases in the amount of calcium per bouton. Presynaptic fibre volley recordings were consistent with single bouton experiments where the N1 component of the field potential curve was also significantly increased by increasing the stimulus intensity confirming the possibility of the recruitment of a different fibre type at higher stimulus intensities (figure 4-16). SyGCaMP2 fluorescence also showed a positive relationship with both the stimulus number and intensity except there was a decrease in the SyGCaMP2 fluorescence at 100 Hz (figure 4-6 & 7). With SyGCaMP2-mCherry, it was possible to detect responses to single stimuli

(Okorocha, 2016) as it is the case for the GCaMP6 sensor. In our hands, increasing stimuli intensity, number and frequency of stimulation showed a prominent uniform pattern of SyGCaMP2 response makes it a useful tool for calcium signalling monitoring in the CNS.

4.3.2 A comparative study of adenosine receptor manipulation showed the sensitivity and confirmed the presynaptic locus of SyGCaMP2-Mcherry sensor in CA1 microcircuit of SyG37 transgenic mouse model.

Adenosine reduced SyG37 responses in the presence of AP5 and on washout, responses recovered and even potentiated. These effects were accompanied by a reduction in fEPSP size and an increase in PPR (figure 4-8 & 9). Together, these results suggest a presynaptic site of action of adenosine and indicate that this effect includes a reduction in presynaptic calcium. MP experiments using the whole frame of the response to SC/AC stimulation revealed the same basic effects as epifluorescence imaging (figure 4-17). If only responding boutons were examined, the effect was consistent but less clear giving the impression that this population of responding boutons was somehow more resistant to adenosine. The numbers of boutons contributing clearly reduced upon application of adenosine but measurements of the fibre volley showed that there was no reduction in fibre recruitment. These results suggest, therefore, that adenosine may have reduced calcium influx so much in some terminals to have made their response too small for us to identify them as responding, giving the appearance that boutons were not activated. It is interesting to speculate why some boutons are not affected by adenosine. They might reflect a separate population of presynaptic terminals from either a different population of cells, or represent heterogeneity within the same population of cells. Further experiments and a more detailed data analysis may be needed to determine if we can divide these presynaptic boutons into different groups according to their ability to recover from adenosine. Zhang and Linden (2012) found that parallel fibre boutons located in the outer molecular layer have a lower calcium clearance rate than boutons located in the inner molecular layer. They suggested that cerebellar granule cell boutons should be regarded as different subpopulations of boutons which may

exhibit different properties rather than forming a homogeneous population. In general, the reduction in SyGCaMP2 fluorescence is due to a reduction in the amount of calcium influx per terminal, as opposed to a reduction in the number of contributing terminals.

Our results with adenosine on SyGCaMP2 responses are largely consistent with those of Wu and Saggau, and others, who showed that adenosine reduced presynaptic calcium as this suppression is thought to be of presynaptic origin as it changes synaptic paired-pulse facilitation in the hippocampus (Wu and Saggau, 1994, Gundlfinger *et al.*, 2007). The effects of adenosine were mediated via A_1 receptors since they were blocked by DPCPX (Lohse *et al.*, 1987a). Of the three optical models used only the SyG37 model reliably detected the effects of DPCPX and revealed that DPCPX is acting to inhibit a tonic, inhibitory effect of adenosine within the CA1 region of the hippocampus (figure 4-10).

Experiments repeated in presence of blocking synaptic transmission produced results that were very similar and provide further confirmation of the results of Wu and Saggau (1994) that adenosine reduces calcium influx within the terminals of SC fibres (figure 4-13 & 14). Even when synaptic transmission was blocked, SyG37 responses were still present and more than 70% of the signal originated from SC/AC terminals (figure 4-12). In our hands, blockade of GABA-ergic and Glutamatergic ionotropic receptors reduced intrinsic autofluorescence measurements almost completely indicating that autofluorescence measurements are largely postsynaptic in origin (figure 4-12). It was therefore not surprising that neither adenosine nor DPCPX (even at higher doses) had any noticeable effect under these conditions. Moreover, presynaptic loading of terminals with organic calcium dyes, fluo-4, was not as sensitive as the SyG37 model. This is most probably due to dye redistribution or leaking from cells over time, non-uniform dye loading, cell size differences and photobleaching (Gee et al., 2000, Paredes et al., 2008). So, we have been able to confirm previous results but using a potentially better and easier model for measuring presynaptic calcium.

One surprising observation was that in the experiments where PTX, AP5 and DNQX were pre-incubated, the baseline peak responses were larger than those measured just with AP5 present (figure 4-15). This was surprising because when

these receptor antagonists were added after a stable baseline of responses had been established, responses decreased. Zhao *et al*., (2011) found that there was an increase in the amount of presynaptic calcium in response to an action potential following a chronic decrease in the activity of the neuronal network which lead to a form of homosynaptic plasticity (Zhao *et al.*, 2011). The reason for this is not entirely clear but Ripley *et al* (2011) reported that there was a strong correlation between the stability of presynaptic inputs and the presence of postsynaptic AMPA receptors. It is possible therefore that in the absence of long-term AMPA receptor activity, presynaptic signals increase in a compensatory manner leading to an increase in responsiveness. These observations suggested that postsynaptic AMPA receptors might play a crucial role in regulating synapse stability (Ripley *et al.*, 2011). Results in this chapter demonstrate that of the four different models tested, the SyG37 model is the most sensitive method. It allows presynaptic calcium to be measured in isolation and because it is possible to measure responses even in the presence of synaptic blockers, it is useful tool to examine the contribution of presynaptic calcium to cell signalling.

4.3.3 CAMP-PKA signalling cascade required for SC-CA1 pathway activity with the possibility of presynaptic calcium contribution.

In the CA1 hippocampal area, forskolin potentiates synaptic transmission through postsynaptic mechanisms which may involve phosphorylation of AMPA receptors (Sokolova et al., 2006). According to Otmakhov (2004), cLTP induced by forskolin and rolipram requires NMDARs since it was blocked by AP5 (Otmakhov et al., 2004). In our experiments, we applied AP5 and so any effects of forskolin/rolipram are unlikely to be postsynaptic or at least NMDAR dependent. Many studies have shown that forskolin can have presynaptic effects. For example, in the CA1 area of rat hippocampal slices, cAMP activation enhances evoked and spontaneous release of neurotransmitter in SC terminals. This was evident from a significant increase in mEPSC frequency (Chavez-Noriega and Stevens, 1994, Carroll et al., 1998). Luchkina *et al.* (2014) found that forskolin has effects on both pre and postsynaptic terminals but the postsynaptic effects are dependent on the presence of GluA4 which is high in immature synapses but

disappears over time. In our experiments, forskolin and rolipram produce a reduction in SyGCaMP2 fluorescence, in a dose dependent manner, but a very small increase in the slope of the fEPSP **(**figure 4-18 & 19). This effect was reversed in the presence of DPCPX revealing a small increase in SyGCaMP2 responses, fEPSP slope and a concomitant reduction in PPR (figure 4-20). These results are largely consistent with those of Lu and Gean (1999). They found that potentiation induced by forskolin in the presence of a type 1 Adenosine receptor antagonist (DPCPX) was PKA-dependent, insensitive to the NMDAR antagonist AP5 and accompanied by a reduction in the PPR. However, they found that application of forskolin with the type 4 specific PDE inhibitor (RO-20-1724) did produce LTP suggesting that it was adenosine, a breakdown product of cAMP that was responsible for masking potentiation. In our hands, using a different PDE4 inhibitor Rolipram, this was not the case. The explanation for this is not clear. Moreover, the level of potentiation we observed was very small compared to that seen previously. It is possible that our fEPSP recordings were a mixture of fEPSP and population spike which are differently affected by forskolin but this does not account for the small effects on presynaptic calcium unless the effect on calcium is relatively small compared to the effect on transmitter release. This small increase in the presynaptic calcium may be also due to the effect of collecting these data at room temperature, since the short-term plasticity as a presynaptic indicator, is temperature-dependent at CA3-CA1 synapses (Klyachko and Stevens, 2006, Gundlfinger, 2008). Another possibility is the effect of animal age as forskolin may only have effects in less mature synapses (Luchkina et al., 2014) which might have some influence on our data. In general, these results confirmed the cAMP/PKA pathway's importance in basal synaptic transmission in CA1 area with a possible contribution of the presynaptic calcium as this detected by SyGCaMP2-mCherry sensor. The sensitivity of SyGCaMP2-mCherry sensor make the SyG37 mouse a useful model for long-term cellular imaging of neuronal populations in the intact brain.

Chapter 5: Evaluation of the SyGCaMP2-mCherry sensor within the MF-CA3 pathway of SyG37 mice.

5.1 Introduction

Presynaptic calcium may play a significant role in certain types of longer-term plasticity of presynaptic origin including LTP at the synapses formed between mossy fibres and pyramidal cells within the CA3 region of the hippocampus (Henze *et al.*, 2000b, Nicoll and Schmitz, 2005). Mossy fibre LTP involves numerous receptors and second messengers, but it is of presynaptic origin and involves the second messenger cAMP (Huang *et al.*, 1994a, Weisskopf *et al.*, 1994, Trudeau *et al.*, 1996). Mossy fibre LTP, as well as the analogous release of transmitter from synaptosomes extracted from this region, is enhanced by the activation of cAMP with the adenylate cyclase activator (forskolin), and is blocked by PKA inhibitors such as H-89 (Rodriguez-Moreno and Sihra, 2004). In this chapter, experiments on the MF-CA3 pathway were carried out in the same way as for those described in Chapter 4. The adenosine receptor modulation experiments were repeated in the presence of DNQX and PTX to block AMPA- and GABA/Glycinergic transmission to ensure that the recorded responses were not from presynaptic terminals of secondary neurones. As in chapter 4, a combination of imaging (SyG37) and field potential recordings were carried out using electrical stimulation and pharmacology. In all cases, care was taken to ensure that the optical and electrophysiological recorded responses from SyG37 mice were from mossy fibres. Consequently, to ensure that responses underwent a substantial level of paired-pulse facilitation and were selectively blocked by addition of DCG-IV, which is an mGluR-2 agonist (Lanthorn *et al.*, 1984, Yokoi *et al.*, 1996).

5.2 RESULTS

5.2.1 Electrode positions for SC-CA1 pathway activation and recording.

Data here were collected and presented in the same way as Chapter 4, section 4.2.1. For MF-CA3 experiments, stimulating electrodes were placed in the *st. granulosum* of the dentate gyrus and the recording electrode was placed in the *st. lucidum* layer of CA3. DCG-IV (an mGluR-2 agonist) was routinely applied to hippocampal slices after experiments as mossy fibre terminals are reported to be selectively sensitive to DCG-IV. Activation of mGluR-2 receptors inhibits glutamate release and, as a consequence, synaptic transmission (Lanthorn *et al*., 1984, Yokoi *et al*., 1996). Therefore, in all MF-CA3 recordings, 1 μM DCG-IV (a group II mGlu receptor agonist) was applied at the end of the experiments. Data were included if responses were reduced by more than 90%, confirming that we were recording from the MF-CA3 pathway with minimal contamination from other pathways. Mossy fibre responses also have characteristically large degrees of paired-pulse facilitation. Figure 5.1-C illustrates a typical field potential recording with large PPF.

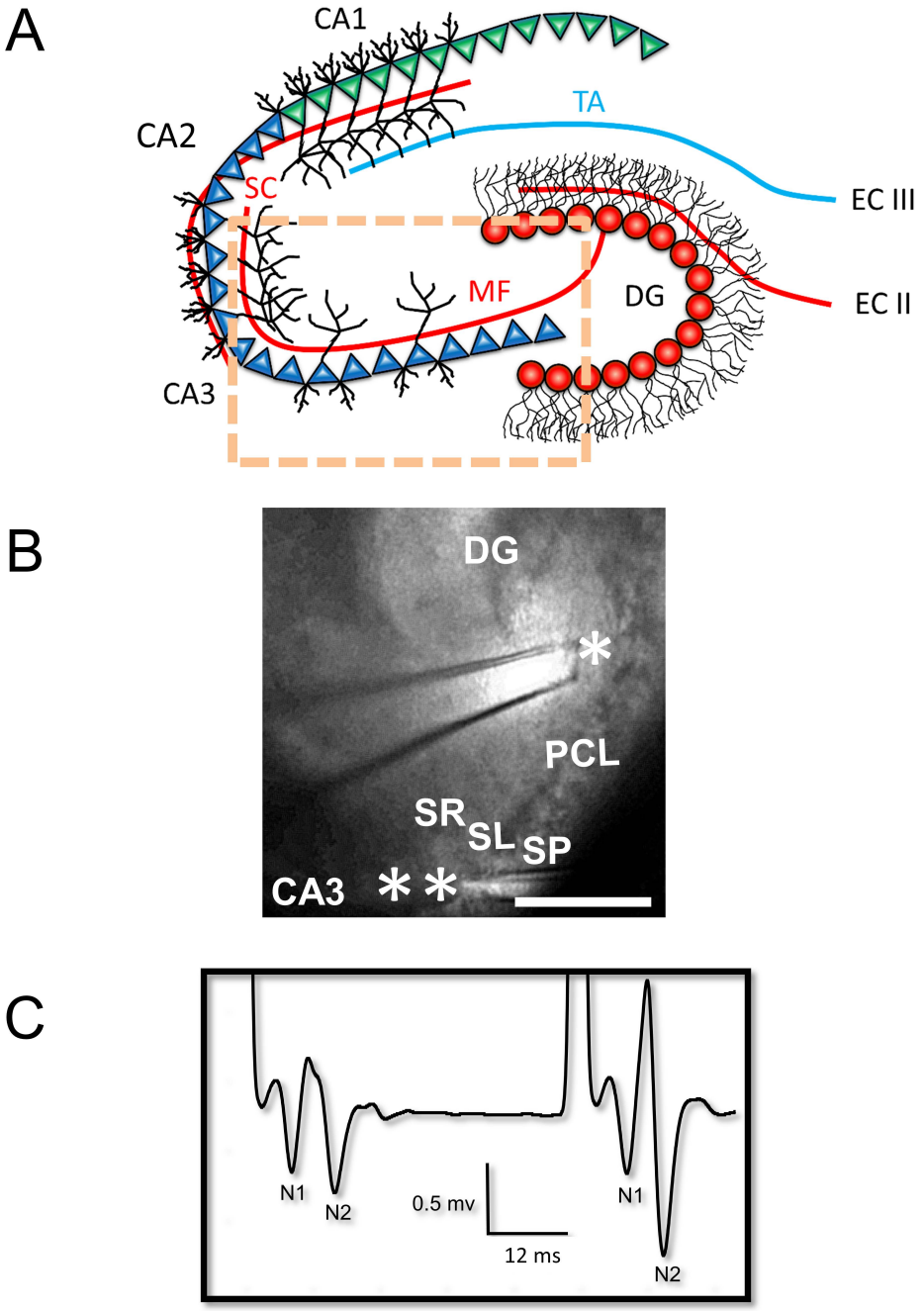

Figure 5.1. Schematic drawings illustrating the synaptic pathways of the hippocampus and the positions of stimulating and recording electrodes within the CA3 region.

A. shows a schematic diagram of transverse section of the mouse hippocampus. B. shows the light transmission image of a transferase section of SyG-37 mouse CA3 region of the hippocampus illustrating stimulating and recording electrode positions and shows different layers and regions of the hippocampal CA3 area, which contains the following layers: SO = *stratum oriens*, PCL = Pyramidal cell layers, SL= *stratum lucidum* and *stratum radiatum*. The single asterisk indicates

the stimulating electrode position and the double asterisks indicate the recording electrode position. C. shows the N1 and N2 components of the field recordings in the *stratum lucidum* of the hippocampal CA3 area as a result of the mossy fibre activation. The scale bar in B is 50 µm.

5.2.2 Electrical activation studies of the MF-CA3 pathway of the SyG37 mouse model.

In this study, we used the SyGCaMP2-mCherry sensor within the SyG37 transgenic mouse to characterise the properties of presynaptic calcium signalling upon activation of the MF-CA3 pathway. The same parameters described in the previous chapter were used to examine the effects of stimulus intensity and the effects of changing the number and frequency of stimuli on SyGCaMP2 responses.

5.2.2.1 The effects of altering the stimulus intensity on the MF-CA3 pathway of the SyG37 mouse model.

In a first set of experiments, the intensity of stimuli applied to the MF pathway was increased from 0 to 70 V using a fixed number of 10 stimuli delivered at 20 Hz. The example illustrated in figure 5.2 demonstrates that SyGCaMP2 fluorescence increased in a roughly linear manner with stimulus intensity with no obvious sign of saturation. The maximal response recorded at 70 V elicited a response which was approximately twice the size of responses recorded at 20V (figure 5.2-A & B). The effects of stimulus intensity on the decay time constant are shown in figure 5.2-C. The effects of stimulus intensity of the N2 component of the field potential recorded from the *stratum lucidum* and are shown in figure 5.2 D-F as well, showing same trend as imaging data. The paired-pulse ratio shows a gradual increase up to a peak at 20 V (figure 5.2-F).

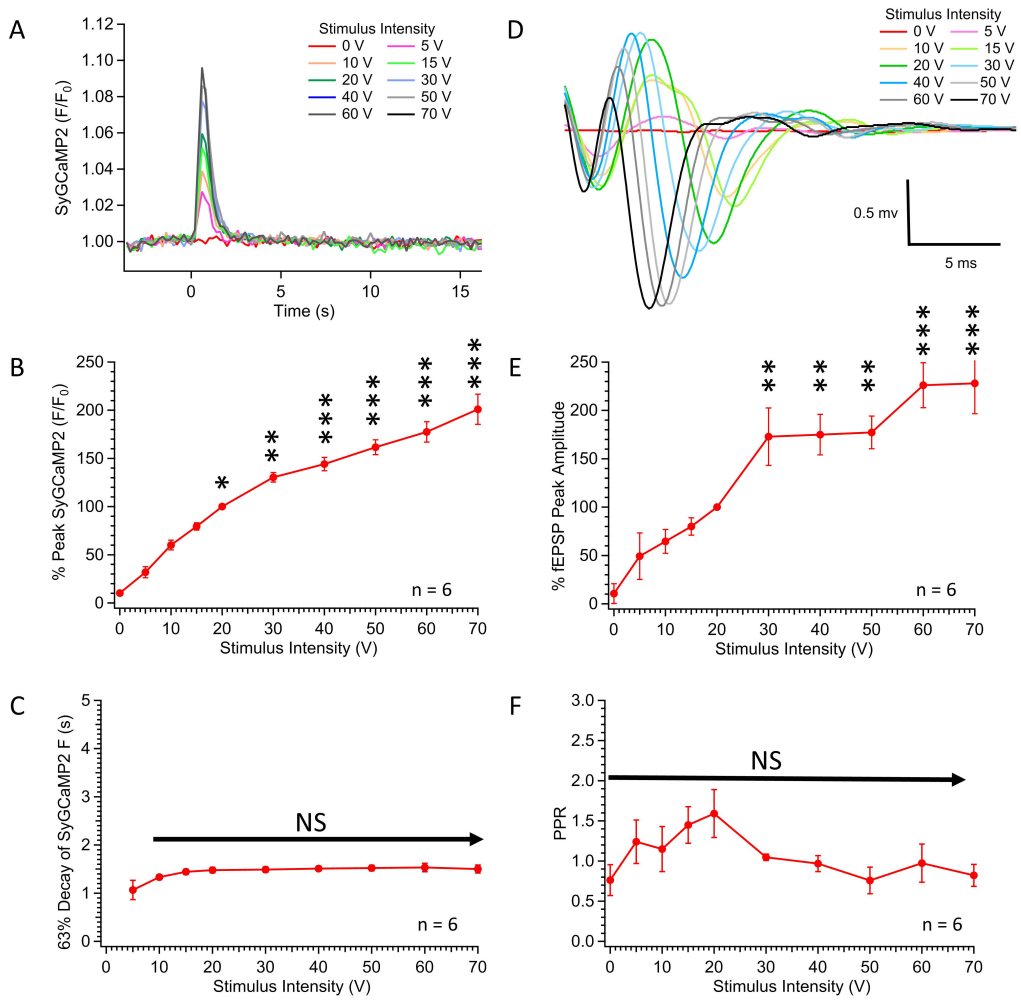

Figure 5.2. The effect of increasing stimulus intensity on SyGCaMP2 fluorescence and fEPSP responses in the hippocampal CA3 region after MF-CA3 activation.

A. shows the mean responses to different stimulus intensities from ROIs placed within the *stratum lucidum* of the CA3 hippocampal region as plotted against time. B. and C. illustrate the effects of increasing stimulus intensity on the peak and 63% decay times, respectively. D. illustrates the effects of increasing stimulus intensity on fEPSPs; each trace is the average of six sweeps. E. and D. show the change in peak amplitude and PPR of field excitatory postsynaptic potentials (fEPSPs), respectively. Values in B and E are normalized to the response at 20 V. Statistical differences are indicated with asterisks with *, ** or *** according to the level of significance. The means and standard errors from 6 separate experiments are shown. The statistical tests were performed between 0V and other stimulus intensities. Statistics: (B), 20V, P=0.0169; 30V, P=0.0029; 40V, P=0.0002; 50V, P=0.0001; 60V, P=<0.0001; 70V, <0.0001. (E), 30V, 0.0040;

40V, 0.0015; 50V, 0.0017; 60V, P=<0.0001; 70V, <0.0001; Kruskal-Wallis test followed by Dunn's multiple comparisons test. (C & F), no significant difference was observed; Ordinary one-way ANOVA followed by Dunnett's multiple comparisons test.

5.2.2.2 The effects of altering stimulus frequency on the SyGCaMP2 and fEPSP responses of MF-CA3 pathway.

The effects of different frequencies of stimulation were tested at a fixed stimulus intensity (20 V) and a fixed stimulus number (10 AP). Imaging data showed that the peak amplitude of SyGCaMP2 fluorescence responses increased in a roughly linear manner up to approximately 20 Hz, which then reached a peak at around 50 Hz. There was a subsequent decline in the SyGCaMP2 fluorescence at 100 Hz, as shown in figure 5.3-A and B. The decay time was also measured; an inverse relationship between the increase in stimulus frequency and the 63% decay time of SyGCaMP2 fluorescence (figure 5.3-C) was observed.

Field potential recordings showed a different trend compared to the imaging results. The peak amplitude and the slope of the N2 component of the last pulse in the train of the field potential were slightly increased by increasing the stimulus frequency with the 10 V required to elicit a suitable response in the *stratum lucidum* and with 100 Hz eliciting a maximal response. At 50 Hz, the peak amplitude decreased slightly, as shown in figure 5.3-D and E. Again, the effect at lower frequencies is more pronounced for SyGCaMP2 fluorescence than on field potential recordings. There was no that clear effect of changing stimulus frequency on the paired-pulse ratio (figure 5.3-F).

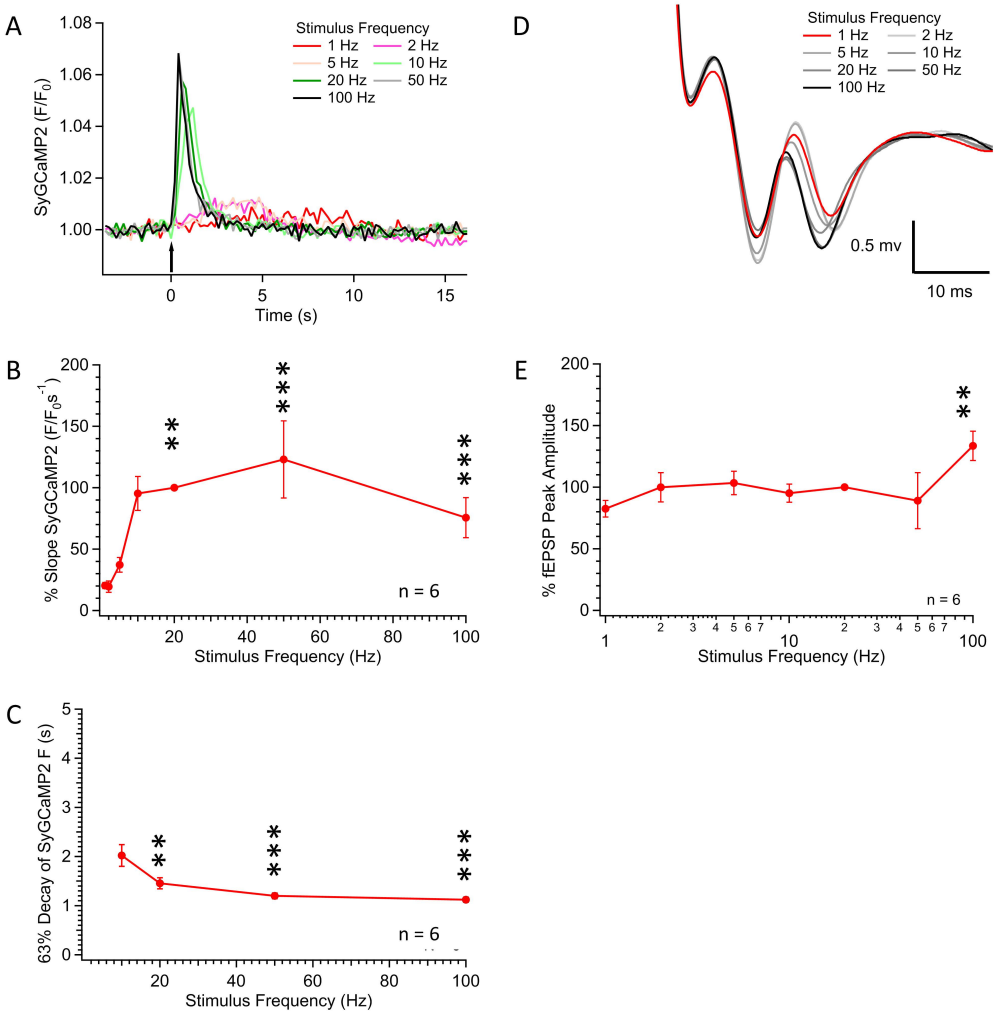

Figure 5.3. The effect of increasing stimulus frequency on both SyGCaMP2 fluorescence and its corresponding fEPSP in the hippocampal CA3 region after MF-CA3 activation.

A. shows the mean responses to different Hz stimulation from ROIs placed within the stratum lucidum of the CA3 hippocampal region plotted against time. B. and C. illustrate the effects of increasing stimulus frequency on the peak and 63% decay time over time for SyGCaMP2 fluorescence, respectively. D. shows field recordings curve illustrating the action of increasing stimulus frequency on MF-CA3 activation. E. and F. show the change in peak amplitude and PPR of field excitatory postsynaptic potentials (fEPSPs) whilst increasing stimulus frequency. The values shown are mean values ± SEM; values in B and E are normalized to the response at 20 Hz. The statistical tests were performed between 0Hz and other stimulus intensities. Statistics: (B), 20Hz, P=0.0069; 50Hz, P=<0.0001; 100Hz, <0.0001. (E), 70Hz, P=0.0029; Kruskal-Wallis test followed by Dunn's multiple comparisons test. (C), 20Hz, P=0.0081; 50Hz, P=0.0003; 100Hz,

P=0.0003, Ordinary one-way ANOVA followed by Dunnett's multiple comparisons test.

5.2.2.3 The effects of altering the stimulus number on the MF-CA3 pathway of the SyG37 mouse model.

In this section, we tested the effects of changing stimulus number on SyGCaMP2 fluorescence and its corresponding fEPSP using a fixed frequency of 20 Hz and fixed intensity of 20 V. The peak amplitude of the SyGCaMP2 fluorescence responses were observed to increase steadily with increasing stimulus number (figure 5.4-A, and B). Increasing the stimulus number from 1 to 20 AP increased the SyGCaMP2 fluorescence in a roughly linear manner. Responses reached a plateau at around 30 stimuli with no clear, subsequent decline, even at 100 stimuli. The time taken to decay to 63% of the peak response was measured as well, showing a positive relationship with stimulus number as shown in figure 5.4-C.

Field potential recordings were consistent with imaging data. The peak amplitude of the N2 component of the field potential were also increased by increasing the stimulus intensity, with 10-20 stimuli required to elicit a suitable response in the *stratum lucidum*; with the peak response reaching to near maximum after 20 stimuli, with only further small increases at 100 stimuli (figure 5.4-D and E). An inverse relationship between the stimulus number and paired-pulse ratio was observed, where the PPR was larger at smaller stimulus numbers and plateaued after 20 stimuli, as shown in figure 5.4-F. In general, as for the stimulus frequency results, the effect at lower stimulus numbers was more pronounced on SyGCaMP2 fluorescence than on field potential recordings. The SyGCaMP2-mCherry sensor shows a high sensitivity to any change in stimulus number, even at 1 action potential, where it detects any calcium increase with successive stimuli by increasing its fluorescence.

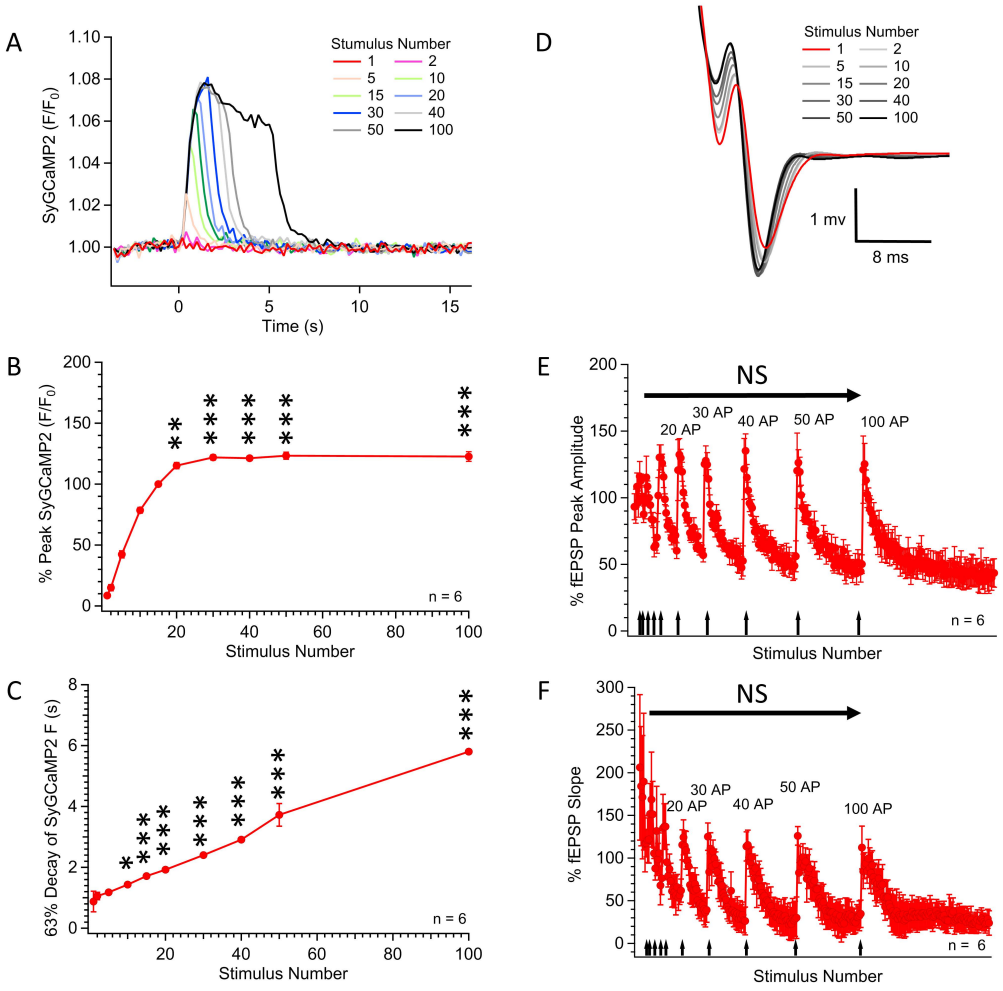

Figure 5.4. The effect of increasing stimulus number on both SyGCaMP2 fluorescence and its corresponding fEPSP in the hippocampal CA3 region after MF-CA3 activation.

A. shows the mean responses to different stimulus number stimulations from ROIs placed within the stratum lucidum of the CA3 hippocampal region plotted against time. B. and C. illustrate the effects of increasing stimulus number on Peak and 63% decay time over time on SyGCaMP2 fluorescence, respectively. D. shows field potential recordings illustrating the action of increasing stimulus number on MF-CA3 activation. E and F show the change in the peak amplitude and the slope of field excitatory postsynaptic potentials (fEPSPs) with increasing stimulus number, respectively. The values shown are mean values ± SEM; values in B and E are normalized to response at 20 AP. The statistical tests were performed between 0V and other stimulus intensities. Statistics: (B), 20AP, P=0.0056; 30AP, P=0.0002; 40 AP, P=0.0002; 50 AP, P=0.0001; 100 AP, P=0.0002; Kruskal-Wallis test followed by Dunn's multiple comparisons test. (C),

15AP, P=0.0102; 20AP, P=0.0007; 30AP, P=<0.0001; 40AP, P=<0.0001; 50AP, P=<0.0001; 100AP, P=<0.0001; Ordinary one-way ANOVA followed by Dunnett's multiple comparisons test. (E & F), no significant difference was observed; Kruskal-Wallis test followed by Dunn's multiple comparisons test.

5.2.3 The relative mono- and poly-synaptic contributions of presynaptic SyGCaMP2 fluorescence within the CA3 microcircuit.

We next investigated the effects of various pharmacological manipulations on MF activation in the CA3 area by comparing optical responses of the SyGCaMP2-mCherry sensor in the SyG37 mouse model and field potential recordings. As in chapter 4, we examined the effects of pharmacological manipulations that are known to affect synaptic transmission through presynaptic effects to establish whether these manipulations led to a corresponding change in SyGCaMP2 fluorescence.

5.2.3.1 Effects of adenosine receptor modulation on the CA3 area of a SyG37 mouse.

We first examined the effects of adenosine as this has been shown to reduce synaptic transmission at CA3 synapses through presynaptic processes (Wu and Saggau, 1994). We then examined the effects of the removal of the adenosine tone by using DPCPX as a specific, competitive A_1 receptor antagonist. Synaptic transmission was blocked in later experiments to investigate the relative mono- and poly-synaptic contributions of presynaptic SyGCaMP2 fluorescence within the CA3 microcircuit.

5.2.3.1.1 Effects of 50 µM adenosine on MF activation in the CA3 area of the SyG37 mouse model.

Experiments were carried out in the same way as for those described in section 4.2.3 in Chapter 4. Adenosine produced a pronounced effect on both SyGCaMP2 fluorescence (~25% reduction) and concurrently recorded field potentials (~70% reduction), reaching a minimum within 10 minutes of application. Both the fluorescence and the N2 component of the field potential were significantly

reduced compared to baseline responses. Both the fluorescence and the fEPSP peak amplitude recovered during the wash-off period (figure 5.5). Adenosine had no effect on the 63% decay time of the SyGCaMP2 fluorescence (figure 5.5-D). Figure 5.5-G shows that application of adenosine increased the magnitude of the PPF from ~1.8 to ~3.0, which is consistent with a presynaptic action of adenosine. Bath application of 1 µM DCG-IV at the end of these experiments reduced both SyGCaMP2 fluorescence and field potential recordings by more than 90%, thereby confirming that we were recording from the MF-CA3 pathway.

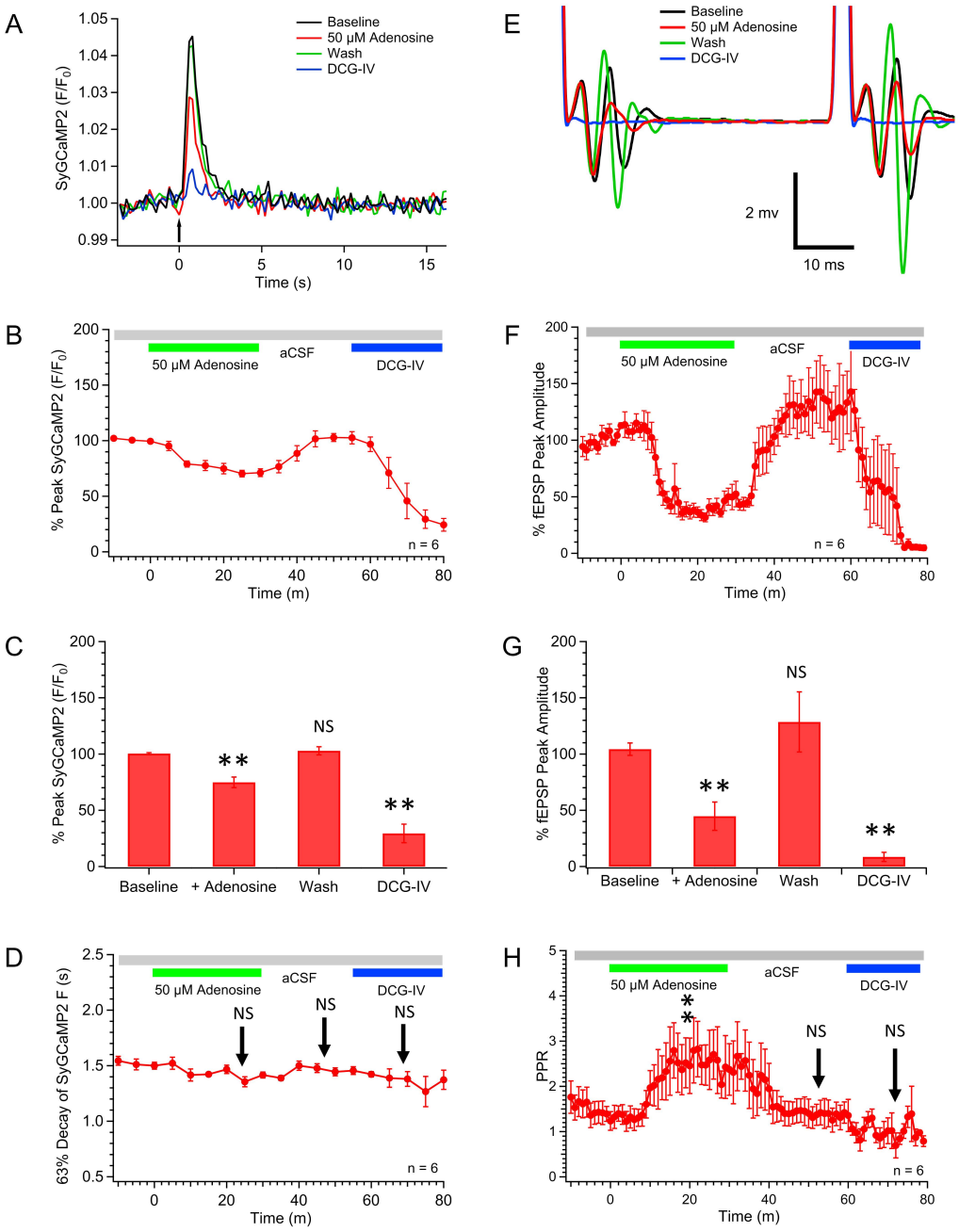

Figure 5.5. Effect of 50 µM adenosine on responses to MF activation in the CA3 area of the SyG37 mouse's hippocampus.

A. shows the mean responses to the effects of adenosine from ROIs placed within the *stratum lucidum* of the CA3 hippocampal region plotted against time. B. and C. show line and bar charts that illustrate the effects of adenosine on SyGCaMP2 fluorescence peak amplitude over time. D. illustrates the effects of adenosine on the SyGCaMP2 fluorescence 63% decay time over time. E. shows the effects of adenosine on traces of the field potential curve collected from the *stratum lucidum*

of the CA3 hippocampal region. E. and F. show line and bar charts illustrating the change in peak amplitude of the field potential before, during, and after addition of adenosine. G. illustrates the effects of adenosine on PPR plotted against time. The gray bar represents aCSF application and the recording from the MF-CA3 pathway was confirmed by DCG-IV bath application at the end of each experiment (blue bar). Statistical differences are indicated with asterisks with *, ** or *** according to the level of significance. Statistics: (C), Adenosine, U= 0, P=0.0022; DCG-IV, U= 0, P=0.0022; (G), Adenosine, U= 0, P=0.0022; DCG-IV, U= 0, P=0.0022; Mann Whitney test. (H), adenosine, t(10) = 2.417, P=0.0362; unpaired t test.

5.2.3.1.2 Effects of the 250 nM A_1-adenosine receptor antagonist DPCPX MF responses in the CA3 area of SyG37 mice.

We next tested the effects of the A1- receptor antagonist, DPCPX on synaptic transmission in the CA3 region. After obtaining stable baselines 250 nM DPCPX was applied for 30 minutes and then washed out for 25 minutes. Application led to a significant increase in SyGCaMP2 responses between control and drug application periods as in figure 5.6-A. B. and C. The N2 component of the field potential was also significantly changed after drug application as was the paired-pulse ratio (figure 5.6-E-H). In both optical and electrophysiological recordings, the effects of DPCPX were not reversible and responses remained significantly different from baseline levels during the wash-off period.

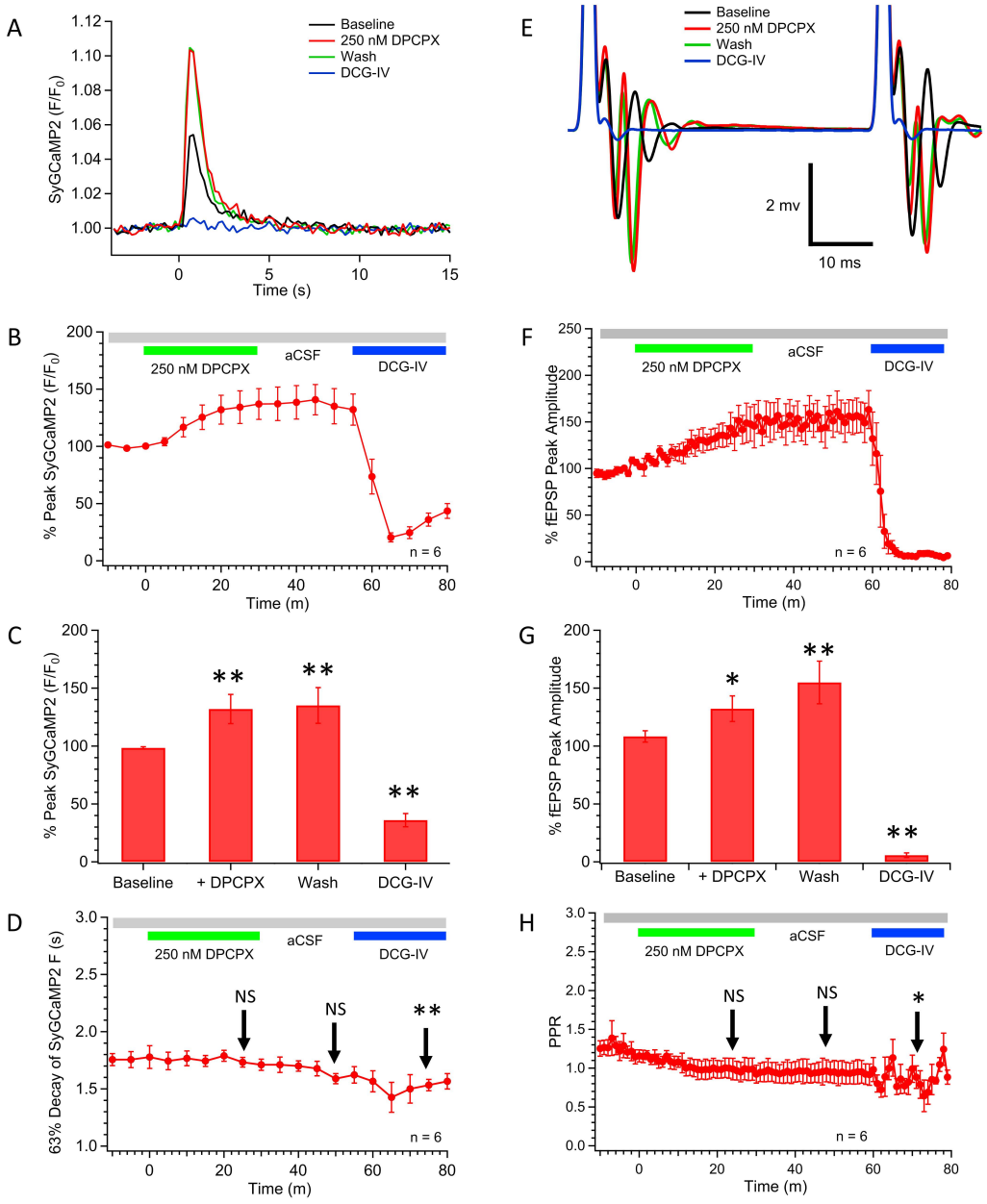

Figure 5.6. Effect of 250 nM DPCPX on responses to MF activation in the CA3 area of the SyG37 mouse's hippocampus.

A. shows the mean responses to the effects of DPCPX from ROIs placed within the stratum lucidum of the CA3 hippocampal region plotted against time. B. and C. line and bar charts illustrate the effects of DPCPX on SyGCaMP2 fluorescence peak amplitude over time, respectively. D. illustrate the effects of DPCPX on SyGCaMP2 fluorescence 63% decay time over time. E. shows the effects of DPCPX on traces of field potential curve collected from the stratum lucidum of the CA3 hippocampal region. B. and C. line and bar charts illustrate the change

in peak amplitude of the field potential before, during, and after addition of DPCPX. D. illustrate the effects of DPCPX on PPR plotted against time. Statistical differences are indicated with asterisks with *, ** or *** according to the level of significance. Statistics: (C), DPCPX, U= 0, P=0.0022; wash, U= 0, P=0.0022; DCG-IV, U= 0, P=0.0022; (G), DPCPX, U= 3, P=0.0152; wash, U= 2, P=0.0087; DCG-IV, U= 0, P=0.0022; Mann Whitney test. (D), DCG-IV, t(10) = 2.84, P=0.0176. (D), DPCPX, t(10) = 2.321, P=0.0427; unpaired t test.

5.2.3.1.3 Effects of 50 µM adenosine in the presence of 250 nM DPCPX on responses to MF activation in the CA3 area SyG37 mice.

The effects of adenosine in the presence of 250 nM DPCPX were next tested in the CA3 region of the hippocampus. For both SyGCaMP2 fluorescence and field potential recordings, adenosine had no effect compared to baseline levels as in figure 5.7. Figure 5.7-D and H reveals that there was no change in either the 63% decay time of the SyGCaMP2 fluorescence or the PPR. The PPR was very small in this series of experiments (~1.1) since due to the fact that DPCPX was present from the beginning.

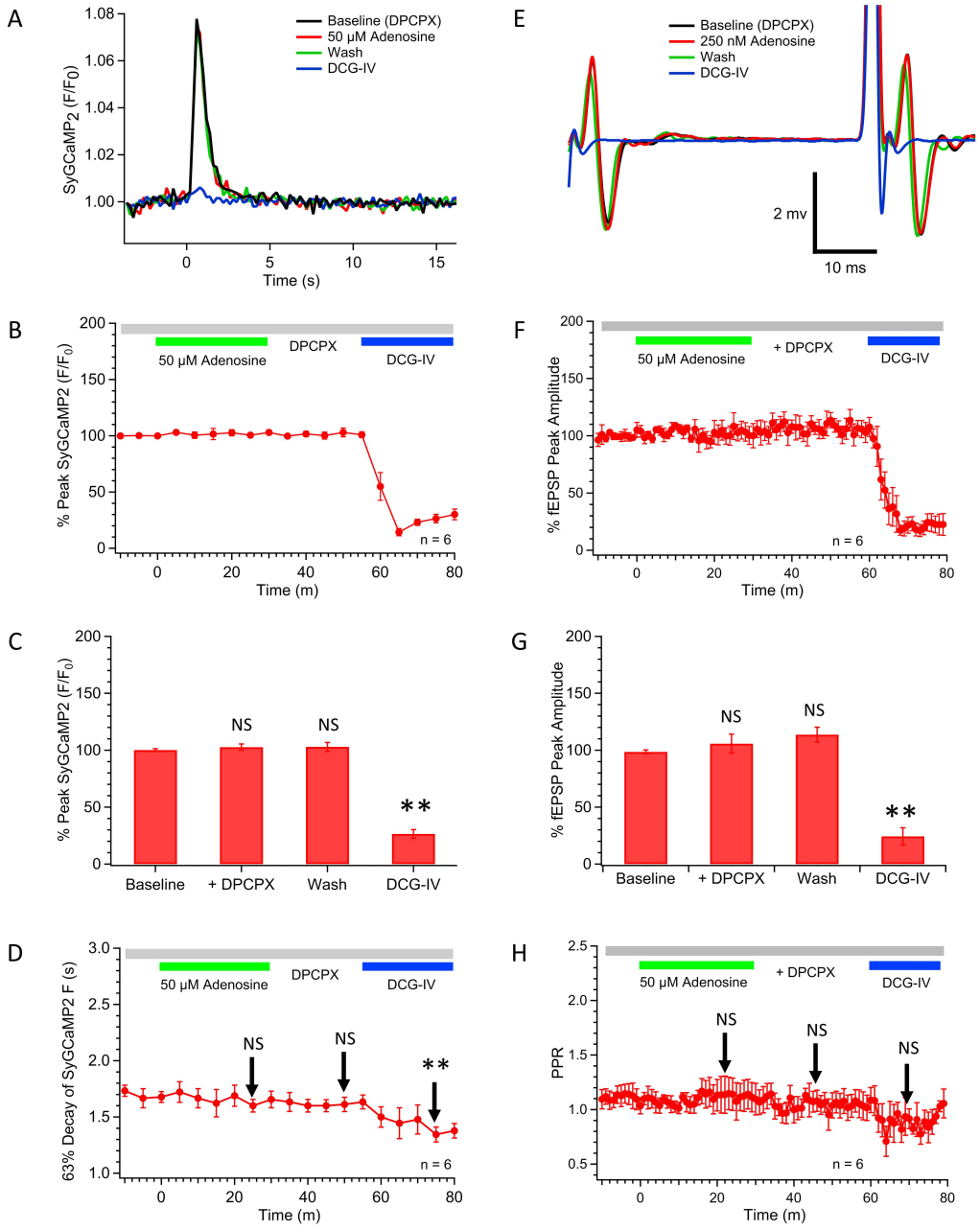

Figure 5.7. Effect of 50 µM adenosine in the presence of 250 nM DPCPX on MF activation in the CA3 area of the SyG37 mouse's hippocampus.

A. shows the mean responses to the effects of adenosine in the presence of DPCPX from ROIs placed within the stratum lucidum of the CA3 hippocampal region plotted against time. B. and C. line and bar charts illustrate the effects of adenosine in the presence of DPCPX on SyGCaMP2 fluorescence peak amplitude over time, respectively. D. illustrate the effects of adenosine in the presence of DPCPX on SyGCaMP2 fluorescence 63% decay time over time. E. shows the effects of adenosine in the presence of DPCPX on traces of field

potential curve collected from the stratum lucidum of the CA3 hippocampal region. B. and C. line and bar charts illustrate the change in peak amplitude of the field potential before, during, and after addition of adenosine in the presence of DPCPX. D. illustrate the effects of adenosine in the presence of DPCPX on PPR plotted against time. Statistical differences are indicated with asterisks with *, ** or *** according to the level of significance. Statistics: (C and G, respectively), DCG-IV, U= 0, P=0.0022; DCG-IV, U= 0, P=0.0022; Mann Whitney test. (D), DCG-IV, t(10) = 0.5758, P=0.0082; unpaired t test.

5.2.3.2 The effects of synaptic transmission blocking and subsequent adenosine receptor manipulation on the CA3 hippocampal area.

We next attempted to establish whether the effects that we observed were mediated primarily at MF terminals or whether there were contributions from presynaptic terminals that were postsynaptic to the MF terminals. We therefore chose to repeat the same experiments as in the CA1 experiments and examine the sequential effects of picrotoxin, AP5 and DNQX, which would be used to block the $GABA_A$/Glycine, NMDA and AMPA receptors, respectively. We then examined the effects of adenosine both alone and in the presence of the A1 receptor blocker, DPCPX, having blocked the major excitatory and inhibitory synaptic pathways formed by the MF terminals.

5.2.3.2.1 Effects of inhibition of AMPA, NMDA and $GABA_A$ / Glycine receptors on responses to MF activation in the CA3 area of a SyG37 mouse model.

Each slice was stimulated as described previously in a drug-free standard extracellular solution before washing cumulatively with 10 µM PTX, then, after 15 minutes, 50 µM AP5, and then 10 µM DNQX after a further 15 minutes. All these drugs were then washed off using the drug-free standard extracellular solution. PTX produced a statistically significant enhancement of SyGCaMP2 fluorescence compared to the baseline. Application of AP5 in the continued presence of PTX caused a reduction in SyGCaMP2 fluorescence but responses were still larger than the baseline values. Application of DNQX led to a further

reduction in the amplitudes of the SyGCaMP2 fluorescence. There was no clear change in the 63% decay time of the SyGCaMP2 fluorescence, as shown in figure 5.8-A to D. Concurrent field potential recordings were also made. The N2 component of the field potential was increased upon addition of PTX and then more increased upon adding AP5, but was reduced significantly when the AMPA receptors were blocked with DNQX. The paired-pulse ratio changed as well, as shown in figure 5.8-H. Responses recovered fully after 30 minutes from wash-off for the SyGCaMP2 fluorescence, but fEPSP recordings did not recover.

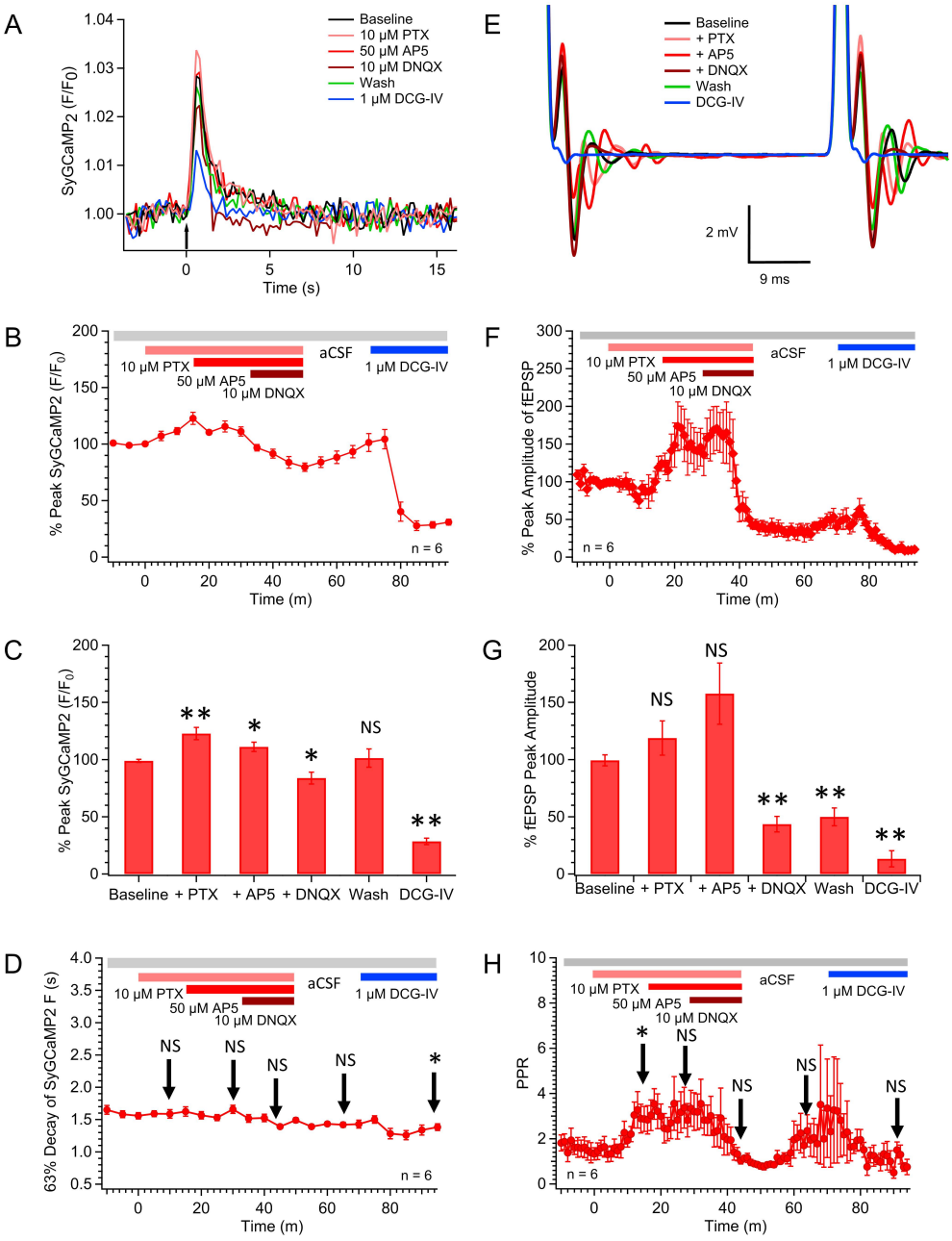

Figure 5.8. Effects of cumulative blockade of GABA/Glycine, NMDA and AMPA receptors on SyGCaMP2 fluorescence and field potential responses to MF activation in the CA3 area of the hippocampus.

A. shows the mean responses to the effects of cumulative applications of 10 µM PTX, 50 µM AP5 and 10 µM DNQX from ROIs placed within the stratum lucidum of the CA3 hippocampal region plotted against time. B. and C. line and bar charts illustrate the effects of cumulative applications of PTX, AP5 and DNQX on SyGCaMP2 fluorescence peak amplitude over time, respectively. D. illustrate the

effects of cumulative applications of PTX, AP5 and DNQX on SyGCaMP2 fluorescence 63% decay time over time. E. shows the effects of cumulative applications of PTX, AP5 and DNQX on traces of field potential curve collected from the stratum lucidum of the CA3 hippocampal region. B. and C. line and bar charts illustrate the change in peak amplitude of the field potential before, during, and after cumulative applications of PTX, AP5 and DNQX. D. illustrate the effects of cumulative applications of PTX, AP5 and DNQX on PPR plotted against time. The statistical test were performed between baseline and the other periods. Statistics: (C), PTX, U= 0, P=0.0022; AP5, U= 3, P=0.0152; DNQX, U= 3, P=0.0154; DCG-IV, U= 0, P=0.0022; (G) DNQX, U= 0, P=0.0022; DCG-IV, U= 0, P=0.0022; DCG-IV, U= 0, P=0.0022; Mann Whitney test; (D) DCG-IV, t(10) = 2.499, P=0.0315. (H) PTX, t(10) = 3.005, P=0.0132; unpaired t test.

5.2.3.2.2 Comparison of the effects of adenosine receptor modulation on responses to MF activation in the CA3 area with and without 10 µM PTX and 10 µM DNQX.

The effects of adenosine and DPCPX were next examined in the presence of a PTX and DNQX to establish the proportion to which their overall effects on the MF-CA3 synaptic pathway were mediated on MF synaptic terminals and, therefore, to estimate the relative contribution of polysynaptic circuits of SyGCaMP2 fluorescence responses to MF-CA3 stimulation. As before, in the presence of PTX and DNQX, application of adenosine produced the same trend as the experiments without these blockers, where adenosine reversibly reduced the size of the presynaptic calcium responses. This inhibitory effect of adenosine was converted to an excitatory effect in the presence of DPCPX, as shown in figure 5.9-A and C. Applications of DPCPX on its own resulted in an increase in SyGCaMP2 fluorescence, as seen in figure 5.9-B (red lines). Interestingly, pre-incubation of slices with PTX and DNQX for at least 30 minutes led to a clear increase in the size of the baseline responses (figure 5.9-D). These results are in agreement with our CA1 data. A two-way ANOVA test was applied to compare the two sets of experiments; in the absence and presence of PTX and DNQX there was a significant difference between the two groups on two occasions; first, in the adenosine alone experimental group, where there was a significant difference at wash-off period. Second, in the presence of PTX, DNQX and

DPCPX, the application of adenosine increased the SyGCaMP2 fluorescence non-significantly, which became significant at the wash-off period. This may be because the adenosine started to stimulate A_{2A} receptors instead, in the presence of these blockers. The inhibitory actions of adenosine observed in the SyG37 model experiments, interestingly, showed the opposite action in the presence of DPCPX when $GABA_A$/Glycine and AMPA/Kainate receptors were blocked. Again, responses recorded from the SyG37 mouse model were, however, still present in the presence of PTX and DNQX, which is consistent with the expression of the SyGCaMP2-mCherry sensor in MF terminals. These results indicated that SyGCaMP2-mCherry is selectively expressed in presynaptic terminals within the hippocampus, as the signal recorded in response to MF-CA3 stimulation is derived mainly from the MF-CA3 terminals themselves.

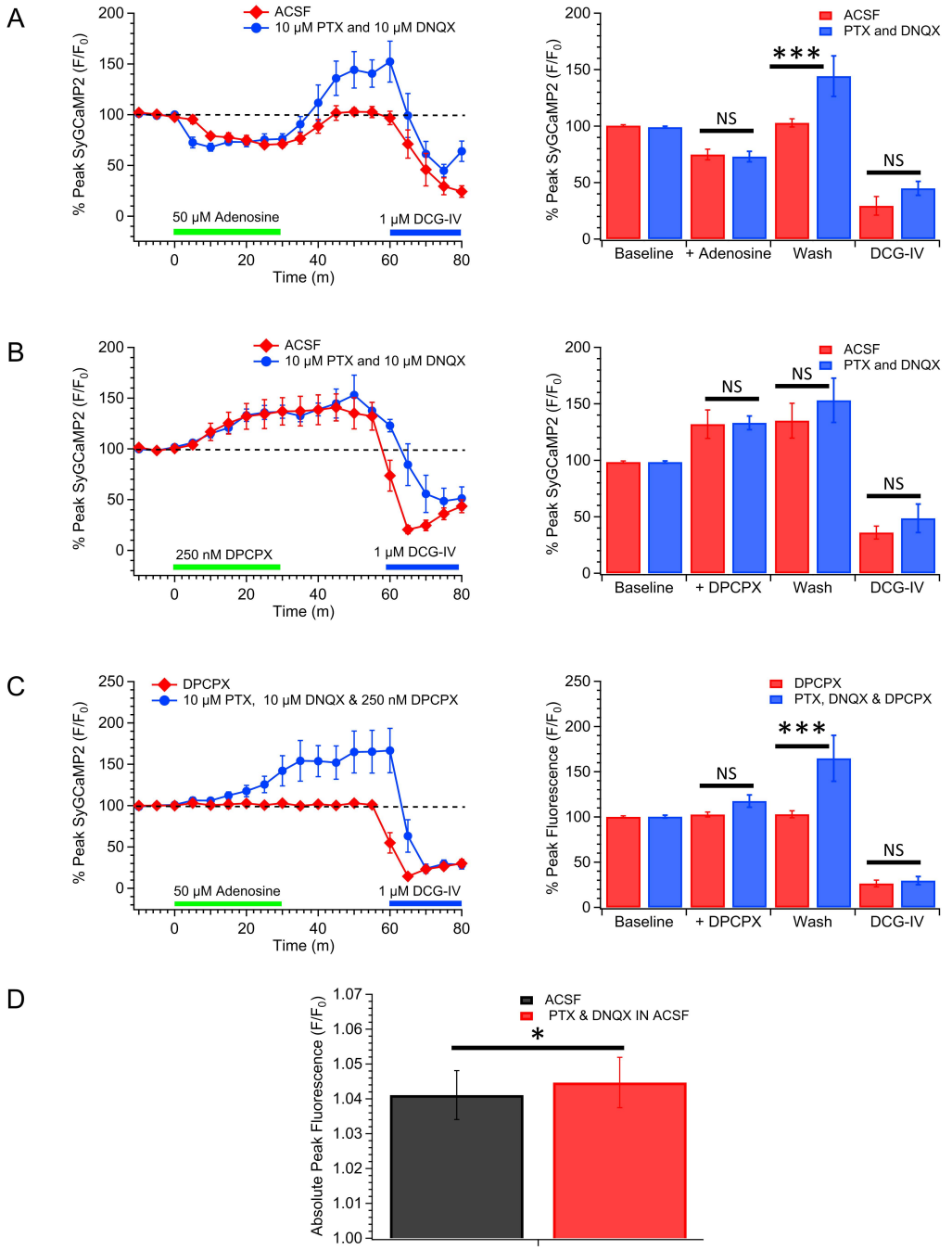

Figure 5.9. The effects of 50 µM adenosine, 250 nM DPCPX, and then both 50 µM adenosine and 250 nM DPCPX, on SyGCaMP2 responses to MF activation in the CA3 area of the hippocampus in the absence and presence of 10 µM PTX and 10 µM DNQX.

A., B. and C. show the pooled data of the effects of adenosine, DPCPX, and then both adenosine and DPCPX, on CA3 area responses in the absence (black) and presence (red) of PTX and DNQX, respectively. D. shows the pooled data of absolute SyGCaMP2 fluorescence collected during stimulation of the MF-CA3

pathway in just aCSF or after the pre-incubation with 10 µM PTX and 10 µM DNQX. The number of experiments in each group was six. Statistics: (A), wash, P=0.0007; (C), wash, P=0.0003; two-way ANOVA followed by Sidak's multiple comparisons test. (D), t(10) = 2.339, P=0.0288; unpaired t test.

5.2.4 The contribution of presynaptic calcium to the cAMP-PKA signalling cascade required for MF-CA3 pathway activity.

PKA plays a fundamental role in the induction and maintenance of the NMDAR-independent form of LTP at MF-CA3 synapses (Hopkins and Johnston, 1988, Huang *et al.*, 1994b, Weisskopf *et al.*, 1994, Calixto *et al.*, 2003, Galvan *et al.*, 2010, Cheng and Yakel, 2014). Kapur et al. (1998) found that brief high-frequency stimulation of MF LTP requires postsynaptic activation of nimodipine sensitive calcium channels, whereas, long high-frequency stimulation induces mossy fiber LTP presynaptically and does not requires postsynaptic activation of nimodipine sensitive calcium channels. Furthermore, a presynaptic form of MF-LTP that requires PKA activation can be enabled by mGLuR7 internalization (Pelkey *et al.*, 2008). Using our mouse model, we therefore aimed to examine whether modulation of the cAMP-PKA signalling cascade with forskolin and rolipram had an effect on SyGCaMP2 responses and on MF-CA3 synaptic transmission.

5.2.4.1 The effects of forskolin and rolipram on responses to MF stimulation in the CA3 area of SyG37 mice.

Experiments were carried out in the same way as for those described in section 4.2.5.1 in Chapter 4. Applications of 25 µM forskolin and 10 nM rolipram to MF responses in CA3 produced small, inconsistent effects on both the peak amplitude and the 63% decay time of the SyGCaMP2 fluorescence, as shown in figures 5.10 A-D. The peak amplitude of the N2 component of the field potential increased, but not significantly. The paired-pulse ratio decreased indicating that the effects of forskolin/rolipram were presynaptic in origin (figure 5-10E-H).

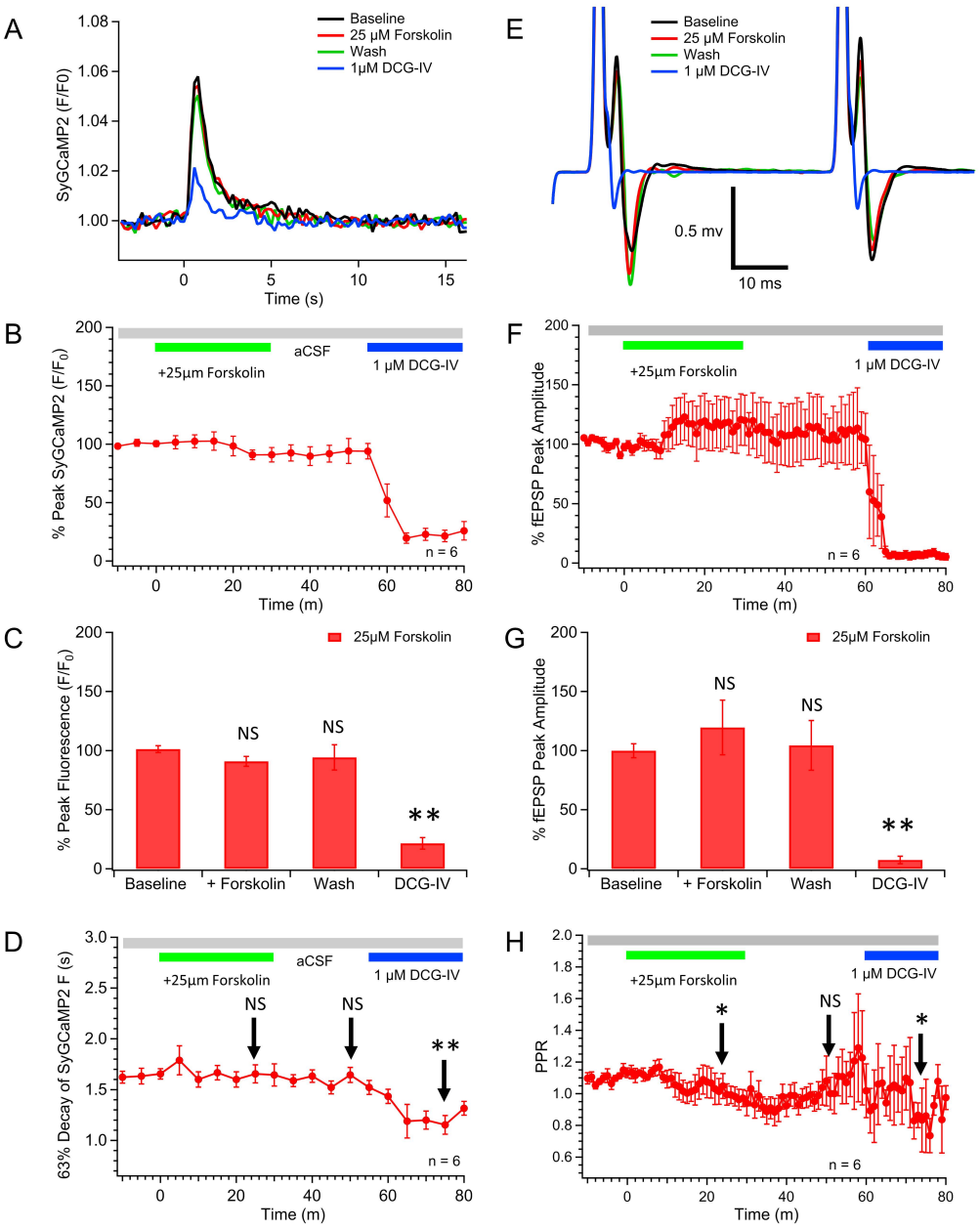

Figure 5.10. The effects of 25 μM forskolin in the presence of rolipram on responses to MF activation of the CA3 area of a SyG37 mouse model.

A. shows the mean responses to the effects of 25 μM forskolin from ROIs placed within the stratum lucidum of the CA3 hippocampal region plotted against time. B. and C. line and bar charts illustrate the effects of 25 μM forskolin on SyGCaMP2 fluorescence peak amplitude over time, respectively. D. illustrate the effects of 25 μM forskolin on SyGCaMP2 fluorescence 63% decay time over time. E. shows the effects of 25 μM forskolin on traces of field potential curve collected from the stratum lucidum of the CA3 hippocampal region. B. and C. line and bar

charts illustrate the change in peak amplitude of the field potential before, during, and after addition of 25 μM forskolin. D. illustrate the effects of 25 μM forskolin on PPR plotted against time. Statistics: (C), DCG-IV, U= 0, P=0.0022; (G) DCG-IV, U= 0, P=0.0022; Mann Whitney test; (D) DCG-IV, t(10) = 4.449, P=0.0016. (H) 25 μM forskolin, t(10) = 2.871, P=0.0132; DCG-IV, t(10) = 2.233, P=0.0496; unpaired t test.

5.2.4.2 Effects of 25 μM forskolin and rolipram on responses to MF activation in the CA3 area in the presence of PKA inhibitor.

As described in the previous section, applications of 25 μM forskolin and 10 nM rolipram produced a small increase in field potential responses but had no significant effect on SyGCaMP2 responses. We next examined whether these effects were mediated via the cAMP-PKA signalling cascade by testing the effects of the cell-permeable protein kinase inhibitor PKI (14-22) amide. Slices were superfused with aCSF containing 100 μM PKI (14-22) amide from the beginning. In the presence of PKI, forskolin and rolipram had no effect on either the peak amplitude or the 63% decay time of the SyGCaMP2 fluorescence responses (figure 5.11.A-D). The peak amplitude of the N2 component of the field potential was reduced significantly and did not recover to the baseline levels (see figures 5.11.E to G. The effects on the paired-pulse ratio were not significant and are shown in figure 5.11-H.

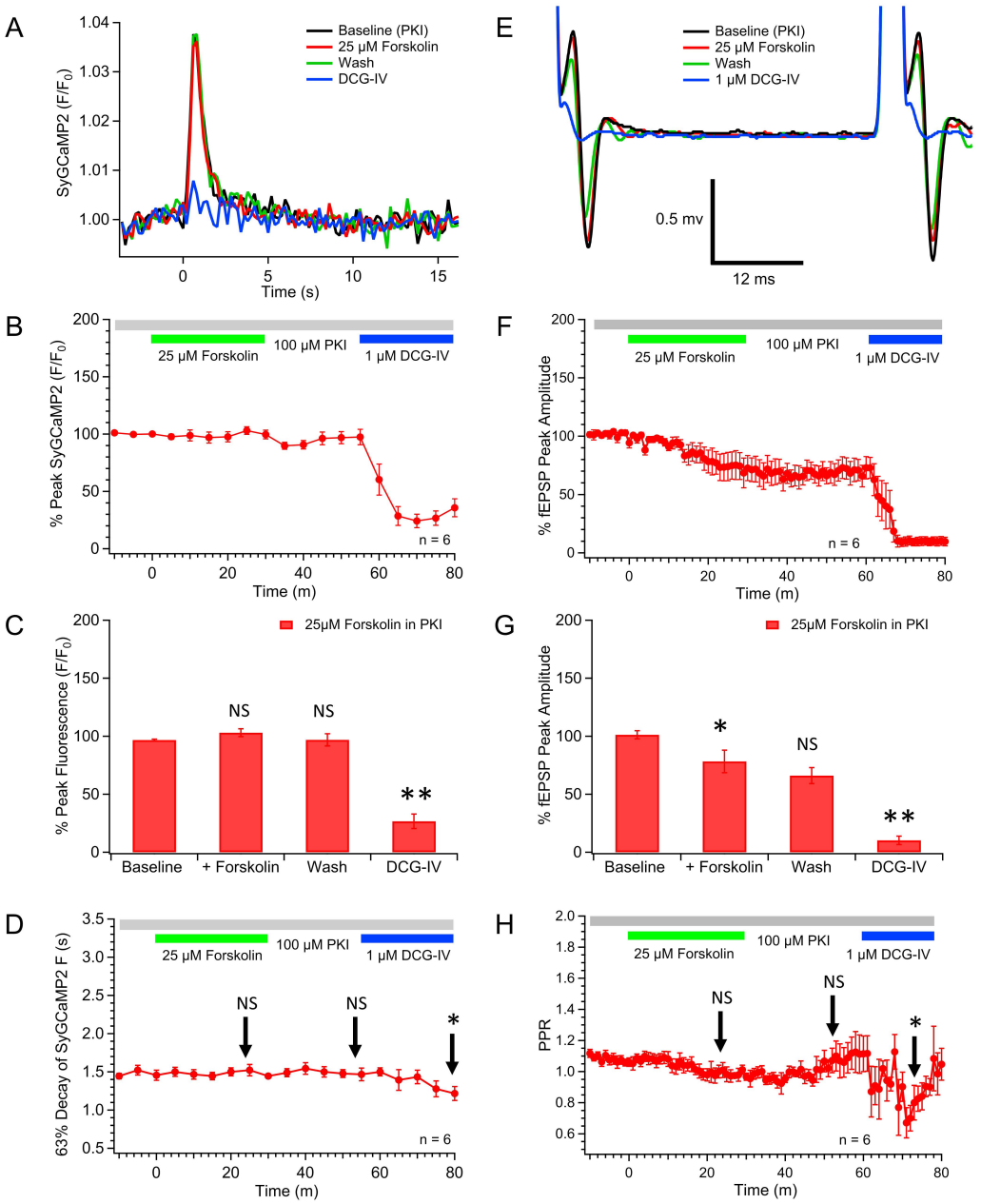

Figure 5.11. The effects of 25 µM forskolin in the presence of both rolipram and protein kinase inhibitor (PKI) on MF activation of the CA3 area of a SyG37 mouse model.

A. shows the mean responses to the effects of 25 µM forskolin in the presence of PKI from ROIs placed within the stratum lucidum of the CA3 hippocampal region plotted against time. B. and C. line and bar charts illustrate the effects of 25 µM forskolin in the presence of PKI on SyGCaMP2 fluorescence peak amplitude over time, respectively. D. illustrate the effects of 25 µM forskolin in the presence of PKI on SyGCaMP2 fluorescence 63% decay time over time. E. shows the effects of 25 µM forskolin in the presence of PKI on traces of field

potential curve collected from the stratum lucidum of the CA3 hippocampal region. B. and C. line and bar charts illustrate the change in peak amplitude of the field potential before, during, and after addition of 25 μM forskolin in the presence of PKI. D. illustrate the effects of 25 μM forskolin in the presence of PKI on PPR plotted against time. Statistics: (C), DCG-IV, U= 0, P=0.0022; (G) 25 μM forskolin, U= 4, P=0.0260; DCG-IV, U= 0, P=0.0022; Mann Whitney test. (D) DCG-IV, t(10) = 3.007, P=0.0132. (H) DCG-IV, t(10) = 2.493, P=0.0318; unpaired t test.

A two-way ANOVA test detected a significant difference between the two field potential recording groups, though not in the imaging recordings (the effect of 25 μM forskolin with and without PKI), where the peak amplitude of the N2 component of the field potential was decreased significantly after PKI application and this inhibition became more significant at the wash-off period as shown in figure 5.12-A and B.

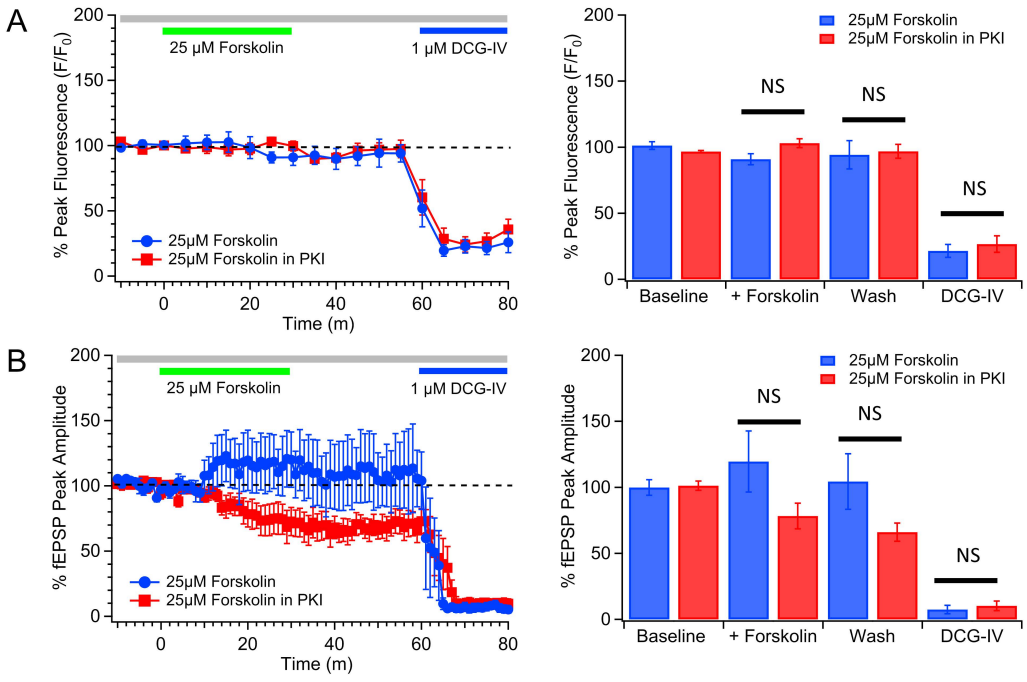

Figure 5.12. Comparison between the effect of 25 μM forskolin and rolipram in the presence and absence of protein kinase inhibitor (PKI) on MF activation in the CA3 area of a SyG37 mouse model.

A. line (left) and bar charts (right) comparing the effects of 25 μM forskolin and 10 nM rolipram in the absence and presence of PKI on the peak amplitude of the SyGCaMP2 fluorescence and the N2 component of the field potential plotted

against time, respectively. The above data are represented as a percentage of averaged means (*n* = 6) of both SyGCaMP2 fluorescence and fEPSP responses recorded from the *stratum lucidum* after a 15-minute control period, 30 minutes after forskolin/rolipram addition and 25 minute washout. DCG-IV confirmed that we were recording from the MF-CA3 pathway. Statistics are presented in the right panel histograms: No observed significant differences; two-way ANOVA followed by Sidak's multiple comparisons test.

5.2.4.3 Effects of cAMP-PKA signalling cascade activation by 50 µM forskolin and rolipram on MF stimulation in the CA3 area of a SyG37 mouse model.

We next tested the effects of 50 µM forskolin. After obtaining stable baselines of evoked responses, 50 µM forskolin and 10 nM rolipram were applied as before. Similarly, forskolin and rolipram produced only small effects on the peak amplitude and the 63% decay time of the SyGCaMP2 fluorescence, as shown in figure 5.13 A. to D. The peak amplitude of the N2 component of the field potential was significantly increased and this increase became more significant during the wash-off period as shown in figure 5.13-E to G. The paired-pulse ratio also changed, indicating possible presynaptic action of forskolin/rolipram (figure 5.13-H).

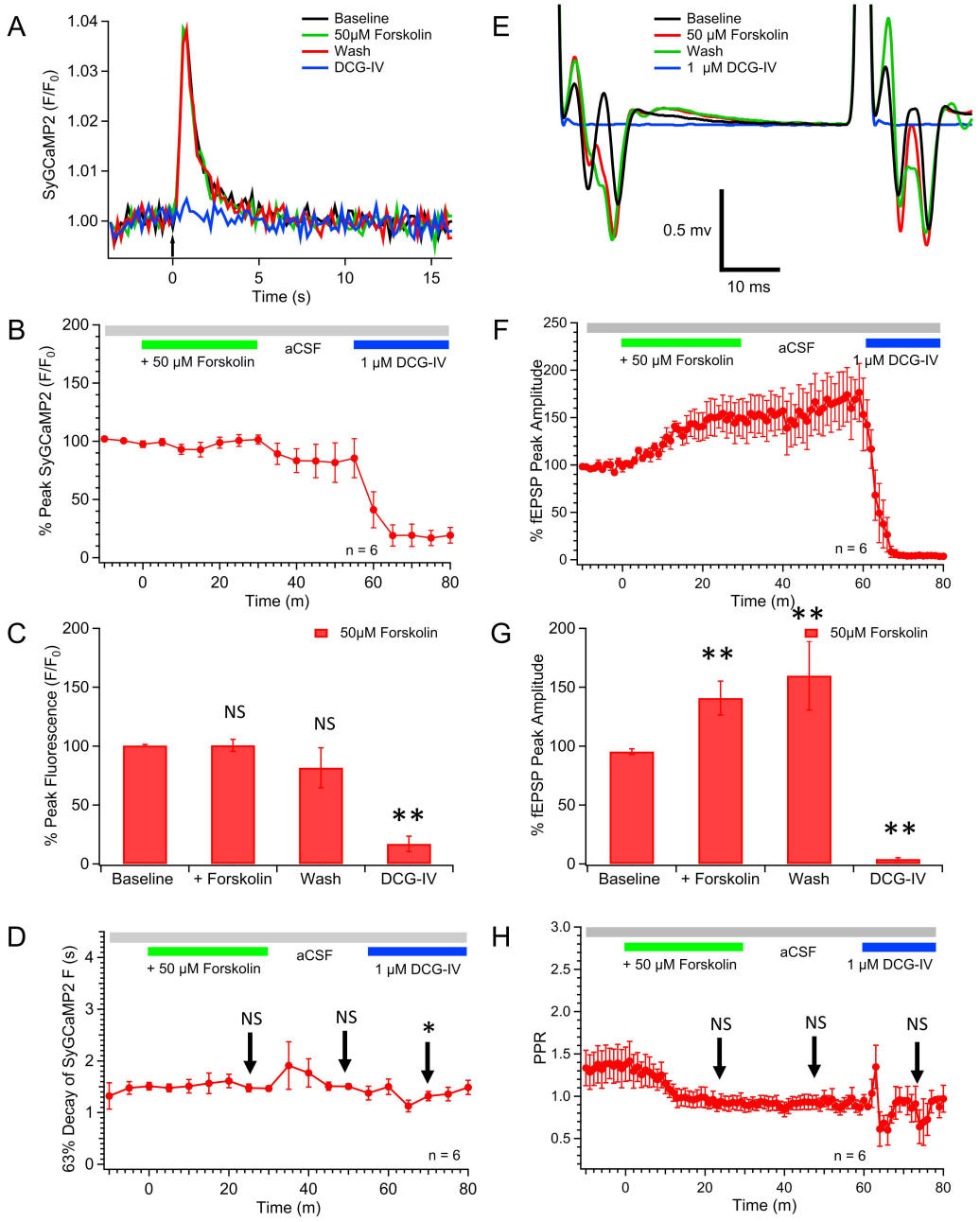

Figure 5.13. The effect of 50 μM forskolin in the presence of rolipram on responses to MF activation of the CA3 area of a SyG37 mouse model.

A. shows the mean responses to the effects of 50 μM forskolin from ROIs placed within the stratum lucidum of the CA3 hippocampal region plotted against time. B. and C. line and bar charts illustrate the effects of 50 μM forskolin on SyGCaMP2 fluorescence peak amplitude over time, respectively. D. illustrate the effects of 50 μM forskolin on SyGCaMP2 fluorescence 63% decay time over time. E. shows the effects of 50 μM forskolin on traces of field potential curve collected from the stratum lucidum of the CA3 hippocampal region. B. and C. line and bar

charts illustrate the change in peak amplitude of the field potential before, during, and after addition of 50 μM forskolin. D. illustrate the effects of 50 μM forskolin on PPR plotted against time. Statistics are presented in the right panel histograms: (C), DCG-IV, U= 0, P=0.0022; (G) 50 μM forskolin, U= 5, P=0.0411; wash, U= 0, P=0.0022; DCG-IV, U= 0, P=0.0022; Mann Whitney test. (D) DCG-IV, t(10) = 4.449, P=0.0132; unpaired t test.

5.2.4.4 Effects of 50 μM forskolin and rolipram on MF activation in the CA3 area in the presence of PKA inhibitor.

In the presence of 100 μM PKI (14-22) amide, 50 μM forskolin and 10 nM rolipram produced no clear effect on either the peak amplitude or the 63% decay time of the SyGCaMP2 fluorescence (figure 5.14.A-D). The peak amplitude of the N2 component of the field potential was reduced during application but recovered towards baseline levels on washout, as shown in figure 5.14.E to G. The paired-pulse ratio also increased during drug application but then recovered on washout (figure 5.14-H).

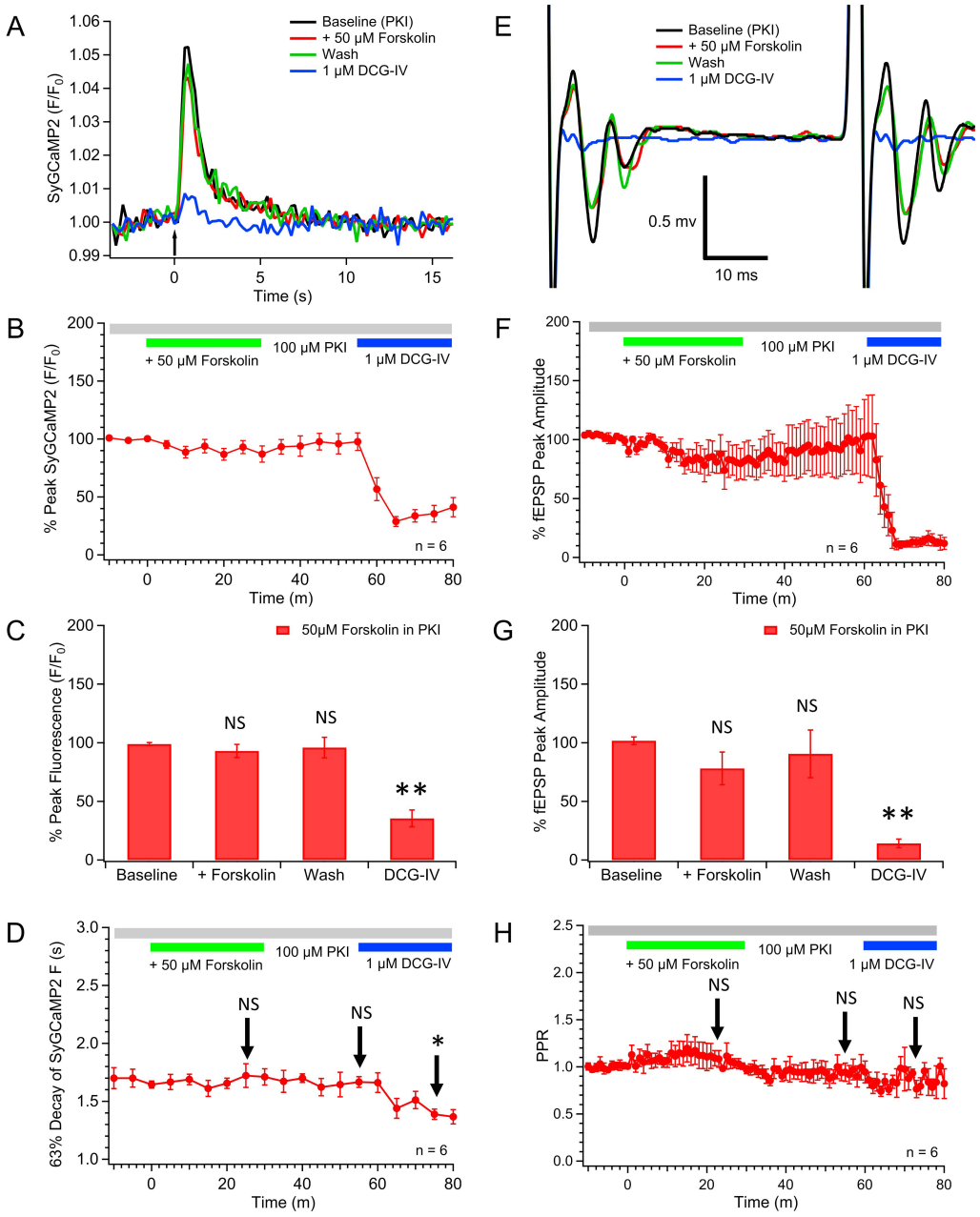

Figure 5.14. The effect of 50 µM forskolin in the presence of both rolipram and protein kinase inhibitor (PKI) on responses to MF activation of the CA3 area of a SyG37 mouse model.

A. shows the mean responses to the effects of 50 µM forskolin in the presence of PKI from ROIs placed within the stratum lucidum of the CA3 hippocampal region plotted against time. B. and C. line and bar charts illustrate the effects of 50 µM forskolin in the presence of PKI on SyGCaMP2 fluorescence peak amplitude over time, respectively. D. illustrate the effects of 50 µM forskolin in the presence of PKI on SyGCaMP2 fluorescence 63% decay time over time. E.

shows the effects of 50 µM forskolin in the presence of PKI on traces of field potential curve collected from the stratum lucidum of the CA3 hippocampal region. B. and C. line and bar charts illustrate the change in peak amplitude of the field potential before, during, and after addition of 50 µM forskolin in the presence of PKI. D. illustrate the effects of 50 µM forskolin in the presence of PKI on PPR plotted against time. Statistics are presented in the right panel histograms: (C), DCG-IV, U= 0, P=0.0022; (G) DCG-IV, U= 0, P=0.0022; Mann Whitney test. (D) DCG-IV, t(10) = 3.839, P=0.0033; unpaired t test.

A two-way ANOVA test revealed a significant difference between the effects of forskolin/rolipram in the presence and absence of PKI on field potentials but not SyGCaMP2 (the effect of 50 µM forskolin with and without PKI). The peak amplitude of the N2 component of the field potential decreased significantly during PKI application and this inhibition became more significant during the wash-off period as shown in figure 5.15-A and B.

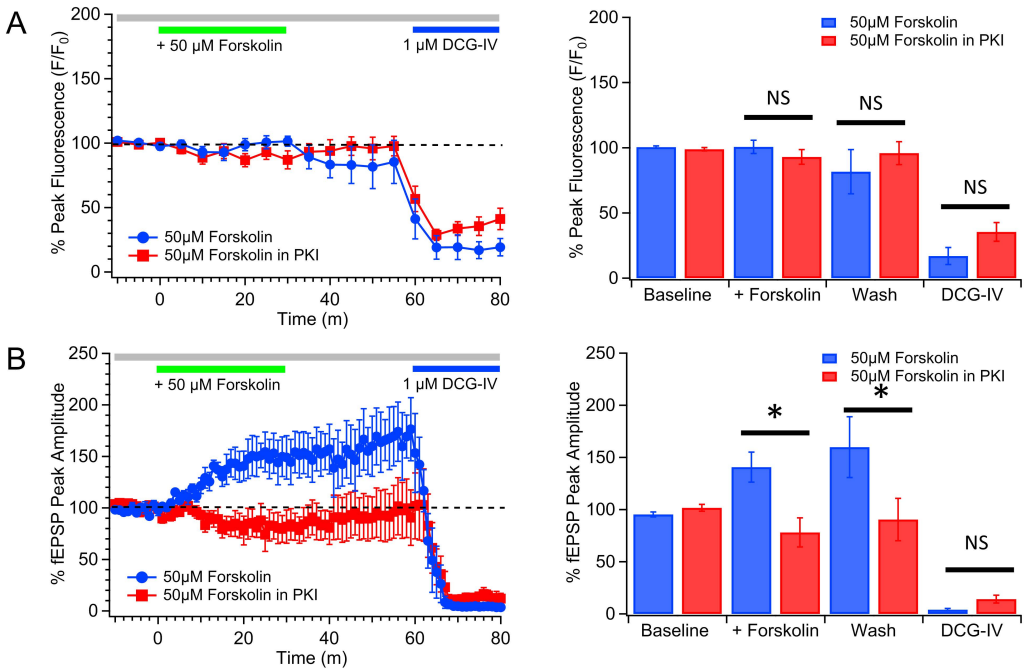

Figure 5.15. Comparison between the effects of 50 µM forskolin and 10 nM rolipram in the presence and absence of protein kinase inhibitor (PKI) on responses to MF activation in the CA3 area of a SyG37 mouse model.

A. Line and bar charts show the effect of 50 µM forskolin and rolipram in the absence and presence of PKI on the peak amplitude of the SyGCaMP2

fluorescence and the N2 component of field potential plotted against time, respectively. The above data is represented as a percentage of averaged means (n = 6) of both SyGCaMP2 fluorescence and fEPSP change in the stratum lucidum at 15 minute control, 30 minute forskolin/rolipram addition and 25 minute washing out periods. DCG-IV confirmed that we are recording from MF-CA3 pathway. Statistics are presented in the right panel histograms: (B), 50 µM forskolin, P=0.0374; wash, P=0.0454; two-way ANOVA followed by Sidak's multiple comparisons test.

Figure 5.16 compares the effects of each concentration of forskolin on SyGCaMP2, fEPSP N2 responses and the N2 PPR.

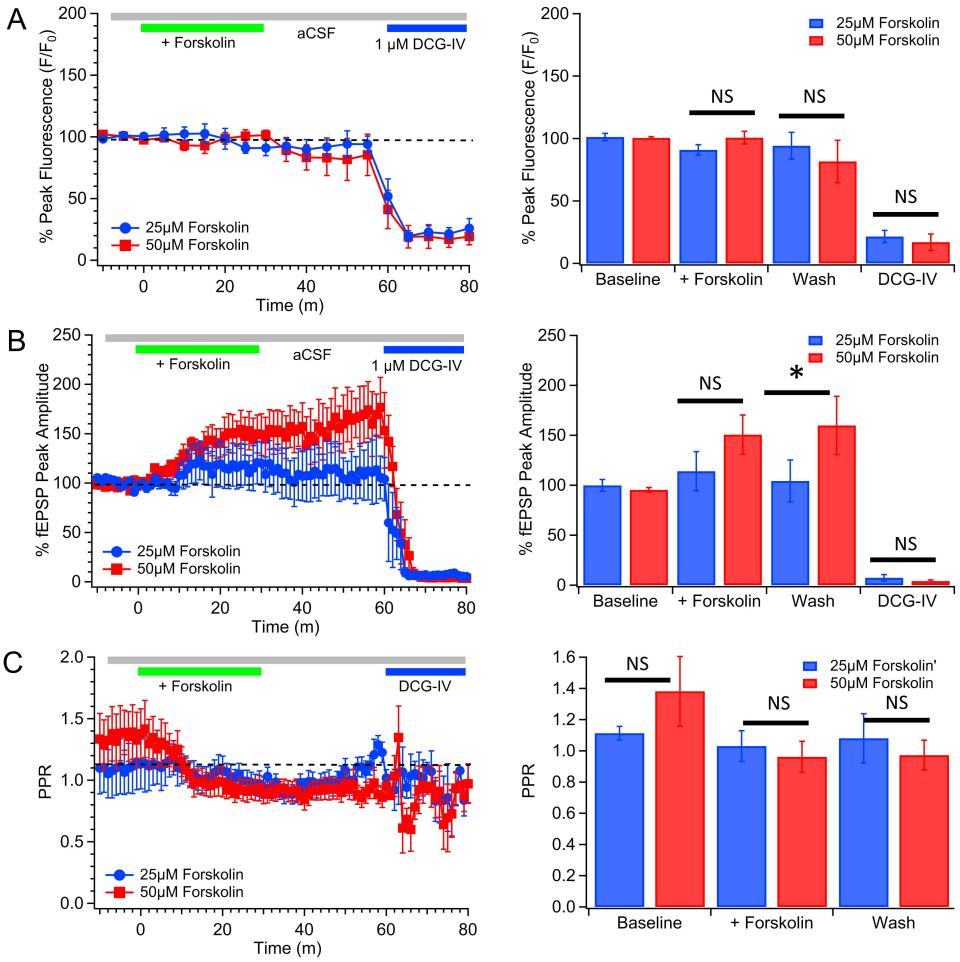

Figure 5.16. Comparison between the effects of two different doses of forskolin (25 and 50 µm), in the presence of rolipram, on responses to MF activation of CA3 area of the SyG37 mouse model.

A. B. and C. Line and bar charts show the effect of 25 and 50 μM forskolin in the presence of rolipram on the peak amplitude of the SyGCaMP2 fluorescence, the N2 component of field potential and PPR plotted against time, respectively. The data in A. and B. are represented as a percentage of averaged means (N = 6) of both SyGCaMP2 fluorescence and fEPSP change in the stratum lucidum at 15 minute control, 30 minute forskolin/rolipram addition and 25 minute washing out periods. DCG-IV confirmed that we are recording from MF-CA3 pathway. Statistics are presented in the right panel histograms: (B), wash, P=0.0152; two-way ANOVA followed by Sidak's multiple comparisons test.

5.2.5 Differences between CA1 and CA3 hippocampal subfields responding to electrical and pharmacological manipulation detected by the SyGCaMP2-mCherry sensor in a SyG37 transgenic mouse model

In this section, the responses to electrical stimulation and effects of the various pharmacological manipulations carried out are compared between CA1 and CA3 to establish highlight differences between these two hippocampal regions.

5.2.5.1 Comparison between electrical activation studies of both SC-CA1 and MF-CA3 pathways of a SyG37 mouse model.

We know that there were fewer stimuli for the CA3 than CA1, however, superimposed absolute data collected from both the SC-CA1 and MF-CA3 pathways, qualitatively, showed that by increasing the stimulus intensity, the SyGCaMP2 fluorescence increased in a roughly linear manner, with 20 V required to elicit a suitable response (figure 5.17-A). CA1 and CA3 areas both responded with a similar trend to the changes in the stimulus number and stimulus frequency, as shown in figure 5.17-B and C.

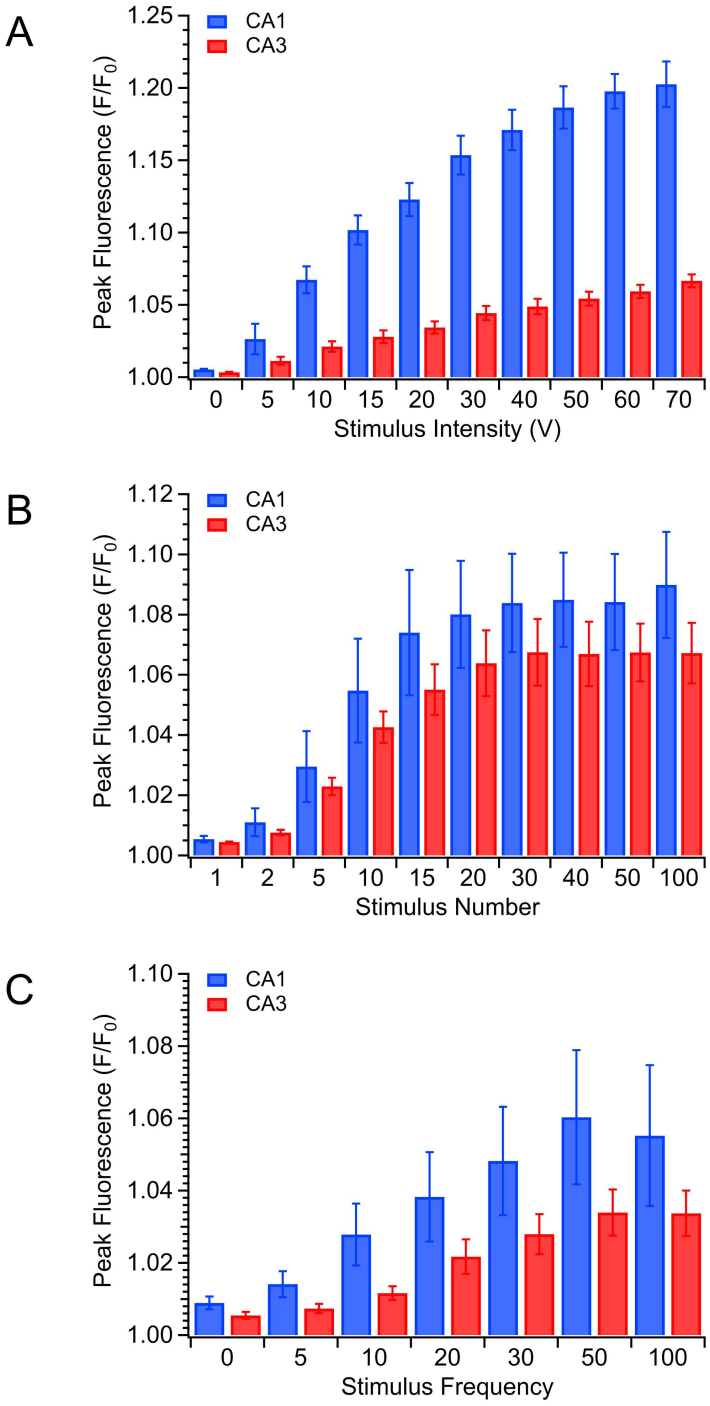

Figure 5.17. The effect of increasing stimulus intensity, stimulus number and stimulus frequency on SyGCaMP2 fluorescence in the hippocampal CA1 and CA3 regions.

A. B. and C. illustrate the effects of increasing stimulus intensity, number and frequency on the peak amplitude of the SyGCaMP2 fluorescence, respectively.

5.2.5.2 Comparison between the effects of adenosine receptor modulation and the relative mono- and polysynaptic contributions of presynaptic calcium in SC-CA1 and MF-CA3 microcircuits of a SyG37 mice.

In the presence of just AP5 in the CA1 experiments, or just drug-free aCSF in the CA3 experiments, adenosine receptor modulation experiments show that the increase of the SyGCaMP2 fluorescence by DPCPX, and the significant blocking of the effects of adenosine on the SyGCaMP2 fluorescence by DPCPX, are consistent with a previews published papers like Wu and Saggau (1994). A two-way ANOVA test was applied to compare the CA1 and CA3 experiments; the CA3 area responded differently in the presence of PTX and DNQX, where there was a significant difference between the two groups on two occasions; first, in the adenosine experimental group, there was a significant difference at wash-off period. Second, in the presence of PTX, DNQX and DPCPX, adenosine application increased the SyGCaMP2 fluorescence significantly, which became more significant at the wash-off period, as shown in figure 5.18. Therefore, in the CA3 experiments, the inhibitory actions of adenosine, interestingly, showed the opposite action in the presence of PTX, DNQX and DPCPX. In general, responses recorded from the SyG37 mouse model were, however, still present in the presence of PTX and DNQX, which is consistent with the expression of the SyGCaMP2-mCherry sensor in both the SC and MF terminals.

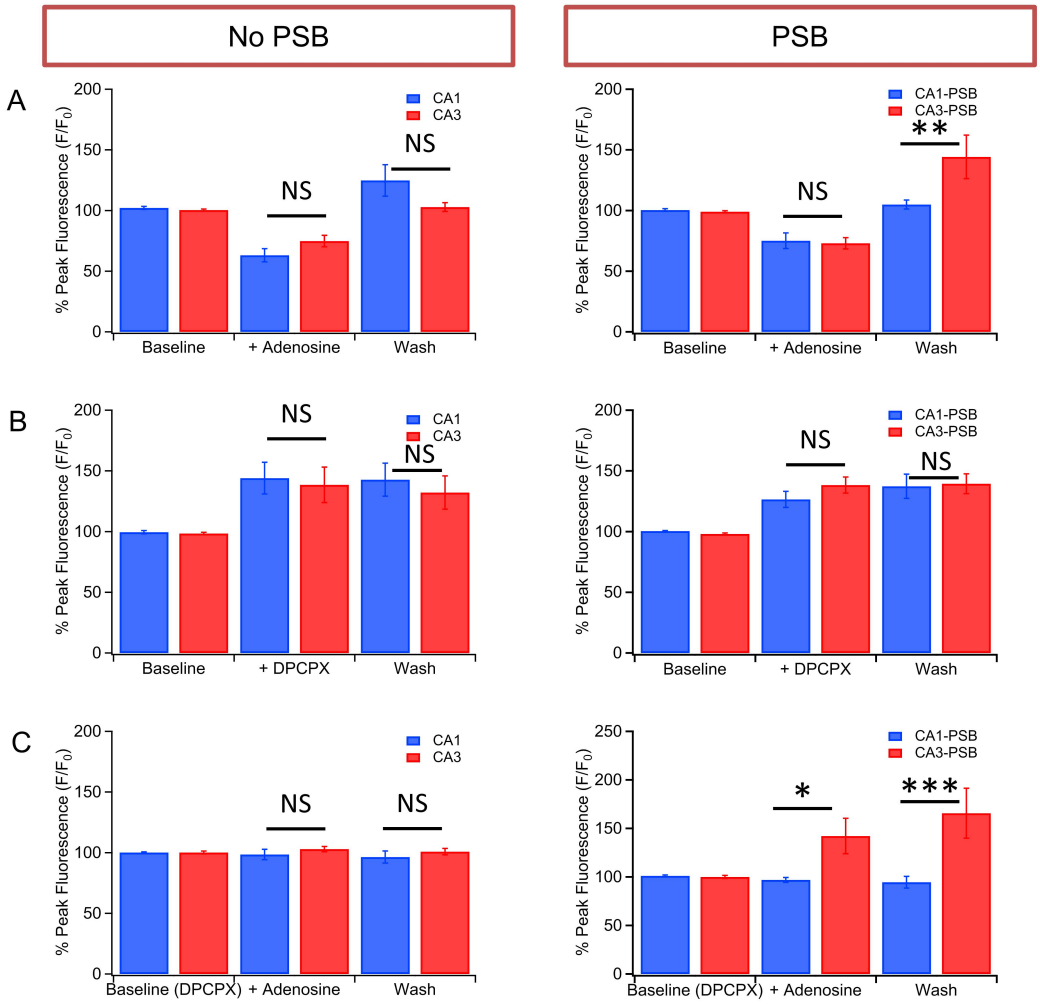

Figure 5.18. Comparison between the effects of 50 µM adenosine, 250 nM DPCPX, and both 50 µM adenosine and 250 nM DPCPX, on SyGCaMP2 fluorescence responses to SC activation in the CA1 area and to MF activation in the CA3 area of the SyG37 hippocampus in the presence and absence of synaptic transmission blockade.

A, B and C. show the pooled analysis of the effects of adenosine, DPCPX and the effects of adding adenosine and DPCPX together on both the CA1 and CA3 areas in the absence (left panel) and presence (right panel) of PTX, AP5 and DNQX (in CA1) or PTX and DNQX (in CA3). Statistics: (A-right panel), wash, P=0.0050; (C-right panel), Adenosine, P=0.0495; wash, P=0.0002; two-way ANOVA followed by Sidak's multiple comparisons test.

5.2.5.3 Comparison of the effects of cAMP-PKA on presynaptic calcium and synaptic transmission in SC-CA1 and MF-CA3 microcircuits of SyG37 mice.

The effects of forskolin/Rolipram in CA1 were measured in the presence of AP5 because postsynaptic LTP in this region is reported to be NMDA receptor dependent. AP5 was not used for experiments in the CA3 region. In CA3 area, forskolin caused a concentration-depending increase in SyGCaMP2 fluorescence. In contrast, in CA1, forskolin produced a concentration dependent reduction in CA1 (see figures. 5.19- A-B and 5.20- A-B). Forskolin/Rolipram had no significant effect on the N2 component of fEPSP recordings in CA1 at either 25 or 50 µM, whereas, in CA3 area had more pronounced effects especially at higher dose (figure 5.19-C and D & 5.20-C and D). A two-way ANOVA test revealed a significant difference between the effect of forskolin on CA1 and CA3, where the SyGCaMP2 fluorescence was significantly higher in CA3 than in CA1 after PKI application in both doses of forskolin, as shown in figures 5.19-E and 5.20-E.

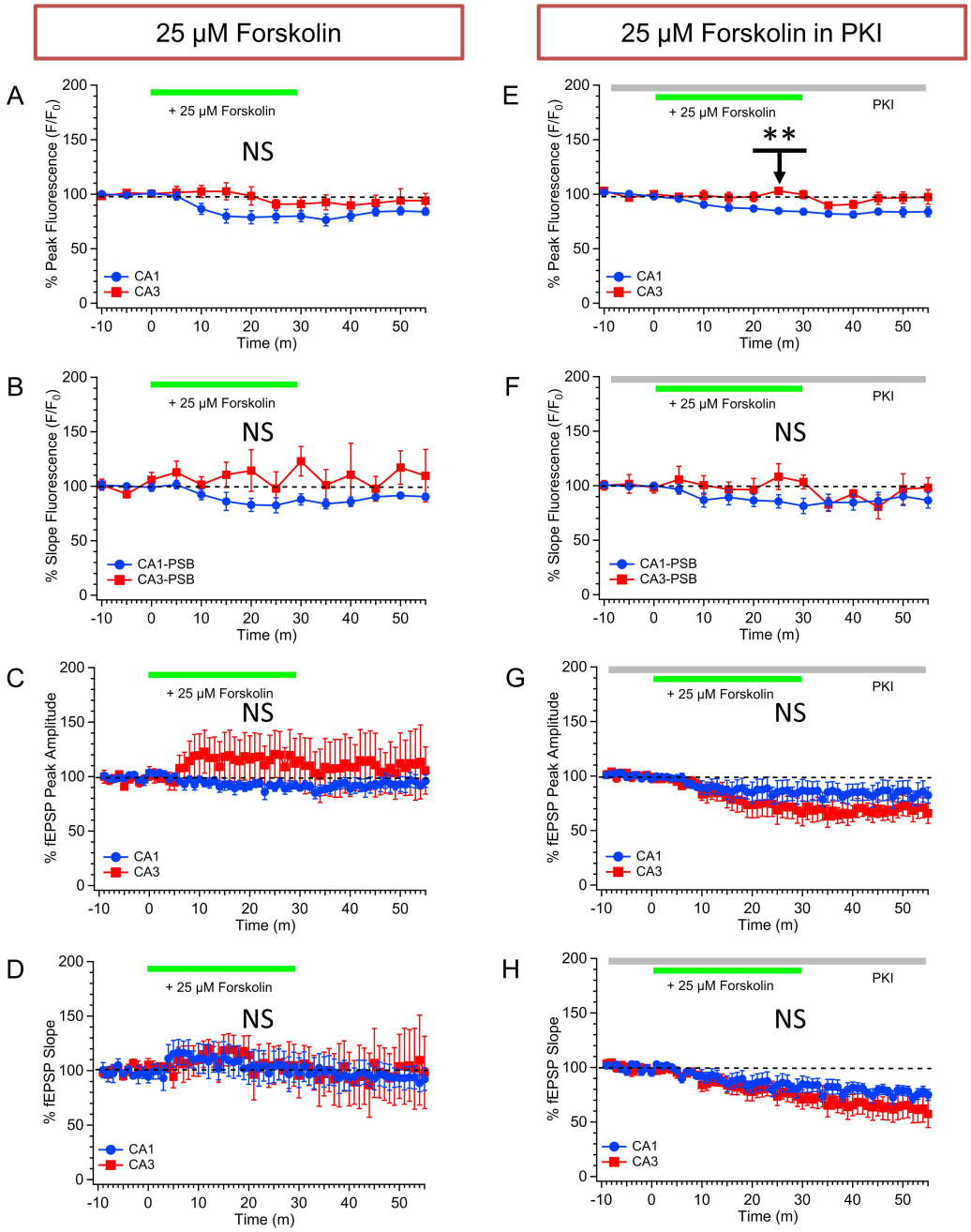

Figure 5.19. Comparison between the effect of 25 μM forskolin and rolipram in the presence and absence of protein kinase inhibitor (PKI) on both SC-CA1 and MF-CA3 synapses of a SyG37 mouse model.

A. B. line charts show the effects of 25 μM forskolin and rolipram in the absence (left panel) and presence of PKI (right panel) on the peak amplitude (A and C) and the slope (B and D) of the SyGCaMP2 fluorescence and the N2 component of the field potential plotted against time, respectively. The CA1 area was represented by a blue line while the CA3 area was represented by a red line. The

above data is represented as a percentage of averaged means (*N* = 6) of both the SyGCaMP2 fluorescence and fEPSP at 15 minute control, 30 minute drug addition and 25 minute washing out periods. Statistics: (E), 25 μM forskolin, P=0.0042; two-way ANOVA followed by Sidak's multiple comparisons test.

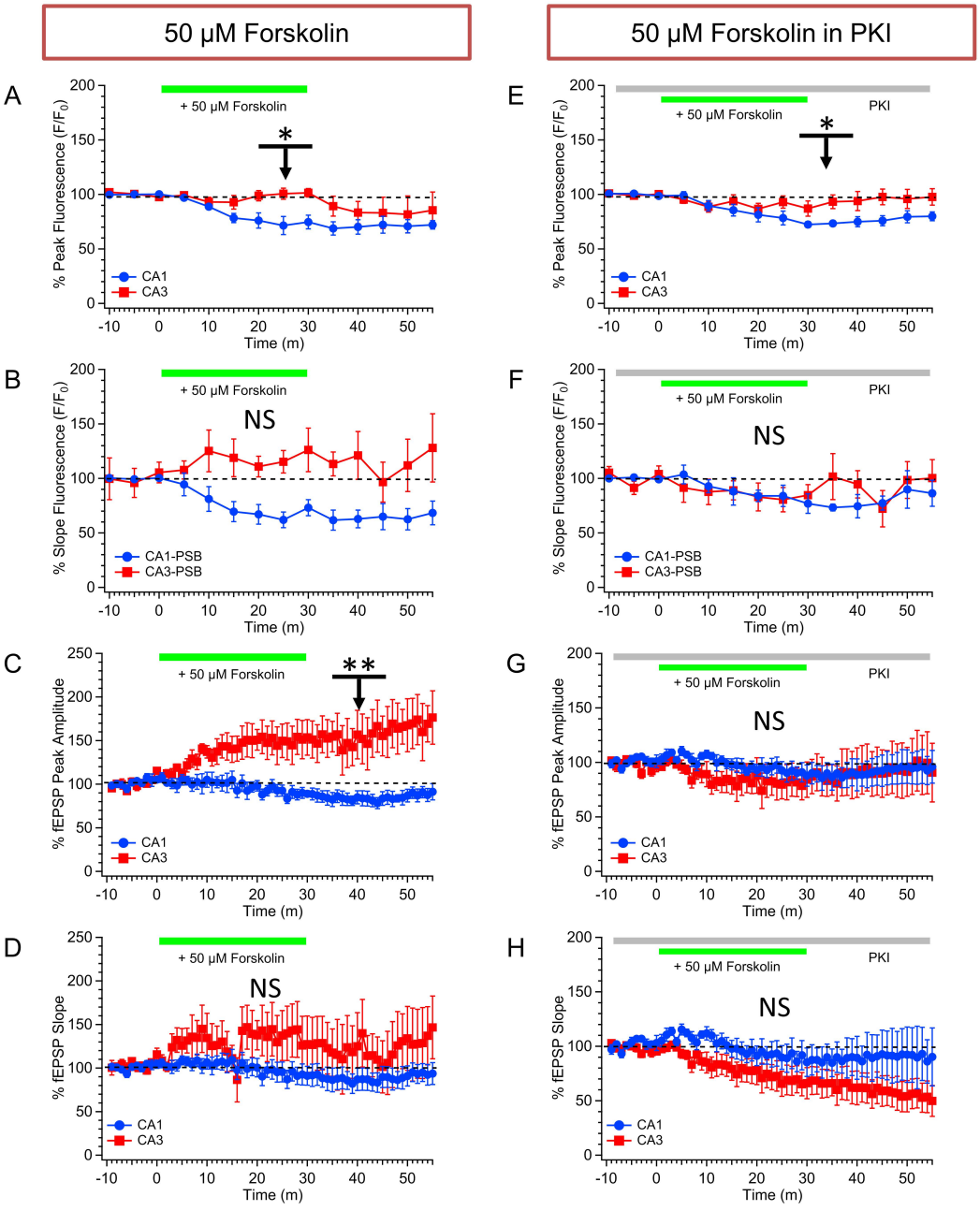

Figure 5.20. Comparison between the effects of 50 μM forskolin and rolipram in the presence and absence of protein kinase inhibitor (PKI) on both SC-CA1 and MF-CA3 synapses of a SyG37 mouse model.

A. B. Line charts show the effect of 25 μM forskolin and rolipram in the absence (left panel) and presence of PKI (right panel) on the peak amplitude (A & C) and the slope (B & D) of the SyGCaMP2 fluorescence and the N2 component of field potential plotted against time, respectively. The CA1 area was represented by blue line while the CA3 area was represented by red line. The above data is represented as a percentage of averaged means (N = 6) of both SyGCaMP2 fluorescence and fEPSP at 15 minute control, 30 minute drug addition and 25 minute washing out periods. DCG-IV confirmed that we are recording from MF-CA3 pathway. Statistics: (A), 25 μM forskolin, P=0.0366; (C), wash, P=0.0037; (E), wash, P=0.0420; two-way ANOVA followed by Sidak's multiple comparisons test.

5.2.5.4 Imaging and IHC data showed possible difference between CA1 and CA3 area in the number of presynaptic boutons (release sites).

The peak amplitude of SyGCaMP2 fluorescence in response to the same intensity, frequency and number of stimuli was always higher in CA1 compared with CA3 (figure 5.21.A). This led us to consider whether this was due to a fundamental difference between the responses of synapses at each site. We therefore revisited IHC experiments and compared the number of mCherry stained presynaptic boutons in both CA1 with CA3 hippocampal areas. ImageJ software was used to subtract the background from IHC images and to count the numbers of presynaptic boutons in identical volumes of tissue. Figure 5.21.B-E indicated that there was an increase in the number of presynaptic boutons in CA1 area than in CA3. The increased response to electrical stimulation in CA1 compared to CA3 may therefore have been due to a larger number of boutons being activated in CA1.

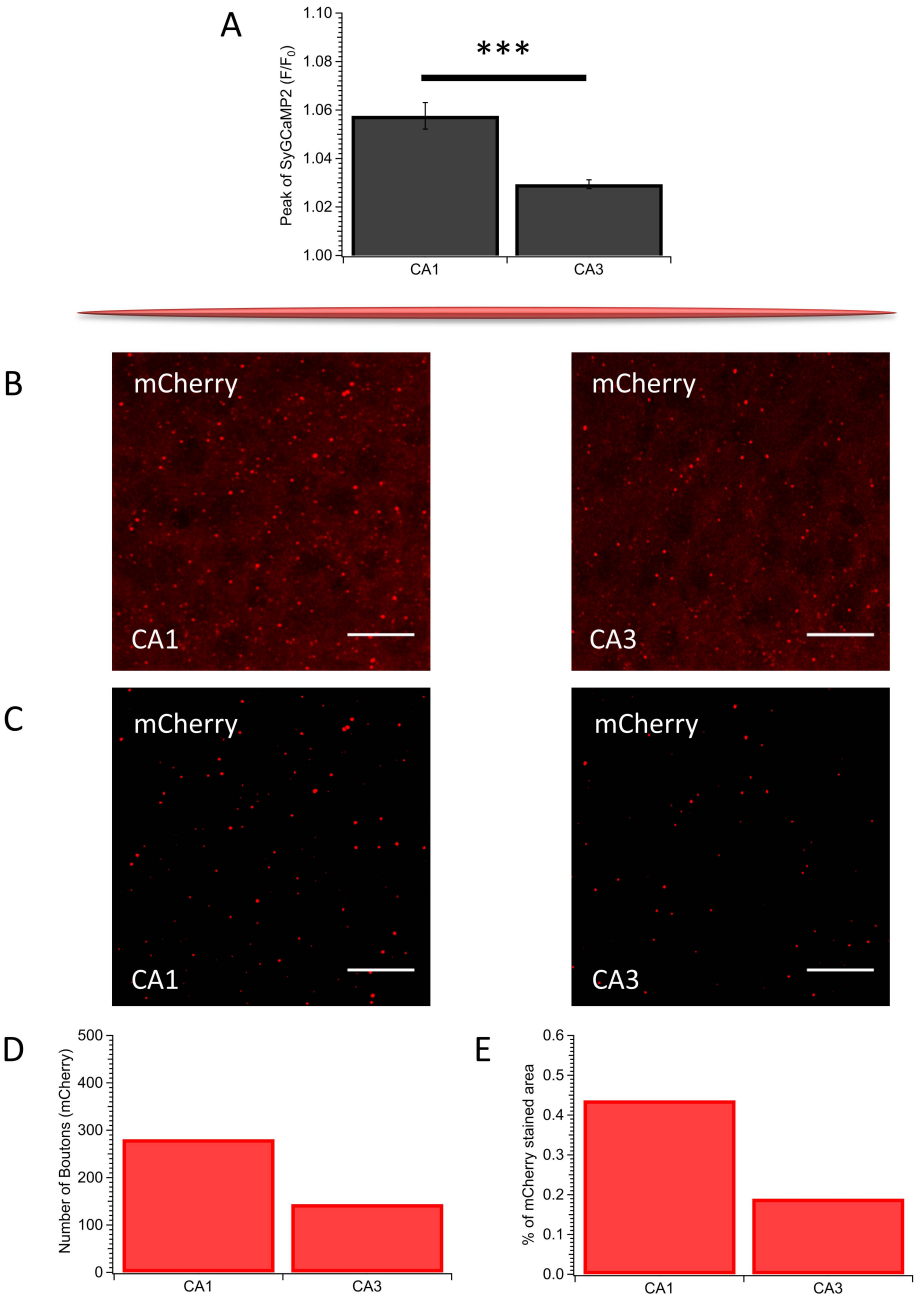

Figure 5.21. Imaging and IHC data showed possible difference between CA1 and CA3 area in the number of presynaptic boutons (release sites).

A. shows the peak amplitude of SyGCaMP2 fluorescence collected from both CA1 and CA3 hippocampal areas. The number of experiments in each series were 6. B and C show anti-mCherry antibody stained presynaptic boutons in both CA1 (left panel) and CA3 areas (right panel), before and after background subtraction, respectively. D and E bar charts show the difference between CA1 and CA3 area in the number of presynaptic boutons and the percentage of mCherry stained areas, respectively. The scale bar in B and C is 10 µm. Statistics: (A), P=<0.0001; unpaired t test.

5.2.5.5 AP5 prevented DCG-IV inhibitory effect on both SC-CA1 and MF-CA3 pathways.

At the end of experiments in the CA3 region, we confirmed that we were recording from the MF-CA3 pathway by suppressing synaptic transmission by bath application of 1 μM DCG-IV. In a series of preliminary experiments, we noticed that AP5 appeared to prevent the inhibitory effect of DCG-IV on the MF-CA3 pathway. We therefore repeated the experiments in which we examined the effects of DPCPX to test whether AP5 antagonised the effects of DCG-IV. As before, after obtaining a stable baseline of synaptic responses, 250 nM DPCPX was applied for 30 minutes and then washed out for 25 minutes. We carried out these experiments in the presence and absence of AP5 to test if there was an interaction between AP5 and DCG-IV. In both sets of experiments, there was a significant and similar increase in SyGCaMP2 fluorescence after adding DPCPX (about 130% of the baseline), as shown in figure 5.22-A. The N2 component of the field potential was also significantly changed after DPCPX application in both cases. The fEPSP in the absence of AP5 is clearly very much enhanced but in the presence of AP5, the increase appears to be a general run up of the response over time (130% and 250%, in the absence and presence of AP5, respectively). The extent of paired-pulse facilitation was unaltered by the application of DPXPX in either the presence or absence of AP5 (figure 5.22-B). Interestingly, in the presence of AP5, suppression of synaptic transmission by bath application of 1 μM DCG-IV was very much reduced.

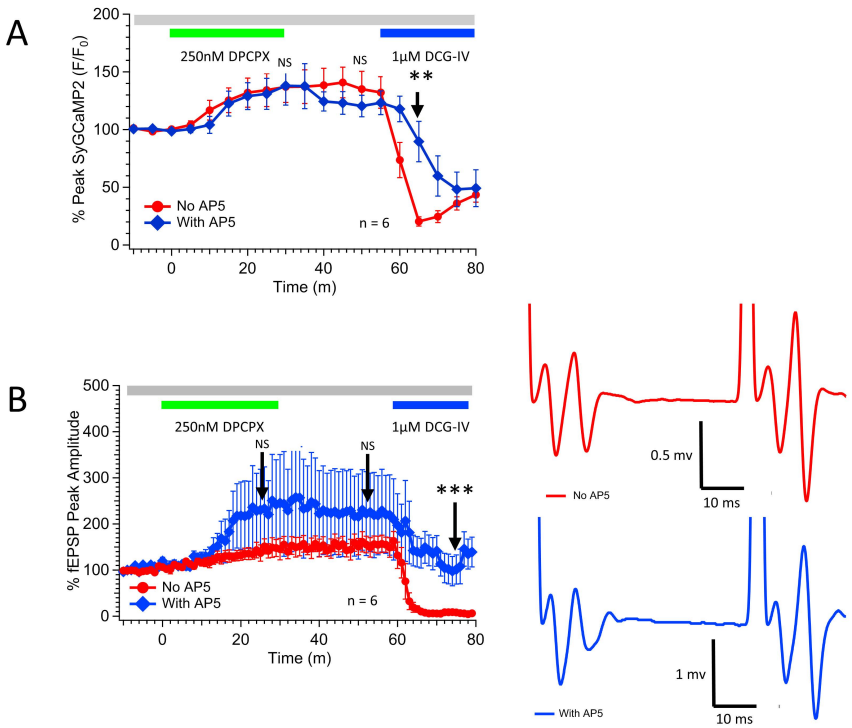

Figure 5.22. Effect of 250 nM DPCPX on MF activation in CA3 area of the SyG37 mouse's hippocampus, with and without AP5.

A. illustrates the effects of DPCPX, in the presence (red) and absence (blue) of AP5, on SyGCaMP2 fluorescence peak amplitude, over time, respectively. B. left panel illustrates the change in peak amplitude of the field potential before, during, and after addition of DPCPX. B the right hand panel shows pairs of field potentials recorded from the *stratum lucidum* of the CA3 hippocampal region in the presence (blue) and absence (red) of AP5. There was no effect of AP5 on PPF recorded from CA3 area. In both imaging and electrophysiology experiments, AP5 prevented DCG-IV inhibitory effect on MF-CA3 pathway. Statistics: (A), DCG-IV, P=0.0034; (B), DCG-IV, P=0.00021; two-way ANOVA followed by Sidak's multiple comparisons test.

It is known that, in CA1 experiments, an NMDA-dependent long term potentiation could arise as a result of repeated stimulation and so the selective NMDA receptor antagonist DL-AP5 was added to the aCSF in all experiments to prevent this phenomenon (Collingridge et al., 1983). In the CA1 region, mGluRs-II receptors are apparently absent (Kamiya *et al.*, 1996) and so we took the opportunity to compare the effects of 1 µM DCG-IV on synaptic transmission in the CA1 and CA3 regions. 1 µM DCG-IV on its own caused a sharp decrease in

both SyGCaMP2 fluorescence and fEPSP responses of both CA1 and CA3 experiments (figure 5.24-A and B, left panel). AP5 prevented the inhibitory effect of DCG-IV on both SC-CA1 and MF-CA3 pathways (figure 5.24-A and B, right panel).

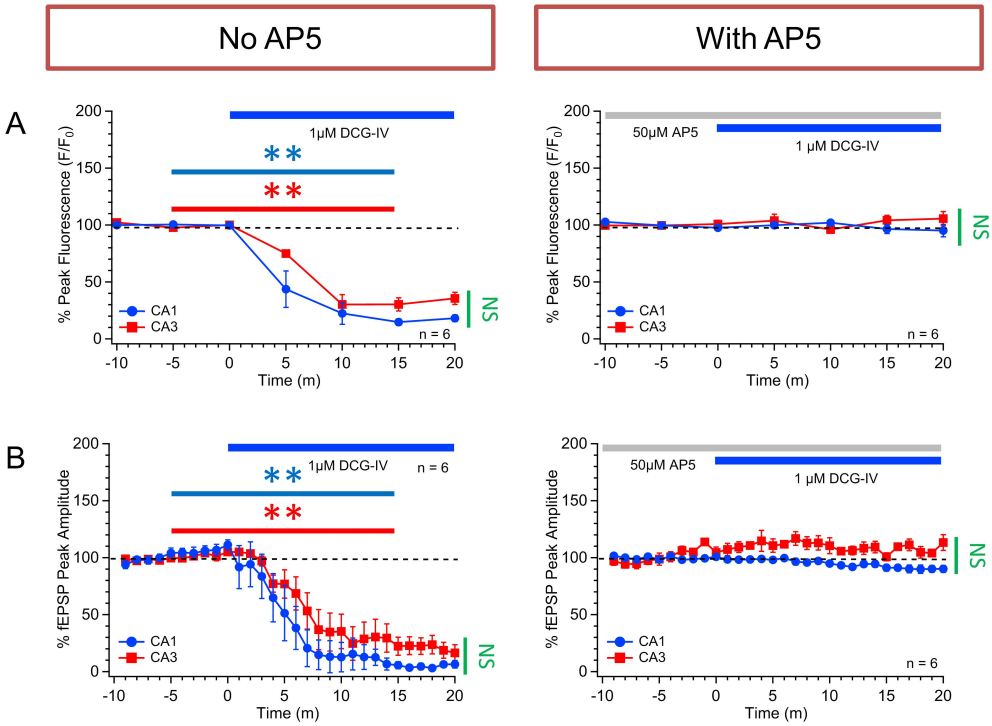

Figure 5.23. Comparison between the effects of 1 μM DCG-IV in the presence and absence of AP5 on responses to both, SC activation in the CA1 and MF activation in the CA3 areas of a SyG37 mouse model.

Imaging (A) and electrophysiological (B) experiments show the effects of DCG-IV in the absence (left panel) and presence (right panel) of AP5 on responses to both, SC activation in the CA1 (blue) and MF activation in the CA3 (red) areas of a SyG37 mouse model. Statistics: (A-left panel-blue), DCG-IV, U=0, P=0.0022; (A-left panel-red), DCG-IV, U=0, P=0.0022. (B-left panel-blue), DCG-IV, U=0, P=0.0022; (B-left panel-red), DCG-IV, U=0, P=0.0022; Mann Whitney test. No significant differences were observed between the two groups; two-way ANOVA followed by Sidak's multiple comparisons test.

5.3 Discussion

In this chapter, we evaluated presynaptic calcium signalling at the MF-CA3 pathway using the SyG37 mouse and compared responses with similar experiments carried out in CA1 to determine the ability of our sensor to detect any differences between these two hippocampal regions.

5.3.1 Electrical activation studies of the MF-CA3 pathway showed a sensitivity of the SyGCaMP2-mCherry sensor.

We examined the effects of altering the electrical activity on the MF-CA3 pathway of the SyG37 mouse model where the SyGCaMP2-mCherry sensor showed that responses to different intensities, frequencies and numbers of stimuli were qualitatively very similar to CA1 region. There was also a positive relationship between SyGCaMP2 fluorescence and the stimulus frequency, with a decrease in the SyGCaMP2 fluorescence at 100 Hz indicating the probability of vesicle exhaustion (figure 5-2, 3 & 4). This agrees with Forsythe *et al.* (1998) and other who found that during presynaptic recordings from the calyx of Held, there was a reduction in calcium entry after prolonged high-frequency stimulation that can contribute to depression (Forsythe et al., 1998, Regehr, 2012).

5.3.2 Adenosine receptor manipulation studies showed the sensitivity, and confirmed the presynaptic locus, of the SyGCaMP2-mCherry sensor in the CA3 microcircuit of a SyG37 transgenic mouse model.

Our results examining the effects of adenosine were consistent with previous observations in the CA3 region of the hippocampus (Wu and Saggau, 1994, Ferrati *et al.*, 2016, Schlicker and Feuerstein, 2017) which showed that adenosine produced a pronounced inhibitory effect on MF responses (figure 5-5). This neural modulation is thought to be due to inhibition of neurotransmitter release by a combination of inhibition of K^+ current activation, reduction of voltage-dependent Ca^{2+} currents, and/or by mechanisms downstream of Ca^{2+} influx (Wu and Saggau, 1994, Bannon *et al.*, 2014). It is thought to be of presynaptic origin as synaptic depression is accompanied by a change in paired-

pulse facilitation (Wu and Saggau, 1994, Gundlfinger et al., 2007). In our experiments, we observed that adenosine directly reduced calcium responses in presynaptic terminals (figure 5-5). This effect remained when experiments were repeated in the presence of DNQX and PTX indicating that the actions of adenosine are on the MF terminals themselves (figure 5-9). The A_1 adenosine receptor antagonist DPCPX (Lohse et al., 1987a) had an effect on both the presynaptic Ca^{2+} transient and on the field excitatory postsynaptic potential (fEPSP) at the MF-CA3 synapses of hippocampal slices. DPCPX enhanced both the Ca^{2+} transient and the fEPSP significantly, suggesting that DPCPX is acting to inhibit a tonic, inhibitory effect of adenosine (figure 5-6). Moreover, this is in agreement with previous research indicating that there are significant amounts of endogenous adenosine accumulated in the extracellular space (Haas and Greene, 1988). The A_1 receptor subtype is GPCR that couples to both G_i- and G_o-proteins in different systems. Therefore, it can impose inhibition of synaptic transmission via a number of transduction mechanisms. These include adenylyl cyclase inhibition, GIRKs activation, Ca^{2+} channel inhibition and phospholipase C activation (for review see; Dunwiddie and Masino, 2001). Pre-incubation with DPCPX antagonized adenosine-mediated reductions in fluorescence and field potential recordings within the CA3 region of the hippocampus (figure 5-7). In the presence of PTX and DNQX the inhibitory effect of adenosine was converted to an excitatory effect in the presence of DPCPX, and the application of DPCPX on its own caused an increase in SyGCaMP2 fluorescence (figure 5-9). In a direct comparison between the two sets of experiments, the absence and presence of PTX and DNQX showed a significant difference between the two groups in two ways: first, in the adenosine alone experimental group, and in the presence of PTX and DNQX, there was a significant increase in the SyGCaMP2 fluorescence at the wash-off period; second, in the presence of PTX, DNQX and DPCPX, adenosine increased the SyGCaMP2 fluorescence non-significantly, which became significant at the wash-off period. In other words, the inhibitory actions of adenosine observed in the SyG37 model experiments showed the opposite action in the presence of DPCPX as when PTX and DNQX are applied. This is may be because adenosine started to significantly stimulate the A_{2A} receptors in the presence of these blockers. This observation that on blockade of inhibitory

A_1 receptors adenosine is able to facilitate synaptic transmission in aged rats, further supports a greater functional impact of A_{2A} receptor activation in aged rats. We also tested the cumulative effect of some blockers on MF-CA3 pathway. PTX was expected to antagonise $GABA_A$/glycine receptors, leading to the removal of tonic inhibition from interneurons (Semyanov *et al.*, 2004). In our experiments, PTX on its own produced a small increase in the SyGCaMP2 fluorescence of a SyG37 mouse model. Addition of PTX, AP5 and DNQX caused a 20% reduction in the SyGCaMP2 fluorescence (figure 5-8). As expected, the N2 component of fEPSP was almost completely abolished as this is largely mediated by AMPA receptors (Wang *et al.*, 1994). These results show that about 80% of the SyGCaMP2 fluorescence originated from mossy fibres (i.e., from the presynaptic side) and the remaining 20% that we assume come from presynaptic boutons which are postsynaptic to mossy fibre. In general, responses recorded from the SyG37 mouse model were, however, still present in the presence of PTX and DNQX, which is consistent with the expression of the SyGCamP2-mCherry sensor in MF terminals.

5.3.3 cAMP-PKA signalling cascade is required for MF-CA3 pathway activity with the possibility of presynaptic calcium contribution.

The effects of forskolin/rolipram on the MF-CA3 pathway were investigated using imaging and field potential recordings. Interestingly, both forskolin doses caused a stimulatory effect on the SyGCaMP2 fluorescence in a dose-dependent manner where 50 µm forskolin had a stronger stimulatory effect than 25µm of forskolin on the peak amplitude of SyGCaMP2 fluorescence (figure 5-16). These changes in SyGCaMP2 fluorescence were accompanied by changes in the paired-pulse ratio, confirming the possible presynaptic locus of forskolin action in this pathway (figure 5-10 & 13). Effects of 50 µM forskolin, but not 25 µM forskolin, on SyGCaMP2 fluorescence were antagonised in the presence of PKI, confirming the possible role of presynaptic calcium in the cAMP-PKA pathway in MF-CA3 synapses (figure 5-11 & 14). This is in agreement with Lonart and Sudhof, (1998) who reported that, in mossy fibres, cAMP may enhance glutamate release via at least three different mechanisms. First, it may increase the size of the readily

releasable pool of vesicles at presynaptic terminals because forskolin potentiates release evoked by treatment with hypertonic sucrose. Second, it may directly enhance calcium entry through voltage-gated calcium channels since forskolin increases release triggered by potassium depolarisation. Third, it may enhance the calcium action on the secretory apparatus since forskolin also increases the response to ionomycin application, which leads to direct elevation of presynaptic calcium (Lonart and Sudhof, 1998). On the other hand, these findings go against those of other researchers, where Kaneko and Takahashi (2004), for instance, found that forskolin had no effect on presynaptic Ca^{2+} currents or K^{+} currents, suggesting that the main target of cAMP is downstream of the Ca2+ influx. Apparently, these results confirm the cAMP/PKA pathway's importance in basal synaptic transmission in MF-CA3 synapses. Under the conditions where cyclic-AMP metabolism is disrupted, high doses of forskolin induce long-term potentiation in the presynaptic region that can be blocked by the cyclic-AMP-dependent protein kinase inhibitor, PKI.

5.3.4 Comparison between the contributions of presynaptic calcium within both SC-CA1 and MF-CA3 microcircuits of a SyG37 mouse model.

5.3.4.1 SyGCaMP2-mCherry sensor detected a difference between SC-CA1 and MF-CA3 microcircuits of a SyG37 mouse model in electrical characterization experiments.

Results show that responses to different intensities, frequencies and numbers of stimuli were qualitatively very similar in both hippocampal regions except that the amplitudes of responses were always smaller in CA3 area (figure 5-17). This might be due to that our sensor is highly expressed in CA1 area compared with CA3 (figure 5-21). Our study showed a loss of linearity at higher stimuli number, with the ability of the SyGCaMP2-mCherry sensor to detect a single AP activation. Moreover, it was able to detect the effect of the residual and the transient calcium (Okorocha, 2016). In general, the SyGCaMP2-mCherry sensor

has sufficient sensitivity to make it a useful tool for monitoring calcium signalling in the hippocampus.

5.3.4.2 In adenosine receptor manipulation experiments, and in the presence of PTX, DNQX and DPCPX, the effect of adenosine is abolished in the CA1 area but is converted into a facilitatory effect in the CA3 area.

In adenosine receptor manipulation experiments, the SyGCaMP2-mCherry sensor detected two differences between the CA1 and CA3 regions where, in the presence of a specific blockers, the CA3 area responded differently in two ways: the first being in the adenosine alone experimental group, where there was an increase in the SyGCaMP2 fluorescence at the wash-off period; and the second in the presence of PTX, DNQX and DPCPX, where adenosine application increased the SyGCaMP2 fluorescence significantly, and which became more significant at the wash-off period (figure 5-18). There is no clear explanation for this, though Rebola et al. (2003b) found that in the CA1 area, application of 50 µM adenosine nearly blocks the fEPSP in both young adult and aged rats. However, in the presence of DPCPX, the effect of adenosine is abolished in young adult rats, but is converted into a facilitatory effect in aged rats that is attenuated in the presence of a highly selective antagonist for the adenosine A_{2A} receptor, ZM241385. In the same study, the possibility of adenosine metabolism modifications in aged rats (Cunha *et al.*, 2001) was excluded using a close chemical analogue of adenosine (2-chloroadenosine) that is less prone to metabolism, and which also facilitated the fEPSP slope in the presence of DPCPX in aged rats (Rebola et al., 2003b). This observation that on the blockade of inhibitory A_1 receptors, adenosine is able to facilitate synaptic transmission in aged rats further supports a greater functional impact of A_{2A} receptor activation in aged rats (Rebola et al., 2003b). Also, it indicates that A_{2A} receptors facilitate synaptic transmission in different mechanisms in aged and in young adult rats, where in young adult rats the A_{2A} receptor-induced facilitation of synaptic transmission was achieved via removal of tonic A_1 receptor-mediated inhibition of synaptic transmission (Lopes *et al.*, 2002), whereas in aged rats the ability of adenosine A_{2A} receptors to facilitate hippocampal synaptic transmission is due to

both a noticeable increase in the A_{2A} receptors binding density in hippocampal nerve terminals, as well as a difference in the hippocampal A_{2A} receptor's main transducing system. In aged rats, the A_{2A} receptors directly facilitate glutamatergic transmission via stimulation of cAMP-PKA-dependent pathways in nerve terminals, and indirect hippocampal synaptic transmission facilitation by tonic A_1 receptor-mediated inhibition attenuation no longer occurs (Cunha et al., 2001, Rebola et al., 2003b). From the above justifications, a question comes to mind: why could we see similar effects in the CA3 area of young mice after the blockade of synaptic transmission? In other words, what is the relationship between the blockade of synaptic transmission and aging? Our sensor could detect the excitatory effect of PTX in CA3 but not in CA1 experiments (figure 4-12 & 5-8). This could be attributed to the $GABA_A$ receptor locations in these different areas, where it is located presynaptically in CA3 area and postsynaptically in the CA1 area, where $GABA_A$ receptors in hippocampal mossy fibres are located presynaptically (Kullmann *et al.*, 2005). This is another indicator of the sensitivity and the presynaptic location of our sensor. CA3 hyperactivity theory is in agreement with other study where they suggested that the hippocampal dysfunction and possibly the limbic seizures observed in mutant mice are contributed to by hyperactive CA3 pyramidal neurones (Calfa *et al.*, 2011). Moreover, when Christian and Dudek (1988) studied the local excitatory circuits in CA3 using low concentrations of picrotoxin to selectively block recurrent inhibition, they lowered extracellular $[K^+]$ to 3 mM and raised both $[Ca^{2+}]$ and $[Mg^{2+}]$ to 4.0 mM to avoid epileptiform activity and decrease cellular excitability in PTX experiments (Christian and Dudek, 1988). Yoshiike *et al.* (2008) assumed that the memory decline in APP/PS1 transgenic mice is mediated by enhanced inhibition of LTP and, therefore, they found that memory deficits in adult APP/PS1 mice could be rescued with a non-epileptic dose of picrotoxin (PTX) for 10 days. In the CA1 area, there was an enhanced modulation of LTP mediated by A_{2A} receptors in aged rats. This was in accordance with an increase in expression and density of A_{2A} receptors in glutamatergic terminals in the age-associated manner. This may explain the ability of A_{2A} receptor antagonists in the prevention of memory dysfunction in aged animals (Costenla *et al.*, 2011). Cunha *et al.* (1994) found that there is a difference between the

CA1 and CA3 areas in the type of adenosine receptor modulation, where they concluded that the electrically evoked release of [3H] ACh in the two areas of the rat hippocampus can be differentially modulated by adenosine. In the CA1 area, ACh release was only modulated by A_1 inhibitory receptors, whereas in the CA3 area, both A_1 inhibitory and A_{2A} excitatory adenosine receptors modulate ACh release. To sum up, the CA3 area behaves differently in the presence of PTX, DNQX and DPCPX. We observed an effect of PTX on the presynaptic calcium in CA3 but not in CA1, which is consistent with the differential expression of $GABA_A$ receptor locations in these two different areas. These results may open up the possibility of an interaction between adenosine and GABA receptors (Rombo *et al*., 2016).

5.3.4.3 Comparison between the contributions of presynaptic calcium in the cAMP-PKA signalling cascade within both SC-CA1 and MF-CA3 microcircuits of a SyG37 mouse model.

We also compared the direct involvement of presynaptic calcium in the cAMP-PKA signalling cascade in both SC-CA1 and MF-CA3 synaptic transmission. We found that in the CA3 area, forskolin caused a small increase in the SyGCaMP2 fluorescence in a dose-dependent manner. By contrast, in the CA1 region a concentration dependent inhibitory effect was observed. These effects were antagonised by PKI indicating that the effects were dependent on the activation of protein kinase A (figure 5-19 & 5-20). It should be noted, however, that CA1 synapses behave very differently from those in CA3, and so whilst these various mechanisms have been observed, it is not clear whether they also exist within the CA1 region. However, in the CA1 area, forskolin-induced long-term potentiation was found to be masked by adenosine accumulation (Lu and Gean, 1999). In chapter 4 we could unmask forskolin-induced long-term potentiation using A_1 adenosine receptor antagonist, DPCPX.

From all of the above, one can hypothesis that depending on the difference between the release probability of the two different hippocampal areas, CA1 and CA3, that if we elicit two presynaptic action potentials with a 50 ms inter-stimulus

interval, paired-pulse ratio (PPR) can be calculated. PPF was observed when the first EPSC was small, as shown during MF-CA3 pathway activation, whereas paired-pulse depression (PPD) was observed when the first EPSC was large, as shown during SC-CA1 pathway activation. If the first action potential, successfully triggers release at most release sites, the PPD will be observed. Therefore, PPD may result from a decrease in quantal content which may be due to short-term depletion of readily releasable vesicles (Debanne *et al*., 1996). If the release probability in the CA1 area is very large, as indicated by the PPD, this might lead to a transient increase in the release of the major excitatory neurotransmitter, glutamate. In neocortical and hippocampal pyramidal neurones, glutamatergic and purinergic neurotransmission occurs at the same nerve terminals (Pankratov *et al.*, 2006). Therefore, the evoked stimulation of the presynaptic terminals will lead to the co-release of both glutamate and ATP. In the hippocampal CA1 region of rats, excitatory glutamatergic synapses are potently inhibited by purines, including adenosine, ATP. The inhibitory effect of purine nucleotides is mediated exclusively by A_1 receptors (Masino *et al.*, 2002). Given the above, one can assume that forskolin induced an increase in neural transmission in CA1 area. The high release probability in the CA1 area led to an increase in glutamate and ATP co-release, which led to purine accumulation that supressed the neurotransmitter release mediated exclusively by A_1 receptors. This mechanism might be working as a negative-feedback mechanism to prevent formation of any epileptic seizures. The opposite may be true in the CA3 area, where there is low release probability, less purine accumulation and, therefore, no masking of the adenosine-induced LTP (figure 5-25). These possibilities mentioned above remain worthy of further consideration and examination.

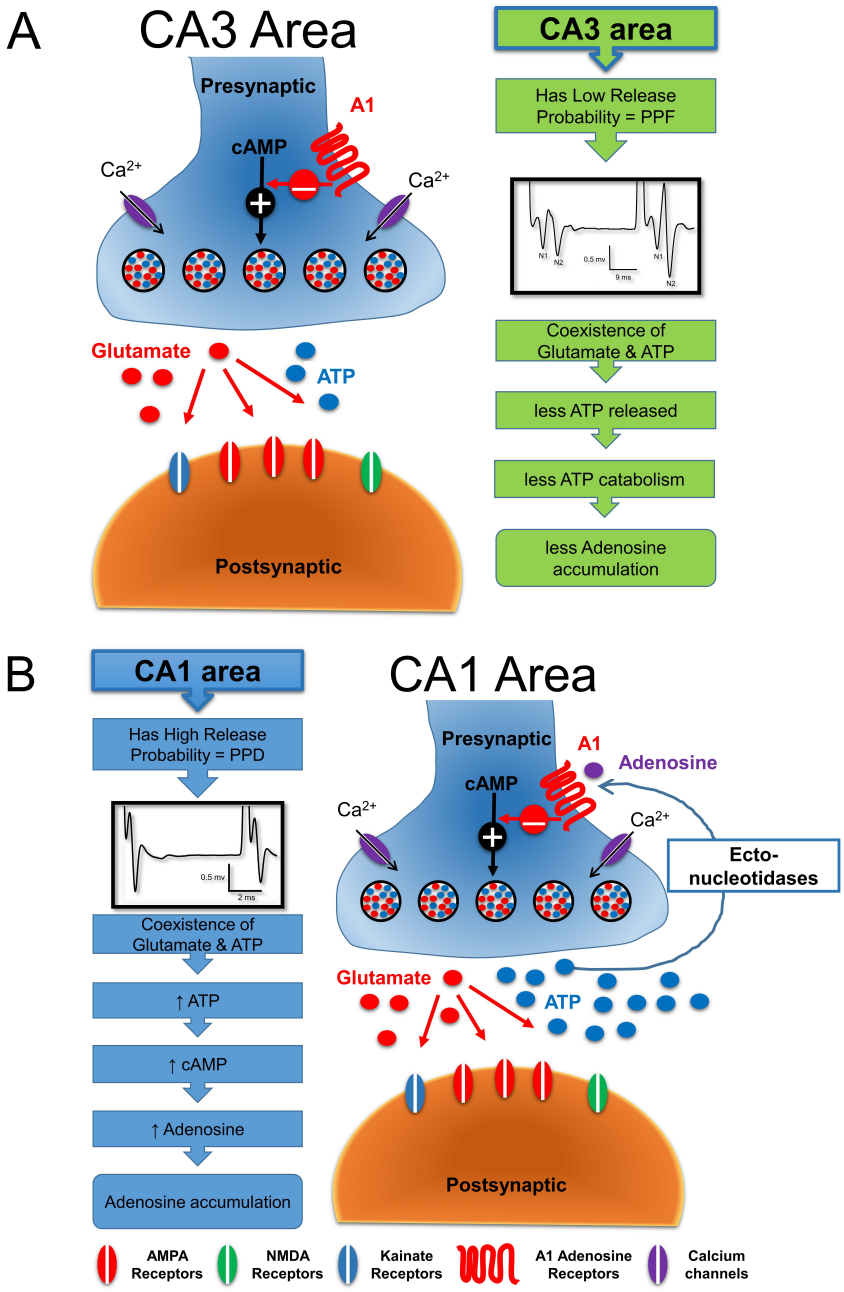

Figure 5.24. Proposed scheme overview of adenosine accumulation in CA1 but not in CA3 hippocampal areas due to the difference in the release probability.

A. schematic diagram showing less adenosine accumulation in the CA3 area due to the low release probability A. scheme diagram showing less adenosine accumulation in the CA1 area due to the low release probability. Presynaptically, localized A_1 adenosine receptors activated by accumulated adenosine directly modulates Ca^{2+} channel activity, causing a decrease in AP-evoked calcium influx and therefore a decrease in transmitter release. Consequently, the EPSC will be reduced markedly on the postsynaptic side.

5.3.4.4 AP5 prevented DCG-IV inhibitory effect on both CA1-SC and MF-CA3 pathways.

We also found that suppression of synaptic transmission in the MF-CA3 pathway by bath application of 1 μM DCG-IV was prevented by AP5. It is known that, in CA1 area experiments, an NMDA-dependent long term potentiation could arise as a result of repeated stimulation and so the selective NMDA receptor antagonist DL-AP5 was added to the aCSF in all experiments to prevent this phenomenon (Collingridge et al., 1983). It has been reported that no mGluR2 receptors exist in the CA1 region (Kamiya et al., 1996). Interestingly, DCG-IV on its own caused a sharp decrease of both SyGCaMP2 Fluorescence and fEPSP in CA1 indicating that despite the apparent absence of mGluR2 receptors, DCG-IV has an inhibitory effect on the SC-CA1 pathway (figure 5-22 & 5-23). Published literature related to the actions of DCG-IV can be divided into three groups. In a group where a lack of effect of DCG-IV in CA1 was reported, slices were pretreated with AP5 before recording from CA1. For example, Kamiya et al (1996) and others claimed that application of DCG-IV reversibly suppressed fEPSP evoked by mossy fibre stimulation. At the same concentration, DCG-IV, did not affect other glutamatergic excitatory transmissions at MF-CA3 or at the SC-CA1 pathways. Therefore, mGluR2/mGluR3 are expressed specifically at mossy fiber synapses in the hippocampal CA3 region (Kamiya et al., 1996, Morishita *et al.*, 1998, Matias *et al.*, 2014, Aksoy-Aksel and Manahan-Vaughan, 2015). A second group found an effect of DCG-IV on different pathways but they did not apply AP5 in their experiments. For example, Tsukamoto *et al.* (2003) and others found that DCG-IV application to hippocampal slices leads to a decrease in synaptic transmission between (1) perforant path and CA1 pyramidal cells, (2) perforant path and CA3, and (3) MF-CA3 (Tsukamoto et al., 2003, Daumas *et al.*, 2009). The third group, mentioned the role of AP5 in preventing the inhibitory effect of DCG-IV on synaptic transmission. For example, Breakwell *et al.* (1997) investigated the synaptic depression induced by DCG-IV in rat CA1 hippocampal area, where a brief bath application of DCG-IV caused a rapid depression of baseline slope of fEPSP. However, the DCG-IV-induced depression could be reversed by AP5. Finally, they suggested that DCG-IV is an agonist at NMDA receptors in area CA1 of rat hippocampus. To sum up, regardless of the hippocampus area, AP5 application will prevent the DCG-IV effect where,

DCG-IV has the ability to suppress synaptic transmission in all hippocampal areas and the NMDA receptor antagonist, AP5, has the ability to block this depressing action of DCG-IV. This might suggest that DCG-IV is an NMDAR agonist as well as mGluR2 agonist. Therefore, it can be used in CA3 which does not have NMDARs but in CA1, the drug is non specific and so affects transmission through perhaps other mechanisms, including direct activation of NMDARs

Chapter 6. General discussion

This study aimed to characterize and test the suitability of the SyGCaMP2-mCherry sensor for measuring synaptic activity in different hippocampal neuronal pathways. Recently, our lab has developed a series of fluorescent protein based sensors that are designed to allow the direct, real time visualisation and quantification of presynaptic calcium signalling, transmitter release and vesicle reuptake. Of these, a SyG37 mouse was created that expresses a fluorescent protein based genetically encoded calcium indicator (GECI) selectively in the presynaptic terminals of neurons. This SyGCaMP2-mCherry sensor is expressed in subsets of CNS neurones under the control of the mouse Thy1 promoter. To characterize it, we used a combination of immunohistochemical, electrophysiological and fluorescent imaging techniques. Our findings indicate that this new ratiometric sensor provides an excellent tool for detecting neural activity in acute brain slices. First, we showed that evoked calcium transients can be detected in acute brain slices prepared from the SyG37 mouse model where electrical activation of SCs or mossy fibres elicited large calcium transients in each of these areas, respectively (figure 5-17). Moreover, in response to electrical stimulation, calcium transients were detectable from as few as one electrical stimulus but increased with increasing stimulus number and frequency (figure 5-17).

Pre and post synaptic information can be collected at the same time using SyGCaMP2 imaging alongside electrophysiological recordings, however, there is a problem that the calcium signal saturates before the electrophysiological signal. In SyGCaMP2-mCherry transgenic mice expression was evident throughout the CNS but was particularly prominent in the hippocampus with a punctate expression in areas CA3 and CA1 (figure 3-3 & 3-4). With immunohistochemistry, we showed that mCherry is preferentially distributed presynaptically in the SyG37 mouse hippocampus with strong expression in the fibre pathways and around cell bodies in the DG, CA3, CA1 and subiculum (figure 3-7). We showed that there was a strong co-localization of mCherry with the presynaptic marker bassoon (Richter et al., 1999) as well as with the excitatory presynaptic marker vGLUT1 and the inhibitory presynaptic marker vGAT; figure

3-8-11 (Chaudhry *et al.*, 1998a, Herzog et al., 2006). No co-localisation was observed with the postsynaptic marker PSD95 (Hunt et al., 1996) or the nuclear stain Hoechst; figure 3-6 & 9 (Latt and Stetten, 1976). The segregation between mCherry and PSD95 and between mCherry and Hoechst confirmed that our sensor is neither expressed in postsynaptic terminals nor in the cell bodies. Therefore, we have provided strong evidence that SyGCaMP2-mCherry expression within the hippocampus is presynaptic and likely to be present in both inhibitory and excitatory terminals.

Using the SyG37 mice, we also demonstrated that blocking glutamergic and GABAregic receptors led to only 25 and 20% reduction in the SyGCaMP2 response amplitude to electrical stimulation in CA1 and CA3 areas, respectively (figure 4-12 & 5-8). Therefore, we assume that only 25 and 20% of transmission originates from presynaptic boutons which are postsynaptic to SCs and mossy fibers, respectively. The SyGCaMP2-mCherry sensor showed it is highly sensitive since it could detect facilitiory effects of PTX in CA3, but not in CA1 experiments (figure 4-12 & 5-8). This may reflect differential locations of $GABA_A$ receptor in each area where it is located presynaptically in CA3 and postsynaptically at CA1 area. Since the activation of presynaptic $GABA_A$ receptors in hippocampal mossy fibres enhance transmission and LTP induction (Kullmann et al., 2005, Ruiz *et al.*, 2010).

To evaluate the suitability of our mouse model for measuring presynaptic activity, we also demonstrated that adenosine receptor manipulation confirmed the presynaptic locus of our sensor. Moreover, we found that in the CA3 area, adenosine behaved differently after blocking synaptic transmission and/or and A_1 receptors (figure 5-18). Finally, in the CA3 area, forskolin caused a small increase in the SyGCaMP2 fluorescence in a dose-dependent manner. However, the effect of forskolin on field potential recordings was very pronounced. In contrast, in the CA1 region, the stimulatory effect of forskolin was converted to an inhibitory effect on SyGCaMP2 fluorescence in a dose-dependent manner (figure 5-19 & 20). This might be because adenosine accumulation in this area could mask the forskolin induced potentiation. In chapter four we were able to unmask forskolin-induced potentiation in CA1, after blocking A1 adenosine receptors; figure 4-19

(Lu and Gean, 1999) with the possibility of presynaptic CA^{2+} contribution. Forskolin effects were antagonised by inhibition of protein kinase A confirming that its effects were mediated by the cAMP-PKA pathway. See tables 6-1, 2 & 3 for the main interesting points reported in this study

This study is part of a wider group of experiments carried out in our lab. In a parallel study, Dr Daniel Pereda as one of our lab members, has been working on aged mice trying to find differences in synaptic transmission between young and aged mice, in terms of the presynaptic calcium effect. As a recommendation for further research, it would be interesting to breed SyG37 mice with other models of age-related deficits or neurodegenerative conditions so that we can compare between the patterns of calcium signalling at presynaptic terminals at each stage of the hippocampal circuit from dentate gyrus to CA1 in young and aged animals and in other disease conditions. It is also noted that the absolute peak amplitude of SyGCaMP2 fluorescence was always higher in CA1 data compared with CA3 (figure 5-17). This might be due to the fact that our sensor appears to be more highly expressed in CA1 compared with CA3, where IHC data supported this possibility (figure 5.21). The interaction between DCG-IV and the NMDA antagonist, AP5 seems to be very interesting topic since we found that AP5 prevented the inhibitory effect of DCG-IV in both hippocampal areas, CA1 and CA3 (figure 5-22 & 23). We hope to re-examine this topic in the future. Moreover, in some preliminary experiments, we could see a presynaptic role of NMDA receptors within CA3 area but not in CA1; it would be better to investigate these interesting results deeply, hoping to change the concept that the synaptic plasticity in CA1 area is NMDA dependant and CA3 area is NMDA independent to a new concept which is that the synaptic plasticity in CA1 area is postsynaptic NMDA dependant and CA3 area is presynaptic NMDA dependant. In experiments where the calcium transients were measured at individual presynaptic boutons, it would have been better to do more experiments, as this type of experiment allowed us to separate whether effects were due to a change in calcium signalling within boutons or a change in the number of contributing boutons or a combination of the two.

One of the limitations of this study was that, we could not always record high levels of paired-pulse facilitation in MF-CA3 experiments. The hippocampal mossy fiber synapse are known to exhibit remarkably pronounced short-term plasticity (Nicoll and Schmitz, 2005). One reason for this may be that we carried out experiments at room temperature and so it would have been interesting to examine the effects of repeating some of the experiments at more physiological temperatures. Nevertheless, all our responses were selectively blocked by DCG-IV, an mGluR-2 agonist (Lanthorn et al., 1984, Yokoi et al., 1996) which is considered to be a characteristic of MF responses. A further limitation of our study is that we did not use the ratiometric feature of our sensor our sensor. This was primarily because it was difficult to separate sensor fluorescence from endogenous fluorophores. Ratiometric measurements are highly dependent on background subtraction and so with this uncertainty, it was felt better to use a more simple approach. Other work carried out in the lab has shown that it is possible to use ratiometric measurements to calibrate absolute calcium in presynaptic terminals and so future work is likely to make use of this feature. Together, these results indicate that SyG37 mice provide a sensitive useful tool to detect patterns of neuronal activity such as residual and transient calcium signalling detection at populations of neurones *in vitro*, as well as at the level of individual neurones and synapses. Now that it has been well characterized in the hippocampus, further studies looking into learning and memory and the effects of different drugs should be possible and useful allowing better distinction of pre- and postsynaptic effects.

Table 6.1. The main differences between the SyG mouse strains.

---- = No Expression, +++ = Expression.

	SYG14 mouse strain	SYG37 mouse strain	Technique
Typical examples of PCR genotyping for detection of a transgene from mouse ear snips from both SyG14 and SyG37 colonies.	+++	+++	PCR
Assessment of SyG14 and SyG37 mice by Western blot analysis of mCherry protein expression.	----	+++	Western blot

Table 6.2. The main differences between optical and electrophysiological techniques used in this study.

Signs: ---- = No effect; ↑, ↑↑, ↑↑↑ = Increase in the effect at different levels. ↓, ↓↓, ↓↓↓ = decrease in the effect at different levels.

	Fluo-4 calcium dye	SYG37 mouse	SYG14 mouse	fEPSP
The effect of 250 nM DPCPX on SC activation in the CA1 area of the hippocampus.	−−−	↑↑↑	−−−	↑↑↑
The effects of 10 μM PTX, 50 μM AP5 and 10 μM DNQX on optically and electrophysiologically recorded responses to SC activation in the CA1 area of the hippocampus.	↓↓	↓	↓↓↓	↓↓↓↓
The effects of pre-incubation of 10 μM PTX, 50 μM AP5 and 10 μM DNQX on the responses of different optical recording methods to SC/AC pathway stimulation.	↓	↑	↓	

Table 6.3. The main different between the responses to both, SC activation in the CA1 and MF activation in the CA3 areas of a SyG37 mouse model.

Signs: ---- = No effect; ↑, ↑↑, ↑↑↑ = Increase in the effect at different levels. ↓, ↓↓, ↓↓↓ = decrease in the effect at different levels.

	CA1	CA3	Technique
mCherry protein expression	↑↑↑	↑↑	IHC and imaging
The effect of increasing stimulus intensity, stimulus number and stimulus frequency on SyGCaMP2 fluorescence in the hippocampal CA1 and CA3 regions.	↑↑↑	↑↑	Imaging and Electrophysiology
The effect of 250 nM DPCPX on SyGCaMP2 fluorescence responses to SC activation in the CA1 area and to MF activation in the CA3 area of the SyG37 hippocampus in the presence of synaptic transmission blockade.	----	↑↑↑	Imaging and Electrophysiology
The effects of 50 µM forskolin and rolipram on both SC-CA1 and MF-CA3 synapses of a SyG37 mouse model.	↓	↑	Imaging and Electrophysiology
The effects of 100 µM DCG-IV in the presence of AP5 on responses to both, SC activation in the CA1 and MF activation in the CA3 areas of a SyG37 mouse model.	----	----	Imaging and Electrophysiology
The effects of 100 µM DCG-IV in the absence of AP5 on responses to both, SC activation in the CA1 and MF activation in the CA3 areas of a SyG37 mouse model.	↓↓↓	↓↓↓	Imaging and Electrophysiology
The effects of 10 µM PTX on responses to both, SC activation in the CA1 and MF activation in the CA3 areas of a SyG37 mouse model.	----	↑	Imaging and Electrophysiology

Appendix 1. SyGCaMP2-mCherry cloning vehicle

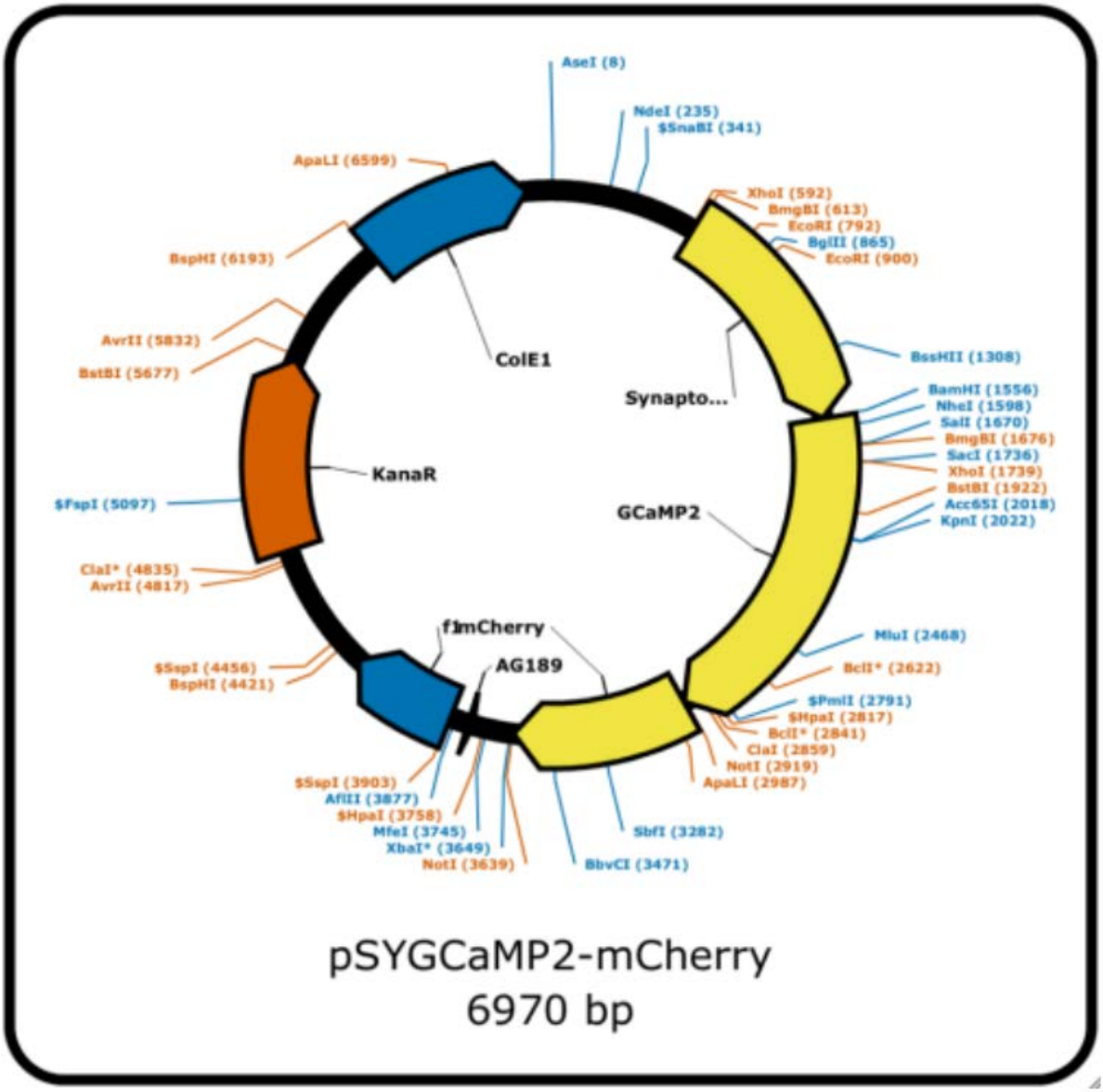

References

ABEL, T. & NGUYEN, P. V. 2008. Regulation of hippocampus-dependent memory by cyclic AMP-dependent protein kinase. *Progress in brain research,* 169**,** 97-115.

ABENAVOLI, A., FORTI, L., BOSSI, M., BERGAMASCHI, A., VILLA, A. & MALGAROLI, A. 2002. Multimodal quantal release at individual hippocampal synapses: evidence for no lateral inhibition. *J Neurosci,* 22**,** 6336-46.

ADAMS, D. J., SHEN, C., LEVENGA, J., BASTA, T., EISENBERG, S. P., MAPES, J., HAMPTON, L., GROUNDS, K., HOEFFER, C. A. & STOWELL, M. H. B. 2017. Synaptophysin is a β-Amyloid Target that Regulates Synaptic Plasticity and Seizure Susceptibility in an Alzheimer's Model. *bioRxiv*.

ADES, E. W., ZWERNER, R. K., ACTON, R. T. & BALCH, C. M. 1980. Isolation and partial characterization of the human homologue of Thy-1. *The Journal of Experimental Medicine,* 151**,** 400-406.

AIGNER, L., ARBER, S., KAPFHAMMER, J. P., LAUX, T., SCHNEIDER, C., BOTTERI, F., BRENNER, H. R. & CARONI, P. 1995. Overexpression of the neural growth-associated protein GAP-43 induces nerve sprouting in the adult nervous system of transgenic mice. *Cell,* 83**,** 269-78.

AKERBOOM, J., RIVERA, J. D. V., GUILBE, M. M. R., MALAVÉ, E. C. A., HERNANDEZ, H. H., TIAN, L., HIRES, S. A., MARVIN, J. S., LOOGER, L. L. & SCHREITER, E. R. 2009. Crystal structures of the GCaMP calcium sensor reveal the mechanism of fluorescence signal change and aid rational design. *Journal of biological chemistry,* 284**,** 6455-6464.

AKSOY-AKSEL, A. & MANAHAN-VAUGHAN, D. 2015. Synaptic strength at the temporoammonic input to the hippocampal CA1 region in vivo is regulated by NMDA receptors, metabotropic glutamate receptors and voltage-gated calcium channels. *Neuroscience,* 309**,** 191-9.

ALEXANDER, S. P. H., CATTERALL, W. A., KELLY, E., MARRION, N., PETERS, J. A., BENSON, H. E., FACCENDA, E., PAWSON, A. J., SHARMAN, J. L., SOUTHAN, C., DAVIES, J. A. & COLLABORATORS, C. 2015. The Concise Guide to PHARMACOLOGY 2015/16: Voltage-gated ion channels. *British Journal of Pharmacology,* 172**,** 5904-5941.

ALZHEIMER, C., SUTOR, B. & TEN BRUGGENCATE, G. 1989. Transient and selective blockade of adenosine A1-receptors by 8-cyclopentyl-1,3-dipropylxanthine (DPCPX) causes sustained epileptiform activity in hippocampal CA3 neurons of guinea pigs. *Neuroscience Letters,* 99**,** 107-112.

AMMANN, D. 2013. *Ion-selective microelectrodes: principles, design and application*, Springer Science & Business Media.

ANDERSON, W. W. & COLLINGRIDGE, G. L. 2007. Capabilities of the WinLTP data acquisition program extending beyond basic LTP experimental functions. *J Neurosci Methods,* 162**,** 346-56.

BACH, M. E., BARAD, M., SON, H., ZHUO, M., LU, Y.-F., SHIH, R., MANSUY, I., HAWKINS, R. D. & KANDEL, E. R. 1999. Age-related defects in spatial memory are correlated with defects in the late phase of hippocampal long-term potentiation in vitro and are attenuated by drugs that enhance the cAMP signaling pathway. *Proceedings of the National Academy of Sciences,* 96**,** 5280-5285.

BAIRD, G. S., ZACHARIAS, D. A. & TSIEN, R. Y. 1999. Circular permutation and receptor insertion within green fluorescent proteins. *Proceedings of the National Academy of Sciences,* 96**,** 11241-11246.

BANKHEAD, P. 2014. Analyzing fluorescence microscopy images
with ImageJ. *Queen's University Belfast,* 2017.

BANNON, N. M., ZHANG, P., ILIN, V., CHISTIAKOVA, M. & VOLGUSHEV, M. 2014. Modulation of synaptic transmission by adenosine in layer 2/3 of the rat visual cortex in vitro. *Neuroscience,* 260**,** 171-184.

BARTLETT, J. M. S. & STIRLING, D. 2003. A Short History of the Polymerase Chain Reaction. *In:* BARTLETT, J. M. S. & STIRLING, D. (eds.) *PCR Protocols.* Totowa, NJ: Humana Press.

BELARDINELLI, L. & PELLEG, A. 2012. *Adenosine and adenine nucleotides: From molecular biology to integrative physiology*, Springer Science & Business Media.

BELLOCCHIO, E. E., REIMER, R. J., FREMEAU, R. T., JR. & EDWARDS, R. H. 2000. Uptake of glutamate into synaptic vesicles by an inorganic phosphate transporter. *Science,* 289**,** 957-60.

BENITAH, J., GOMEZ, A., FAUCONNIER, J., KERFANT, B., PERRIER, E., VASSORT, G. & RICHARD, S. 2002. Voltage-gated Ca 2+ currents in the human pathophysiologic heart: a review. *Basic research in cardiology,* 97.

BENNETT, P. B. & GUTHRIE, H. R. 2003. Trends in ion channel drug discovery: advances in screening technologies. *Trends in biotechnology,* 21**,** 563-569.

BERGET, S. M. 1995. Exon recognition in vertebrate splicing. *J Biol Chem,* 270**,** 2411-4.

BIRD, C. M. & BURGESS, N. 2008. The hippocampus and memory: insights from spatial processing. *Nat Rev Neurosci,* 9**,** 182-94.

BLISS, T. V. & COLLINGRIDGE, G. L. 1993. A synaptic model of memory: long-term potentiation in the hippocampus. *Nature,* 361**,** 31-9.

BLISS, T. V. & LOMO, T. 1973. Long-lasting potentiation of synaptic transmission in the dentate area of the anaesthetized rabbit following stimulation of the perforant path. *J Physiol,* 232**,** 331-56.

BOISON, D. 2012. Adenosine dysfunction in epilepsy. *Glia,* 60**,** 1234-1243.

BOLLEN, E., PUZZO, D., RUTTEN, K., PRIVITERA, L., DE VRY, J., VANMIERLO, T., KENIS, G., PALMERI, A., D'HOOGE, R., BALSCHUN, D., STEINBUSCH, H. M., BLOKLAND, A. & PRICKAERTS, J. 2014. Improved long-term memory via enhancing cGMP-PKG signaling requires cAMP-PKA signaling. *Neuropsychopharmacology,* 39**,** 2497-505.

BORTOLOTTO, Z. A., FITZJOHN, S. M. & COLLINGRIDGE, G. L. 1999. Roles of metabotropic glutamate receptors in LTP and LTD in the hippocampus. *Curr Opin Neurobiol,* 9**,** 299-304.

BOURTCHOULADZE, R., ABEL, T., BERMAN, N., GORDON, R., LAPIDUS, K. & KANDEL, E. R. 1998. Different training procedures recruit either one or two critical periods for contextual memory consolidation, each of which requires protein synthesis and PKA. *Learn Mem,* 5**,** 365-74.

BREAKWELL, N. A., HUANG, L., ROWAN, M. J. & ANWYL, R. 1997. DCG-IV inhibits synaptic transmission by activation of NMDA receptors in area CA1 of rat hippocampus. *Eur J Pharmacol,* 322**,** 173-8.

BREAKWELL, N. A., ROWAN, M. J. & ANWYL, R. 1996. Metabotropic glutamate receptor dependent EPSP and EPSP-spike potentiation in area CA1 of the submerged rat hippocampal slice. *Journal of Neurophysiology,* 76**,** 3126-3135.

BRETTLE, D. & CARMICHAEL, F. 2011. The impact of digital image processing artefacts mimicking pathological features associated with restorations. *British dental journal,* 211**,** 167-170.

BRICKMAN, A. M., KHAN, U. A., PROVENZANO, F. A., YEUNG, L. K., SUZUKI, W., SCHROETER, H., WALL, M., SLOAN, R. P. & SMALL, S. A. 2014. Enhancing dentate gyrus function with dietary flavanols improves cognition in older adults. *Nat Neurosci,* 17**,** 1798-803.

BROCK, R., HINK, M. A. & JOVIN, T. M. 1998. Fluorescence correlation microscopy of cells in the presence of autofluorescence. *Biophys J,* 75**,** 2547-57.

BROSE, N. 2008. For better or for worse: complexins regulate SNARE function and vesicle fusion. *Traffic,* 9**,** 1403-13.

BRUNS, R. F., FERGUS, J. H., BADGER, E. W., BRISTOL, J. A., SANTAY, L. A., HARTMAN, J. D., HAYS, S. J. & HUANG, C. C. 1987a. Binding of the A1-selective adenosine antagonist 8-cyclopentyl-1,3-dipropylxanthine to rat brain membranes. *Naunyn Schmiedebergs Arch Pharmacol,* 335**,** 59-63.

BRUNS, R. F., FERGUS, J. H., BADGER, E. W., BRISTOL, J. A., SANTAY, L. A., HARTMAN, J. D., HAYS, S. J. & HUANG, C. C. 1987b. Binding of the A1-selective adenosine antagonist 8-cyclopentyl-1, 3-dipropylxanthine to rat brain membranes. *Naunyn-Schmiedeberg's archives of pharmacology,* 335**,** 59-63.

BUCKINGHAM, J. 1987. *Dictionary of organic compounds [12] [12],* New York u.a., Chapman and Hall.

BURRI, L. & LITHGOW, T. 2004. A Complete Set of SNAREs in Yeast. *Traffic,* 5**,** 45-52.

BUSCHE, M. A., EICHHOFF, G., ADELSBERGER, H., ABRAMOWSKI, D., WIEDERHOLD, K. H., HAASS, C., STAUFENBIEL, M., KONNERTH, A. & GARASCHUK, O. 2008. Clusters of hyperactive neurons near amyloid plaques in a mouse model of Alzheimer's disease. *Science,* 321**,** 1686-9.

BUSCHE, M. A. & KONNERTH, A. 2016. Impairments of neural circuit function in Alzheimer's disease. *Philosophical Transactions of the Royal Society B: Biological Sciences,* 371**,** 20150429.

CALFA, G., HABLITZ, J. J. & POZZO-MILLER, L. 2011. Network hyperexcitability in hippocampal slices from Mecp2 mutant mice revealed by voltage-sensitive dye imaging. *Journal of Neurophysiology,* 105**,** 1768-1784.

CALHOUN, M. E., JUCKER, M., MARTIN, L. J., THINAKARAN, G., PRICE, D. L. & MOUTON, P. R. 1996. Comparative evaluation of synaptophysin-based methods for quantification of synapses. *Journal of neurocytology,* 25**,** 821-828.

CALIXTO, E., THIELS, E., KLANN, E. & BARRIONUEVO, G. 2003. Early maintenance of hippocampal mossy fiber--long-term potentiation depends on protein and RNA synthesis and presynaptic granule cell integrity. *J Neurosci,* 23**,** 4842-9.

CAMPSALL, K. D., MAZEROLLE, C. J., DE REPENTINGY, Y., KOTHARY, R. & WALLACE, V. A. 2002. Characterization of transgene expression and Cre recombinase activity in a panel of Thy-1 promoter-Cre transgenic mice. *Dev Dyn,* 224**,** 135-43.

CAPPAERT, N. L. M., VAN STRIEN, N. M. & WITTER, M. P. 2015. Chapter 20 - Hippocampal Formation A2 - Paxinos, George. *The Rat Nervous System (Fourth Edition).* San Diego: Academic Press.

CARONI, P. 1997. Overexpression of growth-associated proteins in the neurons of adult transgenic mice. *J Neurosci Methods,* 71**,** 3-9.

CARROLL, R. C., NICOLL, R. A. & MALENKA, R. C. 1998. Effects of PKA and PKC on miniature excitatory postsynaptic currents in CA1 pyramidal cells. *J Neurophysiol,* 80**,** 2797-800.

CAVALIER, M., CROUZIN, N., BEN SEDRINE, A., DE JESUS FERREIRA, M. C., GUIRAMAND, J., COHEN-SOLAL, C., FEHRENTZ, J. A., MARTINEZ, J., BARBANEL, G. & VIGNES, M. 2015. Involvement of PKA and ERK pathways in ghrelin-induced long-lasting potentiation of excitatory synaptic transmission in the CA1 area of rat hippocampus. *Eur J Neurosci,* 42**,** 2568-76.

CHAKRABARTI, L., GALDZICKI, Z. & HAYDAR, T. F. 2007. Defects in Embryonic Neurogenesis and Initial Synapse Formation in the Forebrain of the Ts65Dn Mouse Model of Down Syndrome. *The Journal of Neuroscience,* 27**,** 11483-11495.

CHANCE, B., SCHOENER, B., OSHINO, R., ITSHAK, F. & NAKASE, Y. 1979. Oxidation-reduction ratio studies of mitochondria in freeze-trapped samples. NADH and flavoprotein fluorescence signals. *J Biol Chem,* 254**,** 4764-71.

CHAUDHRY, F. A., REIMER, R. J., BELLOCCHIO, E. E., DANBOLT, N. C., OSEN, K. K., EDWARDS, R. H. & STORM-MATHISEN, J. 1998a. The vesicular GABA transporter, VGAT, localizes to

synaptic vesicles in sets of glycinergic as well as GABAergic neurons. *J Neurosci,* 18**,** 9733-50.

CHAUDHRY, F. A., REIMER, R. J., BELLOCCHIO, E. E., DANBOLT, N. C., OSEN, K. K., EDWARDS, R. H. & STORM-MATHISEN, J. 1998b. The Vesicular GABA Transporter, VGAT, Localizes to Synaptic Vesicles in Sets of Glycinergic as Well as GABAergic Neurons. *The Journal of Neuroscience,* 18**,** 9733-9750.

CHAVEZ-NORIEGA, L. E. & STEVENS, C. F. 1994. Increased transmitter release at excitatory synapses produced by direct activation of adenylate cyclase in rat hippocampal slices. *Journal of Neuroscience,* 14**,** 310-317.

CHEN, C., ARAI, I., SATTERFIELD, R., YOUNG, S. M. & JONAS, P. 2017. Synaptotagmin 2 Is the Fast Ca(2+) Sensor at a Central Inhibitory Synapse. *Cell Reports,* 18**,** 723-736.

CHEN, Q., CICHON, J., WANG, W., QIU, L., LEE, S. J., CAMPBELL, N. R., DESTEFINO, N., GOARD, M. J., FU, Z., YASUDA, R., LOOGER, L. L., ARENKIEL, B. R., GAN, W. B. & FENG, G. 2012. Imaging neural activity using Thy1-GCaMP transgenic mice. *Neuron,* 76**,** 297-308.

CHEN, X., NELSON, C. D., LI, X., WINTERS, C. A., AZZAM, R., SOUSA, A. A., LEAPMAN, R. D., GAINER, H., SHENG, M. & REESE, T. S. 2011. PSD-95 is required to sustain the molecular organization of the postsynaptic density. *J Neurosci,* 31**,** 6329-38.

CHEN, Y. & BARKLEY, M. D. 1998. Toward Understanding Tryptophan Fluorescence in Proteins. *Biochemistry,* 37**,** 9976-9982.

CHENG, Q. & YAKEL, J. L. 2014. Presynaptic α7 nicotinic acetylcholine receptors enhance hippocampal mossy fiber glutamatergic transmission via PKA activation. *Journal of Neuroscience,* 34**,** 124-133.

CHETELAT, G. & BARON, J. C. 2003. Early diagnosis of Alzheimer's disease: contribution of structural neuroimaging. *Neuroimage,* 18**,** 525-41.

CHO, J.-H., SWANSON, C. J., CHEN, J., LI, A., LIPPERT, L. G., BOYE, S. E., ROSE, K., SIVARAMAKRISHNAN, S., CHUONG, C.-M. & CHOW, R. H. 2017. The GCaMP-R family of genetically encoded ratiometric calcium indicators. *ACS Chemical Biology,* 12**,** 1066-1074.

CHRISTIAN, E. P. & DUDEK, F. E. 1988. Characteristics of local excitatory circuits studied with glutamate microapplication in the CA3 area of rat hippocampal slices. *Journal of Neurophysiology,* 59**,** 90-109.

CHUNG, C. & RAINGO, J. 2013. Vesicle dynamics: how synaptic proteins regulate different modes of neurotransmission. *J Neurochem,* 126**,** 146-54.

COLLINGRIDGE, G., KEHL, S. & MCLENNAN, H. 1983. The antagonism of amino acid-induced excitations of rat hippocampal CA1 neurones in vitro. *The Journal of physiology,* 334**,** 19-31.

COLLINS, T. J. 2007. ImageJ for microscopy. *Biotechniques,* 43**,** 25-30.

COLLINSON, N., KUENZI, F. M., JAROLIMEK, W., MAUBACH, K. A., COTHLIFF, R., SUR, C., SMITH, A., OTU, F. M., HOWELL, O., ATACK, J. R., MCKERNAN, R. M., SEABROOK, G. R., DAWSON, G. R., WHITING, P. J. & ROSAHL, T. W. 2002. Enhanced learning and memory and altered GABAergic synaptic transmission in mice lacking the alpha 5 subunit of the GABAA receptor. *J Neurosci,* 22**,** 5572-80.

CONTRACTOR, A., MULLE, C. & SWANSON, G. T. 2011. Kainate receptors coming of age: milestones of two decades of research. *Trends Neurosci,* 34**,** 154-63.

COSTENLA, A. R., DIÓGENES, M. J., CANAS, P. M., RODRIGUES, R. J., NOGUEIRA, C., MAROCO, J., AGOSTINHO, P. M., RIBEIRO, J. A., CUNHA, R. A. & DE MENDONÇA, A. 2011. Enhanced role of adenosine A2A receptors in the modulation of LTP in the rat hippocampus upon ageing. *European Journal of Neuroscience,* 34**,** 12-21.

CUNHA, R. A., ALMEIDA, T. & RIBEIRO, J. 2001. Parallel modification of adenosine extracellular metabolism and modulatory action in the hippocampus of aged rats. *Journal of neurochemistry,* 76**,** 372-382.

CUNHA, R. A., MILUSHEVA, E., VIZI, E. S., RIBEIRO, J. A. & SEBASTIÃO, A. M. 1994. Excitatory and Inhibitory Effects of A1 and A2A Adenosine Receptor Activation on the Electrically Evoked [3H]Acetylcholine Release from Different Areas of the Rat Hippocampus. *Journal of Neurochemistry,* 63**,** 207-214.

DANA, H., CHEN, T.-W., HU, A., SHIELDS, B. C., GUO, C., LOOGER, L. L., KIM, D. S. & SVOBODA, K. 2014. Thy1-GCaMP6 transgenic mice for neuronal population imaging in vivo. *PLoS One,* 9**,** e108697.

DAUMAS, S., CECCOM, J., HALLEY, H., FRANCES, B. & LASSALLE, J. M. 2009. Activation of metabotropic glutamate receptor type 2/3 supports the involvement of the hippocampal mossy fiber pathway on contextual fear memory consolidation. *Learn Mem,* 16**,** 504-7.

DE LEON, M. J., GEORGE, A. E., GOLOMB, J., TARSHISH, C., CONVIT, A., KLUGER, A., DE SANTI, S., MCRAE, T., FERRIS, S. H., REISBERG, B., INCE, C., RUSINEK, H., BOBINSKI, M., QUINN, B., MILLER, D. C. & WISNIEWSKI, H. M. 1997. Frequency of hippocampal formation atrophy in normal aging and Alzheimer's disease. *Neurobiol Aging,* 18**,** 1-11.

DE MATOS, L. L., TRUFELLI, D. C., DE MATOS, M. G. L. & DA SILVA PINHAL, M. A. 2010. Immunohistochemistry as an Important Tool in Biomarkers Detection and Clinical Practice. *Biomarker Insights,* 5**,** 9-20.

DEBANNE, D., GUÉRINEAU, N. C., GÄHWILER, B. H. & THOMPSON, S. M. 1996. Paired-pulse facilitation and depression at unitary synapses in rat hippocampus: quantal fluctuation affects subsequent release. *The Journal of Physiology,* 491**,** 163-176.

DECKERT, J., MORGAN, P. F. & MARANGOS, P. J. 1988. Adenosine uptake site heterogeneity in the mammalian CNS? Uptake inhibitors as probes and potential neuropharmaceuticals. *Life Sciences,* 42**,** 1331-1345.

DEL NIDO, P. J., GLYNN, P., BUENAVENTURA, P., SALAMA, G. & KORETSKY, A. P. 1998. Fluorescence measurement of calcium transients in perfused rabbit heart using rhod 2. *Am J Physiol,* 274**,** H728-41.

DENG, W., AIMONE, J. B. & GAGE, F. H. 2010. New neurons and new memories: how does adult hippocampal neurogenesis affect learning and memory? *Nat Rev Neurosci,* 11**,** 339-50.

DENG, Y., WANG, C. C., CHOY, K. W., DU, Q., CHEN, J., WANG, Q., LI, L., CHUNG, T. K. H. & TANG, T. 2014. Therapeutic potentials of gene silencing by RNA interference: Principles, challenges, and new strategies. *Gene,* 538**,** 217-227.

DIANA, R. A., YONELINAS, A. P. & RANGANATH, C. 2007. Imaging recollection and familiarity in the medial temporal lobe: a three-component model. *Trends Cogn Sci,* 11**,** 379-86.

DIETRICH, D., KIRSCHSTEIN, T., KUKLEY, M., PEREVERZEV, A., VON DER BRELIE, C., SCHNEIDER, T. & BECK, H. 2003. Functional specialization of presynaptic Cav2.3 Ca2+ channels. *Neuron,* 39**,** 483-96.

DREOSTI, E., ODERMATT, B., DOROSTKAR, M. M. & LAGNADO, L. 2009a. A genetically encoded reporter of synaptic activity in vivo. *Nat Methods,* 6**,** 883-9.

DREOSTI, E., ODERMATT, B., DOROSTKAR, M. M. & LAGNADO, L. 2009b. A genetically encoded reporter of synaptic activity in vivo. *Nat.Methods,* 6**,** 883-889.

DUNN, K. W., KAMOCKA, M. M. & MCDONALD, J. H. 2011. A practical guide to evaluating colocalization in biological microscopy. *American Journal of Physiology-Cell Physiology,* 300**,** C723-C742.

DUNWIDDIE, T. V. 1985. The Physiological Role of Adenosine In The Central Nervous System. *International Review of Neurobiology,* 27**,** 63-139.

DUNWIDDIE, T. V. & MASINO, S. A. 2001. The role and regulation of adenosine in the central nervous system. *Annu Rev Neurosci,* 24**,** 31-55.

DURING, M. J. & SPENCER, D. D. 1992. Adenosine: A potential mediator of seizure arrest and postictal refractoriness. *Annals of Neurology,* 32**,** 618-624.

EICHENBAUM, H. 1999. Conscious awareness, memory and the hippocampus. *Nature neuroscience,* 2**,** 775-776.

EICHHOFF, G., KOVALCHUK, Y., VARGA, Z., GARASCHUK, O. & VERKHRATSKY, A. 2010. In Vivo Ca²⁺ imaging of the living brain using multi-cell bolus loading technique. *Neuromethods Neuromethods,* 43**,** 205-220.

EL MOUSTAINE, D., GRANIER, S., DOUMAZANE, E., SCHOLLER, P., RAHMEH, R., BRON, P., MOUILLAC, B., BANERES, J. L., RONDARD, P. & PIN, J. P. 2012. Distinct roles of metabotropic glutamate receptor dimerization in agonist activation and G-protein coupling. *Proc Natl Acad Sci U S A,* 109**,** 16342-7.

ENGELMAN, H. S. & MACDERMOTT, A. B. 2004. Presynaptic ionotropic receptors and control of transmitter release. *Nature Reviews Neuroscience,* 5**,** 135.

ERREGER, K., CHEN, P. E., WYLLIE, D. J. & TRAYNELIS, S. F. 2004. Glutamate receptor gating. *Crit Rev Neurobiol,* 16**,** 187-224.

ESHKIND, L. G. & LEUBE, R. E. 1995. Mice lacking synaptophysin reproduce and form typical synaptic vesicles. *Cell Tissue Res,* 282**,** 423-33.

EVANS, G. J. & COUSIN, M. A. 2005. Tyrosine phosphorylation of synaptophysin in synaptic vesicle recycling. *Biochem Soc Trans,* 33**,** 1350-3.

FABER, E. S., DELANEY, A. J. & SAH, P. 2005. SK channels regulate excitatory synaptic transmission and plasticity in the lateral amygdala. *Nat Neurosci,* 8**,** 635-41.

FALKNER, S., GRADE, S., DIMOU, L., CONZELMANN, K. K., BONHOEFFER, T., GOTZ, M. & HUBENER, M. 2016. Transplanted embryonic neurons integrate into adult neocortical circuits. *Nature,* 539**,** 248-253.

FEIN, A. & TSACOPOULOS, M. 1988. Activation of mitochondrial oxidative metabolism by calcium ions in Limulus ventral photoreceptor. *Nature,* 331**,** 437-40.

FENG, G., MELLOR, R. H., BERNSTEIN, M., KELLER-PECK, C., NGUYEN, Q. T., WALLACE, M., NERBONNE, J. M., LICHTMAN, J. W. & SANES, J. R. 2000. Imaging neuronal subsets in transgenic mice expressing multiple spectral variants of GFP. *Neuron,* 28**,** 41-51.

FERRATI, G., MARTINI, F. J. & MARAVALL, M. 2016. Presynaptic Adenosine Receptor-Mediated Regulation of Diverse Thalamocortical Short-Term Plasticity in the Mouse Whisker Pathway. *Frontiers in Neural Circuits,* 10**,** 9.

FERREIRA, T. & RASBAND, W. 2012. ImageJ user guide. *ImageJ/Fiji,* 1.

FERRER-MONTIEL, A. V. & MONTAL, M. 1996. Pentameric subunit stoichiometry of a neuronal glutamate receptor. *Proc Natl Acad Sci U S A,* 93**,** 2741-4.

FISCHER, H., NYBERG, L., KARLSSON, S., KARLSSON, P., BREHMER, Y., RIECKMANN, A., MACDONALD, S. W., FARDE, L. & BACKMAN, L. 2010. Simulating neurocognitive aging: effects of a dopaminergic antagonist on brain activity during working memory. *Biol Psychiatry,* 67**,** 575-80.

FORSYTHE, I. D., TSUJIMOTO, T., BARNES-DAVIES, M., CUTTLE, M. F. & TAKAHASHI, T. 1998. Inactivation of Presynaptic Calcium Current Contributes to Synaptic Depression at a Fast Central Synapse. *Neuron,* 20**,** 797-807.

FOSTER, T. C. 2007. Calcium homeostasis and modulation of synaptic plasticity in the aged brain. *Aging Cell,* 6**,** 319-25.

FRANKE, T., LANGHORST, M., SERRANO-VELEZ, J. L., RIVERA-RIVERA, N. L., ROSA-MOLINAR, E., SERRANO-VELEZ, J. L., RIVERA-RIVERA, N. L. & ROSA-MOLINAR, E. 2014. Simplified approach makes two-photon Multicolor imaging less costly. *Biophoton Int Biophotonics International,* 21**,** 20-23.

FRERKING, M. & WONDOLOWSKI, J. 2008. Regulation of Neurotransmitter Release by Presynaptic Receptors. *In:* WANG, Z.-W. (ed.) *Molecular Mechanisms of Neurotransmitter Release.* Totowa, NJ: Humana Press.

FRITSCH, B., REIS, J., GASIOR, M., KAMINSKI, R. M. & ROGAWSKI, M. A. 2014. Role of GluK1 kainate receptors in seizures, epileptic discharges, and epileptogenesis. *J Neurosci,* 34**,** 5765-75.

FROSTIG, R. D. 2009. *In vivo optical imaging of brain function,* Boca Raton, CRC Press.

FURUKAWA, N., TAKASUSUKI, T., FUKUSHIMA, T. & HORI, Y. 2008. Presynaptic large-conductance calcium-activated potassium channels control synaptic transmission in the superficial dorsal horn of the mouse. *Neurosci Lett,* 444**,** 79-82.

GALVAN, E. J., COSGROVE, K. E., MAUNA, J. C., CARD, J. P., THIELS, E., MERINEY, S. D. & BARRIONUEVO, G. 2010. Critical involvement of postsynaptic protein kinase activation in long-term potentiation at hippocampal mossy fiber synapses on CA3 interneurons. *J Neurosci,* 30**,** 2844-55.

GARNER, C. C., NASH, J. & HUGANIR, R. L. 2000. PDZ domains in synapse assembly and signalling. *Trends Cell Biol,* 10**,** 274-80.

GEE, K. R., BROWN, K. A., CHEN, W. N. U., BISHOP-STEWART, J., GRAY, D. & JOHNSON, I. 2000. Chemical and physiological characterization of fluo-4 Ca2+-indicator dyes. *Cell Calcium,* 27**,** 97-106.

GEORGAKOUDI, I., JACOBSON, B. C., MULLER, M. G., SHEETS, E. E., BADIZADEGAN, K., CARR-LOCKE, D. L., CRUM, C. P., BOONE, C. W., DASARI, R. R., VAN DAM, J. & FELD, M. S. 2002. NAD(P)H and collagen as in vivo quantitative fluorescent biomarkers of epithelial precancerous changes. *Cancer Res,* 62**,** 682-7.

GERBER, U., GREENE, R., HAAS, H. & STEVENS, D. 1989. Characterization of inhibition mediated by adenosine in the hippocampus of the rat in vitro. *The Journal of Physiology,* 417**,** 567-578.

GINGOLD, H. & PILPEL, Y. 2011. Determinants of translation efficiency and accuracy. *Mol Syst Biol,* 7**,** 481.

GIRAUDO, C. G., GARCIA-DIAZ, A., ENG, W. S., CHEN, Y., HENDRICKSON, W. A., MELIA, T. J. & ROTHMAN, J. E. 2009. Alternative Zippering as an On-Off Switch for SNARE-Mediated Fusion. *Science,* 323**,** 512-516.

GLITSCH, M. D. 2008. Spontaneous neurotransmitter release and Ca2+--how spontaneous is spontaneous neurotransmitter release? *Cell Calcium,* 43**,** 9-15.

GORDON, E. D., MORA, R., MEREDITH, S. C. & LINDQUIST, S. L. 1987. Hypusine formation in eukaryotic initiation factor 4D is not reversed when rates or specificity of protein synthesis is altered. *J Biol Chem,* 262**,** 16590-5.

GORDON, S. L., LEUBE, R. E. & COUSIN, M. A. 2011. Synaptophysin is required for synaptobrevin retrieval during synaptic vesicle endocytosis. *J Neurosci,* 31**,** 14032-6.

GOUAUX, E. 2004. Structure and function of AMPA receptors. *The Journal of Physiology,* 554**,** 249-253.

GOUDER, N., FRITSCHY, J. M. & BOISON, D. 2003. Seizure suppression by adenosine A1 receptor activation in a mouse model of pharmacoresistant epilepsy. *Epilepsia,* 44**,** 877-85.

GRADINARU, V., ZHANG, F., RAMAKRISHNAN, C., MATTIS, J., PRAKASH, R., DIESTER, I., GOSHEN, I., THOMPSON, K. R. & DEISSEROTH, K. 2010. Molecular and Cellular Approaches for Diversifying and Extending Optogenetics. *Cell,* 141**,** 154-165.

GRADY, C. 2012. The cognitive neuroscience of ageing. *Nat Rev Neurosci,* 13**,** 491-505.

GRÜNDIG, B. & KRABISCH, C. 1989. Ion-selective microelectrodes. Principles, design and applications. Berlin, Heidelberg, New York, Tokyo: Springer-Verlag, 1986. 346 pp., 153 fig., 42 tab., DM 158,-, ISBN 3-540-16222-4. *Engineering in Life Sciences,* 9**,** 210-210.

GUNDLFINGER, A. 2008. *The Hippocampal Mossy Fiber Synapse: Transmission, Modulation and Plasticity.* Humboldt-Universität zu Berlin.

GUNDLFINGER, A., BISCHOFBERGER, J., JOHENNING, F. W., TORVINEN, M., SCHMITZ, D. & BREUSTEDT, J. 2007. Adenosine modulates transmission at the hippocampal mossy fibre

synapse via direct inhibition of presynaptic calcium channels. *The Journal of Physiology,* 582**,** 263-277.

GUO, C., STELLA, S. L., HIRANO, A. A. & BRECHA, N. C. 2009. Plasmalemmal and Vesicular γ-Aminobutyric Acid Transporter Expression in the Developing Mouse Retina. *The Journal of comparative neurology,* 512**,** 6-26.

GUO, Y., XIAO, P., LEI, S., DENG, F., XIAO, G. G., LIU, Y., CHEN, X., LI, L., WU, S., CHEN, Y., JIANG, H., TAN, L., XIE, J., ZHU, X., LIANG, S. & DENG, H. 2008. How is mRNA expression predictive for protein expression? A correlation study on human circulating monocytes. *Acta Biochim Biophys Sin (Shanghai),* 40**,** 426-36.

HAAS, L. & GREENE, R. W. 1988. Endogenous adenosine inhibits hippocampal CA1 neurones: further evidence from extra- and intracellular recording. *Naunyn-Schmiedeberg's Archives of Pharmacology,* 337**,** 561-565.

HAMMOND, R. S., BOND, C. T., STRASSMAIER, T., NGO-ANH, T. J., ADELMAN, J. P., MAYLIE, J. & STACKMAN, R. W. 2006. Small-conductance Ca2+-activated K+ channel type 2 (SK2) modulates hippocampal learning, memory, and synaptic plasticity. *J Neurosci,* 26**,** 1844-53.

HASAN, M. T., FRIEDRICH, R. W., EULER, T., LARKUM, M. E., GIESE, G., BOTH, M., DUEBEL, J., WATERS, J., BUJARD, H., GRIESBECK, O., TSIEN, R. Y., NAGAI, T., MIYAWAKI, A. & DENK, W. 2004. Functional Fluorescent Ca(2+) Indicator Proteins in Transgenic Mice under TET Control. *PLoS Biology,* 2**,** e163.

HAUGLAND, R. P., SPENCE, M. T. Z., JOHNSON, I. D. & BASEY, A. 2005. *The Handbook : a guide to fluorescent probes and labeling technologies,* [Eugene, OR], Molecular Probes.

HEIM, N. 2005. Genetically encoded calcium indicators based on troponin C and fluorescent proteins.

HEIM, R., PRASHER, D. C. & TSIEN, R. Y. 1994. Wavelength mutations and posttranslational autoxidation of green fluorescent protein. *Proc Natl Acad Sci U S A,* 91**,** 12501-4.

HENZE, D. A., BORHEGYI, Z., CSICSVARI, J., MAMIYA, A., HARRIS, K. D. & BUZSÁKI, G. 2000a. Intracellular features predicted by extracellular recordings in the hippocampus in vivo. *Journal of neurophysiology,* 84**,** 390-400.

HENZE, D. A., URBAN, N. N. & BARRIONUEVO, G. 2000b. The multifarious hippocampal mossy fiber pathway: a review. *Neuroscience,* 98**,** 407-27.

HERZOG, E., TAKAMORI, S., JAHN, R., BROSE, N. & WOJCIK, S. M. 2006. Synaptic and vesicular co-localization of the glutamate transporters VGLUT1 and VGLUT2 in the mouse hippocampus. *J Neurochem,* 99**,** 1011-8.

HINOI, E., OGITA, K., TAKEUCHI, Y., OHASHI, H., MARUYAMA, T. & YONEDA, Y. 2001. Characterization with [3H]quisqualate of group I metabotropic glutamate receptor subtype in rat central and peripheral excitable tissues. *Neurochem Int,* 38**,** 277-85.

HOOD, E. 2004. RNAi: What's all the noise about gene silencing? *Environmental Health Perspectives,* 112**,** A224-A229.

HOPKINS, W. F. & JOHNSTON, D. 1988. Noradrenergic enhancement of long-term potentiation at mossy fiber synapses in the hippocampus. *J Neurophysiol,* 59**,** 667-87.

HU, S. H., CHRISTIE, M. P., SAEZ, N. J., LATHAM, C. F., JARROTT, R., LUA, L. H., COLLINS, B. M. & MARTIN, J. L. 2011. Possible roles for Munc18-1 domain 3a and Syntaxin1 N-peptide and C-terminal anchor in SNARE complex formation. *Proc Natl Acad Sci U S A,* 108**,** 1040-5.

HUANG, Y. Y., LI, X. C. & KANDEL, E. R. 1994a. cAMP contributes to mossy fiber LTP by initiating both a covalently mediated early phase and macromolecular synthesis-dependent late-phase. *Cell,* 79**,** 69-79.

HUANG, Y. Y., LI, X. C. & KANDEL, E. R. 1994b. cAMP contributes to mossy fiber LTP by initiating both a covalently mediated early phase and macromolecular synthesis-dependent late phase. *Cell,* 79**,** 69-79.

HUNT, C. A., SCHENKER, L. J. & KENNEDY, M. B. 1996. PSD-95 is associated with the postsynaptic density and not with the presynaptic membrane at forebrain synapses. *J Neurosci,* 16**,** 1380-8.

HUSTON, J. P., HAAS, H. L., BOIX, F., PFISTER, M., DECKING, U., SCHRADER, J. & SCHWARTING, R. K. W. 1996. Extracellular adenosine levels in neostriatum and hippocampus during rest and activity periods of rats. *Neuroscience,* 73**,** 99-107.

INOUE, Y., KAMIKUBO, Y., EZURE, H., ITO, J., KATO, Y., MORIYAMA, H. & OTSUKA, N. 2015. Presynaptic protein Synaptotagmin1 regulates the neuronal polarity and axon differentiation in cultured hippocampal neurons. *BMC Neuroscience,* 16**,** 92.

IVANOVA, S. Y., STOROZHUK, M. V. & KOSTYUK, P. G. 2002. Changes in Paired Pulse Depression as an Indicator for the Involvement of Presynaptic Mechanism(s) in Modulation of GABA-ergic Synaptic Transmission in Rat Hippocampal Cell Cultures. *Neurophysiology,* 34**,** 144-146.

IZUMI, Y. & ZORUMSKI, C. F. 2008. Direct cortical inputs erase long-term potentiation at Schaffer collateral synapses. *J Neurosci,* 28**,** 9557-63.

JAHN, R. 2004. Principles of Exocytosis and Membrane Fusion. *Annals of the New York Academy of Sciences,* 1014**,** 170-178.

JANE, D. E., LODGE, D. & COLLINGRIDGE, G. L. 2009. Kainate receptors: pharmacology, function and therapeutic potential. *Neuropharmacology,* 56**,** 90-113.

JANZ, R., SUDHOF, T. C., HAMMER, R. E., UNNI, V., SIEGELBAUM, S. A. & BOLSHAKOV, V. Y. 1999. Essential roles in synaptic plasticity for synaptogyrin I and synaptophysin I. *Neuron,* 24**,** 687-700.

JARRARD, L. E. 1993. On the role of the hippocampus in learning and memory in the rat. *Behav Neural Biol,* 60**,** 9-26.

JENSEN, K., LAMBERT, J. D. & JENSEN, M. S. 1999. Activity-dependent depression of GABAergic IPSCs in cultured hippocampal neurons. *Journal of Neurophysiology,* 82**,** 42-49.

KAESER, P. S. & REGEHR, W. G. 2014. Molecular mechanisms for synchronous, asynchronous, and spontaneous neurotransmitter release. *Annu Rev Physiol,* 76**,** 333-63.

KAMIYA, H., SHINOZAKI, H. & YAMAMOTO, C. 1996. Activation of metabotropic glutamate receptor type 2/3 suppresses transmission at rat hippocampal mossy fibre synapses. *J Physiol,* 493 (Pt 2)**,** 447-55.

KANEKO, M. & TAKAHASHI, T. 2004. Presynaptic mechanism underlying cAMP-dependent synaptic potentiation. *J Neurosci,* 24**,** 5202-8.

KANEKO, T., FUJIYAMA, F. & HIOKI, H. 2002. Immunohistochemical localization of candidates for vesicular glutamate transporters in the rat brain. *J Comp Neurol,* 444**,** 39-62.

KAPUR, A., YECKEL, M. F., GRAY, R. & JOHNSTON, D. 1998. L-Type calcium channels are required for one form of hippocampal mossy fiber LTP. *J Neurophysiol,* 79**,** 2181-90.

KASE, H., RICHARDSON, P. J. & JENNER, P. 1999. *Adenosine receptors and Parkinson's disease*, Academic Press.

KEMSHEAD, J. T., RITTER, M. A., COTMORE, S. F. & GREAVES, M. F. 1982. Human Thy-1: Expression on the cell surface of neuronal and and glial cells. *Brain Research,* 236**,** 451-461.

KENNEDY, M. J. & EHLERS, M. D. 2011. Mechanisms and function of dendritic exocytosis. *Neuron,* 69**,** 856-75.

KESNER, R. P. & ROLLS, E. T. 2015. A computational theory of hippocampal function, and tests of the theory: New developments. *Neuroscience & Biobehavioral Reviews,* 48**,** 92-147.

KIDD, F. L., COUMIS, U., COLLINGRIDGE, G. L., CRABTREE, J. W. & ISAAC, J. T. 2002. A presynaptic kainate receptor is involved in regulating the dynamic properties of thalamocortical synapses during development. *Neuron,* 34**,** 635-46.

KIM, E. & SHENG, M. 2004. PDZ domain proteins of synapses. *Nat Rev Neurosci,* 5**,** 771-81.

KLENCHIN, V. A. & MARTIN, T. F. 2000. Priming in exocytosis: attaining fusion-competence after vesicle docking. *Biochimie,* 82**,** 399-407.

KLYACHKO, V. A. & STEVENS, C. F. 2006. Temperature-Dependent Shift of Balance among the Components of Short-Term Plasticity in Hippocampal Synapses. *The Journal of Neuroscience,* 26**,** 6945-6957.

KLYUCH, B. P., DALE, N. & WALL, M. J. 2012. Deletion of ecto-5'-nucleotidase (CD73) reveals direct action potential-dependent adenosine release. *J Neurosci,* 32**,** 3842-7.

KUCHIBHOTLA, K. V., GOLDMAN, S. T., LATTARULO, C. R., WU, H. Y., HYMAN, B. T. & BACSKAI, B. J. 2008. Abeta plaques lead to aberrant regulation of calcium homeostasis in vivo resulting in structural and functional disruption of neuronal networks. *Neuron,* 59**,** 214-25.

KULLMANN, D. M., RUIZ, A., RUSAKOV, D. M., SCOTT, R., SEMYANOV, A. & WALKER, M. C. 2005. Presynaptic, extrasynaptic and axonal GABA(A) receptors in the CNS: where and why? *Progress in biophysics and molecular biology,* 87**,** 33-46.

KUNZ, W. S. & GELLERICH, F. N. 1993. Quantification of the content of fluorescent flavoproteins in mitochondria from liver, kidney cortex, skeletal muscle, and brain. *Biochem Med Metab Biol,* 50**,** 103-10.

KWAN, A. C., DUFF, K., GOURAS, G. K. & WEBB, W. W. 2009. Optical visualization of Alzheimer's pathology via multiphoton-excited intrinsic fluorescence and second harmonic generation. *Opt Express,* 17**,** 3679-89.

KWON, S. E. & CHAPMAN, E. R. 2011. Synaptophysin regulates the kinetics of synaptic vesicle endocytosis in central neurons. *Neuron,* 70**,** 847-54.

LANTHORN, T. H., GANONG, A. H. & COTMAN, C. W. 1984. 2-Amino-4-phosphonobutyrate selectively blocks mossy fiber-CA3 responses in guinea pig but not rat hippocampus. *Brain Res,* 290**,** 174-8.

LATT, S. A. & STETTEN, G. 1976. Spectral studies on 33258 Hoechst and related bisbenzimidazole dyes useful for fluorescent detection of deoxyribonucleic acid synthesis. *Journal of Histochemistry & Cytochemistry,* 24**,** 24-33.

LAURI, S. E., VESIKANSA, A., SEGERSTRALE, M., COLLINGRIDGE, G. L., ISAAC, J. T. & TAIRA, T. 2006. Functional maturation of CA1 synapses involves activity-dependent loss of tonic kainate receptor-mediated inhibition of glutamate release. *Neuron,* 50**,** 415-29.

LEE, I., RAO, G. & KNIERIM, J. J. 2004. A double dissociation between hippocampal subfields: differential time course of CA3 and CA1 place cells for processing changed environments. *Neuron,* 42**,** 803-15.

LI, L. & CHIN, L. S. 2003. The molecular machinery of synaptic vesicle exocytosis. *Cell Mol Life Sci,* 60**,** 942-60.

LISMAN, J. E. & OTMAKHOVA, N. A. 2001. Storage, recall, and novelty detection of sequences by the hippocampus: elaborating on the SOCRATIC model to account for normal and aberrant effects of dopamine. *Hippocampus,* 11**,** 551-68.

LLANO, I., GONZÁLEZ, J., CAPUTO, C., LAI, F. A., BLAYNEY, L. M., TAN, Y. P. & MARTY, A. 2000. Presynaptic calcium stores underlie large-amplitude miniature IPSCs and spontaneous calcium transients. *Nature Neuroscience,* 3**,** 1256.

LODISH, H. F. 2004. Molecular cell biology. Princeton, N.J.: Recording for the Blind & Dyslexic.

LOHSE, M., KLOTZ, K.-N., LINDENBORN-FOTINOS, J., REDDINGTON, M., SCHWABE, U. & OLSSON, R. 1987a. 8-Cyclopentyl-1,3-dipropylxanthine (DPCPX) — a selective high affinity antagonist radioligand for A1 adenosine receptors. *Naunyn-Schmiedeberg's Archives of Pharmacology,* 336**,** 204-210.

LOHSE, M. J., KLOTZ, K. N., LINDENBORN-FOTINOS, J., REDDINGTON, M., SCHWABE, U. & OLSSON, R. A. 1987b. 8-Cyclopentyl-1,3-dipropylxanthine (DPCPX)--a selective high affinity antagonist radioligand for A1 adenosine receptors. *Naunyn Schmiedebergs Arch Pharmacol,* 336**,** 204-10.

LONART, G. & SUDHOF, T. C. 1998. Region-specific phosphorylation of rabphilin in mossy fiber nerve terminals of the hippocampus. *J Neurosci,* 18**,** 634-40.

LOPES, L. V., CUNHA, R. A., KULL, B., FREDHOLM, B. B. & RIBEIRO, J. A. 2002. Adenosine A2A receptor facilitation of hippocampal synaptic transmission is dependent on tonic A1 receptor inhibition. *Neuroscience,* 112**,** 319-329.

LOVATT, D., XU, Q., LIU, W., TAKANO, T., SMITH, N. A., SCHNERMANN, J., TIEU, K. & NEDERGAARD, M. 2012. Neuronal adenosine release, and not astrocytic ATP release, mediates feedback inhibition of excitatory activity. *Proceedings of the National Academy of Sciences,* 109**,** 6265-6270.

LU, K. T. & GEAN, P. W. 1999. Masking of forskolin-induced long-term potentiation by adenosine accumulation in area CA1 of the rat hippocampus. *Neuroscience,* 88**,** 69-78.

LU, K. T., WU, S. P. & GEAN, P. W. 1999. Promotion of forskolin-induced long-term potentiation of synaptic transmission by caffeine in area CA1 of the rat hippocampus. *Chin J Physiol,* 42**,** 249-53.

LUCHKINA, N. V., HUUPPONEN, J., CLARKE, V. R., COLEMAN, S. K., KEINANEN, K., TAIRA, T. & LAURI, S. E. 2014. Developmental switch in the kinase dependency of long-term potentiation depends on expression of GluA4 subunit-containing AMPA receptors. *Proc Natl Acad Sci U S A,* 111**,** 4321-6.

LUTTRELL, L. M. & LEFKOWITZ, R. J. 2002. The role of β-arrestins in the termination and transduction of G-protein-coupled receptor signals. *Journal of Cell Science,* 115**,** 455-465.

MADISEN, L., GARNER, A. R., SHIMAOKA, D., CHUONG, A. S., KLAPOETKE, N. C., LI, L., VAN DER BOURG, A., NIINO, Y., EGOLF, L., MONETTI, C., GU, H., MILLS, M., CHENG, A., TASIC, B., NGUYEN, T. N., SUNKIN, S. M., BENUCCI, A., NAGY, A., MIYAWAKI, A., HELMCHEN, F., EMPSON, R. M., KNOPFEL, T., BOYDEN, E. S., REID, R. C., CARANDINI, M. & ZENG, H. 2015. Transgenic mice for intersectional targeting of neural sensors and effectors with high specificity and performance. *Neuron,* 85**,** 942-58.

MANABE, T., WYLLIE, D. J., PERKEL, D. J. & NICOLL, R. A. 1993. Modulation of synaptic transmission and long-term potentiation: effects on paired pulse facilitation and EPSC variance in the CA1 region of the hippocampus. *J Neurophysiol,* 70**,** 1451-9.

MARAMBAUD, P., DRESES-WERRINGLOER, U. & VINGTDEUX, V. 2009. Calcium signaling in neurodegeneration. *Mol Neurodegener,* 4**,** 20.

MARRO, P. J., BAUMGART, S., DELIVORIA-PAPADOPOULOS, M., ZIRIN, S., CORCORAN, L., MCGAURN, S. P., DAVIS, L. E. & CLANCY, R. R. 1997. Purine Metabolism and Inhibition of Xanthine Oxidase in Severely Hypoxic Neonates Going onto Extracorporeal Membrane Oxygenation1. *Pediatric research,* 41**,** 513-520.

MARTENS, S. & MCMAHON, H. T. 2008. Mechanisms of membrane fusion: disparate players and common principles. *Nat Rev Mol Cell Biol,* 9**,** 543-556.

MARTINSON, E. A., JOHNSON, R. A. & WELLS, J. N. 1987. Potent adenosine receptor antagonists that are selective for the A1 receptor subtype. *Molecular Pharmacology,* 31**,** 247-252.

MASINO, S. A., DIAO, L., ILLES, P., ZAHNISER, N. R., LARSON, G. A., JOHANSSON, B., FREDHOLM, B. B. & DUNWIDDIE, T. V. 2002. Modulation of hippocampal glutamatergic transmission by ATP is dependent on adenosine A1 receptors. *Journal of Pharmacology and Experimental Therapeutics,* 303**,** 356-363.

MATIAS, C. M., DIONISIO, J. C., SAGGAU, P. & QUINTA-FERREIRA, M. E. 2014. Activation of group II metabotropic glutamate receptors blocks zinc release from hippocampal mossy fibers. *Biol Res,* 47**,** 73.

MATTSON, M. P. 2007. Calcium and neurodegeneration. *Aging Cell,* 6**,** 337-50.

MCENTEE, W. J. & CROOK, T. H. 1993. Glutamate: its role in learning, memory, and the aging brain. *Psychopharmacology,* 111**,** 391-401.

MCINTIRE, S. L., REIMER, R. J., SCHUSKE, K., EDWARDS, R. H. & JORGENSEN, E. M. 1997. Identification and characterization of the vesicular GABA transporter. *Nature,* 389**,** 870-876.

MCMAHON, H. T., BOLSHAKOV, V. Y., JANZ, R., HAMMER, R. E., SIEGELBAUM, S. A. & SÜDHOF, T. C. 1996. Synaptophysin, a major synaptic vesicle protein, is not essential for neurotransmitter release. *Proceedings of the National Academy of Sciences of the United States of America,* 93**,** 4760-4764.

MEEKS, J. P. & MENNERICK, S. 2004. Selective effects of potassium elevations on glutamate signaling and action potential conduction in hippocampus. *Journal of Neuroscience,* 24**,** 197-206.

MEGíAS, M., EMRI, Z., FREUND, T. F. & GULYÁS, A. I. 2001. Total number and distribution of inhibitory and excitatory synapses on hippocampal CA1 pyramidal cells. *Neuroscience,* 102**,** 527-540.

MELDRUM, B. S. 2000. Glutamate as a neurotransmitter in the brain: review of physiology and pathology. *The Journal of nutrition,* 130**,** 1007S-1015S.

MENTER, J. M. 2006. Temperature dependence of collagen fluorescence. *Photochemical & Photobiological Sciences,* 5**,** 403-410.

MEYERSON, J. R., KUMAR, J., CHITTORI, S., RAO, P., PIERSON, J., BARTESAGHI, A., MAYER, M. L. & SUBRAMANIAM, S. 2014. Structural mechanism of glutamate receptor activation and desensitization. *Nature,* 514**,** 328-34.

MI, Z. & JACKSON, E. K. 1998. Evidence for an endogenous cAMP-adenosine pathway in the rat kidney. *J Pharmacol Exp Ther,* 287**,** 926-30.

MILLER, R. J. 1998. Presynaptic receptors. *Annu Rev Pharmacol Toxicol,* 38**,** 201-27.

MIYAWAKI, A., LLOPIS, J., HEIM, R., MCCAFFERY, J. M., ADAMS, J. A., IKURA, M. & TSIEN, R. Y. 1997. Fluorescent indicators for Ca2+ based on green fluorescent proteins and calmodulin. *Nature,* 388**,** 882-7.

MOCELLIN, S. & PROVENZANO, M. 2004. RNA interference: learning gene knock-down from cell physiology. *J Transl Med,* 2**,** 39.

MOECHARS, D., DEWACHTER, I., LORENT, K., REVERSE, D., BAEKELANDT, V., NAIDU, A., TESSEUR, I., SPITTAELS, K., HAUTE, C. V., CHECLER, F., GODAUX, E., CORDELL, B. & VAN LEUVEN, F. 1999. Early phenotypic changes in transgenic mice that overexpress different mutants of amyloid precursor protein in brain. *J Biol Chem,* 274**,** 6483-92.

MONICI, M. 2005. Cell and tissue autofluorescence research and diagnostic applications. *Biotechnology Annual Review.* Elsevier.

MORISHITA, W., KIROV, S. A. & ALGER, B. E. 1998. Evidence for metabotropic glutamate receptor activation in the induction of depolarization-induced suppression of inhibition in hippocampal CA1. *J Neurosci,* 18**,** 4870-82.

MORRIS, R. G., ANDERSON, E., LYNCH, G. S. & BAUDRY, M. 1986. Selective impairment of learning and blockade of long-term potentiation by an N-methyl-D-aspartate receptor antagonist, AP5. *Nature,* 319**,** 774-6.

MORRISON, J. H. & BAXTER, M. G. 2012. The ageing cortical synapse: hallmarks and implications for cognitive decline. *Nat Rev Neurosci,* 13**,** 240-50.

MOSER, E. I., KROPFF, E. & MOSER, M.-B. 2008. Place Cells, Grid Cells, and the Brain's Spatial Representation System. *Annual Review of Neuroscience,* 31**,** 69-89.

MOTA, S. I., FERREIRA, I. L. & REGO, A. C. 2014. Dysfunctional synapse in Alzheimer's disease - A focus on NMDA receptors. *Neuropharmacology,* 76 Pt A**,** 16-26.

MULLIS, K. B., ERLICH, H. A., ARNHEIM, N., HORN, G. T., SAIKI, R. K. & SCHARF, S. J. 1987. Process for amplifying, detecting, and/or-cloning nucleic acid sequences. Google Patents.

NAKAI, J., OHKURA, M. & IMOTO, K. 2001. A high signal-to-noise Ca2+ probe composed of a single green fluorescent protein. *Nat Biotech,* 19**,** 137-141.

NI, B., WU, X., YAN, G. M., WANG, J. & PAUL, S. M. 1995. Regional expression and cellular localization of the Na(+)-dependent inorganic phosphate cotransporter of rat brain. *J Neurosci,* 15**,** 5789-99.

NICHOLSON, D. A., YOSHIDA, R., BERRY, R. W., GALLAGHER, M. & GEINISMAN, Y. 2004. Reduction in size of perforated postsynaptic densities in hippocampal axospinous synapses and age-related spatial learning impairments. *J Neurosci,* 24**,** 7648-53.

NICOLL, R. A. & SCHMITZ, D. 2005. Synaptic plasticity at hippocampal mossy fibre synapses. *Nat Rev Neurosci,* 6**,** 863-76.

O'KEEFE, J. & DOSTROVSKY, J. 1971. The hippocampus as a spatial map. Preliminary evidence from unit activity in the freely-moving rat. *Brain Res,* 34**,** 171-5.

OKOROCHA, A. E. 2016. *Fluorescent protein calcium sensor for monitoring synaptic transmission.* Department of Cell Physiology & Pharmacology.

OTMAKHOV, N., KHIBNIK, L., OTMAKHOVA, N., CARPENTER, S., RIAHI, S., ASRICAN, B. & LISMAN, J. 2004. *Forskolin-Induced LTP in the CA1 Hippocampal Region Is NMDA Receptor Dependent*.

PAK, M. & YETKIN, Y. 2014. The Sources of Extracellular Adenosine in Hippocampus and Neostriatum of the Rat Brain. *World Journal of Neuroscience,* 4**,** 85.

PAK, M. A., HAAS, H. L., DECKING, U. K. M. & SCHRADER, J. 1994. Inhibition of adenosine kinase increases endogenous adenosine and depresses neuronal activity in hippocampal slices. *Neuropharmacology,* 33**,** 1049-1053.

PALMADA, M. & CENTELLES, J. J. 1998. Excitatory amino acid neurotransmission. Pathways for metabolism, storage and reuptake of glutamate in brain. *Front Biosci,* 3**,** d701-18.

PANKRATOV, Y., LALO, U., VERKHRATSKY, A. & NORTH, R. A. 2006. Vesicular release of ATP at central synapses. *Pflugers Arch,* 452**,** 589-97.

PAREDES, R. M., ETZLER, J. C., WATTS, L. T. & LECHLEITER, J. D. 2008. Chemical Calcium Indicators. *Methods (San Diego, Calif.),* 46**,** 143-151.

PARK, J. & GUPTA, R. S. 2013. Adenosine metabolism, adenosine kinase, and evolution. *Adenosine.* Springer.

PAYNE, S. H. 2015. The utility of protein and mRNA correlation. *Trends in biochemical sciences,* 40**,** 1-3.

PELKEY, K. A., TOPOLNIK, L., YUAN, X. Q., LACAILLE, J. C. & MCBAIN, C. J. 2008. State-dependent cAMP sensitivity of presynaptic function underlies metaplasticity in a hippocampal feedforward inhibitory circuit. *Neuron,* 60**,** 980-7.

PETERS, J. M., FRANKE, W. W. & KLEINSCHMIDT, J. A. 1994. Distinct 19 S and 20 S subcomplexes of the 26 S proteasome and their distribution in the nucleus and the cytoplasm. *J Biol Chem,* 269**,** 7709-18.

PICCOLINO, M., PIGNATELLI, A. & RAKOTOBE, L. A. 1999. Calcium-independent release of neurotransmitter in the retina: a “Copernican” viewpoint change. *Progress in Retinal and Eye Research,* 18**,** 1-38.

PINHEIRO, P. S. & MULLE, C. 2008. Presynaptic glutamate receptors: physiological functions and mechanisms of action. *Nat Rev Neurosci Nature Reviews Neuroscience,* 9**,** 423-436.

PRENDERGAST, F. G. & MANN, K. G. 1978. Chemical and physical properties of aequorin and the green fluorescent protein isolated from Aequorea forskalea. *Biochemistry,* 17**,** 3448-3453.

PURVES, D. 2008. *Neuroscience,* Sunderland, Mass., Sinauer.

RAJAPPA, R., GAUTHIER-KEMPER, A., BONING, D., HUVE, J. & KLINGAUF, J. 2016. Synaptophysin 1 Clears Synaptobrevin 2 from the Presynaptic Active Zone to Prevent Short-Term Depression. *Cell Rep,* 14**,** 1369-1381.

RAMIREZ, D. M. & KAVALALI, E. T. 2011. Differential regulation of spontaneous and evoked neurotransmitter release at central synapses. *Curr Opin Neurobiol,* 21**,** 275-82.

RAMÓN Y CAJAL, S. 1972. *Histologie du systeme nerveux : de l'homme & des vertebres,* Madrid, Raycar.

RAPP, P. R. & GALLAGHER, M. 1996. Preserved neuron number in the hippocampus of aged rats with spatial learning deficits. *Proc Natl Acad Sci U S A,* 93**,** 9926-30.

REBOLA, N., LUJAN, R., CUNHA, R. A. & MULLE, C. 2008. Adenosine A2A receptors are essential for long-term potentiation of NMDA-EPSCs at hippocampal mossy fiber synapses. *Neuron,* 57**,** 121-34.

REBOLA, N., PINHEIRO, P. C., OLIVEIRA, C. R., MALVA, J. O. & CUNHA, R. A. 2003a. Subcellular localization of adenosine A(1) receptors in nerve terminals and synapses of the rat hippocampus. *Brain Res,* 987**,** 49-58.

REBOLA, N., RODRIGUES, R. J., LOPES, L. V., RICHARDSON, P. J., OLIVEIRA, C. R. & CUNHA, R. A. 2005. Adenosine A1 and A2A receptors are co-expressed in pyramidal neurons and co-localized in glutamatergic nerve terminals of the rat hippocampus. *Neuroscience,* 133**,** 79-83.

REBOLA, N., SEBASTIÃO, A. M., DE MENDONÇA, A., OLIVEIRA, C. R., RIBEIRO, J. & CUNHA, R. A. 2003b. Enhanced adenosine A 2A receptor facilitation of synaptic transmission in the hippocampus of aged rats. *Journal of neurophysiology,* 90**,** 1295-1303.

REDBERRY, G. W. 2006. *Gene silencing : new research,* New York, Nova Science Publishers.

REGEHR, W. G. 2012. Short-term presynaptic plasticity. *Cold Spring Harb Perspect Biol,* 4**,** a005702.

REHM, H., WIEDENMANN, B. & BETZ, H. 1986. Molecular characterization of synaptophysin, a major calcium-binding protein of the synaptic vesicle membrane. *The EMBO Journal,* 5**,** 535-541.

REIF, A. E. & ALLEN, J. M. V. 1964. THE AKR THYMIC ANTIGEN AND ITS DISTRIBUTION IN LEUKEMIAS AND NERVOUS TISSUES. *The Journal of Experimental Medicine,* 120**,** 413-433.

REIFF, D. F., IHRING, A., GUERRERO, G., ISACOFF, E. Y., JOESCH, M., NAKAI, J. & BORST, A. 2005. In vivo performance of genetically encoded indicators of neural activity in flies. *Journal of Neuroscience,* 25**,** 4766-4778.

REUTER, H. 1996. Diversity and function of presynaptic calcium channels in the brain. *Curr Opin Neurobiol,* 6**,** 331-7.

RICHARDSON, P. J., BROWN, S. J., BAILYES, E. M. & LUZIO, J. P. 1987. Ectoenzymes control adenosine modulation of immunoisolated cholinergic synapses. *Nature,* 327**,** 232-234.

RICHTER, K., LANGNAESE, K., KREUTZ, M. R., OLIAS, G., ZHAI, R., SCHEICH, H., GARNER, C. C. & GUNDELFINGER, E. D. 1999. Presynaptic cytomatrix protein bassoon is localized at both excitatory and inhibitory synapses of rat brain. *J Comp Neurol,* 408**,** 437-48.

RIEBE, I. 2010. Differences in glutamatergic transmission onto interneurons and pyramidal cells in the rat hippocampus.

RIPLEY, B., OTTO, S., TIGLIO, K., WILLIAMS, M. E. & GHOSH, A. 2011. Regulation of synaptic stability by AMPA receptor reverse signaling. *Proc Natl Acad Sci U S A,* 108**,** 367-72.

RODRIGUEZ-MORENO, A. & SIHRA, T. S. 2004. Presynaptic kainate receptor facilitation of glutamate release involves protein kinase A in the rat hippocampus. *J Physiol,* 557**,** 733-45.

ROLLS, E. T. 1987. Information representation, processing and storage in the brain: analysis at the single neuron level. *The neural and molecular bases of learning***,** 503-540.

ROLLS, E. T. 1996. A theory of hippocampal function in memory. *Hippocampus,* 6**,** 601-20.

ROMBO, D. M., RIBEIRO, J. A. & SEBASTIÃO, A. M. 2016. Hippocampal GABAergic transmission: a new target for adenosine control of excitability. *Journal of Neurochemistry,* 139**,** 1056-1070.

RUIZ, A., CAMPANAC, E., SCOTT, R. S., RUSAKOV, D. A. & KULLMANN, D. M. 2010. Presynaptic GABAA receptors enhance transmission and LTP induction at hippocampal mossy fiber synapses. *Nature neuroscience,* 13**,** 431-438.

RUSINEK, H., DE SANTI, S., FRID, D., TSUI, W. H., TARSHISH, C. Y., CONVIT, A. & DE LEON, M. J. 2003. Regional brain atrophy rate predicts future cognitive decline: 6-year longitudinal MR imaging study of normal aging. *Radiology,* 229**,** 691-6.

RUSSELL, J. T. 2011. Imaging calcium signals in vivo: a powerful tool in physiology and pharmacology. *British Journal of Pharmacology,* 163**,** 1605-1625.

RUTTEN, K., VAN DONKELAAR, E. L., FERRINGTON, L., BLOKLAND, A., BOLLEN, E., STEINBUSCH, H. W., KELLY, P. A. & PRICKAERTS, J. H. 2009. Phosphodiesterase inhibitors enhance object memory independent of cerebral blood flow and glucose utilization in rats. *Neuropsychopharmacology,* 34**,** 1914-25.

SAILER, C. A., KAUFMANN, W. A., KOGLER, M., CHEN, L., SAUSBIER, U., OTTERSEN, O. P., RUTH, P., SHIPSTON, M. J. & KNAUS, H.-G. 2006. Immunolocalization of BK channels in hippocampal pyramidal neurons. *European Journal of Neuroscience,* 24**,** 442-454.

SCHLICKER, E. & FEUERSTEIN, T. 2017. Human presynaptic receptors. *Pharmacology & Therapeutics,* 172**,** 1-21.

SCHMITT, U., TANIMOTO, N., SEELIGER, M., SCHAEFFEL, F. & LEUBE, R. 2009. Detection of behavioral alterations and learning deficits in mice lacking synaptophysin. *Neuroscience,* 162**,** 234-243.

SCHUBERT, P. 1988. Physiological modulation by adenosine: selective blockade of A1-receptors with DPCPX enhances stimulus train-evoked neuronal Ca influx in rat hippocampal slices. *Brain Research,* 458**,** 162-165.

SCHULZ, P. E., COOK, E. P. & JOHNSTON, D. 1994. Changes in paired-pulse facilitation suggest presynaptic involvement in long-term potentiation. *J Neurosci,* 14**,** 5325-37.

SCOTTI, M. M. & SWANSON, M. S. 2016. RNA mis-splicing in disease. *Nat Rev Genet,* 17**,** 19-32.

SCOVILLE, W. B. & MILNER, B. 1957. Loss of recent memory after bilateral hippocampal lesions. *J Neurol Neurosurg Psychiatry,* 20**,** 11-21.

SELKOE, D. J. 2003. Folding proteins in fatal ways. *Nature,* 426**,** 900-904.

SEMYANOV, A., WALKER, M. C., KULLMANN, D. M. & SILVER, R. A. 2004. Tonically active GABA A receptors: modulating gain and maintaining the tone. *Trends Neurosci,* 27**,** 262-9.

SHARIFZADEH, M., SHARIFZADEH, K., NAGHDI, N., GHAHREMANI, M. H. & ROGHANI, A. 2005. Posttraining intrahippocampal infusion of a protein kinase AII inhibitor impairs spatial memory retention in rats. *J Neurosci Res,* 79**,** 392-400.

SHETH, S., BRITO, R., MUKHERJEA, D., RYBAK, L. P. & RAMKUMAR, V. 2014. Adenosine Receptors: Expression, Function and Regulation. *International Journal of Molecular Sciences,* 15**,** 2024-2052.

SHI, L., ADAMS, M. & BRUNSO-BECHTOLD, J. K. 2007. Frontiers in Neuroscience

Subtle Alterations in Glutamatergic Synapses Underlie the Aging-Related Decline in Hippocampal Function. *In:* RIDDLE, D. R. (ed.) *Brain Aging: Models, Methods, and Mechanisms.* Boca Raton (FL): CRC Press/Taylor & Francis

Taylor & Francis Group, LLC.

SHIGEMOTO, R., KINOSHITA, A., WADA, E., NOMURA, S., OHISHI, H., TAKADA, M., FLOR, P. J., NEKI, A., ABE, T., NAKANISHI, S. & MIZUNO, N. 1997. Differential presynaptic localization of metabotropic glutamate receptor subtypes in the rat hippocampus. *J Neurosci,* 17**,** 7503-22.

SIEGEL, F. & LOHMANN, C. 2013. Probing synaptic function in dendrites with calcium imaging. *Exp Neurol,* 242**,** 27-32.

SIEGEL, G. J. 2005. Basic neurochemistry : molecular, cellular and medical aspects ; [software CD included]. Amsterdam [u.a.: Elsevier, Acad. Press.

SMALL, S. A., SCHOBEL, S. A., BUXTON, R. B., WITTER, M. P. & BARNES, C. A. 2011. A pathophysiological framework of hippocampal dysfunction in ageing and disease. *Nat Rev Neurosci,* 12**,** 585-601.

SMITH, T. D., ADAMS, M. M., GALLAGHER, M., MORRISON, J. H. & RAPP, P. R. 2000. Circuit-specific alterations in hippocampal synaptophysin immunoreactivity predict spatial learning impairment in aged rats. *J Neurosci,* 20**,** 6587-93.

SOKOLOVA, I. V., LESTER, H. A. & DAVIDSON, N. 2006. Postsynaptic mechanisms are essential for forskolin-induced potentiation of synaptic transmission. *J Neurophysiol,* 95**,** 2570-9.

SPERLÁGH, B. & SYLVESTER VIZI, E. 2011. The role of extracellular adenosine in chemical neurotransmission in the hippocampus and Basal Ganglia: pharmacological and clinical aspects. *Current topics in medicinal chemistry,* 11**,** 1034-1046.

SPIWOKS-BECKER, I., VOLLRATH, L., SEELIGER, M. W., JAISSLE, G., ESHKIND, L. G. & LEUBE, R. E. 2001. Synaptic vesicle alterations in rod photoreceptors of synaptophysin-deficient mice. *Neuroscience,* 107**,** 127-42.

SPRUSTON, N. 2008. Pyramidal neurons: dendritic structure and synaptic integration. *Nat Rev Neurosci,* 9**,** 206-221.

SQUIRE, L. R. 2013. *Fundamental neuroscience,* Amsterdam; London, Academic Press.

SQUIRE, L. R., STARK, C. E. & CLARK, R. E. 2004. The medial temporal lobe. *Annu Rev Neurosci,* 27**,** 279-306.

STANTON, P. K., BRAMHAM, C. & SCHARFMAN, H. E. 2006. *Synaptic plasticity and transsynaptic signaling*, Springer Science & Business Media.

STOSIEK, C., GARASCHUK, O., HOLTHOFF, K. & KONNERTH, A. 2003. In vivo two-photon calcium imaging of neuronal networks. *Proc Natl Acad Sci U S A,* 100**,** 7319-24.

SUDHOF, T. C. 1995. The synaptic vesicle cycle: a cascade of protein□protein interactions. *Nature,* 375**,** 645-653.

SUDHOF, T. C. 2013. A molecular machine for neurotransmitter release: synaptotagmin and beyond. *Nat Med,* 19**,** 1227-31.

SÜDHOF, T. C., LOTTSPEICH, F., GREENGARD, P., MEHL, E. & JAHN, R. 1987. The cDNA and derived amino acid sequences for rat and human synaptophysin. *Nucleic Acids Research,* 15**,** 9607.

SUDHOF, T. C. & RIZO, J. 2011. Synaptic vesicle exocytosis. *Cold Spring Harb Perspect Biol,* 3.

SUN, H. Y., BARTLEY, A. F. & DOBRUNZ, L. E. 2009. Calcium-Permeable Presynaptic Kainate Receptors Involved in Excitatory Short-Term Facilitation Onto Somatostatin Interneurons During Natural Stimulus Patterns. *Journal of Neurophysiology,* 101**,** 1043-1055.

SUTTON, R. B., FASSHAUER, D., JAHN, R. & BRUNGER, A. T. 1998. Crystal structure of a SNARE complex involved in synaptic exocytosis at 2.4[thinsp]A resolution. *Nature,* 395**,** 347-353.

SZE, C., BI, H., KLEINSCHMIDT-DEMASTERS, B. K., FILLEY, C. M. & MARTIN, L. J. 2001. N-Methyl-D-aspartate receptor subunit proteins and their phosphorylation status are altered selectively in Alzheimer's disease. *J Neurol Sci,* 182**,** 151-9.

TADA, M., TAKEUCHI, A., HASHIZUME, M., KITAMURA, K. & KANO, M. 2014. A highly sensitive fluorescent indicator dye for calcium imaging of neural activity in vitro and in vivo. *The European Journal of Neuroscience,* 39**,** 1720-1728.

TAKAHASHI, A., CAMACHO, P., LECHLEITER, J. D. & HERMAN, B. 1999. Measurement of intracellular calcium. *Physiol Rev,* 79**,** 1089-125.

TALLINI, Y. N., OHKURA, M., CHOI, B. R., JI, G., IMOTO, K., DORAN, R., LEE, J., PLAN, P., WILSON, J., XIN, H. B., SANBE, A., GULICK, J., MATHAI, J., ROBBINS, J., SALAMA, G., NAKAI, J. & KOTLIKOFF, M. I. 2006. Imaging cellular signals in the heart in vivo: Cardiac expression of the high-signal Ca2+ indicator GCaMP2. *Proc Natl Acad Sci U S A,* 103**,** 4753-8.

TANAKA, M., MIYOSHI, J., ISHIZAKI, H., TOGAWA, A., OHNISHI, K., ENDO, K., MATSUBARA, K., MIZOGUCHI, A., NAGANO, T., SATO, M., SASAKI, T. & TAKAI, Y. 2001. Role of Rab3 GDP/GTP Exchange Protein in Synaptic Vesicle Trafficking at the Mouse Neuromuscular Junction. *Molecular Biology of the Cell,* 12**,** 1421-1430.

TANK, D., REGEHR, W. & DELANEY, K. 1995. A quantitative analysis of presynaptic calcium dynamics that contribute to short-term enhancement. *The Journal of Neuroscience,* 15**,** 7940-7952.

TARSA, L. & GODA, Y. 2002. Synaptophysin regulates activity-dependent synapse formation in cultured hippocampal neurons. *Proceedings of the National Academy of Sciences,* 99**,** 1012-1016.

TERUNUMA, M., REVILLA-SANCHEZ, R., QUADROS, I. M., DENG, Q., DEEB, T. Z., LUMB, M., SICINSKI, P., HAYDON, P. G., PANGALOS, M. N. & MOSS, S. J. 2014. Postsynaptic GABAB receptor activity regulates excitatory neuronal architecture and spatial memory. *J Neurosci,* 34**,** 804-16.

THAKAR, S., WANG, L., YU, T., YE, M., ONISHI, K., SCOTT, J., QI, J., FERNANDES, C., HAN, X., YATES, J. R., 3RD, BERG, D. K. & ZOU, Y. 2017. Evidence for opposing roles of Celsr3 and Vangl2 in glutamatergic synapse formation. *Proc Natl Acad Sci U S A,* 114**,** E610-E618.

THANAWALA, M. S. & REGEHR, W. G. 2013. Presynaptic calcium influx controls neurotransmitter release in part by regulating the effective size of the readily releasable pool. *J Neurosci,* 33**,** 4625-33.

THESTRUP, T., LITZLBAUER, J., BARTHOLOMAUS, I., MUES, M., RUSSO, L., DANA, H., KOVALCHUK, Y., LIANG, Y., KALAMAKIS, G., LAUKAT, Y., BECKER, S., WITTE, G., GEIGER, A., ALLEN, T., ROME, L. C., CHEN, T.-W., KIM, D. S., GARASCHUK, O., GRIESINGER, C. & GRIESBECK, O. 2014. Optimized ratiometric calcium sensors for functional in vivo imaging of neurons and T lymphocytes. *Nat Meth,* 11**,** 175-182.

THIBAULT, O. & LANDFIELD, P. W. 1996. Increase in single L-type calcium channels in hippocampal neurons during aging. *Science,* 272**,** 1017-20.

THOMAS, L., HARTUNG, K., LANGOSCH, D., REHM, H., BAMBERG, E., FRANKE, W. W. & BETZ, H. 1988. Identification of synaptophysin as a hexameric channel protein of the synaptic vesicle membrane. *Science,* 242**,** 1050-3.

THOMPSON, S. M., HAAS, H. L. & GÄHWILER, B. 1992. Comparison of the actions of adenosine at pre-and postsynaptic receptors in the rat hippocampus in vitro. *The Journal of Physiology,* 451**,** 347-363.

TIAN, L., HIRES, S. A. & LOOGER, L. L. 2012. Imaging neuronal activity with genetically encoded calcium indicators. *Cold Spring Harb Protoc,* 2012**,** 647-56.

TIAN, L. & LOOGER, L. L. 2008. Genetically encoded fluorescent sensors for studying healthy and diseased nervous systems. *Drug Discov Today Dis Models,* 5**,** 27-35.

TOWBIN, H., STAEHELIN, T. & GORDON, J. 1979. Electrophoretic transfer of proteins from polyacrylamide gels to nitrocellulose sheets: procedure and some applications. *Proc Natl Acad Sci U S A,* 76**,** 4350-4.

TRUDEAU, L. E., EMERY, D. G. & HAYDON, P. G. 1996. Direct modulation of the secretory machinery underlies PKA-dependent synaptic facilitation in hippocampal neurons. *Neuron,* 17**,** 789-797.

TSIEN, R., POZZAN, T. & RINK, T. 1982. Calcium homeostasis in intact lymphocytes: cytoplasmic free calcium monitored with a new, intracellularly trapped fluorescent indicator. *The Journal of Cell Biology,* 94**,** 325-334.

TSIEN, R. Y. 1998. The green fluorescent protein. *Annu Rev Biochem,* 67**,** 509-44.

TSUKAMOTO, M., YASUI, T., YAMADA, M. K., NISHIYAMA, N., MATSUKI, N. & IKEGAYA, Y. 2003. Mossy fibre synaptic NMDA receptors trigger non-hebbian long-term potentiation at entorhino-CA3 synapses in the rat. *The Journal of Physiology,* 546**,** 665-675.

VANZETTA, I. & GRINVALD, A. 1999. Increased cortical oxidative metabolism due to sensory stimulation: implications for functional brain imaging. *Science,* 286**,** 1555-8.

VENG, L. M., MESCHES, M. H. & BROWNING, M. D. 2003. Age-related working memory impairment is correlated with increases in the L-type calcium channel protein alpha1D (Cav1.3) in area CA1 of the hippocampus and both are ameliorated by chronic nimodipine treatment. *Brain Res Mol Brain Res,* 110**,** 193-202.

VERHAGE, M., MAIA, A. S., PLOMP, J. J., BRUSSAARD, A. B., HEEROMA, J. H., VERMEER, H., TOONEN, R. F., HAMMER, R. E., VAN DEN BERG, T. K., MISSLER, M., GEUZE, H. J. & SUDHOF, T. C. 2000. Synaptic assembly of the brain in the absence of neurotransmitter secretion. *Science,* 287**,** 864-9.

VOGLIS, G. & TAVERNARAKIS, N. 2006. The role of synaptic ion channels in synaptic plasticity. *EMBO Rep,* 7**,** 1104-10.

VOLIANSKIS, A., FRANCE, G., JENSEN, M. S., BORTOLOTTO, Z. A., JANE, D. E. & COLLINGRIDGE, G. L. 2015. Long-term potentiation and the role of N-methyl-d-aspartate receptors. *Brain Research,* 1621**,** 5-16.

VOLLERT, C., FORKUO, G. S., BOND, R. A. & ERIKSEN, J. L. 2013. Chronic treatment with DCPCX, an adenosine A1 antagonist, worsens long-term memory. *Neuroscience Letters,* 548**,** 296-300.

WANG, J. Q., DAUNAIS, J. B. & MCGINTY, J. F. 1994. Role of kainate/AMPA receptors in induction of striatal zif/268 and preprodynorphin mRNA by a single injection of amphetamine. *Brain Res Mol Brain Res,* 27**,** 118-26.

WANG, Q., SHUI, B., KOTLIKOFF, M. I. & SONDERMANN, H. 2008. Structural basis for calcium sensing by GCaMP2. *Structure,* 16**,** 1817-27.

WANG, Z.-W. 2008. *Molecular mechanisms of neurotransmitter release* [Online]. [Totowa, N.J.?]: Humana Press. Available: http://site.ebrary.com/id/10361995.

WASHBOURNE, P., THOMPSON, P. M., CARTA, M., COSTA, E. T., MATHEWS, J. R., LOPEZ-BENDITO, G., MOLNAR, Z., BECHER, M. W., VALENZUELA, C. F., PARTRIDGE, L. D. & WILSON, M. C. 2002. Genetic ablation of the t-SNARE SNAP-25 distinguishes mechanisms of neuroexocytosis. *Nat Neurosci,* 5**,** 19-26.

WEI, A. D., GUTMAN, G. A., ALDRICH, R., CHANDY, K. G., GRISSMER, S. & WULFF, H. 2005. International Union of Pharmacology. LII. Nomenclature and molecular relationships of calcium-activated potassium channels. *Pharmacol Rev,* 57**,** 463-72.

WEIMER, R. M. & RICHMOND, J. E. 2005. Synaptic vesicle docking: a putative role for the Munc18/Sec1 protein family. *Curr Top Dev Biol,* 65**,** 83-113.

WEISSKOPF, M., CASTILLO, P., ZALUTSKY, R. & NICOLL, R. 1994. Mediation of hippocampal mossy fiber long-term potentiation by cyclic AMP. *Science,* 265**,** 1878-1882.

WIEDENMANN, B. & FRANKE, W. W. 1985. Identification and localization of synaptophysin, an integral membrane glycoprotein of Mr 38,000 characteristic of presynaptic vesicles. *Cell,* 41**,** 1017-1028.

WILCOX, K. S. & DICHTER, M. A. 1994. Paired pulse depression in cultured hippocampal neurons is due to a presynaptic mechanism independent of GABAB autoreceptor activation. *Journal of Neuroscience,* 14**,** 1775-1788.

WILLOUGHBY, D., WACHTEN, S., MASADA, N. & COOPER, D. M. 2010. Direct demonstration of discrete Ca2+ microdomains associated with different isoforms of adenylyl cyclase. *J Cell Sci,* 123**,** 107-17.

WINN, H., RUBIO, R. & BERNE, R. 1981. Brain adenosine concentration during hypoxia in rats. *American Journal of Physiology-Heart and Circulatory Physiology,* 241**,** H235-H242.

WITTER, M. P., GRIFFIOEN, A. W., JORRITSMA-BYHAM, B. & KRIJNEN, J. L. M. 1988. Entorhinal projections to the hippocampal CA1 region in the rat: An underestimated pathway. *Neuroscience Letters,* 85**,** 193-198.

WU, L. G. & SAGGAU, P. 1994. Adenosine inhibits evoked synaptic transmission primarily by reducing presynaptic calcium influx in area CA1 of hippocampus. *Neuron,* 12**,** 1139-48.

XU-FRIEDMAN, M. A. & REGEHR, W. G. 2004. Structural contributions to short-term synaptic plasticity. *Physiological Reviews,* 84**,** 69-85.

XU, J., PANG, Z. P., SHIN, O. H. & SUDHOF, T. C. 2009. Synaptotagmin-1 functions as a Ca2+ sensor for spontaneous release. *Nat Neurosci,* 12**,** 759-66.

YANG, Y. & CALAKOS, N. 2013. Presynaptic long-term plasticity. *Front Synaptic Neurosci,* 5**,** 8.

YANG, Y. & HONARAMOOZ, A. 2012. Characterization and Quenching of Autofluorescence in Piglet Testis Tissue and Cells. *Anatomy Research International,* 2012**,** 10.

YOKOI, M., KOBAYASHI, K., MANABE, T., TAKAHASHI, T., SAKAGUCHI, I., KATSUURA, G., SHIGEMOTO, R., OHISHI, H., NOMURA, S., NAKAMURA, K., NAKAO, K., KATSUKI, M. & NAKANISHI, S. 1996. Impairment of hippocampal mossy fiber LTD in mice lacking mGluR2. *Science,* 273**,** 645-7.

YOSHIIKE, Y., KIMURA, T., YAMASHITA, S., FURUDATE, H., MIZOROKI, T., MURAYAMA, M. & TAKASHIMA, A. 2008. GABA(A) receptor-mediated acceleration of aging-associated memory decline in APP/PS1 mice and its pharmacological treatment by picrotoxin. *PLoS One,* 3**,** e3029.

YOUNG, P., QIU, L., WANG, D., ZHAO, S., GROSS, J. & FENG, G. 2008. Single-neuron labeling with inducible Cre-mediated knockout in transgenic mice. *Nature neuroscience,* 11**,** 721-728.

YUAN, P., LEONETTI, M. D., PICO, A. R., HSIUNG, Y. & MACKINNON, R. 2010. Structure of the human BK channel Ca2+-activation apparatus at 3.0 A resolution. *Science,* 329**,** 182-6.

ZANDER, J. F., MUNSTER-WANDOWSKI, A., BRUNK, I., PAHNER, I., GOMEZ-LIRA, G., HEINEMANN, U., GUTIERREZ, R., LAUBE, G. & AHNERT-HILGER, G. 2010. Synaptic and vesicular coexistence of VGLUT and VGAT in selected excitatory and inhibitory synapses. *J Neurosci,* 30**,** 7634-45.

ZHANG, W. & LINDEN, D. J. 2012. Calcium influx measured at single presynaptic boutons of cerebellar granule cell ascending axons and parallel fibers. *Cerebellum,* 11**,** 121-31.

ZHAO, C., DREOSTI, E. & LAGNADO, L. 2011. Homeostatic synaptic plasticity through changes in presynaptic calcium influx. *J Neurosci,* 31**,** 7492-6.

ZIEGLER, D. R., CULLINAN, W. E. & HERMAN, J. P. 2002. Distribution of vesicular glutamate transporter mRNA in rat hypothalamus. *J Comp Neurol,* 448**,** 217-29.

ZIMMERMANN, H., VOGEL, M. & LAUBE, U. 1993. Hippocampal localization of 5'-nucleotidase as revealed by immunocytochemistry. *Neuroscience,* 55**,** 105-112.

ZIPFEL, W. R., WILLIAMS, R. M., CHRISTIE, R., NIKITIN, A. Y., HYMAN, B. T. & WEBB, W. W. 2003. Live tissue intrinsic emission microscopy using multiphoton-excited native fluorescence and second harmonic generation. *Proceedings of the National Academy of Sciences,* 100**,** 7075-7080.

ZUCKER, R. S. 1987. The calcium hypothesis and modulation of transmitter release by hyperpolarizing pulses. *Biophysical Journal,* 52**,** 347-350.

ZUCKER, R. S. & REGEHR, W. G. 2002a. Short-term synaptic plasticity. *Annu.Rev.Physiol,* 64**,** 355-405.